P-ISSN 2525-2461 • E-ISSN 2615-9937

Vietnam Journal of Science, Technology and Engineering

MARCH 2021 • VOLUME 63 NUMBER 1

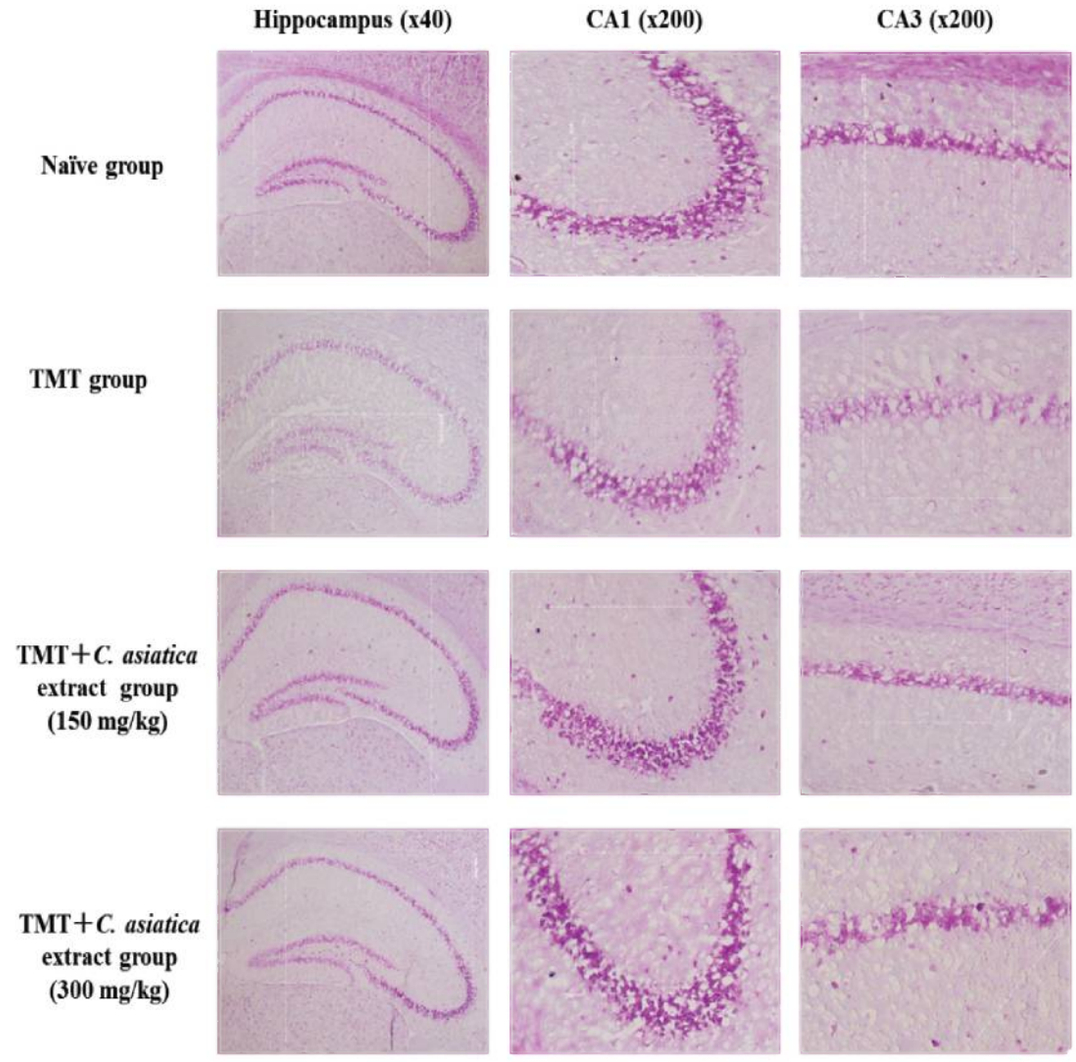

EFFECT OF *CENTELLA ASIATICA* ON COGNITIVE DEFICITS CAUSED IN TRIMETHYLTIN-INDUCED NEUROTOXICITY MODEL MICE

VIETNAM JOURNAL OF SCIENCE, TECHNOLOGY AND ENGINEERING * MARCH 2021 * VOLUME 63 NUMBER 1

vietnamscience.vn or vietnamscience.vjst.vn

Vietnam Journal of Science, Technology and Engineering (VJSTE) **is a quarterly double-blind peer-reviewed academic journal. VJSTE publishes research articles and review articles in all areas of science, technology and engineering with the focus on the physical sciences, life sciences and environmental sciences including the following topics:**

- **Physical Sciences**
- **Agriculture**
- **Medicine**
- **Pharmacology**
- **Biology**
- **Biotechnology**
- **Biomedical Applications**
- **Ecology**
- **Climatology**
- **Environmental Science.**

CLASSIFICATION SCHEME

1. **Mathematics and Computer Science**
   - **1.1. Mathematics**
   - **1.2. Computer Science**
   - **1.3. Computational Science**
2. **Physical Sciences**
   - **2.1. Physics**
   - **2.2. Chemistry**
   - **2.3. Engineering**
3. **Life Sciences**
   - **3.1. Agriculture**
   - **3.2. Medicine**
   - **3.3. Pharmacology**
   - **3.4. Biology**
   - **3.5. Biotechnology**
   - **3.6. Biomedical Applications**
4. **Earth Sciences**
   - **4.1. Geography**
   - **4.2. Geology**
   - **4.3. Geophysics**
   - **4.4. Oceanography**
5. **Environmental Sciences**
   - **5.1. Ecology**
   - **5.2. Climatology**
   - **5.3. Environmental Science**

CONTENTS

MARCH 2021 • VOLUME 63 NUMBER 1

5

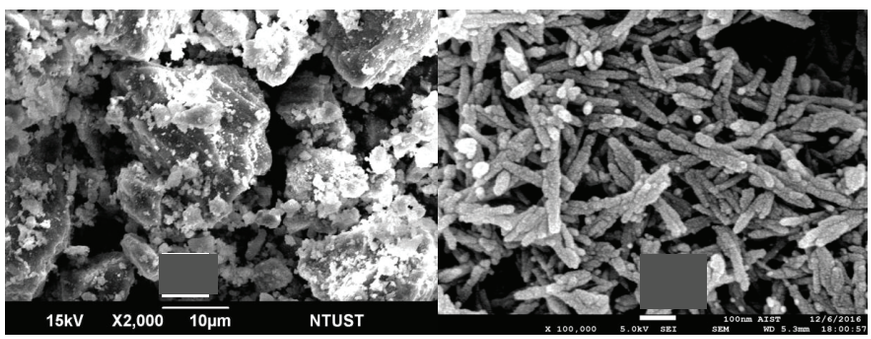

PHYSICAL SCIENCES

3 Microwave-assisted synthesis of nanorod hydroxyapatite from eggshells.
Doan Van Hong Thien, Nguyen Thi Bich Thuyen, Tran Thi Bich Quyen, Nguyen Huu Chiem, Van Pham Dan Thuy, Pham Hung Viet

7 Study on the fluoride-releasing ability of dental GIC materials in deionized water and artificial saliva environments.
Quang Minh Do, Ngoc Tri Huynh Nguyen, Thi Hong Hoa Huynh, Hong Lien Pham, Thi Thu Ho, Do Trung Kien Kieu, Ngoc Minh Huynh

15 Study on extracting hemicellulose, cellulose, and carboxymethyl cellulose from Vietnamese rice straw waste.
Mai Thi Tuyet Phan, Trang Thu La, Thu Hong Anh Ngo

21 Composition of ground granulated blast-furnace slag and fly ash-based geopolymer activated by sodium silicate and sodium hydroxide solution: Multi-response optimisation using Response Surface Methodology.
Hoang-Quan Dinh, Thanh-Bang Nguyen

30 Application of an innovative draw solute in forward osmosis (FO) processes.
Nguyen Cong Nguyen, Hau Thi Nguyen, Shiao-Shing Chen, Xuan Thanh Bui

LIFE SCIENCES

36 Influences of seed priming with *Spirulina platensis* extract on seed quality properties in black gram (*Vigna mungo* L.).
Nguyen Quang Thinh

42 Evaluation of clinical characteristics and lower esophageal sphincter pressure on high resolution manometry in achalasia patients after treatment.
Linh Nguyen Thuy, Trang Tran Thi Thu, Hue Luu Thi Minh, Hang Dao Viet

47 Study on cancer stem cell labeling and inhibition efficiency of LV3 nanocomplex *in vitro*.
Le Nhat Minh, Vo Trong Nhan, Thi Thao Do, Tran Thu Huong, Le Tri Vien, Phung Thi Kim Hue

54 Meningococcal disease in one soldier patient: Case report from Vietnam.
Nguyen Thanh Viet, Nguyen Minh Nam, Nguyen Vu Trung, Do Tuan Anh, Hoang Van Tong

CONTENTS

MARCH 2021 • VOLUME 63 NUMBER 1

52

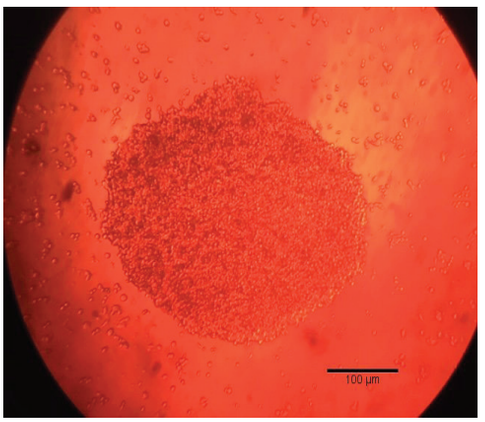

59 Effect of *Centella asiatica* on cognitive deficits caused in trimethyltin-induced neurotoxicity model mice.

Hang Thi Nguyet Pham, Hong Nguyen Tran, Xoan Thi Le, Khoi Minh Nguyen, Hiep Tuan Nguyen, Lap Thi Nguyen, Folk R. William

64 Development of inducer-free expression plasmids using IPTG-inducible P*spac* promoter for *Bacillus subtilis*.

Phuong Thi Bich Chu, Hanh Thi Thu Phan, Hoang Duc Nguyen, Trang Thi Phuong Phan

71 Co-digestion of domestic wastewater and organic fraction of food waste using anaerobic membrane bioreactor: A pilot scale study.

Hong Ha Bui, Lan Huong Nguyen, Thanh Tri Nguyen, Phuoc Dan Nguyen

ENVIRONMENTAL SCIENCES

77 Fluctuations in agriculture and sediment in the Mekong delta of Vietnam due to increased upstream water use.

Viet Hung Bui, Ngoc Diep Nguyen

83 Removal of greenhouse gas in biofilter using organic and inorganic media.

Nguyen Thanh Tung, Wilai Chiemchaisri, Chart Chiemchaisri, Samunya Sanguanpak

90 Sustainability assessment of community-based water resource management of irrigation systems for agriculture.

Huynh Thi Lan Huong, Pham Ngoc Anh

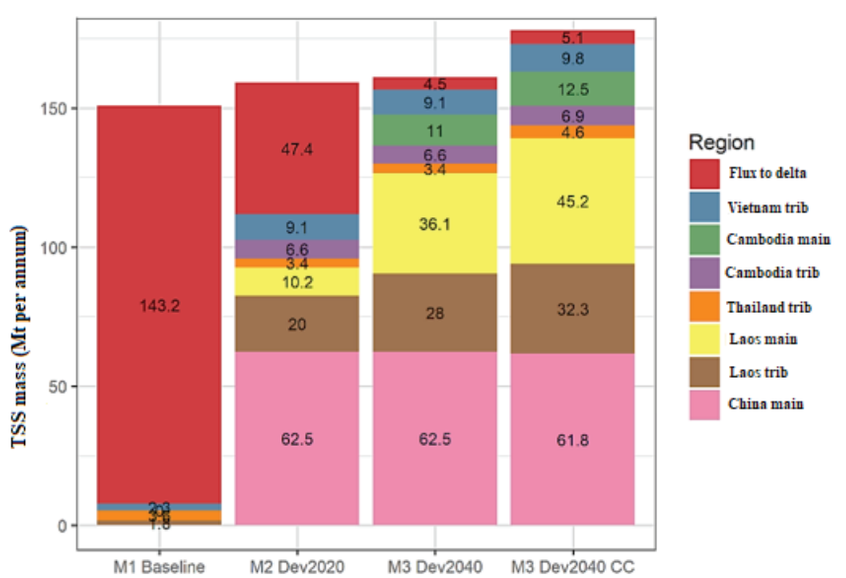

DOI: 10.31276/VJSTE.63(1).03-06

Microwave-assisted synthesis of nanorod hydroxyapatite from eggshells

Doan Van Hong Thien[1*], Nguyen Thi Bich Thuyen[1], Tran Thi Bich Quyen[1], Nguyen Huu Chiem[2], Van Pham Dan Thuy[2], Pham Hung Viet[3]

[1]*Department of Chemical Engineering, Can Tho University, Campus II, 3/2 Street, Xuan Khanh Ward, Ninh Kieu District, Can Tho City, Vietnam*

[2]*Department of Environmental Science, Can Tho University, Campus II, 3/2 Street, Xuan Khanh Ward, Ninh Kieu District, Can Tho City, Vietnam*

[3]*Research Centre for Environmental Technology and Sustainable Development, Vietnam National University, Hanoi, 334 Nguyen Trai Street, Thanh Xuan Trung Ward, Thanh Xuan District, Hanoi, Vietnam*

Received 22 May 2019; 24 October 2019; accepted 8 November 2019

Abstract:

Nanorod hydroxyapatite (HA) was synthesised from eggshells by using a microwave-assisted technique. In recent years, hydroxyapatite [HA, $Ca_{10}(PO_4)_6(OH)_2$] has gained attention because it exhibits excellent biocompatibility with soft tissues, such as muscle, gums, and skin. Every day, millions of tonnes of eggshells are generated around the world as bio-waste. The eggshell occupies about 11% of the total weight of an egg, and it consists of calcium carbonate (94%), calcium phosphate (1%), magnesium carbonate (1%), and organic matter (4%) (protein fibres). With eggshells and phosphoric acid as precursors, the reaction was carried out in a microwave with an irradiation power of 800 W for 45 minutes. The effects of Ca/P molar ratios and the power of microwaves were investigated. The obtained hydroxyapatite was characterised by X-ray diffraction (XRD), scanning electron microscope (SEM), and infrared spectroscopy (IR). During this research, HA nanorods were successfully synthesised from eggshells and phosphoric acid as precursors using microwave-assisted technology. The nanorod-like HA samples were 20-40 nm in diameter and 130-180 nm in length.

Keywords: **eggshell, hydroxyapatite, microwave-assisted synthesis, nanorod.**

Classification number: **2.2**

1. Introduction

In recent years, hydroxyapatite [HA, $Ca_{10}(PO_4)_6(OH)_2$] has gained attention because it exhibits excellent biocompatibility with soft tissues, such as muscle, gums, and skin [1]. Moreover, HA is often used for bone grafting, orthopaedic and dental implants, or the components of implants. In addition, HA is also applied for the adsorption of heavy metal ions. This substance can be produced from fish scales, seashells, bodily fluids, natural calcite, and eggshells [2-8].

Every day, millions of tonnes of eggshells are generated around the world as bio-waste. The eggshell occupies about 11% of the total weight of an egg, and it consists of calcium carbonate (94%), calcium phosphate (1%), magnesium carbonate (1%), and organic matter (4%) (protein fibres) [3, 9]. Sometimes, eggshells are used as a fertiliser because of their high calcium and nitrogen content, as a foodstuff, or for animal use [3]. Due to high calcium carbonate content, eggshells can be used as a material for the synthesis of HA [6-8, 10, 11].

A number of synthetic methods have been used to prepare HA, including sol-gel, spray pyrolysis, as well as hydrothermal and chemical precipitation methods [7, 12]. The hydrothermal method is an effective and convenient way to synthesise HA with diverse controllable morphologies, such as nanospheres, as well as needle- and flower-like structures [4, 5, 11]. The preparation of HA from eggshells consists of two steps. Firstly, the eggshells are calcined to remove organic compounds and obtain calcium oxide. Secondly, the obtained calcium oxide is reacted with orthophosphate hydrothermally for conversion to HA. Then, HA nanostructures with different morphologies are prepared by using organic modifiers. However, the disadvantage of the hydrothermal method is that it is time consuming [13]. Therefore, a microwave-assisted technique can be used as a green energy and to save time for synthesis of HA.

Microwave irradiation is a simple method for the synthesis of HA due to its high reaction rate, time savings, rapid heating, and green energy [14, 15]. In this process, the size and shape of HA molecules can be controlled by the synthesis parameters [13, 15]. The purpose of this work is to prepare nanorod HA by microwave-assisted synthesis with the use of phosphoric acid, with eggshells serving as the calcium source. Furthermore, HA is a potential material for metal ion adsorption.

**Corresponding author: Email: dvhthien@ctu.edu.vn*

2. Materials and methods

2.1. Materials

Eggshells were washed with boiling water to remove the membrane layer and dried overnight at 50°C in a box oven. After drying, the cleaned eggshells were ground into fine powder using a ball milling for 5 hours at 400 rpm. Phosphoric acid and ammonium hydroxide were purchased from Merck.

2.2. Methods

2.2.1. Preparation of hydroxyapatite from eggshells:

The powdered eggshells were calcined at the temperatures of 800, 900, 1,000, and 1,100°C to convert $CaCO_3$ into CaO. Then, CaO (11.2 g) was dissolved in 400 ml of H_2O while being stirred for 1 hour at room temperature to obtain $Ca(OH)_2$ solution. Then, the solution was heated to 75°C. Subsequently, the phosphoric acid (0.3 M) was added to the solution with a dropper. The ratios of Ca/P were 1.65, 1.67, and 1.69. The pH of the solution was maintained between 10 and 12 by using ammonium hydroxide. After ultrasounding for 1 hour, the mixture was placed in a microwave reactor for a chemical reaction. The mixture was irradiated with microwaves at various powers of irradiation (300, 600, 800, and 1,000 W). The precipitate was washed to remove residuals and then dried in a box oven at 100°C for 6 hours to obtain the HA powders.

2.2.2. Characterisations of the decomposition of eggshells and HA:

The chemical compositions of the eggshells were analysed with an X-ray fluorescence spectrometer (XRF) (S2 Ranger, Bruker, Germany). The crystalline phase of HA precipitates was investigated by X-ray diffraction (XRD) (D8 Phaser, Bruker, Germany) over a 2-theta (2θ) range from 10 to 60° with a scanning speed of 0.05°/min using CuKα radiation (λ=1.5406 Å) operating at the accelerating voltage of 40 kV and the current of 40 mA. The Joint Committee on Powder Diffraction Standards (JCPDS: 01-076-0694) was used for HA confirmation; HA formation was observed by Fourier transform infrared spectroscopy (FTIR) (FTS-3500, Bio-Rad, USA) using KBr pellets. The spectrum was scanned over 4,000-400 cm^{-1}. Surface morphology of the HA was observed using scanning electron microscopy (SEM) (JSM-6390LV, JEOL, Japan) at the accelerating voltage of 5 kV after gold coating.

3. Results and discussion

3.1. Effects of calcination temperature for the conversion of $CaCO_3$ into CaO

The chemical composition of eggshells depends on the calcination temperature. From the XRF results, after an increase in calcination temperature from 800 to 1,100°C for 4 hours, the percentage of CaO increased and reached the equilibrium value (95.6%) at 900°C. Therefore, the calcination temperature of 900°C was chosen for further experiments.

3.2. The effect of Ca/P molar ratios on HA formation

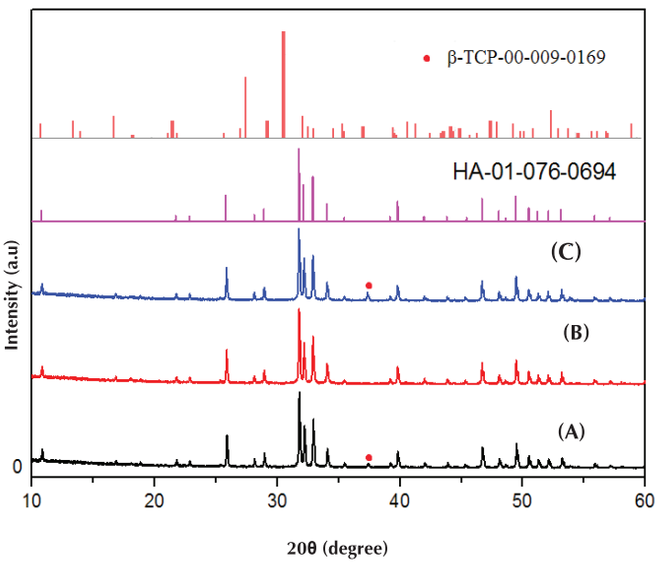

Fig. 1. XRD patterns of hydroxyapatite samples synthesised with the different molar ratios of Ca/P: (A) 1.65, (B) 1.67, and (C) 1.69.

Figure 1 illustrates the XRD patterns of hydroxyapatite samples with different molar ratios of Ca/P. The molar ratio of Ca/P was 1.67, and the characteristic HA peaks at 2θ angles of 25.89, 31.71, 34.06, 39.89, 46.73, 49.53, and 53.21°, corresponding to (002), (211), (202), and (301) Miller's planes, confirmed the formation of HA. No impurities peaks were found in the XRD pattern (Fig. 1B). In Fig. 1(A and C), the characteristic peak at 2θ=37.38° indicates the presence of β-TCP. Thus, the molar ratio of 1.67 for Ca/P was chosen for further experiments.

3.3. The effect of the power of microwave irradiation on HA formation

Figure 2 displays the XRD patterns of hydroxyapatite samples with different powers of microwave irradiation. With a power of microwave irradiation higher than 800 W, the characteristic peaks of HA were observed at 2θ angles of 25.90, 31.77, 32.15, 32.9, 34.04, 39.70, 46.68, 49.39, and 53.10°. All the peaks were indexed to hexagonal HA with no secondary phases, indicating that the HA was pure. The intensity of the highest peak was observed at a 2θ angle of 31.77°, corresponding to the (211) lattice plane, an increase from 80 to 800 W.

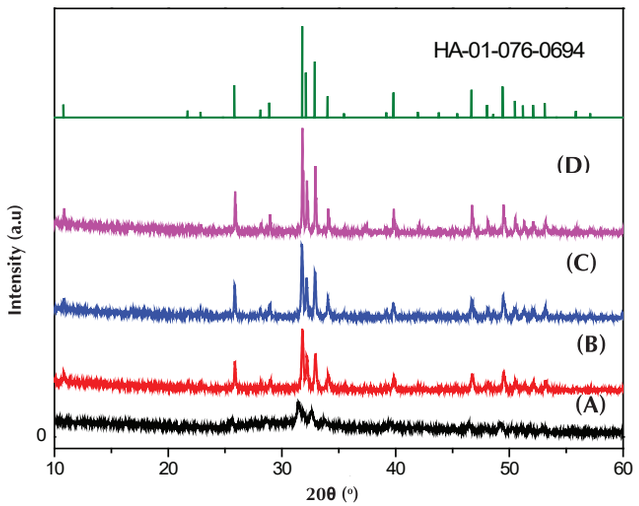

Fig. 2. XRD patterns of hydroxyapatite samples with the different powers of microwave irradiation: (A) 300 W, (B) 600 W, (C) 800 W, and (D) 1,000 W.

Figure 2C indicates that the highest intensity peak was at a 2θ angle of 31.78°. The average crystallite size (t) of HA was determined by the Scherrer equation:

$$t = \frac{0.9\lambda}{B\cos(\theta)}$$

where λ is the X-ray wavelength (λ = 1.5406 Å); θ is the diffraction angle; and B is determined by the "full width at half maximum intensity" located at 2θ. According to the Scherrer equation, the average crystallite size was 26.5 nm. This HA crystallite size is similar to the size of apatite crystals in previous studies [16].

3.4. Characteristics of HA

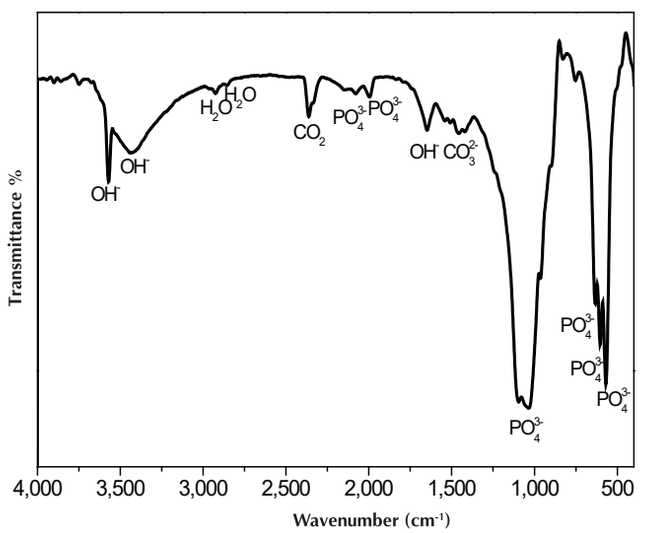

Fig. 3. FTIR spectrum of HA.

The FTIR spectrum of the synthesised HA sample is illustrated in Fig. 3. The characteristic peaks of functional groups of OH^- and PO_4^{3-} were observed in the IR spectrum. The characteristic peaks of the OH^- groups were at the wavelengths of 3,560 cm^{-1} (stretching mode) and 633 cm^{-1} (vibration). The characteristic peaks of the PO_4^{3-} groups were at the wavelengths of 565, 600 cm^{-1} (bending modes), 1,030 and 1,990 cm^{-1} (stretching mode) [17]. Moreover, a broad band observed at 1,630 cm^{-1} was attributed to the stretching modes of water molecules. The peaks of carbonate ions at 870 and 1,455 cm^{-1} were observed due to the substitution of the hydroxyl (-OH) and phosphate sites by the carbonate ions [17].

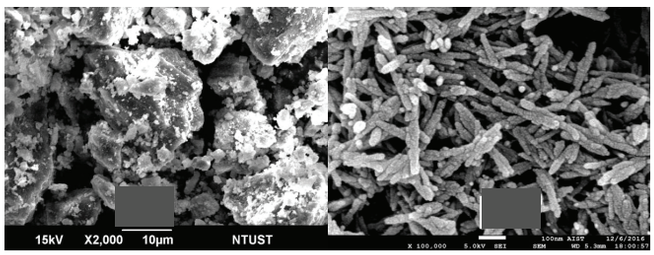

(A) (B)

Fig. 4. SEM images of eggshells (A) and hydroxyapatite sample (B).

Figure 4 contains SEM images of eggshells (Fig. 4A) and HA obtained after microwave-assisted synthesis (Fig. 4B). The eggshell powder was polyhedron. The polyhedron consisted of a multilayer of $CaCO_3$ (Fig. 4A). The HA obtained was uniform, and the morphology of HA was that of a nanorod of 20-40 nm in diameter and 130-180 nm in length. The nanorods of HA were obtained because the growth development of HA is along the c-axis due to its hexagonal symmetry [18]. Similar rod-like morphologies have been reported in previous studies [15, 19]. Besides, HA with flower- and sphere-like morphology has been synthesised by using microwave-assisted methods [9, 13, 14]. Thus, nanorod HA was successful prepared by using a microwave-assisted method in this research.

4. Conclusions

During this research, HA nanorods were successfully synthesised from eggshells and phosphoric acid as precursors using microwave-assisted technology. The temperature for the decomposition of calcium carbonate to form calcium oxide was 900°C. The uniform HA was obtained by applying a microwave irradiation power of 800 W for 45 minutes using XRD, IR, and SEM techniques. The HA produced had a nanorod-like morphology with samples of 20-40 nm in diameter and 130-180 nm in length.

CRediT author statements

Doan Van Hong Thien, Nguyen Thi Bich Thuyen, Tran Thi Bich Quyen: Conceptualization, Methodology, Data curation, Formal analysis, Writing - Review & Editing; Nguyen Huu Chiem, Van Pham Dan Thuy, Pham Hung Viet: Conceptualization, Methodology, Writing original draft preparation, Writing - Review & Editing.

ACKNOWLEDGEMENTS

This work was financially supported by the "Can Tho University Improvement Project VN14-P6, supported by a Japanese ODA loan" under grant number E6.

COMPETING INTERESTS

The authors declare that there is no conflict of interest regarding the publication of this article.

REFERENCES

[1] K. Prabakaran, S. Rajeswari (2009), "Spectroscopic investigations on the synthesis of nano-hydroxyapatite from calcined eggshell by hydrothermal method using cationic surfactant as template", *Spectrochimica Acta Part A: Molecular and Biomolecular Spectroscopy*, **74(5)**, pp.1127-1134, DOI: 10.1016/j.saa.2009.09.021.

[2] G. Gergely, F. Wéber, I. Lukács, et al. (2010), "Preparation and characterization of hydroxyapatite from eggshell", *Ceramics International*, **36(2)**, pp.803-806, DOI: 10.1016/j.ceramint.2009.09.020.

[3] E.M. Rivera, M. Araiza, W. Brostow, et al. (1999), "Synthesis of hydroxyapatite from eggshells", *Materials Letters*, **41(3)**, pp.128-134, DOI: 10.1016/S0167-577X(99)00118-4.

[4] W.F. Ho, H.C. Hsu, S.K. Hsu, et al. (2013), "Calcium phosphate bioceramics synthesized from eggshell powders through a solid state reaction", *Ceramics International*, **39(6)**, pp.6467-6473, DOI: 10.1016/j.ceramint.2013.01.076.

[5] A.R. Ibrahim, Y. Zhou, X. Li, et al. (2015), "Synthesis of rod-like hydroxyapatite with high surface area and pore volume from eggshells for effective adsorption of aqueous Pb(II)", *Materials Research Bulletin*, **62**, pp.132-141, DOI: 10.1016/j.materresbull.2014.11.023.

[6] P. Kamalanathan, S. Ramesh, L.T. Bang, et al. (2014), "Synthesis and sintering of hydroxyapatite derived from eggshells as a calcium precursor", *Ceramics International*, **40(10)**, pp.16349-16359, DOI: 10.1016/j.ceramint.2014.07.074.

[7] A.I. Adeogun, E.A. Ofudje, M.A. Idowu, et al. (2018), "Biowaste-derived hydroxyapatite for effective removal of reactive yellow 4 dye: Equilibrium, kinetic, and thermodynamic studies", *ACS Omega*, **3(2)**, pp.1991-2000, DOI: 10.1021/acsomega.7b01768.

[8] K. Ronan, M.B. Kannan (2017), "Novel sustainable routefor synthesis of hydroxyapatite biomaterial from biowastes", *ACS Sustainable Chemistry & Engineering*, **5(3)**, pp.2237-2245, DOI: 10.1021/acssuschemeng.6b02515.

[9] G.S. Kumar, A. Thamizhavel, E. Girija (2012), "Microwave conversion of eggshells into flower-like hydroxyapatite nanostructure for biomedical applications", *Materials Letters*, **76**, pp.198-200, DOI: 10.1016/j.matlet.2012.02.106.

[10] S.C. Wu, H.K. Tsou, H.C. Hsu, et al. (2013), "A hydrothermal synthesis of eggshell and fruit waste extract to produce nanosized hydroxyapatite", *Ceramics International*, **39(7)**, pp.8183-8188, DOI: 10.1016/j.ceramint.2013.03.094.

[11] D.L. Goloshchapov, V.M. Kashkarov, N.A. Rumyantseva, et al. (2013), "Synthesis of nanocrystalline hydroxyapatite by precipitation using hen's eggshell", *Ceramics International*, **39(4)**, pp.4539-4549, DOI: 10.1016/j.ceramint.2012.11.050.

[12] R. Bardhan, S. Mahata, B. Mondal (2011), "Processing of natural resourced hydroxyapatite from eggshell waste by wet precipitation method", *Advances in Applied Ceramics*, **110(2)**, pp.80- 86, DOI: 10.1179/1743676110Y.0000000003.

[13] G.S. Kumar, G. Karunakaran, E.K. Girija, et al. (2018), "Size and morphology-controlled synthesis of mesoporous hydroxyapatite nanocrystals by microwave-assisted hydrothermal method", *Ceramics International*, **44(10)**, pp.11257-11264, DOI: 10.1016/j.ceramint.2018.03.170.

[14] W. Xiao, H. Gao, M. Qu, et al. (2018), "Rapid microwave synthesis of hydroxyapatite phosphate microspheres with hierarchical porous structure", *Ceramics International*, **44(6)**, pp.6144-6151, DOI: 10.1016/j.ceramint.2017.12.247.

[15] V. Apalangya, V. Rangari, S. Jeelani, et al. (2018), "Rapid microwave synthesis of needle-liked hydroxyapatite nanoparticles via template directing ball-milled spindle-shaped eggshell particles", *Ceramics International*, **44(6)**, pp.7165-7171, DOI: 10.1016/j.ceramint.2018.01.161.

[16] S. Türk, İ. Altınsoy, G. ÇelebiEfe, et al. (2017), "Microwave-assisted biomimetic synthesis of hydroxyapatite using different sources of calcium", *Materials Science and Engineering: C*, **76**, pp.528-535, DOI: 10.1016/j.msec.2017.03.116.

[17] H. Tanaka, E. Tsuda, H. Nishikawa, et al. (2012), "FTIR studies of adsorption and photocatalytic decomposition under UV irradiation of dimethyl sulfide on calcium hydroxyapatite", *Advanced Powder Technology*, **23(1)**, pp.115-119, DOI: 10.1016/j.apt.2011.01.001.

[18] M.S. Shojai, M.T. Khorasani, E.D. Khoshdargi, et al. (2013), "Synthesis methods for nanosized hydroxyapatite with diverse structures", *Acta Biomaterialia*, **9(8)**, pp.7591-7621, DOI: 10.1016/j.actbio.2013.04.012.

[19] K.P. Sanosh, M.C. Chu, A. Balakrishnan, et al. (2009), "Utilization of biowaste eggshells to synthesize nanocrystalline hydroxyapatite powders", *Materials Letters*, **63(24)**, pp.2100-2102, DOI: 10.1016/j.matlet.2009.06.062.

DOI: 10.31276/VJSTE.63(1).07-14

Study on the fluoride-releasing ability of dental GIC materials in deionized water and artificial saliva environments

Quang Minh Do[1, 2], Ngoc Tri Huynh Nguyen[1, 2], Thi Hong Hoa Huynh[1, 2, 3], Hong Lien Pham[1, 2], Thi Thu Ho[1, 2], Do Trung Kien Kieu[1, 2], Ngoc Minh Huynh[1, 2*]

[1]Department of Silicate Materials, Faculty of Materials Technology, Ho Chi Minh City University of Technology, 268 Ly Thuong Kiet Street, Ward 14, District 10, Ho Chi Minh City, Vietnam

[2]Vietnam National University - Ho Chi Minh City, Linh Trung Ward, Thu Duc City, Ho Chi Minh City, Vietnam

[3]Tra Vinh University, 126 Nguyen Thien Thanh Street, Ward 5, Tra Vinh City, Tra Vinh Province, Vietnam

Received 5 June 2019; revised 21 August 2019; accepted 7 September 2019

Abstract:

Glass ionomer cement (GIC) is a particular type of cement used in dentistry. One of the most critical properties of GIC is the ability to release fluoride, which can prevent recurrent tooth decay. This study simultaneously investigated the release of fluoride, the compressive strength, and the apparent density of three GICs in deionized water (DW) and artificial saliva (AS) environments. GICs with 3 different types of glass powders were used to study. Powder B (the original) was the glass powder based on the SiO_2-Al_2O_3-CaF_2-$AlPO_4$-Na_3AlF_6 system, powder HA5 was powder B supplemented with 5 wt. % hydroxyapatite powder (HA), and powder Si_2 was powder B surface-treated with 2 wt. % silane JH-S69. The results of this study showed the amount of fluoride ion (F^-) released during 28 days in AS was lower in comparison to the DW environment, and the rate slowed down significantly after 1 d. The F^- release rate at 1-d age tended to be high as the compression strength was low. In AS, the powder supplemented with 5 wt.% HA improved the compressive strength and the cumulative amount of F^- released by the GIC. After 28 d, the F^- release of the GIC materials were able to be recharged in a NaF solution with 1,018 ppm F^- concentration for 3 min and further fluoride ions were released in both the DW and AS environments.

Keywords: **dental material, fluoride release, glass ionomer cement.**

Classification number: **2.2**

1. Introduction

GIC can be defined as a water-based material that hardens following an acid-base reaction. An ordinary glass ionomer cement consists of 2 parts: the ion-leachable glass powder, which is based on a calcium fluoro-aluminosilicate glass, and an acidic polymer solution of a polyalkenoic acid. The setting occurs in concentrated solutions in water. The final structure of a hardened GIC contains polyalkenoate salts with ionic crosslinks and a substantial amount of unreacted glass, which acts as the filler to reinforce the set cement. Since its introduction in 1971 [1], GICs have been successfully applied in dentistry and hold an important role in today's dental materials [2-4]. Although GICs have lower physical and mechanical properties than amalgam and composite resin materials, their advantages of aesthetics, adhesive properties, and biocompatibility make them very attractive to dental applications [5]. Dental caries or tooth decay is one of the most common health problems. The crucial feature of GICs for dental applications is their ability to release fluoride, which has anti-cariogenic effects. Lots of studies have emphasized the importance of fluoride-containing GIC materials to protect existing tooth structures and prevent secondary tooth decay, which places GIC materials in a better position than other materials [5, 6]. The fluoride release of glass ionomers causes the dentin to be less soluble in acid, increases the mineral regeneration, and changes the bacterial plaque composition in the tooth structure around fillings. Besides, GICs also have a fluoride absorption ability when exposed to F-containing sources. This remarkable feature helps to maintain the material's cariostatic capability in the long term [7]. Fluoride is an essential component of the glasses of GICs. This component has several functions within the glass such as lowering the

*Corresponding author: Email: hnminh@hcmut.edu.vn

fusion temperature, which improves the working behaviour of freshly mixed cement paste by preventing premature gelation. Moreover, fluoride improves the strength of the set cement [8]. However, some previous studies [9] have reported that a high fluoride-release ability could lead to poor mechanical properties. The factors that may affect the release of fluoride are the composition and microstructure of GIC materials (glass powder composition, fluoride content, powder/liquid ratio, substrate composition, and absorption ability of the GIC material), the storage environment (composition, pH, quantity, and frequency of the solution renewal), and regular contact with a local F-source such as toothpaste or mouthwash.

A lot of treatment methods, additives, and/or fillers have been applied to GIC material components to improve or enhance their properties. A mixture of inorganic compounds (glass, mineral, or metal) and organic compounds (rubber, plastic, or polymer) make it difficult to form a fine composite due to surface incompatibility involving the complex interaction of physical and chemical factors. One of the common solutions is the surface modification method using silane coupling agents. These substances are silicon-based chemicals that contain two types of reactivity - inorganic and organic - in the same molecule. The surface treatment of inorganic particles with silanes improves the phase interaction between the substrate and dispersant, thus improving the physical and mechanical properties of materials, and dental GICs are no exception [10-12]. Besides, another way is to increase the density of GICs by the application of various fillers [13] into a polyalkenoate glass component, such as metal powders (silver, stainless steel), carbon fibre, alumino-silicate fiberglass, or inorganic powder (SiO_2, Al_2O_3, ZrO_2, forsterite [14], hydroxyapatite, bioactive glass powder [15]). Among them, hydroxyapatite (HA) [$Ca_{10}(PO_4)_6(OH)_2$] has good biological properties. Therefore, combining HA into GIC may not only improve mechanical properties but also enhance biological compatibility and the fluoride release ability of GIC materials [16, 17].

The modification of GIC components to improve certain properties will no doubt change other properties of the material. The main purpose of this study is to assess the fluoride release from GICs with three different types of glass powders in deionized water and artificial saliva environments, before and after a NaF solution treatment (i.e. fluoride recharge). The change in compressive strength, apparent density, and microstructure of the material was also evaluated simultaneously after immersion periods.

2. Materials and methods

2.1. Materials

2.1.1. Synthesis and characterization of glass powders and liquid of GIC materials:

A high-speed lab milling equipment (Ceramic Instruments Ins) with a 1-l ceramic jar and 7-8-mm diameter zirconia ball was used for preparing the glass batch or for grinding the glass frit. The raw materials/ZrO_2 ball ratio was approximately 250 g/1,000 g. The glass batch was prepared by mixing suitable amounts of reagent-grade raw materials (Al_2O_3, SiO_2, $AlPO_4$, Na_3AlF_6, CaF_2) in the ceramic ball mill jar for 10 min. The homogeneous mixture was melted in a platinum crucible in a Carbolite-1600 furnace at 1,300^{o}C for 90 min. Then, the molten glass was quenched in cool distilled water to form a glass frit. The frit was, in turn, dry-milled for 50 min and sieved through a 45 µm mesh sieve to produce the first glass powder denoted as B. The chemical composition of the base glass powder B (mol% of elements, by x-ray fluorescence) is Al: 25.6, Si: 22.9, Ca: 15.2, P: 10.7, F: 15.3, Na: 10.4. The x-ray diffraction (XRD) patterns by Bruker D2 Phaser equipment with Cu - K_α radiation, 2θ scanning from 10 to 70^o, step size of 0.03^o/2θ, and mean time per step of 42 s, demonstrated that glass powder B was an amorphous material. The average diameter and specific surface area of powder B analysed by laser diffraction were 14.3 µm and 10,358 cm^2/cm^3, respectively.

The second powder denoted HA5 is powder B supplemented with 5 wt.% HA (synthesized hydroxyapatite powder, a research product of grant number B2012-20-09TD). The XRD pattern of the HA powder showed that the peaks corresponded to the standard hydroxyapatite crystal (ICDD standard, HA: JCPDS No. 09-0432). The crystal size of the nano-HA is determined to be about 51.8 nm by using X'Pert High Score software and the Scherrer equation for the (002) peak. The scanning electron microscope (SEM) and transmission electron microscope (TEM) images showed the particle size of HA to be less than 100 nm [18].

The third powder, denoted Si_2, is glass powder B surface-treated with 2 wt.% silane JH-S69 (chemical name: Bis-(3-triethoxysilypropyl) tetrasulfide, ChemSpec, Ltd, USA) to improve the surface compatibility with the acidic polymer solution. The glass powder B (100 g) was well mixed with a solution (60 g) of 3.33% JH-S69 in ethanol in a mortar and then dried at 110°C for 2 h in a dryer to obtain the dried silane-treated powder. This dried powder was, in turn,

re-dispersed in ethanol at 60°C for 30 min by hot magnetic stirrer, then vacuum-filtered (using Whatman No.40 filter paper) to remove any non-bonded residual silane. After being dried again at 60°C for 4 h, it was finely crushed in a mortar and passed through a 45 µm mesh sieve to obtain the surface-modified glass powder Si_2.

The main component of the acidic polymer liquid was a poly(acrylic acid) solution [$(C_3H_4O_2)_n$] (PAA) with average M_w ~ 100,000 and 35 wt. % in H_2O (a product of Sigma-Aldrich). To improve the handling, storage, and reactivity characteristics of the polymer liquid, maleic acid [$C_4H_4O_4$] (5% by mass) and tartaric acid [$C_4H_6O_6$] (5% by mass) were added to the PAA solution.

2.1.2. Preparation of GIC samples: The GIC powder and liquid were mixed at a powder/liquid (P/L) ratio ~1.4 g/1.0 g and shaped at 23±1°C. Cylindrical specimens were fabricated according to ISO 9917-1:2007's instructions, using stainless steel cylindrical moulds with 4.0±0.1 mm diameter and 6.0±0.1 mm height. Thirty minutes after mixing, the ends of the specimen were ground flat and at right angles to its long axis by using wet 400-grade silicon carbide paper. Then, the specimens were immediately removed from the moulds after surfacing and checked visually for air-voids or chipped edges. Any such defective specimen was discarded. Five GIC cylindrical specimens of each composition (B, HA5, or Si_2) were immediately immersed in closed plastic centrifuge tubes (conical bottom) containing 5 ml of deionized water (pH 7.0) or an artificial saliva solution (pH 5.0) at 37±1°C and 100% humidity for 1, 7, 14, and 28 d in an incubator until testing time. The ingredients of the artificial saliva [19] are shown in Table 1.

Table 1. The ingredients of each 50 g of artificial saliva (AS) solution [19].

Ingredients of AS	Amount in 50 g AS solution
Carboxymethylcellulose sodium	0.5 g
Calcium chloride ($CaCl_2.H_2O$)	0.0073 g
Sodium chloride (NaCl)	0.0422 g
Potassium chloride (KCl)	0.06 g
Sorbitol ($C_6H_{14}O_6$)	1.5 g
Magnesium chloride ($MgCl_2.6H_2O$)	0.0026 g
Potassium monohydrogen phosphate (K_2HPO_4)	0.0171 g
Sorbic acid ($C_6H_8O_2$)	0.025 g
Sodium benzoate ($C_7H_5NaO_2$)	0.0295 g
Deionized water	47.8 g

2.2. Compressive strength (CS) test

The CS of the hardened GICs was tested by Testometric M350-10CT equipment (England) at the Faculty of Materials Technology (HCMUT, VNU-HCM), and followed the ISO 9917-1:2007- Annex D with the cross-head speed of 0.75 mm/min. The CS was calculated by using the equation:

$$CS = \frac{4\times P}{\pi\times d^2} \text{ (MPa)}$$

where P is the maximum force applied (N) and d is the measured diameter of the cylindrical specimen (mm).

2.3. Measurement of GICs apparent density

The apparent density, is determined by the Archimedes method:

$$\rho_{ap} = \frac{m_d}{m_d - m_A}\rho_W \quad (g/cm^3)$$

where m_d is the dry specimen mass (specimens were dried at 60°C for 3 h) (g), m_A is the saturated specimen mass in water (g), and ρ_W is the density of distilled water (g/cm^3).

2.4. The microstructure of GICs (Surface examination with scanning electron microscopy)

The surfaces of samples were Pt-sputtered and then analyzed by scanning electron microscope [FE-SEM, Model S-4800 (Hitachi High - Technologies Co., Tokyo, Japan)].

2.5. Fluoride release experiment

The environmental conditions may affect the fluoride release ability of GICs. When the storage solution is replaced every day, the releasing ability is higher than in a fixed storage solution. For the test of fluoride release in this study, the storage solutions have to be renewed daily. The cylindrical specimens of the hardened GICs were prepared as shown in above. The average weight and the surface area of each specimen were 0.149±0.005 g and 1.00±0.02 cm^2, respectively.

The F^- concentration of the storage solution after soaking times (expressed as ppm) was analyzed by the Spectroquant® Spectrophotometer Pharo 100 (Merck) at the Centre for Product Evaluation (CPE) of Tra Vinh University (TVU) with a fluoride test kit with measuring range 0.1-20.0 ppm (µg/ml) and code 114598.0001. The cumulative amount of the released fluoride was obtained by the following equation [7]:

Cumulative released F^- (µg/g/cm^2) = F^- concentration (ppm ~ µg/ml) * total volume of storage solution (ml)/total weight of specimens (g)/total surface area of specimens (cm^2).

The rate of fluoride release as a function of time is expressed as µg/g/cm^2/d.

2.6. Fluoride treatment to simulate a fluoride recharge

After 28 d of storage in the DW or AS environment, the GIC samples were soaked in a NaF solution (F^- concentration: 1,018 ppm) for 3 min to simulate fluoride recharge during practical applications, which models the F^- the GIC could receive from F^--containing oral hygiene products. Then, they were rinsed gently with DW and immersed again in the same storage solution at 37°C. The storage solutions also were replaced every day. The sequential F^- release was tested at the storage age of the next 1, 2, and 3 d.

3. Results and discussion

3.1. Compressive strength (CS) and apparent density (ρ_{ap}) of GICs

Figure 1 represents the mean CS values and the mean ρ_{ap} values of the hardened GICs at 1, 7, and 28 d of age in the AS and DW storage environment. The CS is an important indicator of strength against mastication forces. The change in compressive strength of each GIC sample, according to the storage time, was similar in the AS and DW environments. The mean CS value of all the GICs increased from 1 d to 7 d, while the 28-d value decreased for the B and Si_2 specimens. Because of the recent contact (0.5-1 h after the end of mixing) with the soaking solution of the GICs during the prolonged immersion time, the leaching and diffusing ions from the cement to the immersion environment lead to failure in the material structure [20]. This is one of the disadvantages of GICs in return for their F^- release capability.

Two important factors affecting the strength of the GICs are the compactness and the interior bondings of the material. The ρ_{ap} reflects the consistency of the hardened GIC samples after the immersion time. With increasing ρ_{ap}, an increase in CS should be expected. A silane coupling agent can provide a stable bond between the two different poorly bonded surfaces as well as better wetting of inorganic substrates, which can help reduce the appearance of voids in the process of mixing and shaping the GIC. Thus, when glass powder B was surface-treated with 2% silane JH-S69, the resulting GIC-Si_2 samples possessed a higher apparent density and a more stable compression strength value at an older age (28 d). In the GIC-HA5 sample, the addition of HA nanoparticles with 5% content leads to a wide particle size distribution of the powder mixture. The glass and HA grains could be intertwined to fill the gap and thus increase the cement density. Moreover, HA is also capable of ion exchange [21]; many research results [17, 22, 23] have shown that HA is able to react with GIC through carboxylate groups in polyacids. That fact contributes to the increase in compressive strength of the GIC-HA5.

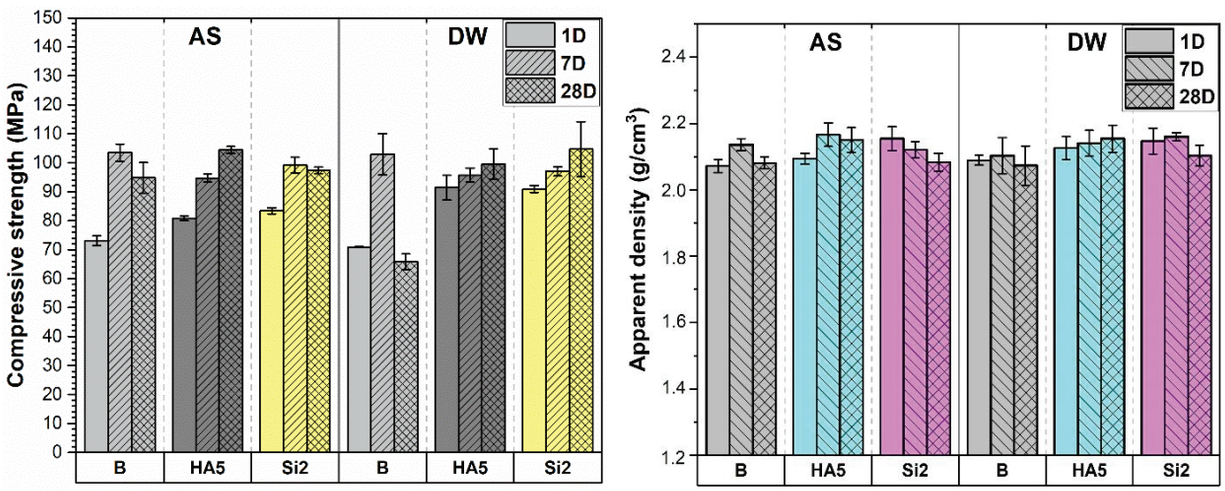

Fig. 1. Mean compressive strength (left) and mean apparent density (right) of GICs in AS and DW environment at 1, 7, and 28 d age.

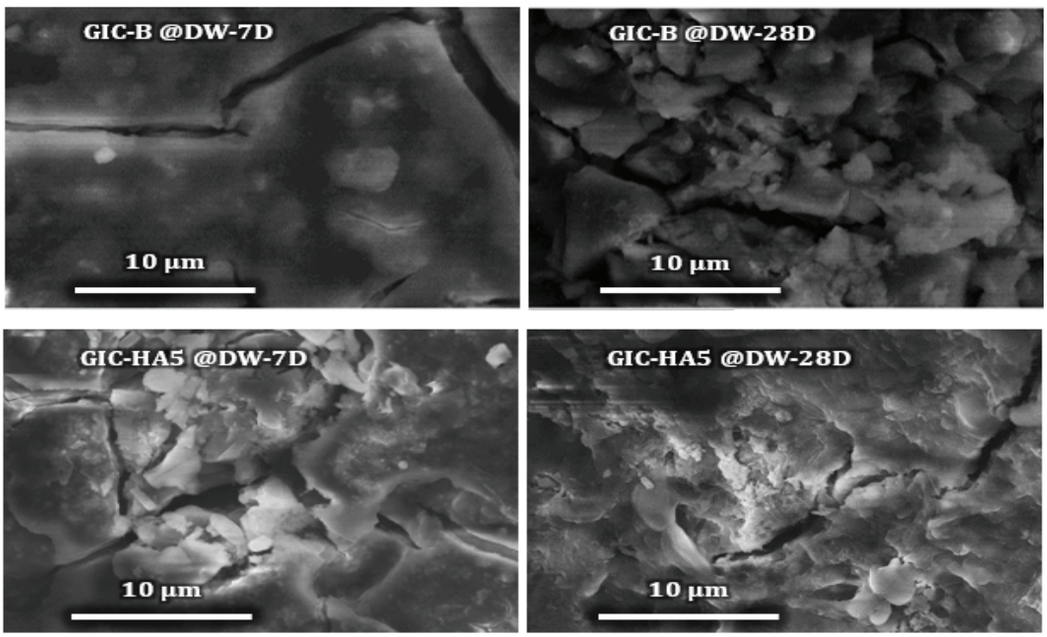

Fig. 2. The SEM images of GIC materials.

3.2. The results of SEM

SEM characterization is carried out to analyze the topography and the morphology of the hardened GICs surfaces. As shown in the SEM images (Fig. 2), the compact structure of the hardened GICs could be observed after 7 d.

The unclear borders around the glass powder grains signified that the glass phase reacted with the matrix phase and created mechanical and chemical bonding. Moreover, micro-clefts and pores could be formed by the mixing, shaping, and shrinkage processes. In general, the microstructure of the GIC samples soaked in the AS or DW environment at the same age was not significantly distinguished by the SEM images. It is noteworthy that the structure of the GIC pellet surface became rougher after 28 d of immersion, especially for sample B. The boundary of the unresponsive glass grains was more visible. It is indicated by the SEM images that the partial dissolution of the material on the surfaces occurred over time. This result might also be deduced from the reduction of the bulk density of the sample at the 28-d age compared to the 7-d age. Therefore, the CS of GICs tended to decrease at the 28-d age, except for the GIC-HA5 sample.

3.3. Fluoride release

F^- release test data resulting from the GICs studied before and after the F^- treatment in a NaF solution (F^- recharge) are shown in Tables 2 and 3 and Fig. 3. The detailed results showed that the synthetic GICs could release fluoride in both DW and AS environments. The cumulative amount of fluoride release increased with curing time. This phenomenon was caused by the fluoride ions dissolved from the glass powder and those that exist in the glass-ions matrix of the GIC. However, the release rate slowed down significantly after 1 d. The released fluoride in both storage environments was still detectable at 28-d age, but at low levels.

Table 2. The cumulative amount of released fluoride from GIC samples in DW and AS environment.

Environment	Sample	Cumulative released F^- (µg/g/cm²)							
		1 day	*7 days*	*14 days*	*28 days*	Fluoride treatment (FT) in NaF solution (1,018 ppm)	*1 day after FT*	*2 days after FT*	*3 days after FT*
AS	B	50.3	54.4	71.4	82.2		484.0	534.6	566.3
	HA5	53.4	100.3	146.3	186.3		375.3	442.2	484.5
	Si_2	45.6	69.7	78.2	93.2		382.4	423.3	450.5
DW	B	204.1	270.4	316.3	389		484.0	534.6	566.3
	HA5	176.9	224.5	244.9	301.4		375.3	442.2	484.5
	Si_2	183.7	224.5	241.5	317.8		382.4	423.3	450.5

Table 3. Fluoride release rate (µg/g/cm²/d) as a function of time of GIC samples in DW and AS environment.

Environment	Sample	F^- release rate (µg/g/cm²/d)							
		1 day	*7 days*	*14 days*	*28 days*		*1 day after FT*	*2 days after FT*	*3 days after FT*
AS	B	50.3	0.7	2.4	0.8	Fluoride treatment (FT) in NaF solution (1,018 ppm)	65.1	42.3	55.3
	HA5	53.4	7.8	6.6	2.9		73.4	60.1	23.4
	Si_2	45.6	4.0	1.2	1.1		87.8	73.8	52.7
DW	B	204.1	11.1	6.6	5.2		94.9	50.6	31.6
	HA5	176.9	7.9	2.9	4.0		73.9	66.9	42.3
	Si_2	183.7	6.8	2.4	5.5		87.8	40.8	27.2

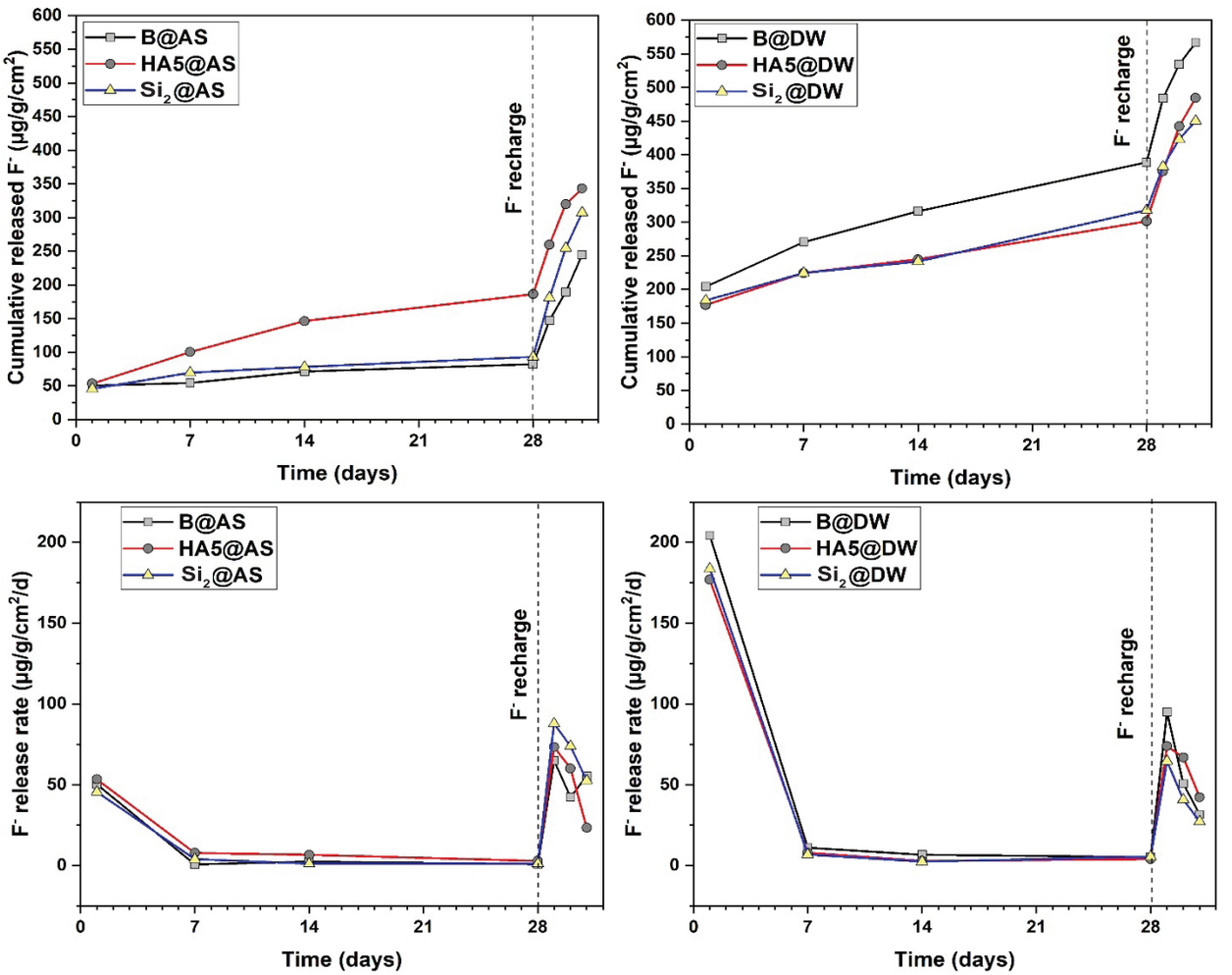

Fig. 3. The plots of cumulative released F^- amount and F^- release rate vs time of storage in AS and DW environments of the GIC samples.

Those results could be explained by the mechanism of ion release. Fluoride ions were released first from the surface of the GIC material with a high rate, then the F^- diffusion from the inside of the GIC structure extended the releasing process at slower rate [8] due to the tight cross-linkage in the mature cement matrix. After being soaked in a NaF solution (1,018 ppm F^-) for 3 min, at 28-d age the increase of F^- release values over the following days indicated that the GICs could be recharged with fluoride.

In Fig. 4, the cumulative release from the three GICs and their CS after 28 d of immersion in AS and DW is

shown. The linear fitting was performed using the analysis tool of Origin Pro 2015. The cumulative F^- release amount of the three GICs observed in AS was less than in the DW environment. That may be explained by the similarity between the ions' composition in the AS environment and the GIC materials, which causes a low diffusion gradient [24]. In the storage solutions, the ions-release phenomena, including F^- release, occurred due to the erosion of the GIC.

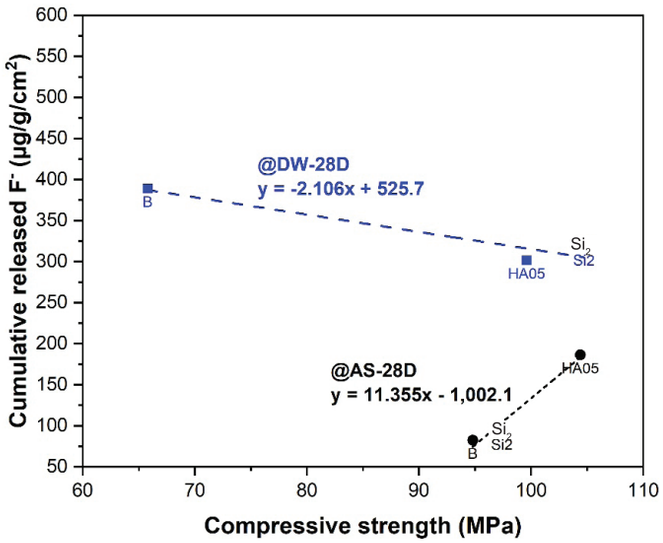

Fig. 4. Plot of cumulative released F^- amount vs compressive strength at 28-d age of the GIC samples in AS and DW environments.

In the case of deionized water, a negative value of the slope of the fit line indicates that a mature GIC sample with a high cumulative amount of F^- release would have a low CS value. During the GIC immersion process in deionized water, the diffusion of ions took place merely from GIC into the water. Conversely, in the process of storage in the AS environment, the saliva components, including calcium and phosphates, could diffuse into the cement structure and contribute to the strengthening of the GICs' surface [25]. Consequently, the CS values of the GIC-B and GIC-HA5 samples in the AS were higher than those in DW. On the other hand, the presence of HA nano-particles has a role in this aspect as the filler that made the apparent density and the CS of GIC-HA5 higher. However, unlike glass grains, HA particles might disrupt the cross-linking of polysalts. Thus, the fluoride release of GIC-HA5 in AS still occurred quite favourably due to the mobility of the small fluoride ions (like hydroxyl ions) in this GIC matrix without any damage [26].

Figure 5 shows the relationship between the F^- release rate and the compressive strength of the GIC samples in the AS and DW environments at 1-d age and 29-d age (i.e. 1 d after F^- recharge). The slopes of the fit lines had negative values. Therefore, for the three GIC samples with different powder compositions, the F^- release rate at 1-d age tended to be high when the compression strength was low. This trend was also expressed in the F^- re-release value on the first day after the GIC samples were recharged with F^-. The modification of glass powder B by the addition of HA (HA5) or the silane surface treatment with JH-S69 (Si_2) has increased the CS and the Pap of the GICs. These factors have limited the release of F^- from the surface, which is the dominant mechanism in the early stages, as a consequence.

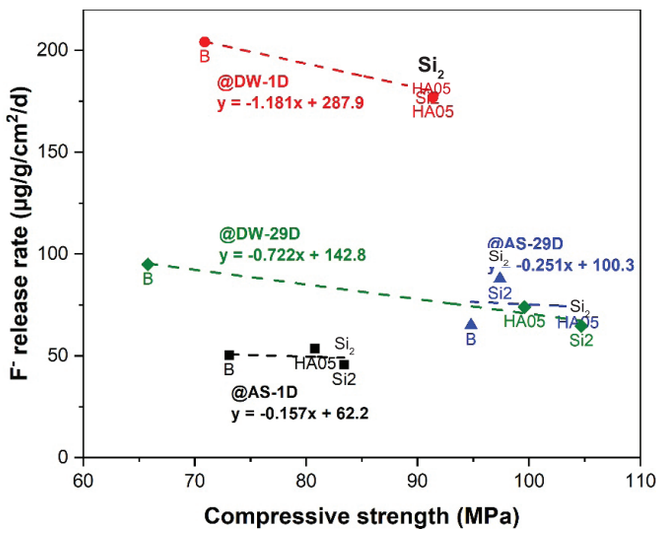

Fig. 5. The F^- release rate vs the compressive strength of GIC samples in AS and DW environments at 1-d age and 29-d age (1 d after F^- recharge).

4. Conclusions

The three GICs synthesized in this study showed satisfactory results in their fluoride-releasing ability over time. The releasing capacity in DW was higher in comparison to AS, and the rate slowed down significantly after 1 d of immersion. The modification of glass powder B by the addition of HA (HA5) or the silane surface treatment with JH-S69 (Si_2) has increased the CS and the ρ_{ap} of the GICs, accordingly, and in the early stages, it limited the release of F^- from the surface in both environments. In AS, the supplement of 5 wt.% HA can improve not only the CS but also the cumulative F^- release amount of GIC. After 28 days of F^- release, the GIC materials were able to be recharged and further released fluoride in the DW and AS environments.

CRedit author statements

Quang Minh Do, Ngoc Tri Huynh Nguyen, Thi Hong Hoa Huynh: Conceptualisation, Methodology, Data curation, Formal analysis, Writing - Review & Editing; Hong Lien Pham, Thi Thu Ho, Do Trung Kien Kieu, Ngoc Minh Huynh: Formal analysis, Writing - Review & Editing, Revise article.

ACKNOWLEDGEMENTS

This research is funded by Vietnam National University, Ho Chi Minh city under grant number C2017-20a-01. We acknowledge the support of time and facilities from Ho Chi Minh city University of Technology (HCMUT), VNU-HCM for this study.

COMPETING INTERESTS

The authors declare that there is no conflict of interest regarding the publication of this article.

REFERENCES

[1] A.D. Wilson, B.E. Kent (1971), "The glass-ionomer cement, a new translucent dental filling material", *J. Appl. Chem. Biotechnol.*, **21(11)**, DOI: 10.1002/jctb.5020211101.

[2] C.L. Davidson (2006), "Advances in glass-ionomer cements", *J. Appl. Oral Sci.*, **14(SPE)**, pp.3-9, DOI: 10.1590/s1678-77572006000700002.

[3] D.C. Smith (1998), "Development of glass-ionomer cement systems", *Biomaterials*, **19(6)**, pp.467-478, DOI: 10.1016/s0142-9612(97)00126-9.

[4] J.W. McLean, A.D. Wilson (2004), "Glass ionomer cements", *Br. Dent. J.*, **196(9)**, pp.514-515, DOI: 10.1038/sj.bdj.4811254.

[5] H. Kusumoto, S. Abolghasemi, B. Woodfine, et al. (2016), "The effect of phosphate, fluorine, and soda content of the glass on the mechanical properties of the glass ionomer (polyalkenoate) cements", *J. Non-Cryst. Solids*, **449**, (Supplement C), pp.94-99, DOI: 10.1016/j.jnoncrysol.2016.06.036.

[6] J.W. Nicholson (2014), "Fluoride-releasing dental restorative materials: An update", *Balk. J. Dent. Med.*, **18(2)**, pp.60-69, DOI: 10.1515/bjdm-2015-0010.

[7] M.G. Gandolfi, S. Chersoni, G.L. Acquaviva, et al. (2006), "Fluoride release and absorption at different pH from glass-ionomer cements", *Dent. Mater.*, **22(5)**, pp.441-449, DOI: 10.1016/j.dental.2005.04.036.

[8] S.K. Sidhu (2016), *Glass-Ionomers in Dentistry*, Springer, DOI: 10.1007/978-3-319-22626-2.

[9] X. Xu, J.O. Burgess (2003), "Compressive strength, fluoride release and recharge of fluoride-releasing materials", *Biomaterials*, **24(14)**, pp.2451-2461, DOI: 10.1016/s0142-9612(02)00638-5.

[10] S. Kato, F. Fusejima, T. Yoshikawa (1996), *Dental Glass Ionomer Cement Composition*, US5520725 A, 15pp.

[11] S. Nakamura, K. Yoshida, K. Kamada, et al. (2004), "Bonding between resin luting cement and glass infiltrated alumina-reinforced ceramics with silane coupling agent", *J. Oral Rehabil.*, **31(8)**, pp.785-789, DOI: 10.1111/j.1365-2842.2004.01304.x.

[12] M. Hirasawa, S. Kato, M. Takuno (2004), *Glass Powder for Glass Ionomer Cement*, US20040067359 A1, 6pp.

[13] T.D. Caluwé, C.W.J. Vercruysse, S. Fraeyman, et al. (2014), "The influence of particle size and fluorine content of aluminosilicate glass on the glass ionomer cement properties", *Dent. Mater.*, **30(9)**, pp.1029-1038, DOI: 10.1016/j.dental.2014.06.003.

[14] F.S. Sayyedan, M.H. Fathi, H. Edris, et al. (2014), "Effect of forsterite nanoparticles on mechanical properties of glass ionomer cements", *Ceram. Int.*, **40(7)**, Part B, pp.10743-10748, DOI: 10.1016/j.ceramint.2014.03.062.

[15] T.D. Caluwé, C.W.J. Vercruysse, I. Ladik, et al. (2017), "Addition of bioactive glass to glass ionomer cements: Effect on the physico-chemical properties and biocompatibility", *Dent. Mater.*, **33(4)**, pp.e186-e203, DOI: 10.1016/j.dental.2017.01.007.

[16] Y.W. Gu, A.U.J. Yap, P. Cheang, et al. (2005), "Effects of incorporation of HA/ZrO_2 into glass ionomer cement (GIC)", *Biomaterials*, **26(7)**, pp.713-720, DOI: 10.1016/j.biomaterials.2004.03.019.

[17] R.A.S. Alatawi, N.H. Elsayed, W.S. Mohamed (2019), "Influence of hydroxyapatite nanoparticles on the properties of glass ionomer cement", *J. Mater. Res. Technol.*, **8(1)**, pp.344-349, DOI: 10.1016/j.jmrt.2018.01.010.

[18] D.Q. Minh, N.K. Son, H.N. Minh, et al. (2014), *Research and Development of The Sintered Material from Hydroxy Apatite (HA) by Hot-pressing Method for Biomaterial*, Final report on the key research project of Vietnam National University, Ho Chi Minh city (VNU-HCM), grant number B2012-20-09TD, 30pp (in Vietnamese).

[19] M.A.M.P. Kashani (2013), *Effect of Cation Substitutions in an Ionomer Glass Composition on The Setting Reaction and Properties of The Resulting Glass Ionomer Cements*, University of Birmingham, 215pp.

[20] F. Barandehfard, M.K. Rad, A. Hosseinnia, et al. (2016), "The addition of synthesized hydroxyapatite and fluorapatite nanoparticles to a glass-ionomer cement for dental restoration and its effects on mechanical properties", *Ceram. Int.*, **42(15)**, pp.17866-17875, DOI: 10.1016/j.ceramint.2016.08.122.

[21] K. Arita, A. Yamamoto, Y. Shinonaga, et al. (2011), "Hydroxyapatite particle characteristics influence the enhancement of the mechanical and chemical properties of conventional restorative glass ionomer cement", *Dent. Mater. J.*, **30(5)**, pp.672-683, DOI: 10.4012/dmj.2011-029.

[22] A.D. Wilson, H.J. Prosser, D.M. Powis (1983), "Mechanism of adhesion of polyelectrolyte cements to hydroxyapatite", *J. Dent. Res.*, **62(5)**, pp.590-592, DOI: 10.1177/00220345830620051801.

[23] A. Moshaverinia, S. Ansari, M. Moshaverinia, et al. (2008), "Effects of incorporation of hydroxyapatite and fluoroapatite nanobioceramics into conventional glass ionomer cements (GIC)", *Acta Biomater.*, **4(2)**, pp.432-440, DOI: 10.1016/j.actbio.2007.07.011.

[24] M.S. Baig, G.J.P. Fleming (2015), "Conventional glass-ionomer materials: A review of the developments in glass powder, polyacid liquid and the strategies of reinforcement", *J. Dent.*, **43(8)**, pp.897-912, DOI: 10.1016/j.jdent.2015.04.004.

[25] K. Okada, S. Tosaki, K. Hirota, et al. (2001), "Surface hardness change of restorative filling materials stored in saliva", *Dent. Mater.*, **17(1)**, pp.34-39, DOI: 10.1016/s0109-5641(00)00053-1.

[26] G.J. Mount, W.R. Hume, H.C. Ngo, et al. (2016), *Preservation and Restoration of Tooth Structure*, John Wiley & Sons, 328pp.

DOI: 10.31276/VJSTE.63(1).15-20

Study on extracting hemicellulose, cellulose, and carboxymethyl cellulose from Vietnamese rice straw waste

Mai Thi Tuyet Phan*, Trang Thu La, Thu Hong Anh Ngo

Faculty of Chemistry - University of Science, Vietnam National University, Hanoi,
334 Nguyen Trai Street, Thanh Xuan Trung Ward, Thanh Xuan District, Hanoi, Vietnam

Received 15 May 2020; revised 24 August 2020; accepted 3 September 2020

Abstract:

Vietnam is an agricultural country with a large amount of rice straw waste amounting to 55-60 million tons annually. Rice straw contains about 35-40% dry weight of cellulose and 25-30% hemicellulose, and 10-15% lignin. Cellulose and hemicellulose were successfully extracted from Vietnamese rice straw waste. The maximum hemicellulose yield of the process was 22.60% with 1.5 M NaOH at 90°C for 1.5 h. The pure cellulose obtained from the rice straw was prepared by refluxing the rice straw powder with a 1.0 M HNO_3 solution at 90°C for 1.5 h. The Vietnamese rice straw cellulose was converted to carboxymethyl cellulose (CMC) by etherification. The extracted cellulose was soaked in a mixed solution of isopropyl alcohol and NaOH solution for 1.5 h. After that, it was reacted with monochloroacetic acid at 70°C for 1.5 h. The optimum conditions for carboxymethylation were 5 g cellulose, 4.0 g monochloroacetic acid, and 15 ml 25% w/v NaOH and the obtained product had a degree of substitution (DS) of 0.70.

Keywords: **carboxymethyl cellulose, cellulose, hemicellulose, Vietnamese rice straw waste.**

Classification number: **2.2**

1. Introduction

Vietnam is an agricultural country with a large amount of rice straw waste amounting to 55-60 million tons annually. Rice straw contains about 35-40% dry weight of cellulose and 25-30% hemicellulose and 10-15% lignin [1, 2]. Therefore, the potential of cellulose and hemicellulose recovery from this waste is quite feasible. Recovering cellulose from rice straw waste will upgrade the rice value chain by adding value to by-product of rice production. To date, many works have mentioned problems with cellulose, hemicellulose and lignin recovery from rice straw by-products [3, 4]. For example, R.C. Sun, et al. (2000) [3] reported that a two-stage treatment of rice straw with 0.25 M NaOH at 55°C for 2 h followed by 0.0-5.0% H_2O_2 at 45°C for 12 h at pH 11.5. From there, 49.3-74.3% of the residual hemicelluloses was released compared to 16.6-25.1 wt.% of the weight of the initial dried rice straw powder. Lignin was also extracted from Vietnamese rice straw using a combination of ultrasound irradiation for 30 min and 2 M NaOH at 90°C for 1.5 h, which yielded a lignin separation of 84.7% of the residual lignin [4]. G. Fan, et al. (2019) [5] extracted cellulose from rice straw and further converted it into microcrystalline cellulose (MCC) in the presence of a hydrochloric acid aqueous solution and the cellulose content reached up to 92.4% MCC. Although, many efforts have been made to identify a suitable solution for cellulose extraction, the determination of a procedure for separating the biomass constituents efficiently is still a major obstacle to its utilization. Therefore, studies on the simultaneous extraction of cellulose and hemicellulose from this waste is essential and important. The purpose of this work is to confirm the potential of using Vietnamese rice straw waste as a raw material for industrial hemicellulose extraction and CMC production.

*Corresponding author: Email: maimophong@gmail.com.

2. Experimental

2.1. Materials and rice straw source

The main chemicals used in this study include monochloroacetic (MCA) (UK) 99.7%, acetic acid 99.9%, nitric acid 65%, and sodium hydroxyl 99.9% (Merck). The solvents include methanol 99.8%, ethanol 99.9%, isopropanol 99.7%, and acetone 99.8% (Merck).

The rice straw waste was collected from Vietnam. Rice straw samples were dried in an oven at 60°C for 24 h before being ground into particles of 1 mm diameter by using a grinding machine.

2.2. Preparation methods

2.2.1. Hemicellulose extraction from Vietnamese rice straw waste

Hemicellulose was recovered from Vietnamese rice straw by alkaline extraction. Ten grams of dried rice straw powder were mixed with 250 ml of diluted *x* M NaOH (*x*=0.50 M, 1.00 M, 1.50 M, 2.00 M, 2.50 M) at 90°C for different periods of time (*t*=60, 90, 120 min) under continuous stirring. The dark slurry obtained was filtered and washed with 250 ml of distilled water to the recover solid part. The residual solid part was put into a clean Erlenmeyer flask for separation of the cellulose. The filtrate was acidified to pH 6 with 25% acetic acid. The hemicellulose was precipitated by using cold ethanol 96% (volume portion of filtrate to ethanol was 1:2). The mixture was soaked overnight to allow the hemicellulose to precipitate (no stirring) and settle to the bottom. The precipitate layer was carefully removed by vacuum filtration. The precipitate was washed 3 times with 70% ethanol solution. The obtained hemicellulose was dried at 40°C for 24 h. The dried hemicellulose was ground into a fine powder. The yield of the hemicellulose was gravimetrically determined and expressed as a weight of the extracted dried hemicellulose to 100 g of the dried rice straw used for extraction. This process was repeated 3 times.

The yield of the hemicellulose was determined by using the below equation:

$$H_H(\%) = \frac{m_H}{m_0} x100$$

where H_H is the yield of hemicellulose, m_H is the weight of obtained hemicellulose, and m_0 is the weight of initial dried rice straw powder.

2.2.2. Cellulose recovery from Vietnam's rice straw waste

Determination of optimum HNO_3 concentration: the solid residual part of the above process was treated with 150 ml of *y* M HNO_3 (y=0.75, 1.00, 1.25 and 1.50 M) and cooked at 90°C for 90 min. This mixture was then filtered and washed with cold distilled water until the indicator paper did not change colour. The residue was dried in an oven at 60°C overnight until the weight was constant. Finally, the dried cellulose was ground and kept in a polyethylene bag for cellulose modification in the next process.

The yield of the cellulose extraction was determined by using the below equation:

$$H_C(\%) = \frac{m_C}{m_0} x100$$

where H_C is the yield of the cellulose extraction, m_c is the weight of the obtained cellulose, and m_0 is the weight of the initial dried rice straw powder.

2.2.3. Synthesis of CMC

Five grams of cellulose extraction obtained from Vietnamese rice straw powder was added to 50 ml of isopropanol under continuous stirring for 30 min. Then, 15 ml of (15%, 20%, 25%, 30% w/v) NaOH was added dropwise into the mixture and further stirred for 1 h at room temperature. The carboxymethylation began when *y* grams of MCA (y=1.0, 2.0, 3.0, 4.0 g and 5.0 g) was added under continuous stirring for another 90 min at 70°C. The solid part was neutralized with acetic acid to pH7 and washed three times by soaking in 20 ml of ethanol for 10 min to remove undesirable by-products. The obtained CMC was filtered and dried at 60ºC until the weight was constant and it was kept in a dry place.

The yield of the CMC was determined by using the below equation [6]:

$$H_{CMC}(\%) = \frac{m_{CMC} - m_C}{m_C} x100$$

where H_{CMC} is the yield of the CMC, m_{CMC} is the weight of the obtained CMC, and m_C is the weight of the cellulose used to synthesis CMC.

2.3. Research methods

2.3.1. Infrared spectroscopy (FTIR)

FTIR spectra were recorded on an FT/IR-6300 spectrometer, with 32 scans and a resolution of 4 cm^{-1} in the wavenumber range of 600-4000 cm^{-1}.

The degree of substitution, DS_{rel}, of the carboxyl group in the CMC can be determined with FTIR spectra by means of taking the ratio of the absorption spectra as shown in the below equation [7]:

$$DS_{rel}(\%) = \frac{A_{1593}}{A_{2918}} - B$$

where is A_{1593} is the absorbance at 1593 cm^{-1}, which is assigned to the stretching vibration of the carboxyl group

(COO^-), A_{2918} is the absorbance at 2918 cm^{-1}, which is assigned to the stretching vibration of methine (C-H), and *B* is a numerical constant corresponding to the A_{1593}/A_{2918} ratio of the cellulose, which was found to be zero. A linear relationship between the absolute and relative values of the degree of substitution was proved by Pushpamalar as shown in the below equation:

$$DS_{abs} = 0.4523 DS_{rel}$$

2.3.2. Viscosity measurement method

The average molecular weight (M) of the polymers was determined by viscometric measurements using an Ubbelohde Capillary Viscometer. This value was calculated according to the Mark and Houwink-Sakurada equation:

$$[\eta] = KxM^{\alpha}$$

where [η] ($dl.g^{-1}$) is the intrinsic viscosity and K and α are the characteristic constants for the used polymer-solvent systems. For CMC at room temperature (25°C), the values of the constants K and α are $7.3x10^{-3}$ (ml/g) and 0.93, respectively, in 6% NaOH solution [1, 8].

3. Results and discussion

3.1. Hemicellulose extraction

3.1.1. Effect of NaOH concentration on the yield of hemicellulose extraction

The results presented in Fig. 1A indicated that the concentration of NaOH solution had a significant impact on the hemicellulose yield from Vietnamese rice straw waste. The maximum yield of hemicellulose was obtained at 1.5 M NaOH. These results indicated that at a low NaOH concentration (0.75 M), a very low yield of hemicellulose is obtained (about 7.8%). Increasing the concentration of NaOH to 1.0 M and 1.5 M increases the yield of extracted hemicellulose to about 18.3 and 22.4%, respectively. This increase can be attributed to the fact that at high concentrations of NaOH, the ester bond cleavage between ferulic acid and hemicellulose increases. However, with further increase of the NaOH concentration to 2 M and 2.5 M, the yield of hemicellulose reduced to 20.3% and 19.1%, respectively. The reduction in the retained hemicellulose at high alkaline concentration was due to the degradation of hemicellulose [9, 10].

3.1.2. Effect of treatment time on the yield of hemicellulose extraction

The yield of hemicellulose extraction at different extraction times is shown in Fig. 1B. The extraction time was maintained at 60, 90, 120, and 150 min for each extraction. The other extraction conditions, such as the ratio of water to rice straw powder, extraction temperature, and NaOH concentration were maintained at 25:1, 90°C, and 1.5 M, respectively. These results show that the yield of hemicellulose increased with extraction time and reached its highest value of 22.4% at treatment time of 90 min. However, further increases in extraction time to 120 min and 150 min resulted in a slight reduction in hemicellulose yield. This could be due to the partial degradation of hemicellulose [10]. Thus, the optimum time of extraction for the maximum yield of hemicellulose was found to be 90 min.

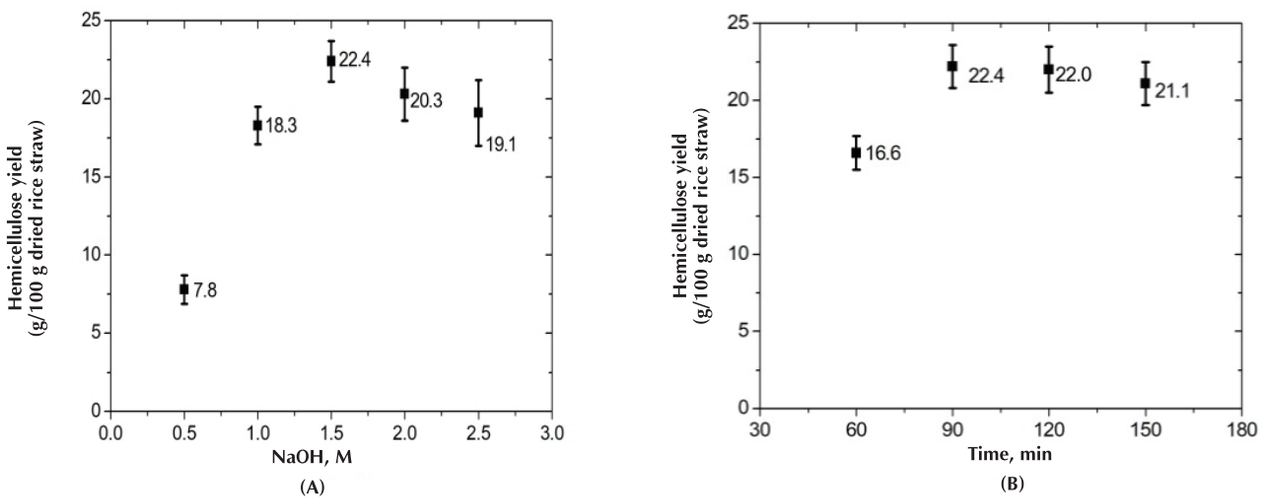

Fig. 1. Effect of (A) NaOH concentration during 90 min and (B) treatment time at 1.5 M NaOH on the yield of hemicellulose extraction.

3.1.3. Characterization of obtained hemicellulose

The obtained hemicellulose was characterized by FTIR spectroscopy and the results are shown in Fig. 2.

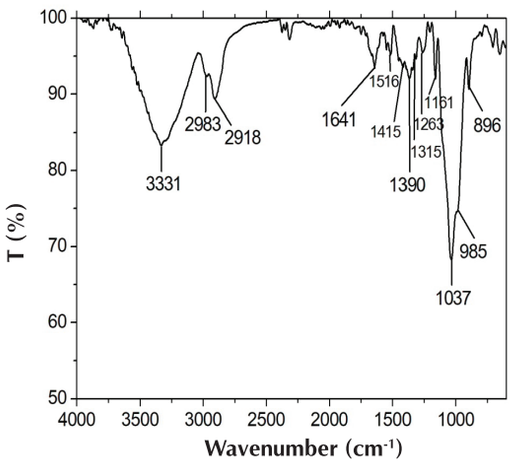

Fig. 2. FTIR spectroscopy of hemicellulose.

The peaks at 1415, 1390, 1315, 1263, 1161, 1037, 985, and 896 cm^{-1} are characteristic peaks of hemicellulose [11, 12]. A predominant absorption at 1037 cm^{-1} is due to the C-O-C stretching of glycosidic linkage of xylans [13]. A low intensity signal at 985 cm^{-1} also indicated the presence of arabinose units [14]. A peak at 896 cm^{-1} can be assigned to the β-(1,4)-glucosidic linkages between the sugar units in the hemicellulose polymers [15, 16]. The peak at 3331 cm^{-1} is represented by the OH stretching mode, while the peak at 2983 cm^{-1} is attributed to the stretching vibration of the CH_2 group. The peaks at 2918 cm^{-1} and 1315 cm^{-1} can be attributed to stretching and deformation vibrations of the C-H group in glucose unit. In the carbonyl stretching region, the peak at 1641 cm^{-1} is characteristic of absorbed water [16]. Furthermore, the peaks at 1390, 1263, and 1161 cm^{-1} represented C-H stretching and O-H or C-O bending vibrations. A very small peak at 1516 cm^{-1} is attributed to the aromatic skeletal vibration, implying the occurrence of a small amount of the lignin. The FTIR spectroscopy results are similar to other authors' results [4, 17].

3.2. Cellulose extraction

The process of cellulose recovery was conducted at various concentrations of HNO_3 solution to determine the optimum treatment conditions. The results are listed in Table 1.

Table 1. Cellulose yield with various HNO_3 concentrations.

Yield of cellulose	HNO_3, (C_M)			
	0.750	*1.00*	*1.25*	*1.50*
H_c (%)	28.50	32.50	30.13	26.20

In this experiment, HNO_3 was used to treat the solid residual part from the hemicellulose extraction process in the previous stage and the yield of cellulose reached the best result at HNO_3 1.00 M. It also can be seen in Table 1 that with the higher levels of HNO_3 concentration (1.25 M and 1.50 M), the cellulose yield decreases gradually. This might be due to the destruction of the cellulose structure at high concentrations of HNO_3 solution. In brief, the highest yield of the cellulose extraction is 32.50% at HNO_3 of 1.00 M.

3.2.1. Characterizations of cellulose by FTIR spectroscopy

The FTIR spectroscopy of cellulose is displayed in Fig. 3. The band at 3313 cm^{-1} can be assigned to the OH stretching mode, while the signal observed at 2918 and 1321 cm^{-1} is attributed to the stretching and deformation vibrations of the C-H groups in the glucose units. The band at 1159 cm^{-1} is assigned to -C-O-C stretch of the β(1,4)-glycosidic linkage is prominent for cellulose samples. The peak at 1105 cm^{-1} is assigned to -C-O group of secondary alcohols and ethers functions existing in the cellulose chain backbone. Lastly, the wavenumber range of about 895-1051 cm^{-1} is associated with the β-(4,1)-glycosidic linkages between the glucose units in cellulose [7]. FTIR spectroscopy of the cellulose extracted from Vietnamese rice straw waste is similar to the result of N.D. Vu, et al. (2017) [4]. In addition, the absence of peaks at 1600-1800 cm^{-1}, normally characterizing the C=O functional groups and the aromatic ring of hemicellulose and lignin molecules [18, 19], proved that hemicellulose and lignin were completely removed. This means that the recovered cellulose is of high purity. This pure cellulose was then used for CMC synthesis.

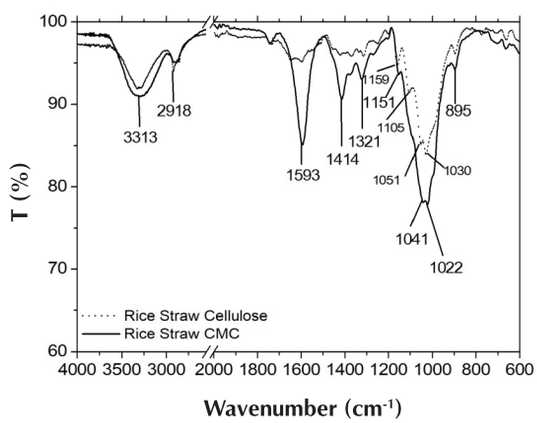

Fig. 3. FTIR spectroscopy of extracted cellulose and CMC.

3.3. CMC synthesis

3.3.1 Effect of NaOH concentration on DS and yield of CMC

NaOH was used as an alkaline reagent to swell the cellulose chains, which provides the ability of substitution by sodium carboxymethyl groups in cellulose units. The DS of the CMC obtained with different concentrations of sodium hydroxide are shown in Table 2.

Table 2. The yield and DS of synthesized CMC with various NaOH concentrations.

	NaOH, %wt			
	15	*20*	*25*	*30*
H_{CMC} (%)	32.1	52.3	63.8	56.6
DS	0.48	0.57	0.70	0.61

As shown in Table 2, the DS of the CMC increased with NaOH concentration and attained the highest DS of 0.70 at a NaOH concentration of 25% (w/v). However, upon further increase in the NaOH concentration, a reduction in DS value was observed. This can be explained by the degradation effect of high concentrations of the alkali reagent on CMC polymer chains. These results are similar to that of B. Xiao, et al. (2001) [17] and S. Sunardi, et al. (2017) [20].

3.3.2. Effect of MCA weight on DS and yield of CMC

The effect of the MCA weight on the DS value was determined by changing the amount of MCA from 2.0 g to 5.0 g. The result is shown in Table 3, where the DS of the CMC increased with an increasing amount of MCA in a range of 2.0-4.0 g and then decreased slightly with further increase of the MCA amount. The highest DS value was observed at an MCA weight of 4.0 g. The reason behind this observation is that an undesired side reaction occurred that dominated CMC production with the greater availability of the MCA molecules. This range of DS value (from 0.48-0.70) is similar to another author's report [7] for bagasse waste. Table 3 also shows that the trend in the change of CMC yield is similar to that of the DS.

Table 3. The yield and DS of CMC synthesized with various amount of MCA.

	Amount of MCA (g)			
	2.0	*3.0*	*4.0*	*5.0*
H_{CMC} (%)	43.7	63.8	75.0	72.2
DS	0.50	0.61	0.70	0.67

The optimum condition for carboxymethylation was 5 g cellulose, 4.0 g chloroacetic acid, and 15 ml of 25% w/v NaOH solution. The obtained CMC had a DS of 0.70.

3.3.3. Characterizations of CMC

The FTIR spectroscopy of the synthesized CMC is shown in Fig. 3. The broad absorption peak at around 3313 cm^{-1} in the spectra indicates the free OH stretching vibration as well as inter and intramolecular hydrogen bonds in the cellulose molecules. The band at 2918 cm^{-1} is attributed to the stretching vibration of the C-H groups. The bands at 1041 cm^{-1} and 1022 cm^{-1} are relevant to the β-(1,4)-glycosidic linkages between the glucose units in cellulose [7, 18]. The presence of strong absorption bands at 1593 and 1414 cm^{-1} are attributed to C=O stretching, which confirms the presence of the -COO and -COONa groups, indicating the successful etherification of cellulose. This peak does not exist in the FTIR spectroscopy of cellulose (Fig. 2). The above analysis results are similar to those of earlier publications of B. Xiao, et al. (2001) [17] for bagasse waste and S. Sunardi, et al. (2017) [20] for purun tikus.

The average molecular weight (M) is an important parameter of CMC. It affects swelling, the solubility of CMC in the water, its structure, and other properties. Fig. 4 displays the Mark and Houwink-Sakurada plots for synthesized CMC in 6% NaOH at 25°C.

Extrapolation of reduced viscosity [η_{red}] to zero concentration provides the intrinsic viscosity, [η], such that:

$$[\eta] = \lim_{C\to 0}\frac{\eta_{sp}}{C} = \lim_{C\to 0}\eta_{red}$$

where $\eta_r = t/t_0$, $\eta_{sp} = \eta_r - 1$, and t and t_0 are the flow time for the CMC solution and pure solvent, respectively.

The intrinsic viscosity as functions of average molecular weight are usually represented by the widely used Mark-Houwink-Sakurada empirical equation:

$[\eta] = KxM^{\alpha}$

The Mark-Houwink constant, K, and α for CMC were $7.3x10^{-3}$ ml/g and 0.93, respectively [8].

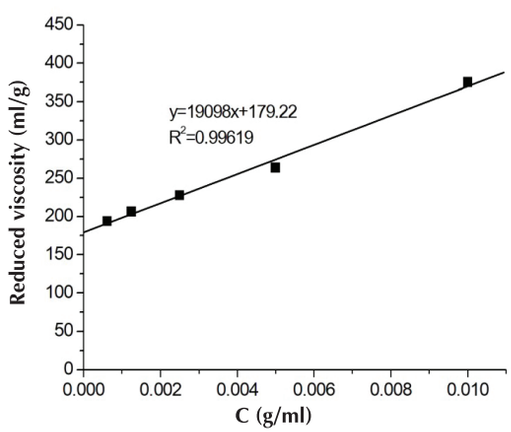

Fig. 4. Mark and Houwink-Sakurada plot for CMC in 0.1 M NaOH at 25°C.

The [η] values can be estimated from the intercept of the plot, where [η]=179.22 (ml/g). The average molecular weight of CMC is 52.535±251 g/mol.

Conclusions

Hemicellulose was successfully extracted from Vietnamese rice straw waste with a maximum hemicellulose extraction yield of 22.4% with 1.5 M NaOH for 90 min at 90°C. The obtained hemicellulose was confirmed by FTIR spectra. Cellulose was successfully recovered from Vietnamese rice straw waste with yield of 32.5% at 1 M HNO_3 for 90 min at 90°C. CMC has been obtained by etherifying cellulose with monochloroacetic acid. The optimal condition for carboxymethylation was 5 g cellulose, 4.0 g chloroacetic acid, and 15 ml of 25% w/v NaOH solution. The optimised CMC products have a DS of 0.70. The chemical structure of the CMC was confirmed by FTIR spectra, which indicated the C=O group at 1593 cm^{-1}. These results show that the simultaneous separation of cellulose and hemicellulose from Vietnamese rice straw waste has great potential and feasibility from both economic and environmental viewpoints.

CRedit author statements

Mai Thi Tuyet Phan, Trang Thu La, Thu Hong Anh Ngo: Conceptualization, Methodology, Data curation, Formal analysis, Writing - Review & Editing.

ACKNOWLEDGEMENTS

This research is funded by Hanoi Department of Sciences and Technology (Grant number 01C-03/04-2020-03).

COMPETING INTERESTS

The authors declare that there is no conflict of interest regarding the publication of this article.

REFERENCES

[1] S. Zhang, F. Li, J. Yu, et al. (2009), "Disolved state and viscosity properties of cellulose in a NaOHcomplex solvent", *Cellul. Chem. Technol.*, **43(7-8)**, pp.241-249.

[2] G. Gou, W. Wei, M. Jiang, et al. (2018), "Environmentally friendly method for the separation of cellulose from steam-exploded rice straw and its high-value application", *Pulp and Paper Processing*, DOI: 10.5772/intechopen.79014.

[3] R.C. Sun, J. Tomkinson, P.L. Ma, et al. (2000), "Comparative study of hemicelluloses from rice straw by alkali and hydrogen peroxide treatments", *Carbohydr. Polym.*, **42(2)**, pp.111-122, DOI: 10.1016/S0144-8617(99)00136-8.

[4] N.D. Vu, H.T. Tran, N.D. Bui, et al. (2017), "Lignin and cellulose extraction from Vietnam's rice straw using ultrasound assisted alkaline treatment method", *International Journal of Polymer Science*, DOI: 10.1155/2017/1063695.

[5] G. Fan, K. Luo, Y. Wang, et al. (2019), "Preparation of convertible cellulose from rice straw using combined organosolv fractionation and alkaline bleaching", *IOP Conf. Series: Earth and Environmental Science*, **237**, DOI: 10.1088/1755-1315/237/5/052053.

[6] T.T.M. Phan, T.S. Ngo (2020), "Pectin and cellulose extraction from passion fruit peel waste", *Vietnam Journal of Science, Technology and Engineering*, **62(1)**, pp.32-37, DOI: 10.31276/VJSTE.62(1).32-37.

[7] K.M. Koh (2013), *Preparation and Characterization of Carboxymethyl Cellulose from Sugarcane Bagasse*, Universiti TunkuAbdul Rahman, 110pp.

[8] M.J. Nayef (2006), *Structure Rheology of Carboxymethyl Cellulose (CMC)*, Nahrain University, 106pp.

[9] I. Egües, C. Sanchez, I. Mondragon, et al. (2012), "Effectof alkaline and autohydrolysis processes on the purity of obtained hemicelluloses from corn stalks", *Bioresour. Technol.*, **103(1)**, pp.239-248, DOI: 10.1016/j.biortech.2011.09.139.

[10] X. Peng, S. Nie, X. Li, et al. (2019), "Characteristics of the water and alkali-soluble hemicellulose fractionated by sequential acidification and graded ethanol from sweet maize stems", *Molecules*, **24**, pp.212-221, DOI: 10.3390/molecules24010212.

[11] N.H. Zulyadi, S.H. Saleh, S.H. Sarijo (2016), "Fractionation of hemicellulose from rice straw by alkaline extraction and ethanol precipitation", *Malaysi. J. Analyti. Sci.*, **20(2)**, pp.329-334, DOI: 10.17576/mjas-2016-2002-15.

[12] R. Sun, J.M. Lawther, W.B. Banks (1996), "Fractional and structural characterization of wheat straw hemicelluloses", *Carbohydr. Polym.*, **29(4)**, pp.325-331, DOI: 10.1016/S0144-8617(96)00018-5.

[13] C. Moine, P. Krausz, V. Chaleix, et al. (2007), "Structural characterization and cytotoxic properties of a 4-*O*-methylglucuronoxylan from *Castanea sativa*", *J. Nat. Prod.*, **70**, pp.60-66, DOI: 10.1021/np060354p.

[14] A. Ebringerova, Z. Hromadkova, J. Alfoldi, et al. (1992), "Structure and solution properties of corn cob heteroxylans", *Carbohydr. Polym.*, **19**, pp.99-105, DOI: 10.1016/0144-8617(92)90119-B.

[15] M.A.K. Azad, F. Wang, H.R. Kim (2015), "Identification of a novel sugar compound from korean pine seeds", *Food Sci. Biotechnol.*, **24**, pp.2011-2015, DOI: 10.1007/s10068-015-0265-y.

[16] H. Cheng, H. Zhan, S. Fu, et al. (2011), "Alkali extraction of hemicellulose from depithed corn stover and effects on soda-AQ pulping", *BioResources*, **11(1)**, pp.196-206, DOI: 10.15376/biores.6.1.196-206.

[17] B. Xiao, X.F. Sun, R. Sun (2001), "Chemical, structural, and thermal characterizations of alkali-soluble lignins and hemicelluloses, and cellulose from maize stems, rye straw, and rice straw", *Polym. Degrad. Stab.*, **74(2)**, pp.307-319, DOI: 10.1016/S0141-3910(01)00163-X.

[18] J. Chumee, D. Seeburin (2014), "Cellulose extraction from Pomelo Peel: Synthesis of carboxymethyl cellulose", *Inter. J. Mater. Metallurgical Eng.*, **8(5)**, pp.435-437.

[19] W. Xu, N. Reddy, Y. Yang (2009), "Extraction, characterization and potential applications of cellulose in corn kernels and Distillers' dried grains with solubles (DDGS)", *Carbohydr. Polym.*, **76**, pp.521- 527, DOI: 10.1016/j.carbpol.2008.11.017.

[20] S. Sunardi, M.F. Nina, B.J. Ahmad (2017), "Preparation of carboxymethyl cellulose produced from purun tikus (*Eleocharis dulcis*)", *AIP Conference Proceedings*, DOI: 10.1063/1.499509.

DOI: 10.31276/VJSTE.63(1).21-29

Composition of ground granulated blast-furnace slag and fly ash-based geopolymer activated by sodium silicate and sodium hydroxide solution: Multi-response optimization using Response Surface Methodology

Hoang-Quan Dinh[1*], Thanh-Bang Nguyen[2]

[1]Thuyloi University, 175 Tay Son Street, Trung Liet Ward, Dong Da District, Hanoi, Vietnam
[2]Vietnam Academy for Water Resources, 171 Tay Son Street, Trung Liet Ward, Dong Da District, Hanoi, Vietnam

Received 13 August 2020; revised 5 November 2020; accepted 10 November 2020

Abstract:

Geopolymers are a class of new binder manufactured by activating aluminosilicate source materials in a highly alkaline medium. This binder is considered "environmentally friendly" due to the recycling of industrial waste sources such as fly ash and blast furnace slag. However, in order to be widely used, this binder has to ensure both quality and economic efficiency. This paper focuses on the optimization of the composition of ground granulated blast-furnace slag and fly ash-based geopolymers activated by sodium silicate and sodium hydroxide solutions. Statistical models are developed to predict the compressive strength and cost of 1 ton of binder using Response Surface Methodology (RSM). In this regard, the effects of three principal variables (%Na_2O, M_s and %GGBS) were investigated in which: %Na_2O - mass ratio of Na_2O in the alkali-activated solution and total solids; M_s - mass ratio of SiO_2 and Na_2O in the activated solution; %GGBS - mass ratio of ground granulated blast-furnace slag (GGBS), and total binder. Quadratic models were proposed to correlate the independent variables for the 28-d compressive strength and cost of 1 ton of binder by using the Central Composite Design (CCD) method. The study reveals that M_s has a minor effect on the strength of mortar in comparison with %Na_2O and %GGBS. The optimized mixture proportions were assessed using the multi-objective optimization technique. The optimal values found were %Na_2O=5.18%, M_s=1.16, and %GGBS=50%, with the goals of maximum compressive strength, the largest amount of fly ash, and reasonable cost for one ton of binder. The experimental results show that the compressive strength of the samples ranged between 62.95-63.54 MPa and were consistent with the optimized results (the variation between the predicted and the experimental results was obtained less than 5%).

Keywords: **alkali-activated slag, fly ash, geopolymer, GGBS, optimization, Response Surface Methodology.**

Classification number: **2.3**

1. Introduction

Alkali-activated binders were first investigated in the 1940s by Purdon's research [1] with the use of GGBS activated with NaOH solution. In 1991, Davidovits developed and patented binders obtained from the alkaline activation of metakaolin named "Geopolymer" [2]. The chemistry of geopolymers are different from Portland cement (OPC). It is well known that OPC is a fine powder obtained by grinding a mixture of clinker, which is made by heating limestone, clay, and other materials such as fly ash with a few percent of gypsum ($CaSO_4.2H_2O$) or anhydrite ($CaSO_4$) to a high temperature (approximately 1450°C). The main binding product, which is derived from the hydration of clinker with water, is calcium silicate hydrate gels known as "C-S-H" gels. The formation of C-S-H, which is an apparently amorphous phase of variable composition, is principally responsible for strength development and matrix formation in Portland cement.

Unlike Portland cement, an alkali-activated binder can be synthesized by exposure of aluminosilicate materials to concentrated alkaline hydroxide (NaOH, KOH) and/or alkali silicate (Na_2SiO_3) solutions, which are then curing at room temperature or slightly elevated temperature [2]. Source materials for alkali-activated binder synthesis should be rich in silicon and aluminium. These could be natural minerals such as kaolinite or metakaolin or one with an empirical

*Corresponding author: Email: dinhhoangquan@tlu.edu.vn

formula containing Si, Al, and oxygen. Alternatively, by-product materials such as fly ash, silica fume, slag, rice husk ash, and red mud could also be used as source materials. The choice of precursor for making an alkali-activated binder depends on factors such as availability, cost, type of application, and specific demand of end users.

According to D.M. Roy (1999) [3] and A. Palomo, et al. (1999) [4], source materials for alkali-activated binder synthesis can be classed into two groups:

- 1st group: aluminosilicate materials such as metakaolin and class F fly ash produce N-A-S-H gel, also called poly(sialates) gel or "geopolymer" when activated by an alkaline solution.

- 2nd group: alkali-earth enriched aluminosilicate materials such as blast furnace slag and class C fly ash produce C-(A)-S-H gel like hydrated calcium silicate gel with high amounts of tetracoordinated Al in its structure, as well as Na^+ ions in the interlayer spaces when activated by an alkaline solution.

Several authors suggested that blending these two groups may produce both N-A-S-H and C-S-H gels in the matrix. F. Puertas, et al. (2011) [5] studied the hydration products of a geopolymer paste made by a mixture of 50% fly ash and 50% slag activated with 10 M NaOH and cured at 25°C using XRD, FTIR, and MAS-NMR analysis. They found that the main reaction product in these pastes is a hydrated calcium silicate, like C-S-H gel, with high amounts of tetracoordinated Al in its structure as well as Na^+ ions in the interlayer spaces. Z. Yunsheng, et al. (2007) [6] reported that a geopolymer synthesized by 50% metakaolin and 50% slag activated with water glass at 20°C had both N-A-S-H and C-(A)-S-H gels forming within its matrix.

Previous studies on alkali-activated slag/fly ash binders show that their mechanical properties are influenced by many factors such as precursor materials, type, dosage of alkali-activated solution, and curing conditions [7-9]. However, experimental design methods in these studies stop at univariate analysis or combine simple multivariate with orthogonal design to determine the optimal value through a limited number of experiments. Response Surface Methodology (RSM) allows one to determine the optimal condition of multiple factors accurately and takes into account the effects of these factors and their interactions with one or more response variables with reliability. Some authors have used RSM to optimize the composition of alkali-activated binders. Research by C. Pinheiro, et al. (2020) [10] focused on predicting equations for compressive and flexural strength at 7 d and 28 d based on three input variables (activator index, precursor index and sodium hydroxide concentration). The ideal composition obtained for the alkaline cement was a mixture constituted by 75% sodium silicate and 25% sodium hydroxide, 50% slag and 50% fly ash, and a sodium hydroxide concentration equal 10 M. This mixture achieved 8.70 MPa of flexural strength and 44.25 MPa of compressive strength. Besides, other authors have used a two-input-variable model in their research. For example, B.S. Mohammed, et al. (2019) [11] focused on the mass ratio of GGBS and total binder and the mass ratio of sodium metasilicate anhydrous and total solid. In addition, J.F. Rivera, el al. (2019) [12] studied SiO_2/Al_2O_3 and Na_2O/SiO_2 molar ratios with a fixed ratio of fly ash and slag. These studies selected compressive strength as the target function to optimize the binder composition. However, a product requires not only good features but also a reasonable cost. Therefore, using cost for one ton of binder as an objective function is necessary.

Additionally, most previous studies have selected input parameters when preparing the alkali solution as the mass ratio of sodium silicate to sodium hydroxide (SS/SH=1.5/1-2.5/1) and the molarity of sodium hydroxide solution (8-14 M). These studies all use sodium silicate liquid with a silica modulus (SiO_2/Na_2O) of 2.0 while the water glass produced in Vietnam and some other countries has silica moduli ranging from 1.5 to 2.7. Therefore, preparation in this manner is detrimental to practical application because the quality of the concrete can be very different with different types of water glass.

In this study, by using RSM, statistical models are developed to predict the compressive strength and cost for one ton of binder. For better quantification when preparing the alkali solution, this study selected input parameters $\%Na_2O$ and M_s, in which: $\%Na_2O$ - mass ratio of Na_2O in the alkali-activated solution and total solids (FA, GGBS and solids in alkali solution); M_s - mass ratio of SiO_2 and Na_2O in the activated solution. Therefore, liquid sodium silicate, sodium hydroxide, and added water were blended in different proportions providing the required M_s and $\%Na_2O$. Additionally, the precursor index was characterized by the input parameter of %GGBS - mass ratio of GGBS and total binder (FA, GGBS). The effects of these principal variables ($\%Na_2O$, M_s and %GGBS) and their interactions were investigated. Thus, the optimal compositions of ground granulated blast-furnace slag and fly ash-based geopolymers (AAFS) were determined through optimization analysis.

2. Materials and experimental program

2.1. Materials

2.1.1. Fly ash

Most of the thermal power plants in Vietnam uses poor quality coal, resulting from the high loss on ignition

(LOI) fly ash products (LOI>6%). Therefore, research on the use of FA with a high LOI content (this FA is not allowed to be used as mineral additives for cement) will bring great economic benefits. In this inquiry, 3 types of class F fly ash, according to the Vietnamese national code TCVN 10302:2014 [13], were used as the main binder. The chemical constituents were identified by X-ray fluorescence (XRF) and displayed in Table 1. These FAs with different LOI were obtained from the Hai Phong (HP) Thermal Power Plant (LOI=11.32%), Pha Lai (PL) Thermal Power Plant (LOI=10.93%), and Formosa (FO) Thermal Power Plant (LOI=1.83%). These three FA types were selected to evaluate the effect of LOI on compressive strength.

2.1.2. Ground granulated blast-furnace slag

Ground granulated blast-furnace slag was used as the secondary binder in this study. GGBS was obtained from Hoa Phat Steel Joint Stock Company with finesses and chemical constituents displayed in Table 1. The partial replacement of FA with GGBS was expected to produce high strength samples under room temperature curing condition.

Table 1. Chemical composition of FA and GGBS (percentage by weight).

Chemical oxide	FA from HP	FA from PL	FA from FO	GGBS
SiO_2	49.31	47.45	53.48	36.15
Al_2O_3	21.68	20.55	28.84	10.59
Fe_2O_3	8.76	5.17	4.73	0.35
CaO	1.27	8.3	4.12	39.13
MgO	1.62	1.6	2.31	7.59
SO_3	0.42	0.81	0.32	1.47
K_2O	4.36	3.84	1.25	0.95
Na_2O	0.13	0.24	0.85	0.2
TiO_2	0.98	0.76	1.8	0.54
MnO	0.08	0.05	0.04	2.25
P_2O_5	0.13	0.14	0.26	<0.01
LOI	11.32	10.93	1.83	-
Specific gravity (g/cm^3)	2.24	2.24	2.15	2.85
Blaine fineness (cm^2/g)	2935	2863	3617	3503

2.1.3. Alkali-activated solution

Alkali-activated solution includes sodium hydroxide (NaOH) in powder form of 99% purity and sodium silicate as a solution (Na_2SiO_3), or called waterglass, with 6.7% SiO_2, 9.84% Na_2O and 63.46% H_2O by weight. Liquid sodium silicate, sodium hydroxide, and added water were blended in different proportions providing the required M_s and $\%Na_2O$.

2.2. Experimental design

2.2.1. Input variables

The composition of alkali-activated binder includes FA, GGBS, and an alkali solution. The water-to-solids ratio and the sand-to-solids ratio were constant at 0.35 and 3.0 respectively. Therefore, the input parameters were selected as $\%Na_2O$, M_s, and %GGBS. The surveyed domain, coded value, and the real value are shown in Table 2.

Table 2. Surveyed domain, the coded value and the real value of input variables.

Input variables	- Alpha	Lower limit	Center point	Higher limit	+ Alpha
	(-1.6818)	*(-1)*	*(0)*	*(+1)*	*(+1.6818)*
$\%Na_2O$	1.64%	3%	5%	7%	8.36%
M_s	0.83	1	1.25	1.5	1.67
%GGBS	7.96%	25%	50%	75%	92.04%

2.2.2. Experimental design

Design Expert software has been used for the experimental design. Based on the Central Composite Design (CCD) for three independent variables, the mix design formulations of the alkali-activated pastes were randomly selected. The results of this work are the 28-d compressive strength and cost for one ton of binder. The software developed $(2^3+2x3+6)=20$ mixtures for these responses with five randomized duplications. The five duplications are the central points used by the software to improve the experiment's accuracy against any likely errors. Thus, for three types of fly ash (HP, PL and FO), the number of mixtures is 3x20=60. The composition of mortar specimens are shown in Table 3.

2.2.3. Mixing procedure, curing and testing of specimens:

The mixing and preparation of the specimens used to investigate strength development was done according to the European code EN196-1 [14] with the exception that the water-to-binder ratio (w/b) was not 0.50. A water/solid ratio (w/s) of 0.35 was used instead of the w/b ratio when preparing the geopolymer mortars to give more consistent workability due to the high quantity of solid (Na_2O and SiO_2) contained in the alkaline activator. According to EN 196-1, 40x40x160 mm prism specimens were cast. The test apparatus and measurement of the flow diameter is shown in Fig. 1. After 24 h, hardened mortars were removed from the moulds and cured in water until the test period. At 28-d age, three sets of the specimens were used to conduct the compressive strength test. Each compressive strength, R_{28}, is the average of six experimental results.

Fig. 1. Flow test apparatus and measurement of the flow diameter [15].

3. Results and discussion

3.1. Statistical models of 28-d compressive strength and the cost for 1 ton of binder

The effects of the three input variables (%Na_2O, M_s, and %GGBS) and their interactions with the responses (the 28-d compressive strength and the cost for one ton of binder) were conducted by a quadratic function as follows:

$$\sum_{i=0}^{k} \beta_i X_i + \sum_{i=0}^{k} \beta_{ii} {X_i}^2 + \sum_{i,j=0}^{k} \beta_{ij} X_i X_j$$

where Y represents the response value, X represents the input variable, β_o is the interception coefficient, β_i is the coefficient of the linear effect, β_{ii} is the coefficient of the quadratic effect, and β_{ij} is the coefficient of the interaction effect.

The software Design Expert version 11 was used for multiple regression analysis of the obtained experimental data. An F-test was employed to evaluate the statistical significance of the quadratic polynomial. The multiple coefficients of correlation, R, and the determination coefficient of correlation, R^2, were calculated to evaluate the performance of the regression equation.

The mixture proportions and the test results of the 60 prepared mixtures to derive the CCD models are summarized in Table 3.

Table 3. Composition of mortar specimens and the experimental results.

Run	Input variables			Composition of mortar specimens (gam)						28-d Compressive strength (MPa)			Cost for 1 ton of binder
	%Na_2O	*M_s*	*%GGBS*	*Sand*	*GGBS*	*FA*	*Na_2SiO_3 (liquid)*	*NaOH (powder)*	*H_2O (extra)*	*HP-R_{28}*	*PL-R_{28}*	*FO-R_{28}*	
1	3%	1	75%	1350	317.3	105.8	51.9	11	124	28.1	30.5	36.1	$49.86
2	8.36%	1.25	50%	1350	182.7	182.7	180.9	26.2	40.9	49.4	46.3	51.2	$112.58
3	7%	1	75%	1350	290.3	96.8	121.2	25.7	79.4	62.8	64.1	65.2	$93.43
4	5%	1.67	50%	1350	195	195	144.5	11.2	64.2	55.5	55.8	52.0	$80.47
5	1.64%	1.25	50%	1350	216.7	216.7	35.5	5.1	134.7	0.0	0.0	0.0	$32.45
6	5%	1.25	50%	1350	199.7	199.7	108.2	15.7	87.6	56.8	62.1	60.2	$72.52
7	5%	1.25	92.04%	1350	367.6	31.8	108.2	15.7	87.6	59.1	68.3	63.5	$78.93
8	5%	1.25	7.96%	1350	31.8	367.6	108.2	15.7	87.6	5.9	14.3	12.9	$66.10
9	5%	0.83	50%	1350	204.4	204.4	71.8	20.2	111	58.5	55.8	46.2	$64.56
10	3%	1	25%	1350	105.8	317.3	51.9	11	124	6.5	9.8	0.0	$41.79
11	5%	1.25	50%	1350	199.7	199.7	108.2	15.7	87.6	59.4	58.9	56.8	$72.52
12	5%	1.25	50%	1350	199.7	199.7	108.2	15.7	87.6	62.1	62.5	60.7	$72.52
13	7%	1.5	25%	1350	92.8	278.4	181.7	18.2	40.4	29.9	40.3	36.0	$99.45
14	5%	1.25	50%	1350	199.7	199.7	108.2	15.7	87.6	62.1	61.6	59.8	$72.52
15	3%	1.5	75%	1350	312.2	104.1	77.9	7.8	107.3	25.4	37.4	32.1	$55.48
16	7%	1	25%	1350	96.8	290.3	121.2	25.7	79.4	28.7	36.1	32.0	$86.04
17	7%	1.5	75%	1350	278.4	92.8	181.7	18.2	40.4	63.0	70.4	62.3	$106.54
18	5%	1.25	50%	1350	199.7	199.7	108.2	15.7	87.6	58.7	62.2	59.8	$72.52
19	5%	1.25	50%	1350	199.7	199.7	108.2	15.7	87.6	56.6	60.3	60.2	$72.52
20	3%	1.5	25%	1350	104.1	312.2	77.9	7.8	107.3	1.5	1.5	1.3	$47.53

The ANOVA response models for 28-d compressive strength of HP, PL and FO specimens are shown in Table 4-6, respectively. The model's F-values of 75.1, 188.8, and 188.0 for HP, PL, and FO mixtures, respectively, show that the models are significant. There is only a 0.01% chance that an F-value this large could occur due to noise. P-values less than 0.0500 indicate the model terms are significant and those greater than 0.1000 indicate the model terms are not significant. The resulting p-values in Tables 4-6 show that factors like %Na_2O and %GGBS were important at a confidence level of 95% and thus were accepted as crucial parameters on the test results. However, M_s has a minor effect on the 28-d compressive strength in comparison with %Na_2O and %GGBS. This result is consistent with the study of J.K. Prusty, et al. (2020) [16]. The model's quality could be assessed on the basis of lack of fit, for example, the smaller lack of fit value indicates the worthiness of the models. The lack of fit for the F-value was 4.05, 4.92, and 4.83 in the models of HP, PL, and FO mixtures, respectively, implies that there was 7.54, 5.25, and 5.44% chance that the lack of fit for an F-value this large could occur due to noise. The lack of fit for the p-value in all models was larger than 0.05, which indicates "not significant" and thus implies good fitness for all the model's responses.

Table 4. ANOVA response models for 28-d compressive strength of HP specimens.

Source	Sum of squares	Degrees of freedom	Mean Square	F-value	p-value	Remark
Model	10102.5	9	1122.50	75.11	<0.0001	significant
A-%Na_2O	2806.7	1	2806.65	187.79	<0.0001	
B-Ms	9.4	1	9.43	0.63	0.4456	
C-%BFS	3302.5	1	3302.49	220.97	<0.0001	
AB	0.2	1	0.21	0.01	0.9077	
AC	58.9	1	58.86	3.94	0.0753	
BC	10.4	1	10.35	0.69	0.4247	
A^2	2627.3	1	2627.27	175.79	<0.0001	
B^2	62.5	1	62.49	4.18	0.0681	
C^2	1663.7	1	1663.66	111.32	<0.0001	
Residual	149.5	10	14.95			
Lack of fit	119.9	5	23.97	4.05	0.0754	not significant
Pure error	29.6	5	5.92			
Cor total*	10252.0	19				

*Cor total: totals of all information corrected for the mean.

Table 5. ANOVA response models for 28-d compressive strength of PL specimens.

Source	Sum of squares	Degrees of freedom	Mean square	F-value	p-value	Remark
Model	9795.5	9	1088.39	188.80	<0.0001	significant
A-%Na_2O	2715.3	1	2715.27	471.01	<0.0001	
B-Ms	6.1	1	6.06	1.05	0.3293	
C-%BFS	3625.6	1	3625.56	628.92	<0.0001	
AB	37.4	1	37.41	6.49	0.0290	
AC	0.3	1	0.28	0.05	0.8296	
BC	17.7	1	17.70	3.07	0.1103	
A^2	2829.2	1	2829.22	490.78	<0.0001	
B^2	87.8	1	87.77	15.23	0.0030	
C^2	831.2	1	831.17	144.18	<0.0001	
Residual	57.7	10	5.76			
Lack of fit	47.9	5	9.58	4.92	0.0525	not significant
Pure error	9.7	5	1.95			
Cor total	9853.1	19				

Table 6. ANOVA response models for 28-d compressive strength of FO specimens.

Source	Sum of squares	Degrees of freedom	Mean square	F-value	p-value	Remark
Model	9719.0	9	1079.89	188.02	<0.0001	significant
A-%Na_2O	3306.7	1	3306.73	575.75	<0.0001	
B-Ms	4.9	1	4.87	0.85	0.3789	
C-%BFS	3263.0	1	3263.03	568.14	<0.0001	
AB	18.6	1	18.60	3.24	0.1021	
AC	6.8	1	6.84	1.19	0.3006	
BC	1.8	1	1.80	0.31	0.5874	
A^2	2319.0	1	2319.02	403.78	<0.0001	
B^2	276.1	1	276.07	48.07	<0.0001	
C^2	976.3	1	976.25	169.98	<0.0001	
Residual	57.4	10	5.74			
Lack of fit	47.6	5	9.52	4.83	0.0544	not significant
Pure error	9.9	5	1.97			
Cor total	9776.4	19				

Table 7 shows the model for the cost of 1 ton of binder. The model's F-value of 1505.28 implies the model is significant. The resulting p-value shows that all factors were important. However, %Na_2O has a significant effect on the cost for one ton of binder in comparison with M_s and %GGBS.

Table 7. ANOVA response models for the cost of 1 ton of binder.

Source	Sum of squares	Degrees of freedom	Mean square	F-value	p-value	Remark
Model	8664.81	3	2888.27	1505.28	<0.0001	significant
A-%Na_2O	8150.72	1	8150.72	4247.90	<0.0001	
B-Ms	327.55	1	327.55	170.71	<0.0001	
C-%BFS	186.53	1	186.53	97.22	<0.0001	
Residual	30.70	16	1.92			
Lack of fit	30.70	11	2.79			
Pure error	0.0000	5	0.0000			
Cor total	8695.51	19				

The cost for one ton of binder and the 28-d compressive strength of GGBS-FA geopolymer mortar for the HP, PL, and FO mixtures can be predicted using the analysis of variance (ANOVA). The relationships and influence between the variables (%Na_2O, M_s and %GGBS) and their responses were achieved through variance analysis and are presented in Eqs. (1), (2), (3), and (4).

$$R_{28}\text{ of HP} = -155.763 + 37.8043 * \%Na_2O + 69.2449 * M_s + 1.84237 * \%GGBS + 0.325 * \%Na_2O * M_s + 0.05425 * \%Na_2O * \%GGBS + 0.182 * M_s * \%GGBS - 3.37552 * \%Na_2O^2 - 33.3171 * M_s^2 - 0.017191 * \%GGBS^2 \quad (1)$$

$$R_{28}\text{ of PL} = -146.623 + 36.485 * \%Na_2O + 67.8557 * M_s + 1.55059 * \%GGBS + 4.325 * \%Na_2O * M_s + 0.00375 * \%Na_2O * \%GGBS + 0.238 * M_s * \%GGBS - 3.50285 * \%Na_2O^2 - 39.4861 * M_s^2 - 0.0121511 * \%GGBS^2 \quad (2)$$

$$R_{28}\text{ of FO} = -253.679 + 44.231 * \%Na_2O + 188.911 * M_s + 1.93268 * \%GGBS - 3.05 * \%Na_2O * M_s - 0.0185 * \%Na_2O * \%GGBS + 0.076 * M_s * \%GGBS - 3.17133 * \%Na_2O^2 - 70.0289 * M_s^2 - 0.0131689 * \%GGBS^2 \quad (3)$$

$$\text{Cost of 1 ton of binder} = -20.7913 + 12.215 * \%Na_2O + 19.5896 * M_s + 0.14783 * \%GGBS \quad (4)$$

It should be noted that Eq. (4) was established based on the unit price of material as shown in Table 8. Therefore, Eq. (4) is of reference only because the unit price of the material can change over time, for example, by taxes or transportation distance.

Table 8. Unit price of material.

Materials	GGBS	FA	Sodium silicate liquid	Sodium hydroxide
Unit price* (USD per ton)	21.49	4.30	171.90	567.25

Unit price includes taxes and transportation costs.

Table 9 shows high R^2 values of 0.985, 0.994, and 0.964 for the 28-d compressive strength models of the HP, PL, and FO mixtures, respectively, which indicate a good measure of the correspondence between the predicted and experimental results. The predicted R^2 values are in reasonable agreement with the adjusted R^2 as the differences are less than 0.2. All models have sufficient precision values of more than 4, indicating that the models could be used to navigate the design space. The predicted vs actual results are plotted in Fig. 2 and show that the predicted response model was precise. The points were fitted smoothly to a straight line, which indicates a good relationship between experimental and predicted outcomes in the established models.

Table 9. Validation properties of response model.

Response	28-d compressive strength			Cost for 1 ton of binder
	for HP mixture	*for PL mixture*	*for FO mixture*	
Standard deviation	3.87	2.4	2.4	1.39
Mean	41.5	44.91	42.41	72.16
C.V. %	9.32	5.35	5.65	1.92
R^2	0.9854	0.9941	0.9941	0.9965
Adjusted R^2	0.9723	0.9889	0.9888	0.9958
Predicted R^2	0.9074	0.9583	0.9617	0.9934
Adequate precision	25.2553	43.6859	39.7157	132.6476

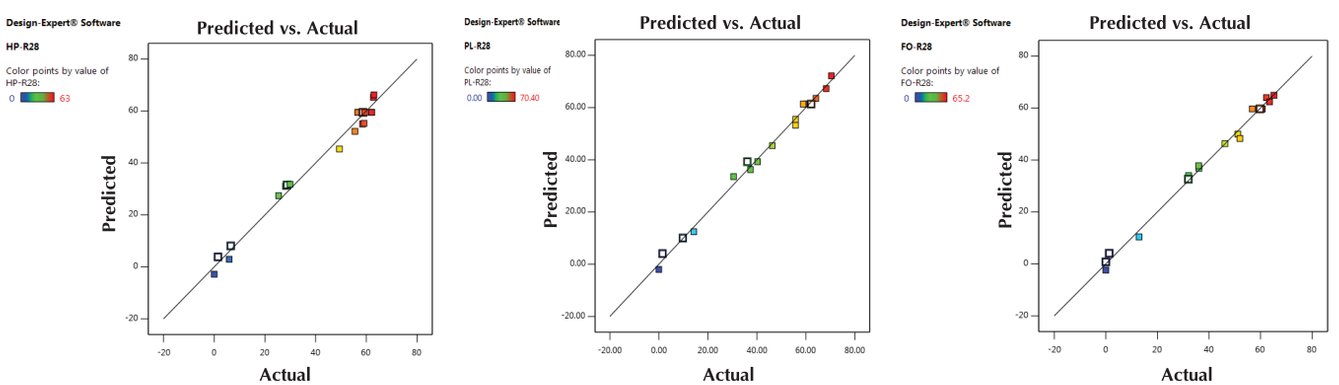

(A) (B) (C)

Fig. 2. Predicted vs actual plot of 28-d compressive strength models for the (A) HP mixture, (B) PL mixture, and (C) FO mixture - effect of %GGBS and %Na_2O.

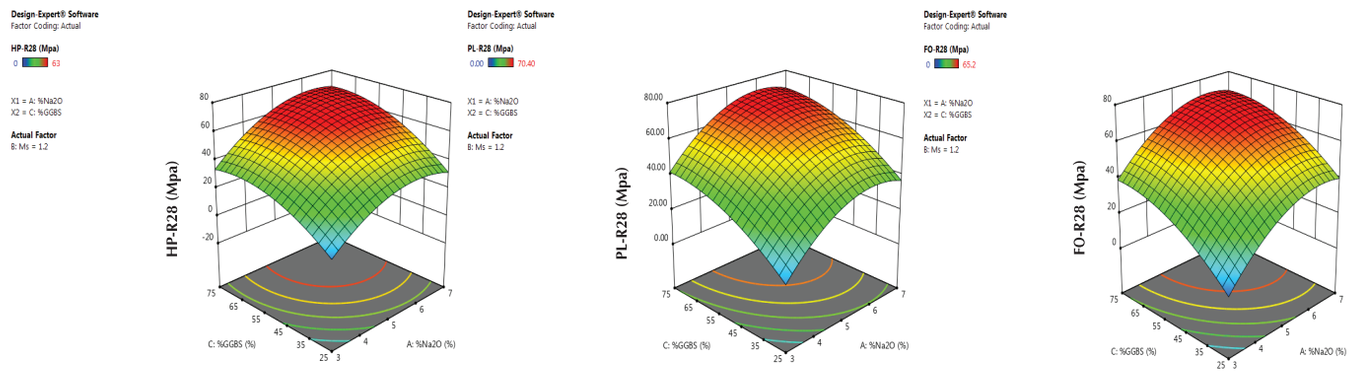

(A) (B) (C)

Fig. 3. 3D surface plots of 28-d compressive strength models for the (A) HP mixture, (B) PL mixture, and (C) FO mixture - effect of %GGBS and %Na_2O.

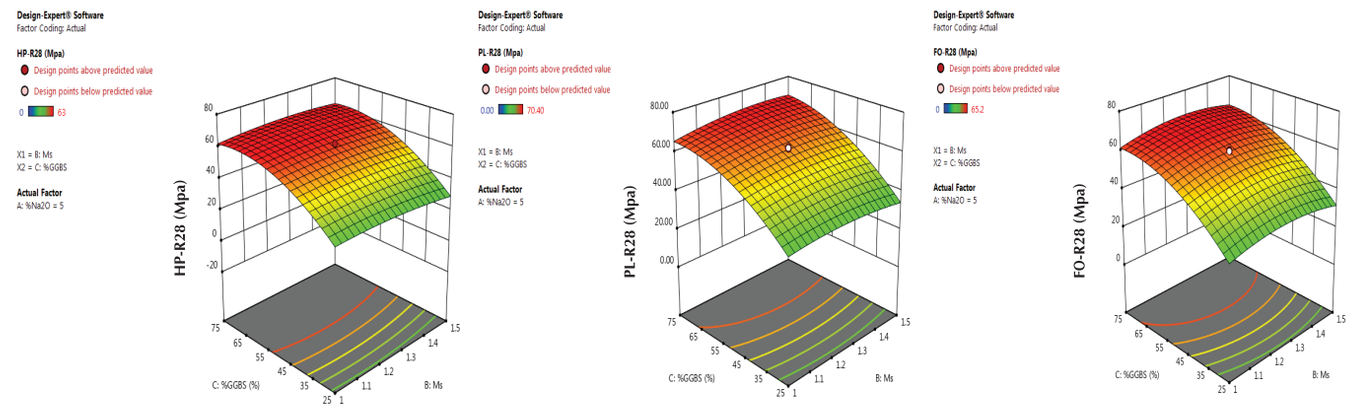

(A) (B) (C)

Fig. 4. 3D surface plots of 28-d compressive strength models for the (A) HP mixture, (B) PL mixture, and (C) FO mixture - effect of %GGBS and M_s.

Three-dimensional surface plots were generated for the pairwise combination of the three factors while keeping one constant. The graphs are given here to highlight the roles played by the various factors in the 28-d compressive strength. Fig. 3 shows the effect of %GGBS and %Na_2O while Fig. 4 shows the effect of %GGBS and M_s on the 28-d compressive strength of mortar. It is noteworthy that the sources of FA with different LOI have minor effect on the compressive strength of mortar. In other words, although fly ash is obtained from different factories, it is only necessary to ensure that the class F fly ash is in accordance with the Vietnamese national code TCVN 10302:2014 and contains less than 12% of LOI. With those two conditions met, it can be used to make a high strength alkali-activated binder. It is also noteworthy that M_s has a very small effect when compared to the other factors (%Na_2O and %GGBS). This result opens up a promising research direction; instead of the standard combination of sodium silicate and sodium hydroxide, 100% sodium silicate can be used as an activator. With the properties that exist in powder form ($Na_2SiO_3.5H_2O$) and are not heat generating like sodium hydroxide, we can pre-mix $Na_2SiO_3.5H_2O$ with FA and GGBS in the appropriate ratio for bagging to use as traditional cement.

3.2. Optimizations

Although alkali-activated binders are considered to have many good properties and are environmentally friendly, it has not been widely used as Portland cement due to its high cost. Therefore, an optimisation of binder composition should be performed to ensure both high strength and reasonable cost. Furthermore, most of the thermal power plants in Vietnam use poor quality coal, which results in high-LOI fly ash products (LOI>6%). Therefore, the increased use of FA with high LOI content (this FA is not allowed to be used as mineral additives for cement), the more environmental and economic benefits. Based on the purpose of optimisation, the characteristic goals of the factors and their response for the multi-response optimization process are shown in Table 10.

Table 10. Definitions for the factors and the responses in the optimization process.

Factors and response	1st goal	2nd goal	Lower	Upper
A:%Na_2O	is in range	is in range	3	7
B:Ms	is in range	is in range	1	1.5
C:%GGBS	is in range	minimize	25	75
HP-R_{28}	maximize	maximize	0	63
PL-R_{28}	maximize	maximize	0	70.4
FO-R_{28}	maximize	maximize	0	65.2
Cost	none	minimize	31.076	113.248

Based on the purpose of optimization, the numerical optimization solutions are presented in Table 11. According to those results, for the 1st goal, the optimal values were %Na_2O=6.15%, M_s=1.30, and %GGBS=73% with predicted 28-d compressive strengths of 69.84, 74.06, and 71.07 MPa. For the 2nd goal, the optimal values were %Na_2O=5.18%, M_s=1.16, and %GGBS=50% with predicted 28-d compressive strengths of 60.69, 61.84 and 60.19 MPa.

To validate the appropriateness of the optimization results and the entire response model, an additional set of investigations were carried out using the optimized mixture proportions. The experimental results were consistent with predicted results with errors between them less than 5% as shown in Table 11. However, the specimens containing 73% GGBS (for the 1st goal) a microcracking network developing on the surface was visible (Fig. 5). This phenomenon was also found in the study of M.F. Zawrah, et al. (2018) [17] with samples containing more than 70% GGBS. This result may have contributions from the high autogenous and drying shrinkage of the alkali-activated slag (AAS). A.J. Thomas, et al. (2012) [18] proposed a hypothesis that this effect was due to part of the greater chemical shrinkage of the

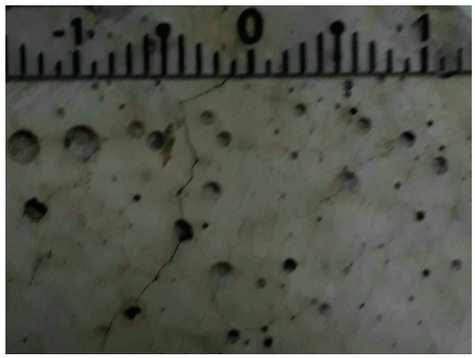

Fig. 5. A visual micro cracking network developing on the surface of the specimens containing 73% GGBS.

alkali activated slag. Additionally, the effect of autogenous shrinkage may be exacerbated by the fact that incorporating GGBS yields a lower permeability of the AAS samples, which prevents excess water into the specimens during saturated curing, which leads to differential stresses that can cause cracking. This phenomenon was not observed in the samples containing 50% GGBS (for the 2nd goal). It is said that the higher replacement of GGBS with fly ash, the lower shrinkage of AAFS mortars [19] and also lower compressive strength.

4. Conclusions

This study focused on the effects of the input variables %Na_2O, M_s, and %GGBS as well as the interaction between them on the target responses of 28-d compressive strength and the cost for one ton of binder. The following conclusions were drawn:

- Although fly ash can be obtained from different factories, it is only necessary to ensure that the class F fly ash in accordance with the Vietnamese national code TCVN 10302:2014 and contains less than 12% of LOI. Then, it

Table 11. Optimization results and model verification.

Optimization goal	Response	%Na_2O	M_s	%GGBS	Predicted results	Experimental results	Error (%)
1st Goal	28-d compressive strength for HP mixture (MPa)	6.15	1.30	73	69.84	71.75	2.73%
	28-d compressive strength for PL mixture (MPa)				74.06	73.99	-0.10%
	28-d compressive strength for FO mixture (MPa)				71.07	72.71	2.30%
	Cost of 1 ton of binder (USD)				$90.59		
2nd Goal	28-d compressive strength for HP mixture (MPa)	5.18	1.16	50	60.69	62.95	3.72%
	28-d compressive strength for PL mixture (MPa)				61.84	63.54	2.75%
	28-d compressive strength for FO mixture (MPa)				60.19	63.11	4.85%
	Cost of 1 ton of binder (USD)				$72.49		

can be used to make high strength alkali-activated binder. Moreover, the sources of FA with different LOI have minor effects on the compressive strength of mortar.

- M_s has a very small effect compared to the other factors (%Na_2O and %GGBS). This result opens up a promising research direction; instead of the standard combination of sodium silicate and sodium hydroxide, 100% sodium silicate may be used as an activator.

- The optimal values were %Na_2O=5.18%, M_s=1.16, and %GGBS=50% with the goals of maximum compressive strength, the largest amount of fly ash, and reasonable cost. The experimental results show that the compressive strength of the samples were between 62.95 and 63.54 MPa and consistent with the optimized results (the variation between the predicted and the experimental results was less than 5%).

For future work, with emphasis on the properties that exist in powder form ($Na_2SiO_3.5H_2O$) and the lack of heat generation like sodium hydroxide, research will be conducted to pre-mix $Na_2SiO_3.5H_2O$ with FA and GGBS in an appropriate ratio for bagging for use as a traditional cement.

CRedit author statements

Hoang-Quan Dinh, Thanh-Bang Nguyen: Conceptualization, Methodology, Data curation, Formal analysis, Writing - Review & Editing.

ACKNOWLEDGEMENTS

This study is a part of the national project KC08.21/16-20. The authors would like to admit the program KC08/16-20, Ministry of Science and Technology, Vietnam for the research financial support.

COMPETING INTERESTS

The authors declare that there is no conflict of interest regarding the publication of this article.

REFERENCES

[1] A.O. Purdon (1940), "The action of alkalis on blast furnace slag", *Journal of The Society of Chemical Industry*, **59**, pp.191-202.

[2] J. Davidovits (1991), "Geopolymer: Inorganic polymeric new materials", *Journal of Thermal Analysis*, **37**, pp.1633-1656.

[3] D.M. Roy (1999), "Alkali-activated cements: Opportunities and challenges", *Cement and Concrete Research*, **29**, pp.249-254, DOI: 10.1016/S0008-8846(98)00093-3.

[4] A. Palomo, M.W. Grutzeck, M.T. Blanco (1999), "Alkali-activated fly ashes: A cement for the future", *Cement and Concrete Research*, **29**, pp.1323-1329, DOI: 10.1016/S0008-8846(98)00243-9.

[5] F. Puertas, M. Palacios, H. Manzano, et al. (2011), "A model for the C-A-S-H gel formed in alkali-activated slag cements", *Journal of the European Ceramic Society*, **31(12)**, pp.2043-2056, DOI: 10.1016/j.jeurceramsoc.2011.04.036.

[6] Z. Yunsheng, S. Wei, C. Qianli, et al. (2007), "Synthesis and heavy metal immobilization behaviors of slag based geopolymer", *Journal of Hazardous Materials*, **143(1-2)**, pp.206-213, DOI: 10.1016/j.jhazmat.2006.09.033.

[7] A. Wardhono, D.W. Law, A. Strano (2015), "The strength of alkali-activated slag/fly ash mortar blends at ambient temperature", *Procedia Engineering*, **125**, pp.650-656, DOI: 10.1016/j.proeng.2015.11.095.

[8] S. Kumar, J. Vasugi, P.S. Ambily, et al. (2013), "Development and determination of mechanical properties of fly ash and slag blended geopolymer concrete", *International Journal of Scientific & Engineering Research*, **4(8)**, 5pp.

[9] P. Abhilash, C. Sashidhar, I.V.R. Reddy (2016), "Strength properties of fly ash and GGBS based geopolymer concrete", *International Journal of ChemTech Research*, **9(3)**, pp.350-356.

[10] C. Pinheiro, S. Rios, A.V. Fonseca, et al. (2020), "Application of the response surface method to optimize alkali activated cements based on low-reactivity ladle furnace slag", *Construction and Building Materials*, **264**, DOI: 10.1016/j.conbuildmat.2020.120271.

[11] B.S. Mohammed, S. Haruna, M.M.A. Wahab, et al. (2019), "Optimization and characterization of cast in-situ alkali-activated pastes by response surface methodology", *Construction and Building Materials*, **225**, pp.776-787, DOI: 10.1016/j.conbuildmat.2019.07.267.

[12] J.F. Rivera, N. Cristelo, A.F. Jiménez, et al. (2019), "Synthesis of alkaline cements based on fly ash and metallurgic slag: optimisation of the SiO_2/Al_2O_3 and Na_2O/SiO_2 molar ratios using the response surface methodology", *Construction and Building Materials*, **213**, pp.424-433, DOI: 10.1016/j.conbuildmat.2019.04.097.

[13] Vietnamese National Standard, TCVN 10302:2014 (2014), *Activity Admixture - Fly Ash for Concrete, Mortar and Cement* (in Vietnamese).

[14] European Standard, EN196-1 (2006), *Methods of Testing Cement - Part 1: Determination of Strength*, pp.1-33.

[15] ASTM International, ASTM C230/C230M-20 (2020), *Standard Specification for Flow Table for Use in Tests of Hydraulic Cement*.

[16] J.K. Prusty, B. Pradhan (2020), "Multi-response optimization using Taguchi-Grey relational analysis for composition of fly ash-ground granulated blast furnace slag-based composition of fly ash-ground granulated blast furnace slag based", *Construction and Building Materials*, **241**, DOI: 10.1016/j.conbuildmat.2020.118049.

[17] M.F. Zawrah, R. Gado, R. Khattab (2018), "Optimization of slag content and properties improvement of Metakaolin-slag geopolymer mixes", *The Open Materials Science Journal*, **12**, pp.40-57, DOI: 10.2174/1874088X01812010040.

[18] A.J. Allen, J.J. Thomas, H.M. Jennings (2012), "Density and water content of nanoscale solid C-S-H formed in alkali-activated (AAS) paste and implications for chemical shrinkage", *Cement and Concrete Research*, **42**, pp.377-383, DOI: 10.1016/j.cemconres.2011.11.003.

[19] M. Chi, R. Huang (2013), "Binding mechanism and properties of alkali-activated fly ash/slag mortars", *Construction and Building Materials*, **40**, pp.291-298, DOI: 10.1016/j.conbuildmat.2012.11.003.

DOI: 10.31276/VJSTE.63(1).30-35

Application of an innovative draw solute in forward osmosis (FO) processes

Nguyen Cong Nguyen[1*], Hau Thi Nguyen[1], Shiao-Shing Chen[2], Xuan Thanh Bui[3]

[1]Faculty of Environment and Natural Resources, Dalat University, 1 Phu Dong Thien Vuong Street, Ward 8, Dalat City, Lam Dong Province, Vietnam
[2]Institute of Environmental Engineering and Management, National Taipei University of Technology, 1, Sec. 3, Zhongxiao Street, Da'an District, Taipei City, Taiwan
[3]Faculty of Environment and Natural Resources, University of Technology, Vietnam National University - Ho Chi Minh City, 268 Ly Thuong Kiet Street, Ward 14, District 10, Ho Chi Minh City, Vietnam

Received 20 November 2019; revised 20 February 2020; accepted 2 March 2020

Abstract:

More attention is being paid to forward osmosis (FO) as a breakthrough technology to tackle environmental pollution due to advantages such as high contaminant removal and low energy consumption. Nevertheless, FO applications remain limited by the lack of ideal draw solutes that simultaneously achieve high permeate flux and low salt leakage flux. Therefore, this paper aims to increase water flux while maintaining low reverse salt diffusion by using a low concentration of a highly charged organic EDTA compound coupled with inorganic NaCl salt as a novel draw solute. Results of the FO performance revealed that a draw solute of 0.3 M EDTA-2Na mixed with 0.6 M NaCl yielded a higher water flux (J_w=8.82 l/m² h) when compared to 0.9 M NaCl only (J_w=7.61 l/m² h). Moreover, the FO-membrane distillation system produced good quality drinking water with a total dissolved solid (TDS) of <5 mg/l from the permeate stream originating from influent brackish water with a TDS of 6000 mg/l. The analysis results from scanning electron microscopy and energy dispersive X-ray spectroscopy (SEM-EDX) images observed a cake layer of NaCl on the FO membrane surface.

Keywords: **brackish water, distillation, forward osmosis, membrane draw solute, reverse salt flux.**

Classification number: **2.3**

1. Introduction

Nowadays, climate change has significantly impacted the life of people especially as rising sea levels lead to an increase in salinity intrusion of many water sources such as the Vietnamese Mekong river delta and the Cau Do river [1]. Saltwater intrusion has caused a lot of problems for drinking water treatment plants using coagulation-sedimentation-filtration-disinfection technology because these traditional technologies are not equipped to treat brackish water. Therefore, water scarcity by salinity intrusion is an increasingly serious global problem and clean water production through the treatment of brackish water is receiving more attention as a solution to freshwater shortages. Among suggested technologies, reverse osmosis (RO) is the most widely employed technology for brackish desalination [2, 3]. However, RO processes consume large amounts of energy because they require high pressure. The limitations of RO membrane technology include severe membrane fouling, scaling, and low water recovery. Furthermore, the discharge of RO concentrate streams are damaging to the environment [4-6]. Hence, it is essential and urgent to investigate a sustainable and environmentally friendly water production technology.

Forward osmosis is a green technology for clean water production [7-10]. Unlike RO process, FO uses natural osmotic pressure to draw permeate water from a feed solution to a draw solution. The semipermeable membrane allows clean water to pass through but rejects solutes [8, 11-13]. Therefore, the FO process can be operated at low or negligible pressure. Many studies have reported that FO is a feasible process because of its low energy consumption, low fouling propensity, and high rejection of various contaminants [11, 14-16]. Although FO has been widely used in brackish desalination and wastewater reclamation [7-9], exploring an appropriate draw solute remains a particularly crucial and major challenge. High permeate stream, minimal salt leakage, nontoxicity, as well as efficient

*Corresponding author: Email: nguyennc@dlu.edu.vn

regeneration, should be maintained in an ideal draw solute [6, 17-19].

Over the past few years, many categories of materials such as inorganic salts and organic solutes have been studied and evaluated as potential optimized draw solutions [17, 20-23]. These draw solutions are easily recovered using an RO membrane, are inexpensive, and produce a relatively high permeate stream. However, both problems of severe reverse solute fluxes during the FO process and high energy consumption during the regeneration process hinder their application. Furthermore, some new draw solutes such as polydiallyldimethylammonium chloride [24], 2-methylimidazole-based compounds [25], and hexavalent phosphazene salts [26] have shown promising results with low salt leakage and easy recovery. Despite these advantages, most of these synthetic draw solutes produce a lower water flux than conventional draw solutions. In our group's previous research, EDTA-2Na was explored as a draw solution for a hybrid FO-nanofiltration (NF) process [27]. These draw solutions, with large molecular size and high osmotic pressure, have received considerable attention [28, 29] because they performed much better than others in terms of relatively high water flux and low reverse solute flux. However, the high viscosity and limitation of the solubility of EDTA-2Na at high concentration remain as challenges for FO applications, which is the main reason for the author to conduct this research.

To the best of our knowledge, a mixed draw solute of highly charged organic EDTA with highly soluble NaCl salt has not yet been used in an FO-membrane distillation (FO-MD) system to simultaneously achieve a high water flux and maintain a low reverse salt flux. Therefore, this study aims to do the following: (1) assess the influence of various draw solute concentrations on FO system; (2) evaluate the efficiency of the application of NaCl mixed with EDTA-2Na as draw solute in FO/MD for desalinating brackish water; and (3) investigate the water quality from the permeate stream of an MD system.

2. Materials and methods

2.1. FO and MD membranes

In this study, we used cellulose triacetate with an embedded support cartridge-type (CTA.ES) FO membrane provided from Hydration Technology Innovations (American). Its characteristics are shown in Table 1. We used an MD membrane, namely, a polytetrafluoroethylene (PTFE) membrane, with 0.45 µm pore sizes and 114±4° contact angle, delivered by the Ray.E.Creative Taiwanese Company. Before use in the MD process, the membrane was washed with clean water and dried at room temperature.

Table 1. Characteristics of CTA.ES FO membrane.

CTA.ES FO membrane	Value
Size for each piece	15×22 cm^2
Contact angle	60-80°
pH range	2-8
Salt rejection	95-99%
Post treatment	Soak in DI water

2.2. Preparation of feed solution and draw solution

We used EDTA-2Na with purity >99% from Sigma-Aldrich Co., Ltd., (Germany) and NaCl salt with purity >99% from Vietnamese salt Co., Ltd., (Vietnam). The draw solutions were prepared using a combination of 0.3 M EDTA-2Na and different concentrations of NaCl. To all draw solutions, NaOH solution was added to adjust to pH 8 and they were stirred for 1 d before being used in the FO process. DI water was used as feed solution in FO to test water flux and reserve salt flux. Synthetic brackish water served as the feed solution for the FO desalination process. The synthetic brackish water was made with a total dissolved solid concentration of 6000 mg/l by mixing NaCl salt into DI water.

2.3. FO-MD process

All FO-MD experiments were conducted with a lab-scale FO-MD setup, as illustrated in Fig. 1. The CTA.ES FO membrane was used for all FO experiments. The FO cell was composed of two semi-cells, each of which was engraved to form a rectangular flow channel with length×width×height of 9.2×4.5×0.2 cm, respectively. The membrane coupons were inserted in the membrane cell such that the active layer faced the feed solution (FO mode) and the flow rate of the feed and draw solutions were both fixed at 500 ml/min. Furthermore, 0.3 M EDTA-2Na mixed with different concentrations of NaCl (0.1, 0.2, 0.4, 0.6 and 0.8 M) were prepared as the draw solutions. Synthetic brackish water served as the feed solution for FO desalination process. We prepared 1 l for the feed solution and draw solution, and then placed it on a scale (BW12KH, Shimadzu, Japan) to monitor weight variations versus time. Then, the mass change of the feed solution was converted to volume change based on the density of the feed solution.

The experimental water flux (J_w, l/m^2 h) was calculated according to the volume variation in the feed tank with time:

$$J_w = \frac{\Delta V}{A\Delta t} \quad (1)$$

where A is the membrane area (m^2) and ΔV is the increased water volume (l) of draw solution obtained in a time interval Δt (h).

The reverse salt flux of the draw solution (J_s, g/m^2 h) was determined from the amount of salt accumulated in the feed tank:

$$J_s = \frac{V_t.C_t - V_0.C_0}{A.t} \quad (2)$$

where C_t and C_0 are the concentration of the feed solution measured at time t (h) and initial time (t=0 h), respectively, and V_t and V_0 are the volume of the feed solution at time t (h) and initial time (t=0 h), respectively.

Following the FO tests, the MD process was conducted to recover the diluted draw solution using an MD cell module (Sterlitech, USA). The FO membrane module was produced from acrylic material and composed of two semicells with a flow channel 0.2 cm deep, 4.5 cm wide, and 9.2 cm long. We pumped and circulated the distillate and feed through each semicell with a velocity of 500 ml/min. Moreover, 0.3 M EDTA-2Na mixed with 0.6 M NaCl was used as the hot feed solution and was temperature controlled at 55±0.5°C, whereas cold DI water used as the original distillate was maintained at 25±0.5°C. The feed solution and distillate were continuously pumped from their reservoirs through each semicell membrane and then back to the reservoirs. The permeate water from the distillate tank that overflowed into the clean water tank was weighted by a digital weighing scale. Using Eq. (1), the water flux was calculated from the volume changes of the MD permeate.

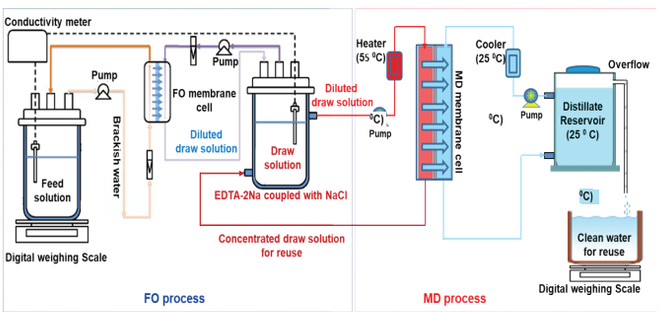

Fig. 1. Illustration of FO-MD system for desalinating brackish water.

Rejection of TDS can be calculated by the equation:

$$R = (1 - \frac{C_P}{C_F}).100\% \quad (3)$$

where R is the TDS rejection, C_P (mg/l) is the TDS concentration in the permeate, and C_{Fi} (mg/l) is the initial feed concentration.

2.4. Analytical methods

Viscosity was obtained using a Viscometer from Japanese Company and conductivity was determined by a conductivity meter (China). Furthermore, we used CAM 100 (Opto-Mechatronics P Ltd., India) to measure the membrane contact angle. Membrane fouling was detected through scanning electron microscopy and energy dispersive X-ray spectroscopy (SEM-EDX). Osmolality was measured using an Osmometer (Model 3320, Advanced Instruments, Inc., USA) on the basis of the freezing-point depression method. The concentration of permeation solutions was analysed using a total organic carbon (TOC) analyser from Japanese Shimadzu Company.

3. Results and discussion

3.1. The influence of draw solution concentrations on water flux and reverse salt flux

Figure 2 presents the variations in the water flux and reverse salt flux for different NaCl concentrations (from 0.1 to 0.8 M) coupled with 0.3 M EDTA-2Na as the draw solutes. The FO experiments were conducted in the membrane orientation of the active layer facing the feed solution of the DI water. The water flux gradually increased from 5.73 to 9.24 l/m^2 h when the concentration of NaCl increased from 0.1 to 0.8 M due to the increase in the osmolality (from 896 to 1584 mOsm/kg) in the draw solution (Fig. 3). Clearly, the increase in FO water flux was not linear with increasing osmolality of the draw solution. This non-linearity could be explained by the rise in viscosity from 1.41 to 1.79 cp (Fig. 3) when the draw solution concentration rose from 0.1 to 0.8 M NaCl, which led to the prevention of permeable water through the FO membrane. Moreover, the reverse salt flux rose from 1.42 to 2.95 g/m^2 h as NaCl concentrations increased from 0.1 to 0.8 M into the 0.3 M EDTA-2Na draw solution, as shown in Fig. 2.

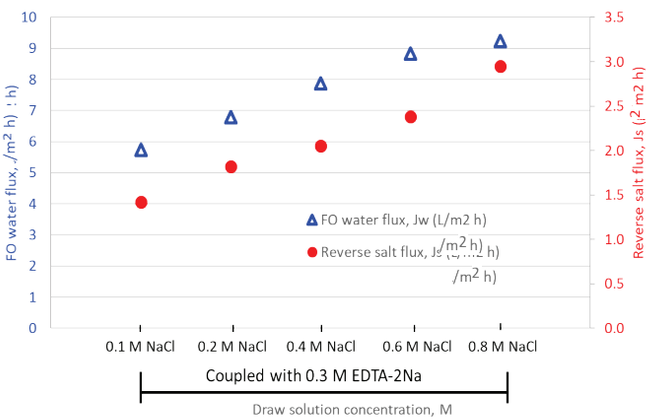

Fig. 2. Variation of reverse salt and water flux using 0.3 M EDTA-2Na mixed with various NaCl concentrations as draw solution.

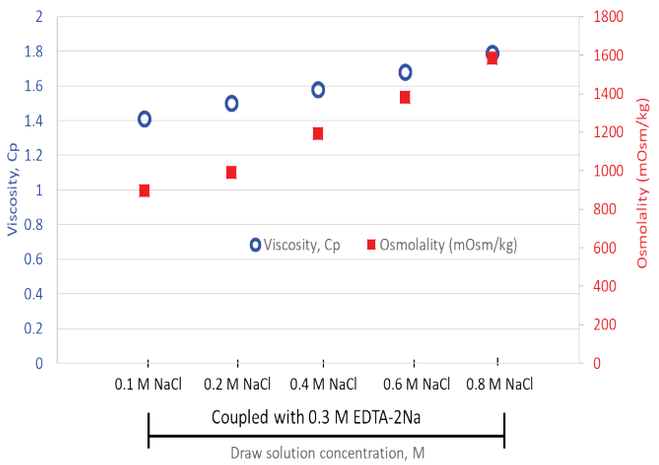

Fig. 3. Variation of osmolality and viscosity using 0.3 M EDTA-2Na mixed with various NaCl concentrations as draw solution.

Meanwhile, the reverse salt fluxes of 0.4 M-1.1 M NaCl as the only draw solution quickly increased from 3.18 to 5.93 g/m^2 h, which is much higher than the measured value of EDTA-2Na mixed with NaCl as the draw solutions (Fig. 4). The reason for the different reverse salt flux of the two kinds of draw solution can be explained by the influence of the complexation and highly charged compounds present in the EDTA-2Na and NaCl mixed draw solution. For instance, we observed 14.4% of Na[EDTA]$^{3-}$complexion and 81% of trivalent compound of H[EDTA]$^{3-}$(complexion and charge formation are observed by Mineql+ software) when coupling 0.3 M EDTA-2Na into NaCl, which resulted in a reduced reverse salt flux [18, 19, 30]. This is the most noteworthy aspect of using the mixed highly charged draw solution of EDTA-2Na into NaCl.

As seen in Fig. 2, between the 0.6 M NaCl concentration coupled with 0.3 M EDTA-2Na (J_w=8.82 l/m^2 h) and 0.8 M NaCl coupled with 0.3 M EDTA-2Na (J_w=9.24 l/m^2 h), the difference in water flux was negligible, however, the reverse salt flux of 0.8 M NaCl coupled with 0.3 M EDTA-2Na (J_s=3.01 g/m^2 h) was much higher than that of 0.6 M NaCl coupled with 0.3 M EDTA-2Na (J_s=2.38 g/m^2 h). These results revealed that 0.6 M NaCl coupled with 0.3 M EDTA-2Na proved to be the optimum concentration of a draw solution in the FO process for simultaneously obtaining low reverse salt flux (J_s=2.38 g/m^2 h) and high water flux (J_w=8.82 l/m^2 h).

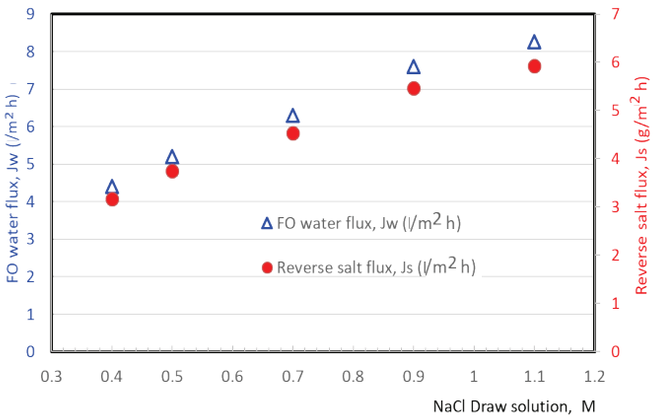

Fig. 4. Variation of water flux and reverse salt flux using pure NaCl with various NaCl concentrations as draw solution.

3.2. Application of EDTA-2Na mixed with NaCl as the draw solute in FO/MD for desalinating the brackish water

Concerning the optimum FO performance among the various NaCl concentrations, 0.6 M NaCl mixed with 0.3 M EDTA-2Na was selected as the draw solution for studying brackish desalination through the FO-MD hybrid system. Fig. 5 depicts the water flux of the FO process for desalinating the synthetic brackish water of 6000 mg/l TDS concentration. The FO water flux decreased from 6.78 l/m^2 h (over the first two hours) to 6.01 l/m^2 h (over the last ten hours). After the 10-h operation, the FO water flux was reduced by 10.32%. A possible reason for the decline in FO permeate flux is the increase in TDS of the feed solution (from 6000 mg/l to 8100 mg/l), which caused an increase in the osmotic pressure of the feed solution, which then reduced the net driving force across the FO membrane.

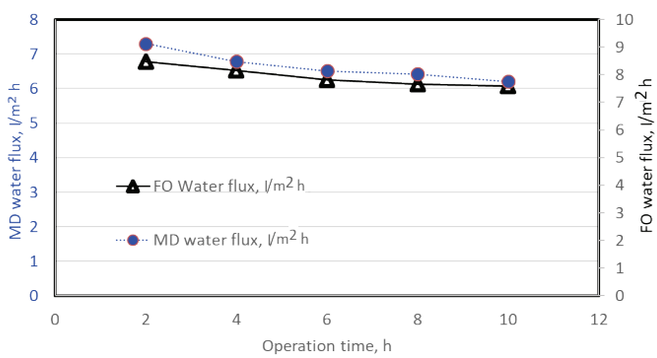

Fig. 5. Variation of FO water flux and MD water flux for the desalination of brackish water versus operation time (0.3 M EDTA-2Na coupled with 0.6 M NaCl as draw solute, MD membrane: PTFE 0.45 µm; hot stream: 55±0.5°C; distillate stream: 25±0.5°C).

Moreover, the reduction in water flux can be attributed to the concentration polarization (CP) effect because of the salt accumulation (NaCl) on the active layer of the FO membrane. In fact, salt accumulation on the FO membrane surface can be observed in Fig. 6A with 6000 mg/l of NaCl as the feed solution. There were some cake layers of NaCl attached to the FO membrane that were identified by EDS through the appearance of peaks indicating the elements Na and Cl (Fig. 6B). This result agrees with that reported by Alnaizy, et al. [22], who showed that the water flux decreased as feed concentration was increased due to a reduced osmotic pressure gradient between feed and draw solution and increased concentration polarization phenomenon.

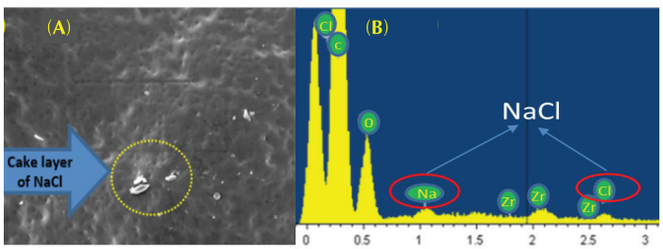

Fig. 6. (A) SEM picture and (B) EDS graph of a used membrane (0.3 M EDTA-2Na coupled with 0.6 M NaCl as draw solute, 6000 mg NaCl/l as feed solution, draw solution facing the support layer, pH of 8, temperature of 25±0.5°C).

As can be seen from Fig. 5, 0.45 µm PTFE was used as an MD membrane for diluted draw solution recovery and the slight decrease in MD water flux from 9.12 to 7.75 l/m^2 h can be attributed to membrane fouling. This outcome agrees with Elzahaby, et al. [31], who observed that a high feed tank temperature could lead to membrane fouling and reduce its performance.

3.3. Water quality from permeate stream of MD system

The recovery of the diluted draw solute (0.3 M EDTA-2Na coupled with 0.6 M NaCl) from FO was induced by the MD process to reuse the draw solution and separate the clean water under the conditions of a hot stream of 55±0.5°C and a distillate stream of 25±0.5°C. Table 2 illustrates the variation of TOC and TDS in the permeate stream from the MD system using the 0.45 µm PTFE MD membrane during 10-h operation. The results showed that the 0.45 µm PTFE efficiently removed almost all ions (more than 99.9%) from the diluted draw solution during the 10-h operation. The overall high salt rejection observed here can be largely attributed to the MD process in which only water vapour is transported through the membrane pores. The concentration of TOC in the permeate stream had a slight increasing trend versus operating time (from 0.48 to 0.93 mg/l), however, the TOC concentration is still lower than that of the drinking water standard. In addition, the TDS concentration in the permeate stream of the MD system slightly rose from 0.95 to 4.54 mg/l after the 10-h operation, which was lower than that of the National Technical Regulation on drinking water quality (QCVN 01:2009/BYT with TDS<1000 mg/l). This result demonstrated that the FO-MD hybrid system can produce high quality drinking water from brackish water.

Table 2. Water quality from permeate stream of MD system for desalinating of synthetic brackish water.

Operating time, h	2	4	6	8	10
TOC in permeate stream, mg/l	0.48	0.59	0.72	0.84	0.93
TDS in permeate stream, mg/l	0.95	1.16	1.47	2.48	4.54
TDS rejection, %	99.99	99.99	99.98	99.96	99.92

Experimental condition: MD membrane: PTFE 0.45 µm; hot stream: 55±0.5°C; distillate stream: 25±0.5°C; Feed and distillate velocity: 500 ml/min; diluted draw solute as feed: 0.3 M EDTA-2Na coupled with 0.6 M NaCl.

Conclusions

The highly charged organic EDTA-2Na compound coupled with highly soluble inorganic NaCl salt creates a suitable draw solute for simultaneously achieving a low reverse salt flux and high water flux in the FO process. The results revealed that the relatively high water flux of 8.82 l/m^2 h and low reverse salt flux of 2.38 g/m^2 h were obtained when 0.3 M EDTA-2Na coupled with 0.6 M NaCl was used as the draw solute and DI water served as the feed solution. Moreover, 0.3 M EDTA-2Na was mixed with 0.6 M NaCl in the brackish desalination process, yielding average water fluxes of 6.35 l/m^2 h when brackish water with a TDS of 6000 mg/l was used as the feed solution in the FO process. Notably, a diluted draw solution was successfully recovered using a 0.45 µm PTFE MD membrane, with an average water flux of 8.30 l/m^2 h and more than 99.9% rejection of salinity.

CRediT author statements

Nguyen Cong Nguyen, Hau Thi Nguyen: Conceptualization, Methodology, Data curation, Formal analysis, Writing - Review & Editing; Shiao-Shing Chen, Xuan Thanh Bui: Conceptualization, Methodology, Writing original draft preparation, Writing - Review & Editing.

ACKNOWLEDGEMENTS

The authors would like to acknowledge the financial support from National Foundation for Science and Technology Development (NAFOSTED) No. 105.08-2017.311, Ministry of Science and Technology (Vietnam) and Ministry of Education (Vietnam) No. B2019-DLA-01.

COMPETING INTERESTS

The authors declare that there is no conflict of interest regarding the publication of this article.

REFERENCES

[1] P.S.J. Minderhoud, L. Coumou, G. Erkens, et al. (2019), "Mekong delta much lower than previously assumed in sea-level rise impact assessments", *Nature Communications*, **10(3847)**, pp.1-13, DOI: 10.1038/s41467-019-11602-1.

[2] L.F. Greenlee, D.F. Lawler, B.D. Freeman, et al. (2009), "Reverse osmosis desalination: water sources, technology, and today's challenges", *Water Research*, **43(9)**, pp.2317-2348, DOI: 10.1016/j.watres.2009.03.010.

[3] K.P. Lee, T.C. Arnot, D. Mattia (2011), "A review of reverse osmosis membrane materials for desalination-development to date and future potential", *Journal of Membrane Science*, **370(1-2)**, pp.1-22, DOI: 10.1016/j.memsci.2010.12.036.

[4] M.A. Shannon, P.W. Bohn, M. Elimelech, et al. (2008), "Science and technology for waterpurification in the coming decades", *Nature*, **452**, pp.301-310, DOI: 10.1038/nature06599.

[5] N. Ghaffour, S. Lattemann, T. Missimer, et al. (2014), "Renewable energy-driven innovative energy-efficient desalination technologies", *Applied Energy*, **136**, pp.1155-1165, DOI: 10.1016/j.apenergy.2014.03.033.

[6] T.-S. Chung, S. Zhang, K.Y. Wang, et al. (2012), "Forward osmosis processes: Yesterday, today and tomorrow", *Desalination*, **287**, pp.78-81, DOI: 10.1016/j.desal.2010.12.019.

[7] T.Y. Cath, A.E. Childress, M. Elimelech (2006), "Forward osmosis: Principles, applications, and recent developments", *Journal of Membrane Science*, **281**, pp.70-87, DOI: 10.1016/j.memsci.2006.05.048.

[8] J.-J. Qin, W.C.L. Lay, K.A. Kekre (2012), "Recent developments and future challenges of forward osmosis for desalination: A review", *Desalination and Water Treatment*, **39(1-3)**, pp.123-136, DOI: 10.1080/19443994.2012.669167.

[9] S. Zhao, L. Zou, C.Y. Tang, et al. (2012), "Recent developments in forward osmosis: Opportunities and challenges", *Journal of Membrane Science*, **396**, pp.1-21, DOI: 10.1016/j.memsci.2011.12.023.

[10] D.Y. Kim, B. Gu, J.H. Kim, et al. (2013), "Theoretical analysis of a seawater desalination process integrating forward osmosis, crystallization, and reverse osmosis", *Journal of Membrane Science*, **444**, pp.440-448, DOI: 10.1016/j.memsci.2013.05.035.

[11] B. Mi, M. Elimelech (2010), "Organic fouling of forward osmosis membranes: Fouling reversibility and cleaning without chemical reagents", *Journal of Membrane Science*, **348**, pp.337-345, DOI: 10.1016/j.memsci.2009.11.021.

[12] S. Zhao, L. Zou (2011), "Effects of working temperature on separation performance, membrane scaling and cleaning in forward osmosis desalination", *Desalination*, **278**, pp.157-164, DOI: 10.1016/j.desal.2011.05.018.

[13] P. Li, S.S. Lim, J.G. Neo, et al. (2014), "Short-and long-term Performance of the thin-film composite forward osmosis (TFC-FO) hollow fiber membranes for oily wastewater purification", *Industrial & Engineering Chemistry Research*, **53(36)**, pp.14056-14064, DOI: 10.1021/ie502365p.

[14] D. Li, X. Zhang, J. Yao, et al. (2011), "Stimuli-responsive polymer hydrogels as a new class of draw agent for forward osmosis desalination", *Chemical Communications*, **47**, pp.1710-1712, DOI: 10.1039/C0CC04701E.

[15] Y. Liu, B. Mi (2012), "Combined fouling of forward osmosis membranes: synergistic foulant interaction and direct observation of fouling layer formation", *Journal of Membrane Science*, **407-408**, pp.136-144, DOI: 10.1016/j.memsci.2012.03.028.

[16] Y. Gu, Y.N. Wang, J. Wei, et al. (2013), "Organic fouling of thin-film composite polyamide and cellulose triacetate forward osmosis membranes by oppositely charged macromolecules", *Water Research*, **47**, pp.1867-1874, DOI: 10.1016/j.watres.2013.01.008.

[17] A. Achilli, T.Y. Cath, A.E. Childress (2010), "Selection of inorganic-based draw solutions for forward osmosis applications", *Journal of Membrane Science*, **364**, pp.233-241, DOI: 10.1016/j.memsci.2010.08.010.

[18] W.A. Phillip, J.S. Yong, M. Elimelech (2010), "Reverse draw solute permeation in forward osmosis: modeling and experiments", *Environmental Science & Technology*, **44(13)**, pp.5170-5176, DOI: 10.1021/es100901n.

[19] N.T. Hancock, W.A. Phillip, M. Elimelech, et al. (2011), "Bidirectional permeation of electrolytes in osmotically driven membrane processes", *Environmental Science & Technology*, **45**, pp.10642-10651, DOI: 10.1021/es202608y.

[20] R.W. Holloway, A.E. Childress, K.E. Dennett, et al. (2007), "Forward osmosis for concentration of anaerobic digester centrate", *Water Research*, **41(17)**, pp.4005-4014, DOI: 10.1016/j.watres.2007.05.054.

[21] E.M.G. Castello, J.R. McCutcheon, M. Elimelech (2009), "Performance evaluation of sucrose concentration using forward osmosis", *Journal of Membrane Science*, **338(1-2)**, pp.61-66, DOI: 10.1016/j.memsci.2009.04.011.

[22] R. Alnaizy, A. Aidan, M. Qasim (2013), "Copper sulfate as draw solute in forward osmosis desalination", *Journal of Environmental Chemical Engineering*, **1(3)**, pp.424-430, DOI: 10.1016/j.jece.2013.06.005.

[23] K.S. Bowden, A. Achilli, A.E. Childress (2012), "Organic ionic salt draw solutions for osmotic membrane bioreactors", *Bioresource Technology*, **122**, pp.207-216, DOI: 10.1016/j.biortech.2012.06.026.

[24] M.J.A. Hamad, E.M.N. Chirwa (2019), "Forward osmosis for water recovery using polyelectrolyte PolyDADMAC and DADMAC draw solutions as a low pressure energy saving process", *Desalination*, **453**, pp.89-101, DOI: 10.1016/j.desal.2018.11.016.

[25] S.K. Yen, N.F.M. Haja, M. Su, et al. (2010), "Study of draw solutes using 2-methylimidazole-based compounds in forward osmosis", *Journal of Membrane Science*, **364(1-2)**, pp.242-252, DOI: 10.1016/j.memsci.2010.08.021.

[26] M.L. Stone, A.D. Wilson, M.K. Harrup, et al. (2013), "An initial study of hexavalent phosphazene salts as draw solutes in forward osmosis", *Desalination*, **312**, pp.130-136, DOI: 10.1016/j.desal.2012.09.030.

[27] N.T. Hau, S.S. Chen, N.C. Nguyen, et al. (2014), "Exploration of EDTA sodium salt as novel draw solution in forward osmosis process for dewatering of high nutrient sludge", *Journal of Membrane Science*, **455**, pp.305-311, DOI: 10.1016/j.memsci.2013.12.068.

[28] G. Gwak, B. Jung, S. Han, et al. (2015), "Evaluation of poly (aspartic acid sodium salt) as a draw solute for forward osmosis", *Water Research*, **80**, pp.294-305, DOI: 10.1016/j.watres.2015.04.041.

[29] Y. Zhao, Y. Ren, X. Wang, et al. (2016), "An initial study of EDTA complex based draw solutes in forward osmosis process", *Desalination*, **378**, pp.28-36, DOI: 10.1016/j.desal.2015.09.006

[30] N.T. Hancock, T.Y. Cath (2009), "Solute coupled diffusion in osmotically driven membrane processes", *Environmental Science & Technology*, **43(17)**, pp.6769-6775, DOI: 10.1021/es901132x.

[31] A.M. Elzahaby, A.E. Kabeel, M.M. Bassuoni, et al. (2016), "Direct contact membrane water distillation assisted with solar energy", *Energy Conversion and Management*, **110**, pp.397-406, DOI: 10.1016/j.enconman.2015.12.046.

DOI: 10.31276/VJSTE.63(1).36-41

Influences of seed priming with *Spirulina platensis* extract on seed quality properties in black gram (*Vigna mungo* L.)

Nguyen Quang Thinh*

Field Crop Research Institute, Vietnam Academy of Agricultural Sciences, Lien Hong Commune, Hai Duong City, Hai Duong Province, Vietnam

Received 18 February 2019; revised 11 June 2019; accepted 24 June 2019

Abstract:

Black gram (*Vigna mungo* L.) is a high nutrient pulse crop. Its seed quickly and easily deteriorates after harvest, resulting in poor planting material production that must be improved accordingly by seed enhancement methods. The blue-green microalgae *Spirulina platensis* contains variously beneficial substances, including macro and micro nutrients, vitamins, amino acids and antioxidants. The aim of this study is to improve the vigour and germination of black gram by priming its seeds with *Spirulina platensis* extract to prevent seed deterioration. Medium vigour black gram seeds were subjected to hydropriming for three hours (T_2); other seeds were primed with *Spirulina platensis* extract at 1.5% for three hours (T_3) while unprimed seeds served as control (T_1). Then, the seeds were artificially aged under 40±1°C and 95±5% relative humidity for five days. The results revealed that the hydropriming and control of black gram seeds were significantly lower in all physiological and biochemical seed quality parameters than seeds primed with *Spirulina platensis* extract at 1.5% for three hours. Consequently, *Spirulina platensis* extract can effectively enhance black gram seeds and use agents in.

Keywords: **black gram, seed priming, seed quality, *Spirulina platensis* extract.**

Classification number: **3.1**

1. Introduction

Black gram (*Vigna mungo* L.) is an important food crop cultivated in most countries throughout Asia. India is the major producer and consumer of black gram, producing approximately 2.199 million tonnes of black gram in an area of 4.02 million hectares during 2015-2016. The crop is of great importance as about 70% of the world's black gram production comes from India [1] and comprises10-12% of India's total pulse crop production [2]. Black gram is highly nutritious containing 24% protein content, 983 mg/100 g of potassium, 138 mg/100 g of calcium, 7.57 mg/100 g of iron, 1.447 mg/100 g niacin, 0.273 mg/100 g of thiamine, and 0.254 mg/100 g of riboflavin. Black gram is an important part of diets in India and other Asian countries are because it complements essential amino acids, high protein, and carbohydrates. Additionally, black gram has been found to be useful in mitigating elevated cholesterol levels. It also improves soil fertility through biological nitrogen fixation and thus plays an important role in sustainable agriculture.

Cyanobacteria (blue-green microalgae) are found in alkaline volcanic lakes and warm water areas. *Spirulina platensis,* a biomass of blue-green algae, produces a protein called phycocyanin belonging to the photosynthetic apparatus; it contains soft cell walls made of complex sugars and proteins and includes antioxidant and free radical scavenging properties [3]. The component analysis revealed that the *Spirulina* extract contains 85.1 g/kg of flavonoids, 77.8 g/kg of b-carotene, 113.2 g/kg of vitamin A and 3.4 g/kg of α-tocopherol, which contribute significantly to their high antioxidant activity. The main fatty acids in the extract are palmitic acid (35.32%), linolenic acid (21.66%), and linoleic acid (20.58%). As a natural biofertilizer, cyanobacteria's ability to fix N_2 improves the growth and yield of crops through the production of growth promoters such as gibberellins, cytokinins, auxins, vitamins, antibiotics and amino acids [4].

*Email: quangthinhsst@gmail.com

Seed priming is a hydration and dehydration process during pre-germination in which seeds absorb water and prevent radicle protrusion; the seeds are dried to their original moisture level [5]. Seed priming has been successfully demonstrated to improve germination and emergence in seeds of many crops. Primed seeds are able to complete the process of germination in a short time and can cope with environmental stresses [6]. Therefore, application of *Spirulina platensis* extract for seed priming to improve seed vigour and viability is a useful technology as it replaces the chemical utilities with organic nutrient supplements for seed quality improvement. Therefore, the present study is proposed to harness the potential use of *Spirulina platensis* extract to improve black gram seed quality.

2. Materials and methods

2.1. Seed material

Genetically pure, medium vigour seeds of black gram (*Vigna mungo* (L) Hepper) cv. CO 6 obtained from the Department of Pulses at Tamil Nadu Agricultural University, Coimbatore were used for this study.

2.2. Preparation of materials

Commercial *Spirulina platensis* powder taken from iGreen Firm, Coimbatore, Tamil Nadu was initially dried under sunlight followed by oven drying for 24 hours at 60°C and used for preparation of extract. Two hundred grams of *Spirulina platensis* powder was taken and added with 400 ml of acetone: methanol solvent [ratios of 1:1 (v/v)] and kept overnight after vigourous shaking. The solution was decanted and filtered through Whatman filter paper and stored in refrigerated conditions at 4°C until usage [7]. This *Spirulina platensis* extract was used as 100% concentrated stock for further studies.

2.3. Treatments

Black gram seeds were subjected to hydro-priming with distilled water for three hours and dried to their original moisture content of approximately 9% (T_2). Other black gram seeds were primed with *Spirulina platensis* extract at 1.5% concentration by soaking for three hours, then were dried to their original moisture content (T_3). The non-primed seeds were used as control (T_1). Then the seeds were artificially aged under 40±1°C and 95±5% RH (accelerated ageing) for five days.

2.4. Observations

Physiological and biochemical seed quality parameters were recorded in aged and non-aged seeds involving germination percentage, root length, shoot length, dry matter production [8], vigour index [9], speed of germination [10], dehydrogenase activity [11], free sugars in seed leachate [12], protein content [13], α-amylase activity [14], gibberellic acids content [15], and lipid peroxidation [16].

2.5. Statistical analysis

The data obtained from different treatments were analyzed for the 'F' test of significance following the methods described by V.G. Panse, et al. (1985) [17]. Wherever necessary, the percent values were transformed to angular (arcsine) values before analysis. The critical differences (CD) were calculated at 5% probability level. The data were tested for statistical significance.

3. Results and discussion

3.1. Physiological changes in black gram seeds due to priming with Spirulina platensis extract

The results revealed that the black gram seeds primed with *Spirulina platensis* extract at 1.5% concentration (T_3) recorded a maximum germination of 98%, higher than hydroprimed (T_2) and control (T_1) seeds, which recorded only 89 and 82% germination, respectively. The percentage of germination increased due to priming with *Spirulina platensis* extract was 9% and 16% over the hydropriming and control, respectively. Additionally, after accelerated ageing, the seeds primed with *Spirulina platensis* extract at 1.5% (T_3) recorded significantly higher germination (62%) which was 11% and 18% higher than the hydroprimed and control seeds, respectively.

Similarly, the root length of the seeds primed with *Spirulina platensis* extract at 1.5% (T_3) were significantly longer both before ageing (16.23 cm) and after ageing (11.97 cm) than the hydroprimed and non-primed seeds (control). The shoot lengths of the seedling were 14.67 cm before ageing and 10.17 cm after ageing in seeds primed with *Spirulina platensis* extract at 1.5%, which were significantly longer than those of the hydropriming and control seeds (Table 1). Soaking the seeds in *Spirulina platensis* extract might have improved not only the availability of seed food reverses but also maintained the cell structure, leading to increased seed vigour and germination in addition to preventing seed deterioration during accelerated ageing. Similar results were also reported by P.B. Ratan, et al. (1993) [18] in annona; J. Vijaya (1996) [19] in black gram and cowpea; H. Asgedom, et al. (2001) [20] in cereal; and S. Benaseer (2016) [21] in black gram hey concluded that sowing might have enhanced absorption of imbibition water and suitable nutrient concentration, resulting in quick initiation of the germination process and improving physiological parameters.

Table 1. Effects of seed priming with *Spirulina platensis* extract on seed germination, root length and shoot length in black gram CO 6.

Treatment	Germination (%)			Root length (cm)			Shoot length (cm)		
	Primed (P)	*Primed + Aged (A)*	*Mean*	*Primed (P)*	*Primed + Aged (A)*	*Mean*	*Primed (P)*	*Primed + Aged (A)*	*Mean*
T_1	82 (64.90)	44 (41.56)	63 (52.54)	14.23	11.00	12.62	13.03	8.93	10.89
T_2	89 (70.63)	51 (45.57)	70 (56.79)	15.20	11.10	13.15	13.57	9.93	11.75
T_3	98 (81.87)	62 (51.94)	80 (64.16)	16.23	11.97	14.10	14.67	10.17	12.42
Mean	90 (71.57)	52 (46.15)		15.22	11.36		13.76	9.68	
	P	A	PxA	P	A	PxA	P	A	PxA
SEd	0.236	0.192	0.333	0.036	0.029	0.051	0.038	0.031	0.054
CD (p=0.05)	0.514	0.419	0.726	0.078	0.064	0.111	0.068	0.166	0.119

Control, T_2: hydropriming, T_3: priming with *Spirulina platensis* extract at 1.5%. Figures in parenthesis indicate arcsine values.

Table 2. Effects of seed priming with *Spirulina platensis* extract on speed of germination, dry matter production and vigour index in black gram CO 6.

Treatment	Speed of germination			Dry matter production (mg/10 seedlings)			Vigour index		
	Primed (P)	*Primed + Aged (A)*	*Mean*	*Primed (P)*	*Primed + Aged (A)*	*Mean*	*Primed (P)*	*Primed + Aged (A)*	*Mean*
T_1	16.87	10.53	13.70	225.3	147.7	186.5	2168	855	1511
T_2	17.97	12.63	15.30	230.7	161.7	196.2	2501	1095	1798
T_3	22.13	15.87	19.35	250.0	173.0	211.5	2925	1393	2159
Mean	18.99	13.01		235.3	160.8		2531	1114	
	P	A	PxA	P	A	PxA	P	A	PxA
SEd	0.014	0.011	0.019	0.76	0.62	1.07	15.24	12.45	21.57
CD (P=0.05)	0.030	0.024	0.042	1.65	1.35	2.33	33.23	27.13	46.99

T_1: control, T_2: hydropriming, T_3: priming with *Spirulina platensis* extract at 1.5%.

Speed of germination was one of the best methods of analyzing the vigour potential of seeds. The speed of germination of seeds primed with *Spirulina platensis* extract at 1.5% for three hours (T_3) was 22.13 in primed seeds before ageing and 15.87 after accelerated ageing, which was significantly higher than hydropriming (T_2) and control (T_1). *Spirulina platensis* extract consisting of biological chemicals and nutrients involved in the priming process might have triggered the germination process early in primed seeds (Table 2). S.K. Khalil, et al. (2010) [22] also reported that seed priming enhanced the speed and uniformity of germination.

Seeds primed with *Spirulina platensis* extract at 1.5% recorded significantly higher dry matter production (250.0 mg 10 seedling^{-1} before ageing and 173.0 mg 10 seedling^{-1} after accelerated ageing) than hydroprimed and non-primed seeds. The computed vigour index value also recorded a similar trend as that of germination, root and shoot length, speed of germination, and dry matter production. The vigour index of seeds primed with *Spirulina platensis* extract at 1.5% recorded 2925 before ageing of primed seeds and 1393 after accelerated ageing, which was significantly higher than for hydroprimed and control seeds (Table 2). The results are in accordance with S. Benaseer (2016) [21], who reported that dry matter production and vigour index of seed priming with chitosan 400 ppm + PPFM 2% for three hours was higher than other treatments for black gram. These results demonstrated that physiological parameters of seeds primed with *Spirulina platensis* extract at 1.5% were superior to those in hydroprimed and control seeds.

3.2. Biochemical changes in black gram seeds due to priming with Spirulina platensis extract

The biochemical analysis of the black gram seeds revealed that the protein content in primed seeds was higher than that in non-primed seeds (control). However, seeds primed with *Spirulina platensis* extract at 1.5% for three hours (T_3) recorded the highest value of 22.78% while

control (T_1) seeds recorded 22.25% of protein content before ageing. After accelerated ageing, seeds primed with *Spirulina platensis* extract at 1.5% for three hours recorded 18.65% of protein content compared to 17.71% measured in the control (T_1) (Fig. 1). K.H. Koehler, et al. (1997) [23] reported that priming of seed promotes germination by repairing the damaged proteins, RNA, and DNA. In the present study as well, the vitamins, nutrients, and amino acids in the *Spirulina platensis* extract might have influenced the protein content of black gram seeds.

Amylase is an important enzyme that breaks down starch into the most commonly transportable form of sugar. Among the treatments, the α-amylase activity increased significantly in primed treatments compared to non-primed seeds. However, seeds primed with *Spirulina platensis* extract at 1.5% (T_3) registered the maximum α-amylase activity of 14.67 mg maltose/minutes while control seeds (T_1) recorded only 14.36 mg maltose/minutes. Additionally, after artificially ageing, the α-amylase activity was significantly higher in seeds primed with *Spirulina platensis* extract, which recorded 12.12 mg maltose/minute than the control and hydroprimed seeds. Seed priming with *Spirulina platensis* extract improved the seed structure leading it to maintain the seed metabolism to synthesis α-amylase during germination (Fig. 1). Z. Li, et al. (2017) [24] also reported that seed priming enhanced α-amylase content under chilling stress in maize.

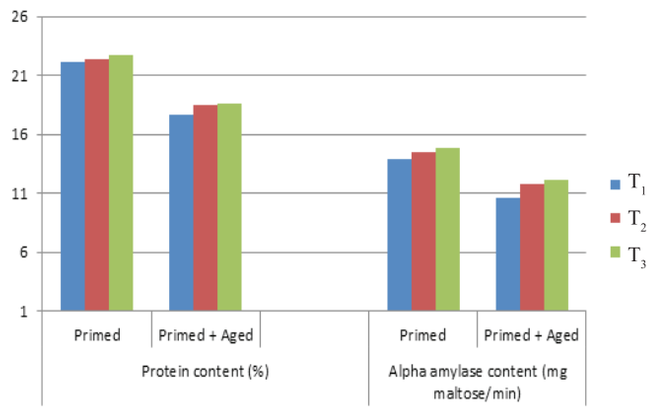

T_1: control, T_2: hydropriming, T_3: priming with *Spirulina platensis* extract 1.5%.

Fig. 1. Effects of seed priming with *Spirulina platensis* extract on protein content and alpha-amylase activity in black gram CO 6.

Gibberillic acid, which is considered an important growth hormone, is quite useful for promotion of seed germination. The seeds primed with *Spirulina platensis* extract at 1.5% (T_3) recorded the highest gibberellic acid content of 80.33 µg/g of fresh weight of seeds while control seeds (T1) recorded the lowest gibberellic acid content of 64.7 µg/g of fresh weight of seeds (Fig. 2). Similar results were also reported by M. Nakaune, et al. (2012) [25], which indicated that gibberellic acid is the major bioactive molecule involved in seed germination. The gibberellic acid content after accelerated ageing was also significantly higher in seeds primed with *Spirulina platensis* extract at 1.5% than in the hydroprimed seeds and non-primed control seeds. The *Spirulina platensis* contains more growth regulators, including gibberellic acids, which might be supplied to the seeds during the soaking and drying process.

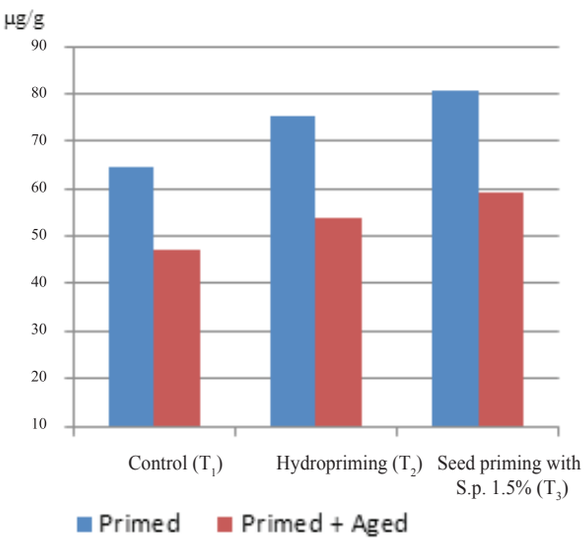

Fig. 2. Effects of seed-priming with *Spirulina platensis* extract on gibberellic acid content in black gram CO 6.

Dehydrogenase is an enzyme that seed germination [26]. All of the living seeds those respiration produce enzymes called dehydrogenase. The results of the study demonstrated that the dehydrogenase enzyme activity in the seeds primed with *Spirulina platensis* extract (T_3) was significantly higher (2.053) compared to hydroprimed (1.561) and control (1.353) seeds. Additionally, after accelerated ageing, seeds primed with *Spirulina platensis* extract recorded higher enzyme activity than hydroprimed and unprimed seeds. Since, *Spirulina platensis* extract includes antioxidants, growth regulators, vitamins, and macro and micro nutrients involved in repair maintenance of the cells, they contributed to promote the dehydrogenase activity in primed seeds and maintained it even under accelerated ageing (Fig. 3).

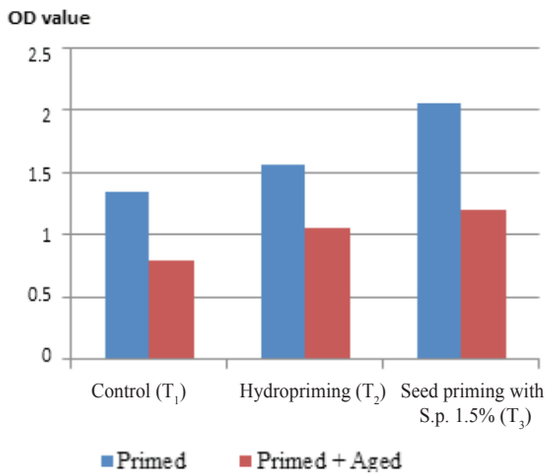

Fig. 3. Effects of seed-priming with *Spirulina platensis* extract on dehydrogenase activity in black gram CO 6.

Lipid peroxidation is the oxidative degradation of lipids. It is the process in which free radicals steal electrons from the lipids in cell membranes, resulting in cell damage. Therefore, lipid peroxidation is a factor indicated for degree of seed deterioration. In this study, seeds primed with *Spirulina platensis* extract (T_3) recorded a lower lipid peroxidation value (0.089) than the control (T_1) seeds, which recorded the highest value (0.135). Artificially aged seeds demonstrated an increase in lipid peroxidation, however, seeds primed with 1.5% *Spirulina platensis* extract recorded a minimum value (0.176), significantly lower than hydroprimed (0.190) and control (0.212) seeds. These results indicated that seeds primed with the *Spirulina platensis* extract demonstrated improved seed vigour by mitigating lipid peroxidation (significantly lower than in non-primed seeds) he seed vigour welleven under accelerated ageing. It might be due to the antioxidants in the *Spirulina platensis* extract react with lipids and the free radicals, leading to seed quality and reduced deterioration (Fig. 4).

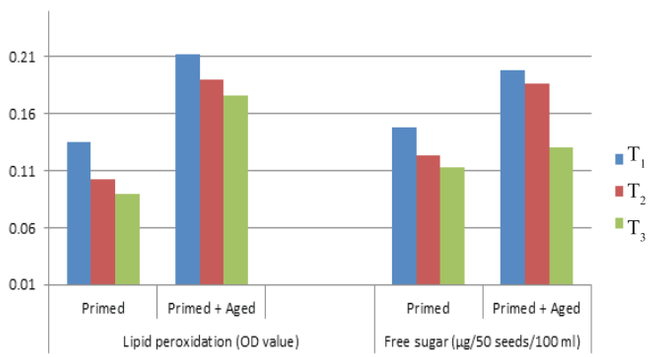

T_1: control, T_2: hydropriming, T_3: priming with *Spirulina platensis* extract 1.5%.

Fig. 4. Effects of seed priming with *Spirulina platensis* extract on lipid peroxidation and free sugar in black gram CO 6.

Free sugar content in seed leachate is an index of cell membrane integrity and seed vigour. The leachate of seeds primed with *Spirulina platensis* extract for three hours (T_3) recorded the minimum free sugar content (0.113 µg/50 seeds/100 ml) while the control (T1) recorded 0.148 µg/50 seeds/100 ml. This trend was noticed even after accelerated ageing of seeds. Conversely, non-primed and hydroprimed seeds recorded higher free sugar content both before and after accelerated ageing (Fig. 4). It could be the seeds primed with *Spirulina platensis* extract maintained cell membrane integrity and tolerance to accelerated ageing. K. Chiu, et al. (2002) [27] reported that improvement in germination by priming might be due to enhanced repair of membranes that are disrupted during maturation drying. This is indirectly supported by the reduced leakage of electrolytes from primed seeds, since electrolyte leakage is in part a result of damaged cell membranes. However, electrolytes may be leaked out during priming, resulting in lower levels of electrolytes in primed seeds than in control seeds.

The results of these studies indicated that the seeds primed with *Spirulina platensis* extract at 1.5% for three hours might have trigger seed germination, vigour, and control over seed deterioration and the mechanism of seed ageing. Moreover, it is reasonable to assume that the priming also affected the rearrangement of cell membrane structure lost during seed ageing and increased the membrane integrity as suggested by E.W. Simon, et al. (1972) [28], J.S. Knyple, et al. (1980) [29], and A.B. Rudrapal, et al. (1988) [30].

4. Conclusions

From this study, it could be concluded that the seeds primed with *Spirulina platensis* extract at 1.5% for three hours significantly improved physiological parameters such as seed germination, speed of germination, dry matter production, seedling length, and vigour index. Additionally, the seeds primed with *Spirulina platensis* extract also recorded vigour associated with biochemical parameters such as protein content, gibberellic acids content, α-amylase activity, and dehydrogenase activity accompanied with lower lipid peroxidation and free sugar in seed leachate of black gram seeds.

COMPETING INTERESTS

The author declares that there is no conflict of interest regarding the publication of this article.

REFERENCES

[1] U. Singh, B. Singh (1992), "Tropical grain legumes as important human foods", *Econ. Bot.*, **46(3)**, pp.310-321, DOI: 10.1007/BF02866630.

[2] P.S. Basu (2011), *Vision 2030*, Indian Institute of Pulses Research, Kanpur, India, pp.1-5.

[3] S. Benedetti, S. Rinalducci, F. Benvenuti, et al. (2006), "Purification and characterization of phycocyanin from the blue-green alga Aphanizomenon flos-aquae", *Journal of Chromatography B: Analytical Technologies in the Biomedical and Life Sciences*, **833(1)**, pp.8-12, DOI: 10.1016/j.jchromb.2005.10.010.

[4] L. Wang, B. Pan, J. Sheng, et al. (2007), "Antioxidant activity of *Spirulina platensis* extracts by supercritical carbon dioxide extraction", *Food Chemistry*, **105(1)**, pp.36-41, DOI: 10.1016/j.foodchem.2007.03.054.

[5] K.J. Bradford (1986), "Manipulation of seed water relations via osmotic priming to improve germination under stress conditions", *Hort. Science*, **21(5)**, pp.1105-1112, DOI: 10.21273/HORTSCI.21.5.1105.

[6] M. Farooq, S.M. Barsa, A. Wahid (2006), "Priming of field-sown rice seed enhances germination, seedling establishment, allometry and yield", *Plant Growth Regulation*, **49(2-3)**, pp.285-294, DOI: 10.1007/s10725-006-9138-y.

[7] K. Ramamoorthy, K. Sujatha (2007), "Effect of seaweed extracts on the ageing of black gram seeds", *Seaweed Res. Utiln.*, **29(1&2)**, pp.119-127, DOI: 10.22271/chemi.2020.v8.i3j.9300.

[8] ISTA (2015), *International Rules for Seed Testing*, International Seed Testing Association, pp.25-30.

[9] A.A.A. Baki, J.D. Anderson (1973), "Vigour determination in soybean seed by multiple criteria", *Crop Sci.*, **13(6)**, pp.630-633, DOI: 10.2135/cropsci1973.0011183X001300060013x.

[10] J.D. Maguire (1962), "Speed of germination - aid in selection and evaluation of seedling emergence and vigour", *Crop Sci.*, **2(2)**, pp.176-177, DOI: 10.2135/cropsci1962.0011183X000200020033x.

[11] D.L. Kittock, A.G. Law (1968), "Relationship of seedling vigor to respiration and tetrazolium chloride reduction by germinating wheat seeds", *Agron. J.*, **60(3)**, pp.286-288, DOI: 10.2134/agronj1968.00021962006000030012x.

[12] M. Somogyi (1952), "Notes on sugar determination", *J. Biol. Chem.*, **195(1)**, pp.19-23.

[13] S.T.Á. Khan, C.G. Young (1973), "Variation in protein content of field peas", *Can. J. of Pl. Sci.*, **53(1)**, pp.37-41, DOI: 10.4141/cjps73-005.

[14] A.K. Paul, S.M. Erji, S.M. Sircar (1970), "Metabolic changes in rice seeds during storage", *Ind. J. Agric. Sci.*, **40(12)**, pp.1031-1036.

[15] A.A. Holbrook, W.J.W. Edge, F. Bailey (1961), *Spectrophotometric Method for Determination of Gibberellic Acid in Gibberellin*, A.C.S. Publications, DOI: 10.1021/ba-1961-0028.ch018.

[16] F. Bernheim, M.L.C. Bernheim, K.M. Wilbur (1948), "The reaction between thiobarbituric acid and oxidation products of certain lipids", *J. Biol. Chem.*, **174(1)**, pp.257-264.

[17] V.G. Panse, P.V. Sukhatme (1985), *Statistical Methods for Agricultural Workers*, Indian Council of Agricultural Research Publication, pp.87-89.

[18] P.B. Ratan, S.E. Reddy, Y.N. Reddy (1993), "Influence of water soaking on *Annona squamosa* L. seed germination and subsequent seedling growth", *South Indian Horticultural Journal*, **41(3)**, pp.171-173.

[19] J. Vijaya (1996), *Standardisation of Pre Sowing Seed Management Technique for Pulses*, MSc. (Ag.) Thesis, Tamil Nadu Agricultural University, Coimbatore.

[20] H. Asgedom, M. Becker (2001), *Effects of Seed Priming with Nutrient Solutions on Germination, Seedling Growth and Weed Competitiveness of Cereals in Eritrea*, Paper presented at the Deutscher Tropentag, 282pp.

[21] S. Benaseer (2016), *Studies on Seed Priming and Foliar Treatments on Enhancement of Seed Vigour, Productivity and Seed Storability in Blackgram*, MSc. (Ag.) Thesis, Tamil Nadu Agricultural University, Coimbatore.

[22] S.K. Khalil, S. Khan, A. Rehman, et al. (2010), "Seed priming and phosphorus application enhance phenology and dry matter production of wheat", *Pak. J. Bot.*, **42(3)**, pp.1849-1856.

[23] K.H. Koehler, B. Voight, H. Spittler, et al. (1997), "Biochemical events after priming and Osmoconditioning of seeds", *Basic and Applied Aspects of Seed Biology*, pp.531-536, DOI: 10.1007/978-94-011-5716-2_58.

[24] Z. Li, J. Xu, Y. Gao, et al. (2017), "The synergistic priming effect of exogenous salicylic acid and H_2O_2 on chilling tolerance enhancement during maize (*Zea mays* L.) seed germination", *Frontiers in Plant Science*, **8**, DOI: 10.3389/fpls.2017.01153.

[25] M. Nakaune, A. Hanada, Y.G. Yin, et al. (2012), "Molecular and physiological dissection of enhanced seed germination using short-term low-concentration salt seed priming in tomato", *Plant Physiology and Biochemistry*, **52**, pp.28-37, DOI: 10.1016/j.plaphy.2011.11.005.

[26] F.J.M. Sung, Y.H. Chang (1993), "Biochemical activities associated with priming of sweet corn seeds to improve vigour", *Seed Sci. & Technol.*, **21(1)**, pp.97-105.

[27] K. Chiu, C. Chen, J. Sung (2002), "Effect of priming temperature on storability of primed *sh*-2 sweet corn seed", *Crop Science*, **42(6)**, pp.1996-2003, DOI: 10.2135/cropsci2002.1996.

[28] E.W. Simon, R.M. Raja Harun (1972), "Leakage during seed imbibition", *J. Exp. Bot.*, **23(7)**, pp.1076-1085.

[29] J.S. Knyple, K.M. Janas, A. Radzziwonoska-Jozwiak (1980), "Is enhanced vigor in soybean (*Glycine max*) dependent on activation of protein turnover during controlled hydration of seed", *Physiol. Veg.*, **18(1)**, pp.157-161.

[30] A.B. Rudrapal, S. Nakamura (1988), "Use of halogens in controlling eggplant and radish seed deterioration", *Seed Sci. & Technol.*, **16**, pp.115-122.

DOI: 10.31276/VJSTE.63(1).42-46

Evaluation of clinical characteristics and lower esophageal sphincter pressure on high resolution manometry in achalasia patients after treatment

Linh Nguyen Thuy[1], Trang Tran Thi Thu[1], Hue Luu Thi Minh[1], Hang Dao Viet[1, 2*]

[1]The Institute of Gastroenterology and Hepatology, 9 Dao Duy Anh Street, Kim Lien Ward, Dong Da District, Hanoi, Vietnam
[2]Hanoi Medical University, 1 Ton That Tung Street, Kim Lien Ward, Dong Da District, Hanoi, Vietnam

Received 2 July 2020; revised 19 September 2020; accepted 2 October 2020

Abstract:

Objective: To describe the clinical characteristics and lower esophageal sphincter (LES) pressures on high-resolution manometry (HRM) in patients with achalasia pre- and post-treatment. Methods: A case series study was conducted in achalasia patients. Clinical symptoms, Eckardt score, upper gastrointestinal endoscopy, esophageal barium swallow, and HRM results were collected on baseline and Eckardt score and HRM results on follow-up were collected. Results: From June 2018 to December 2019, 14 patients were recruited including 6 males and 8 females with mean age of 34.6±10.5 y. The proportion of achalasia type I, II, and III were 28.6, 64.3, and 7.1%, respectively. The Eckardt score, LES resting pressure (for both baseline period and swallow phase) and 4-s integrated resting pressure (IRP4s) significantly decreased after treatment ($p<0.05$). There was a correlation between pre-treatment LES resting pressure (in swallow phase) and change in chest pain score ($p=0.044$, $r=0.546$) and a correlation between pre-treatment IRP4s and change in Eckardt score ($p=0.041$, $r=0.549$). IRP4s had no significant difference between treatment success and recurrence groups. After treatment, 11 patients had clinical success and 3 patients recurred/failed after a median of 4 mo. The diagnosis on HRM after treatment included 5 achalasia (4 type I and 1 type II), 1 esophagogastric junction outflow obstruction (EGJOO), 1 distal esophageal spasm (DES), 6 absent contractility, and 1 ineffective esophageal motility (IEM). Conclusion: Eckardt score, LES pressure, and IRP4s improved significantly after treatment. Besides the role of classification and treatment option, HRM could be used to predict the treatment outcome in achalasia.

Keywords: **achalasia, high resolution manometry (HRM), lower esophageal sphinte, treatment.**

Classification number: **3.2**

1. Introduction

Achalasia is a rare disease characterized by the absence of normal esophageal peristalsis and impaired lower esophageal sphincter (LES) relaxation. The incidence is 1.1-2.2 per 100,000 population and the prevalence is 10-15.7 per 100,000 population [1, 2]. Typical symptoms include difficulty swallowing, regurgitation, chest pain, heartburn, and weight loss.

Current guidelines recommend high-resolution manometry (HRM) as the gold standard in diagnosing and classifying achalasia [1, 2]. The Chicago classification version 3.0 (CC3.0) classifies achalasia into three subtypes, I, II and III, based on the manometric pattern of esophageal peristalsis [3]. These subtypes each have a different prognosis in treatment responses with type III having the highest risk of treatment failure and recurrence. Thus, diagnosis and classification are valuable for the management of achalasia [4, 5]. The primary treatment goal is to alleviate symptoms and to improve patient's quality of life [1, 6]. However, it is reported that nearly 50% of patients fail to respond to treatment and about 10% of patients recur [7, 8].

*Corresponding author: Email: hangdao.fsh@gmail.com

In such cases, physicians usually need to evaluate clinical symptoms, timed barium (for esophageal emptying), and HRM before deciding which treatment is appropriate [1, 9].

T.X. Hung, et al. (2017) [10] studied the changes in clinical symptoms, endoscopy, and barium study in Vietnamese achalasia patients with pneumatic dilatation (PD). They found that the Eckardt score significantly improved after treatment and there was a correlation between and treatment outcomes. The authors, however, did not use esophageal manometry to confirm the diagnosis and classify the subgroups. Therefore, in this study, we aimed to evaluate changes in HRM parameters as well as clinical symptoms in treated achalasia patients.

2. Methods

2.1. Subjects

We conducted a retrospective study on patients who were diagnosed with achalasia on HRM (using CC3.0), treated for achalasia, and performed HRM again after treatment between June 2018 and December 2019 at the Institute of Gastroenterology and Hepatology. Data were collected from archived medical records.

2.2. Study design

2.2.1. Study procedures: Collected retrospective data included clinical symptoms, Eckardt score, findings on upper gastrointestinal endoscopy and esophageal barium swallow, and HRM results on baseline and Eckardt score and HRM results on follow-up. Patients often visited for follow-up after 1 mo of treatment or when they had symptoms suggesting recurrence.

Treatment outcome was evaluated by the follow-up Eckardt score: treatment success (Eckardt score ≤3) and recurrence/failure (Eckardt score >3) [1].

All HRM investigations were measured by the Solar GI system (Laborie) with a 22-channel water-perfused catheter.

2.2.2. Statistical analysis: Data was entered by EpiData version 3.1 and analysed by SPSS version 23.0. Qualitative variables are presented as number and percentage. Quantitative variables are presented as mean (standard deviation) or median (interquartile range). Differences among independent groups were tested by the paired *t*-test or Wilcoxon signed-rank test.

3. Results

3.1. Patient characteristics

Between June 2018 and December 2019, 14 patients were eligible. The most common subtype was type II (64.3%). Table 1 presents baseline characteristics of the patients in the study.

Table 1. Patient characteristics.

Characteristic	Result*
Age (mean±SD)	34.6±10.5
Gender: female/male	8/6
Clinical symptoms	
Dysphagia	13 (92.9)
Globus	5 (35.7)
Vomiting/nausea	10 (71.4)
Chest pain	6 (42.9)
Heartburn	1 (7.1)
Regurgitation	12 (85.7)
Eckardt score	6.5 (1.3), 3-9
Symptom duration (months)	21 (75), 10-142
Endoscopic findings	
Reflux esophagitis	2 (14.3)
Los Angeles classification: A/B/D	2/0/0
Barrett's esophagus	0 (0)
Achalasia	
Endoscopy diagnosis	12 (85.7)
Barium swallow diagnosis	10 (71.4)
HRM subtypes	
Type I	4 (28.6)
Type II	9 (64.3)
Type III	1 (7.1)

*: qualitative variables are presented as number (%); quantitative variables are presented as mean±standard deviation, min - max or median (interquartile range), min - max.

3.2. Changes in clinical symptoms and HRM metrics after treatment

The median follow-up duration was 71 days (min-max 22-330). Of all the patients, 9 (64.2%), 3 (21.4%), 1 (8.2%), and 1 (8.2%) were treated with peroral endoscopic myotomy (POEM), pneumatic dilatation, surgery, and pharmacologic therapy, respectively. At follow-up time, 11 patients had an Eckardt score ≤3 and 3 patients had an Eckardt score >3.

The mean Eckardt score decreased from 6.5 (1.3) to 2 (2.3) (p=0.001). All component scores, except chest pain, improved significantly (Table 2).

Table 2. Changes in Eckardt score and HRM metrics.

Characteristic	Baseline	After treatment	p
Eckardt score	6.5 (1.3), 3-9	2 (2.3), 0-8	0.001
Weight loss	1 (1.3), 0-2	0 (0), 0-2	0.008
Dysphagia	3 (0.3), 0-3	1 (1), 0-3	0.006
Chest pain	1 (1.0), 0-2	0 (1), 0-1	0.083
Regurgitation	2 (2.0), 1-3	0 (1), 0-2	0.002
HRM metrics			
Resting LESP, baseline (mmHg)	34.6±10.0	21.3±11.7	0.005
Resting LESP, swallow (mmHg)	33.3±7.2	21.0±10.3	0.003
IRP4s (mmHg)	26.3±6.2	15.1±9.2	0.003
LES length (cm)	3.6±0.8	3.2±0.5	0.053

LESP: lower esophageal sphincter pressure; significant p-values are in bold.

Baseline and swallow LES resting pressure and IRP4s significantly decreased after treatment ($p<0.05$). There was no difference in LES length before and after treatment (p=0.053).

The correlation between changes in pre-treatment HRM metrics and the change in Eckardt score after treatment is listed in Table 3. There was a correlation between the mean LES pressure (swallow phase) and the change in chest pain score (p=0.044, r=0.546) and between IRP4s and the change in Eckardt score (p=0.042, r=0.549).

Table 3. Correlation between pre-treatment HRM metrics and changes Eckardt scores (p values).

Eckardt score	LES (resting baseline)	LES (swallow phase)	IRP4s
Δ weight loss	0.967	0.863	0.803
Δ dysphagia	0.725	0.734	0.184
Δ chest pain	0.152	0.044	0.055
Δ regurgitation	0.917	0.976	0.224
Δ total score	0.417	0.295	0.042

Δ = before - after; significant p-values are in bold.

3.3. Comparison characteristics between treatment success and recurrence/failure group

The post-treatment HRM diagnoses included achalasia type I (4 patients), achalasia type II (1), absent contractility (6), esophagogastric junction outflow obstruction-EGJOO (1), distal esophageal spams-DES (1), and ineffective esophageal motility-IEM (1) (Fig. 1).

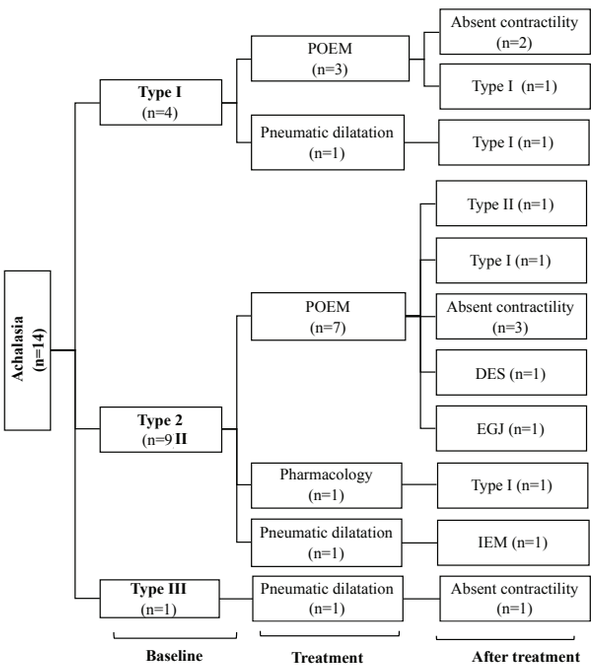

Fig. 1. HRM diagnosis after treatment.

The overall success rate was 78.6%. The success rates of type I, II, and III were 75.0%, 77.98%, and 100% (1 patient), respectively. In the success group, the number of patients receiving POEM, PD and surgery was 7, 3, and 1, respectively. There were 3 patients in the recurrence/failure group, 2 patients were performed POEM and 1 patient received pharmacologic therapy (Table 4). There were no differences in age, gender, symptom duration, Eckardt score, LES pressures (both baseline and swallow), IRP4s, and LES length before treatment between the 2 groups. After treatment, there was no significant difference in post-treatment HRM metrics between 2 groups (Table 5).

Table 4. Characteristics of patients in recurrence/failure group.

Case no.	Age	Gender	Type		Treatment	Erkardt score		Resting LESP baseline (mmHg)		Resting LESP swallow (mmHg)		IRP4s (mmHg)		LES length (cm)	
			Baseline	*After treatment*		*Baseline*	*After treatment*	*Baseline*	*After treatment*	*Baseline*	*After treatment*	*Baseline*	*After treatment*	*Baseline*	*After treatment*
1	54	M	Type II	Type II	POEM	9	8	23.8	23.9	24.2	24.2	19.3	19.2	4.0	3.8
2	20	F	Type I	Absent contractility	POEM	5	4	41.3	21.7	36.6	21.9	23.9	14.2	3.4	3.0
3	34	M	Type II	Type I	Pharmacology	6	5	36.0	29.8	32.4	24.2	26.3	20.6	3.0	3.0

Table 5. Comparison clinical HRM metrics between treatment success and recurrence/failure group.

Characteristics	Success (n = 11)	Recurrence/failure (n = 3)	p*
HRM metrics			
IRP4s	14.6±9.9	18.0±3.4	0,582
IRP4s ≥15 mmHg	45.5%	66.7%	0.515
Δ resting LESP (baseline) (mmHg)	13.2 (-11.1-40,8)	6.2 (-1-19.6)	0.586
Δ resting LESP (swallow) (mmHg)	16.3 (-5.9-34.3)	8.2 (0-14.7)	0.499
Δ IRP4s (mmHg)	11.9 (-5.2-36.8)	5.7 (0.1-9.7)	0.392
Δ LES length (cm)	0.4 (-0.7-2.3)	0.2 (0-0.4)	0.696

Δ = before - after; LESP: lower esophageal sphincter pressure; data are presented as mean±standard deviation, min - max or median (interquartile range), min - max; significant p-values are in bold.
*Mann-Whitney U test.

4. Discussion

In this study, we described the changes in clinical symptoms and lower esophageal sphincter pressure on HRM in post-treatment achalasia patients.

At baseline, type II achalasia was the most common subtype (64.3%), which is in line with previous studies where type II accounted for about two-thirds of achalasia patients [5, 6]. Type II patients often have more favourable outcomes and type III patients have the worst prognosis and are at a higher risk of recurrence (up to 30%) [5]. Therefore, HRM is required to confirm the diagnosis of achalasia and subtypes before selecting treatment modality [1, 2].

POEM was the most common treatment choice in our study. It is a safe treatment with a low rate of serious adverse events, comparable efficacy to surgery, and has a lower rate of recurrence than pneumatic dilatation (PD) after a 2-year follow-up [1, 11]. A preliminary Vietnamese study evaluating the response to POEM found a significant improvement in the Eckardt score at 7 months of follow-up [12]. Therefore, POEM is more frequently indicated for achalasia patients, especially for type III achalasia [1]. Two of nine patients in our study failed to respond to POEM. In such cases, Heller myotomy is preferable because it is more effective than PD [1, 8].

The total Eckardt score and its weight loss, dysphagia, and regurgitation scores, improved significantly after treatment. W.O. Rohof, et al. (2013) [13] found no difference in weight loss score before and after achalasia treatment by pneumatic dilatation or surgery. Both the weight loss and chest pain components in the Eckardt score have been shown to be less reliable, which means they might not reflect treatment response very well [14]. There are several explanations for this. Weight loss is a less common symptom, and the Eckardt score cannot determine whether weight changes result directly from patient's improvement after intervention or from other causes. Chest pain, despite a more common symptom, is caused by obstruction or spasm. Treatment only resolves obstruction and improves esophageal motility but not esophageal spasm, which may result in persistent chest pain after treatment.

In this study, we found that HRM metrics including LES pressures and IRP4s, significantly decreased after treatment. However, 5 patients remained having IRP4s >19 mmHg (cut-off value for water perfused catheter).

Persistent or recurrent achalasia significantly affects quality of life. The most common symptoms in these patients are dysphagia and regurgitation. Dysphagia can suggest post-treatment conditions such as incomplete myotomy, fibrosis, gastroesophageal reflux disease (GERD), absent contractility or functional dysphagia [1]. GERD occurs frequently after treatment (10-31% post PD, 5-35% post-Heller surgery and up to 60% post POEM) but is often effectively managed by proton pump inhibitor (PPI) therapy [1]. Patients with recurrent symptoms should be reassessed for another optimal therapy.

LES pressure and IRP4s in the success group were lower than in the recurrence/failure group, but the difference was not significant. In some previous studies [9], HRM was used to evaluate short-term response to treatment for 3 mo and IRP4s below the cut-off value were used as a factor to define the technical treatment success. Although some patients in our study responded well to treatment, others had persistent achalasia or developed other motility disorders (for example, absent contractility or DES). This suggests follow-up assessment after treatment cannot be based solely on clinical evaluation but requires HRM to examine LES relaxation and other conditions that patients might develop.

Pre-treatment resting LES pressure (in swallow phase) was correlated with the change in the chest pain score and pre-treatment IRP4s was correlated with the change in the total Eckardt score. This suggests that higher LES pressures and IRP4s could predict better improvement after treatment. Similarly, R. Mehta, et al. (2005) [15] showed that the successful group had higher LES pressure than the nonresponse group. Some studies on Heller myotomy also found that high preoperative LES pressure is an independent factor of a good treatment. However, the difference in LES pressure between a responder and nonresponder after achalasia treatment is inconsistent among distinct studies [16]. In a Y. Tang, et al's. study (2015) [17], the changes in the total Eckardt score and weight loss were positively correlated with baseline IRP, and IRP changes after POEM were positively correlated with the Eckardt score changes. These results suggest that a prognostic model to predict

treatment outcomes of achalasia can be developed based on clinical symptoms and HRM metrics.

Small sample size is our major limitation. Future large cohort studies with longer follow-up times are needed to provide a comprehensive picture for achalasia patients treated with different modalities and whether a prognostic model can be developed from HRM metrics as well as clinical parameters.

5. Conclusions

The Eckardt score and IRP4s significantly decreased in achalasia patients after treatment. HRM is important in the diagnosis and classification of achalasia and can help select appropriate treatment and predict outcome.

CRediT author statements

Linh Nguyen Thuy, Trang Tran Thi Thu: Conceptualization, Methodology, Data curation, Formal analysis, Writing - Review & Editing; Hue Luu Thi Minh, Hang Dao Viet: Conceptualization, Methodology, Writing original draft preparation, Writing - Review & Editing.

COMPETING INTERESTS

The authors declare that there is no conflict of interest regarding the publication of this article.

REFERENCES

[1] R. Oude Nijhuis, G. Zaninotto, S. Roman, et al. (2020), "European guidelines on achalasia: United European gastroenterology and European society of neurogastroenterology and motility recommendations", *United European Gastroenterol. J.*, **8(1)**, pp.13-33, DOI: 10.1177/2050640620903213.

[2] M.F. Vaezi, J.E. Pandolfino, M.F. Vela (2013), "ACG clinical guideline: Diagnosis and management of achalasia", *Am. J. Gastroenterol*., **108(8)**, pp.1238-1249, DOI: 10.1038/ajg.2013.196.

[3] P.J. Kahrilas, A.J. Bredenoord, M. Fox, et al. (2015), "The Chicago classification of esophageal motility disorders, v3.0", *Neurogastroenterol. Motil.*, **27(2)**, pp.160-174, DOI: 10.1111/nmo.12477.

[4] J.E. Pandolfino, M.A. Kwiatek, T. Nealis, et al. (2008), "Achalasia: A new clinically relevant classification by high-resolution manometry", *Gastroenterology*, **135(5)**, pp.1526-1533, DOI: 10.1053/j.gastro.2008.07.022.

[5] R. Salvador, M. Costantini, G. Zaninotto, et al. (2010), "The preoperative manometric pattern predicts the outcome of surgical treatment for esophageal achalasia", *J. Gastrointest. Surg*., **14(11)**, pp.1635-1645, DOI: 10.1007/s11605-010-1318-4.

[6] M. Müller (2015), "Impact of high-resolution manometry on achalasia diagnosis and treatment", *Annals of Gastroenterology*, **28(1)**, pp.3-9.

[7] R. Frankhuisen, M.A. Herwaarden, R. Heijkoop, et al. (2007), "Persisting symptoms and decreased health-related quality-of-life in a cross-sectional study of treated achalasia patients", *Aliment. Pharmacol. Ther.*, **26(6)**, pp.899-904, DOI: 10.1111/j.1365-2036.2007.03423.x.

[8] F.B. Hoeij, F.A. Ponds, Y. Werner, et al. (2018), "Management of recurrent symptoms after per-oral endoscopic myotomy in achalasia", *Gastrointest. Endosc.*, **87(1)**, pp.95-101, DOI: 10.1016/j.gie.2017.04.036.

[9] P.J. Kahrilas, A.J. Bredenoord, M. Fox, et al. (2017), "Expert consensus document: advances in the management of oesophageal motility disorders in the era of high-resolution manometry: A focus on achalasia syndromes", *Nat. Rev. Gastroenterol. Hepatol.*, **14(11)**, pp.677-688, DOI: 10.1038/nrgastro.2017.132.

[10] T.X. Hung, V.T. Khanh, D.V. Long (2017), "Short term therapeutic effects of pneumatic balloon dilatation for the treatment of achalasia under endoscopic guidance", *Journal of Vietnam Association of Gastroenterology*, **47**, pp.2939-2944 (in Vietnamese).

[11] F.A. Ponds, P. Fockens, A. Lei, et al. (2019), "Effect of peroral endoscopic myotomy vs pneumatic dilation on symptom severity and treatment outcomes among treatment-naive patients with achalasia: A randomized clinical trial", *JAMA*, **322(2)**, pp.134-144, DOI: 10.1001/jama.2019.8859.

[12] L.Q. Nhan (2019), "Short-term result of peroral endoscopic myotomy for achalasia at University Medical Center at Ho Chi Minh city", *25th National Scientific Congress on Gastroenterology.*

[13] W.O. Rohof, R. Salvador, V. Annese, et al. (2013), "Outcomes of treatment forachalasia depend on manometric subtype", *Gastroenterology*, **144(4)**, pp.718-725, DOI: 10.1053/j.gastro.2012.12.027.

[14] T.H. Taft, D.A. Carlson, J. Triggs, et al. (2018), "Evaluating the reliability and construct validity of the Eckardt symptom score as a measure of achalasia severity", *Neurogastroenterology and Motility: The Official Journal of The European Gastrointestinal Motility Society*, **30(6)**, DOI: 10.1111/nmo.13287.

[15] R. Mehta, A. John, S. Sadasivan, et al. (2005), "Factors determining successful outcome following pneumatic balloon dilation in achalasia cardia", *Indian J. Gastroenterol.*, **24(6)**, pp.243-245.

[16] R.A.B.O. Nijhuis, L.I. Prins, N. Mostafavi, et al. (2020), "Factors associated with achalasia treatment outcomes: Systematic review and meta-analysis", *Clin. Gastroenterol. Hepatol.*, **18(7)**, pp.1442-1453, DOI: 10.1016/j.cgh.2019.10.008.

[17] Y. Tang, C. Xie, M. Wang, et al. (2015), "Association of high-resolution manometry metrics with the symptoms of achalasia and the symptomatic outcomes of peroral endoscopic myotomy", *PLOS ONE*, **10(9)**, DOI: 10.1371/journal.pone.0139385.

DOI: 10.31276/VJSTE.63(1).47-53

Study on cancer stem cell labeling and inhibition efficiency of LV3 nanocomplex *in vitro*

Le Nhat Minh[1], Vo Trong Nhan[1], Thi Thao Do[2], Tran Thu Huong[3], Le Tri Vien[4], Phung Thi Kim Hue[1*]

[1]*Hung Vuong Gifted High School, 48 Hung Vuong Street, Ia Kring Ward, Pleiku City, Gia Lai Province, Vietnam*
[2]*Institute of Biotechnology, Vietnam Academy of Science and Technology, 18 Hoang Quoc Viet Street, Nghia Do Ward, Cau Giay District, Hanoi, Vietnam*
[3]*Institute of Materials Science, Vietnam Academy of Science and Technology, 18 Hoang Quoc Viet Street, Nghia Do Ward, Cau Giay District, Hanoi, Vietnam*
[4]*Institute of Health Research and Educational Development in Central Highlands, 3 Le Hong Phong Street, Dien Hong Ward, Pleiku City, Gia Lai Province, Vietnam*

Received 2 March 2020; revised 9 May 2020; accepted 22 May 2020

Abstract:

Cancer stem cells (CSCs) are the cancer cells that have abilities to self-renew, differentiate into defined progenies, and to initiate and maintain tumour growth. They also contribute to cancer metastasis and therapeutic resistance, both of which are the principal causes of cancer mortality. Therefore, finding efficient fluorescent materials for CSC labelling and basic research is an urgent need. Thus, this research is focused on using a rare-earth element, which is the fluorescent Tb^{3+} nano-ion, and the CD133 monoclonal antibody to create a CSC-targeting nanocomplex (LV3). Tb^{3+} nanorods were silica-surface treated and $-NH_2$ activated before being conjugated with the monoclonal antibody (mAb) against CD133, a typical CSC surface marker. The use of robust fluorescent Tb^{3+} nanorods was to decrease the toxicity of a high-dose prober while the CD133 mAb would increase the CSC's specific binding capacity of the LV3. The fluorescent properties of the coupled LV3 complex were measured and CSC-targeting label activities on the pluripotent human embryonal carcinoma cell line (NTERA-2) were observed. The obtained results presented fluorescent images of LV3 exposed to NTERA-2 cells under microscopy. LV3 also demonstrated that it effectively labelled up to 99.68% of the tested NTERA-2 cells. By contrast, LV3 only labelled 1.44% of the CCD-18Co human healthy cells. On the other hand, LV3 exhibited anti-CSC activity, which inhibited 11.14% *in vitro* and 30.5% tumourspheroid growth of NTERA-2 cells. In conclusion, LV3 showed its efficiency in specific CSC target labelling and inhibition, which could be further applied to fundamental and preclinical research.

Keywords: **cancer stem cells, CCD-18Co, CD133 monoclonal antibody, ion Tb^{3+}, LV3, NTERA-2.**

Classification number: **3.2**

1. Introduction

Despite abundant ongoing research efforts, cancer remains one of the most challenging diseases to treat globally. Due to the heterogeneous nature of cancer, one of the major clinical challenges is the ability of cancer to develop resistance in therapeutic development. It has been hypothesized that cancer stem cells (CSCs) are the cause of this resistance and targeting their treatment will lead to tumour regression [1]. CSCs accounts for a small percentage of tumours and can regenerate into various tumorous cell types causing the growth and expansion of malignancy. CSCs present drug-resistant abilities and overcome radiotherapy. Then, the survival of cancer stem cells after treatment allows the tumour to recur and spread throughout the body. Therefore, CSCs are considered a promising target for research and discovery of more effective anticancer drugs or therapies. CSCs are characterized by several specific surface markers. A pentaspan transmembrane glycoprotein, CD133, has been suggested to mark cancer stem cells in various tumour types. However, the accuracy of CD133 as a cancer stem cell biomarker has been highly controversial [1]. CD133 is known as prominin-1, a transmembrane glycoprotein, and is a common surface marker for CSCs, which are inside of various cancer tumours. This transmembrane CD133 glycoprotein includes an extracellular N-terminus and an intracellular C-terminus, which have been used as an efficacious typical surface antigen to detect and to isolate CSCs [2]. As recognized, traditionally nanotechnological biomedicine heighten pharmaceutical properties and reduce the systemic toxicity of chemotherapy through selectively targeting and effectively transferring anticancer drugs to tumours. Nanoparticles usually improve the therapeutic index of the chemotherapeutic drugs that are enveloped inside or combined with the nanoparticle surfaces. For

*Corresponding author: Email: whitelily109@gmail.com

example, rare-earth elements such as Tb^{3+} nano-materials or cation terbium (III) emitting green fluorescence would effectively assist in detection and treatment [3]. Thus, experimental and clinical applications of CSC labelling and tracking are interesting to evaluate cell location. Rare-earth-based nanotechnology would be very helpful [4].

Also, several studies on nanomaterial labelling effects targeting cancer cells have been reported elsewhere [5, 6]. According to the previous report from the authors in this study [7], Tb^{3+} a rare-earth ion could constitute a fluorescent nanomaterial as terbium orthophosphate monohydrate ($TbPO_4.H_2O$) in the form of hexagonal crystal structure. Fluorescent spectra of $TbPO_4.H_2O$ nanomaterials at pH=2, incubated at 200°C for 24 h, coated by silica, and functionalized with $-NH_2$ measured at 355 nm was determined by iHR55 system (Jobin-Yvon). The fluorescent images of human colorectal adenocarcinoma cells (HT-29) were observed by the effects of the complex of the surface-functionalized $TbPO_4.H_2O$-NH_2 and the anti-CD133 mAb [7]. Our previous study also reported that the fluorescent Tb^{3+} nano-ion and CD133 mAb conjugation (ET complex) gave marks on 26.89% (of colorectal cancer cells) [8] and 97.74% (of NTERA-2 cells) compared to the control, respectively [9]. To continue this study, we modify the content of one component of the RT2 [9] complex to make LV3 and attempted to evaluate the CSC growth inhibition activities of the LV3 complex.

2. Material and method

2.1. Materials

LV3 is made from nano Tb^{3+}-monoclonal antibody (RT) transport system [9].

The pluripotent human embryonal carcinoma cell line (NTERA-2) and the human healthy cell line (CCD-18Co) were kindly provided by Dr. P. Wongtrakoongate, Mahidol University, Thailand, and Prof. Chi-Ying Huang, National Yang-Ming University, Taiwan. Cells were maintained in DMEM medium supplement with 10% foetal bovine serum and 1% antibiotics (antibiotics-antimycotics solution, Invitrogen, Carlsbad, CA, USA) in a humidified incubator with 5% CO_2 at 37°C.

Cultured medium so-called Dulbecco's Modified Eagle Medium (DMEM), Foetal bovine serum (FBS), Trypsin-EDTA, antibiotics (antibiotics-antimycotics) were purchased from Invitrogen (Carlsbad, CA, USA). Human CD133 monoclonal antibody and human CD133 antibody conjugated with FITC (FITC-CD133) were from Miltenyi Biotec (Bergisch Gladbach, Germany). Other chemicals were provided by Sigma Aldrich (St. Louis, MO, USA).

2.2. In vitro cell culture

The *in vitro* cell culture was carried out by following the protocols from ATCC Cell Bank (American Type Culture Collection, USA). Accordingly, NTERA-2 and CCD-18Co cells were cultured in T75 flask with DMEM supplemented by 2 mM L-glutamine, 10% foetal bovine serum (FBS), and 1% antibiotic (Anti-Anti solution). The cells were subcultured every 3-5 d with a ratio of 1:3 and incubated in humid conditions of 37°C and 5% CO_2.

2.3. Labelling cells with LV3

- Cancer stem cells and healthy cells imaging: Using LV3: NTERA-2 and CCD-18Co, cells were pre-seeded into a 96-well plate at 10,000 cells/well and incubated at 37°C, 5% CO_2 for 24 h. Then, the culture medium was replaced with 10% formaldehyde to fix the cells for 10 min at room temperature. The cells were triple rinsed with phosphate buffered saline (PBS) to thoroughly remove formaldehyde. Then, 10 µl of LV3 in 190 µl of PBS were placed into each well and incubated at 4°C for 1 h. The unbound sample was removed and triple rinsed with PBS. Finally, 100 µl PBS was added to the wells before observation using an Olympus Scan^R fluorescence microscope (Olympus Europa SE & Co.KG, Hamburg, DE).

- Determining the number of marked cells (through CD133 surface marker) by flow-cytometry: Cancer stem cells (NTERA-2) and healthy cells (CCD-18Co) were seeded into a 6-well plate and incubated at 37°C, 5% CO_2 overnight. After 24 h of incubation, the cells were harvested with trypsin-EDTA and collected into a falcon tube. Cells were re-suspended with DMEM medium containing 2% FBS, LV3, or anti-CD133-FITC mAb and then incubated at 4°C for 10-15 min while protected from light. The number of labelled cells (out of 10000-12000 counting cells) were measured and analysed by Novocyte flow cytometry system (ACEA Bioscience Inc.) and NovoExpress software.

2.4. LV3 cytotoxic determination

The MTT assay was employed according to T. Mosmann (1983) [10] to measure the cytotoxic activity of the LV3 nanocomplex. In short, cells were seeded in 96-well plates and triplicated, then treated with LV3 at various concentrations for 72 h at 37°C, 5% CO_2. Then, 10 µl MTT (5 mg/ml) was added to each well and incubated at

37°C for 4 h. The medium was discarded and the formazan crystal was dissolved by using 50 µl/well dimethlysulfoxide (DMSO). The OD values were measured at 540 nm by a spectrophotometer (BioTek, ELx800). The number of survived cells was calculated by the formula:

$$\% \text{ survived} = \frac{OD(reagent) - OD(blank)}{OD(control) - OD\ (blank)} x100$$

2.5. Measurement of 3D tumoursphere growth inhibitive activities

BALB/c mice macrophages were isolated using a Macrophage Mouse Isolation Kit (Peritoneum) (Miltenyi Biotech., Bergisch Gladbach, Germany). The isolated cells were cultured in DMEM medium containing 10% FBS and 1% antibiotics at 37°C and 5% CO_2.

In order to form tumour spheroids, the hanging drop method was performed. The 1500 NTERA-2 cells in 20 µl of medium were dropped onto the bottom of the 60 mm tissue culture dish lid before inverting that lid onto the 5-ml medium filled bottom dish. The dish was then incubated at 37°C, 5% CO_2, and 95% humidity. After 3-d incubation, cell aggregates formed. These 3D tumourspheres were further co-cultured with macrophages in a 96-well plate. Wells were covered with 1% agarose before the spheroids were transferred to the wells. The macrophage cells were then co-cultured with the spheroids in the wells. The LV3 treatment was performed by directly adding LV3 into the co-culture wells and further incubated for 3 d. The growth of the spheroids was observed under microscopy. The images were analysed using ImageJ software.

2.6. Statistical analysis

The data was reported as mean±standard deviation (SD) and analysed by the GraphPad Prism 7 software using an unpaired *t*-test. A $p<0.05$ was considered statistically significant.

3. Results and discussion

3.1. Probing NTERA-2 and CCD-18Co cells and with LV3 fluorescent nanocomplex

The results exhibited that the NTERA-2 cells were labelled by LV3 and displayed strong fluorescence under fluorescence microscopy (Fig. 1, Table 1). The healthy cells known as CCD-18Co did not emit any corresponding signal under the same condition (Fig. 2). Therefore, LV3 could be specifically targeting cancer stem cells. The obtained results were consistent with the research of L.N. Minh, et al. (2019) [9].

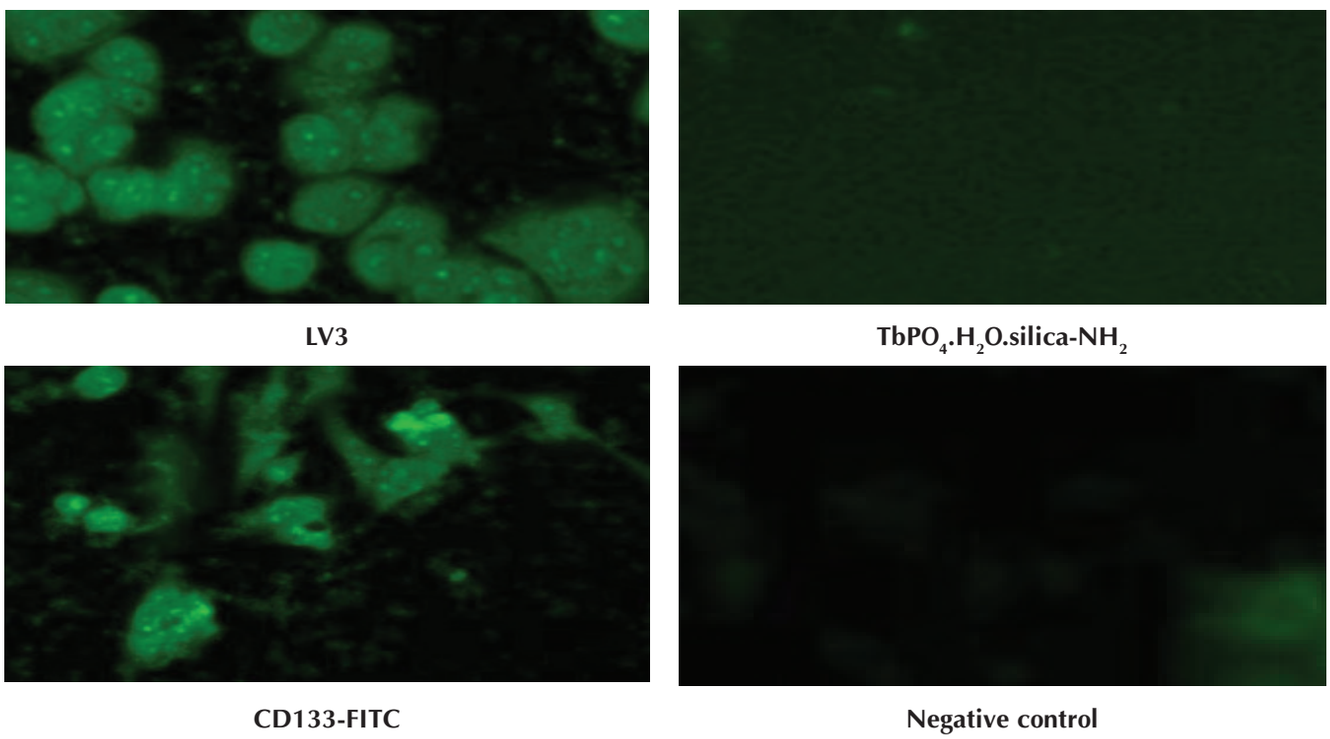

Fig. 1. NTERA-2 cells was probed after 1 h of incubation either with LV3, $TbPO_4.H_2O$.silica-NH_2, CD133-FITC, or without LV3 (negative control) by fluorescence microscopy on an Olympus Scan^R.

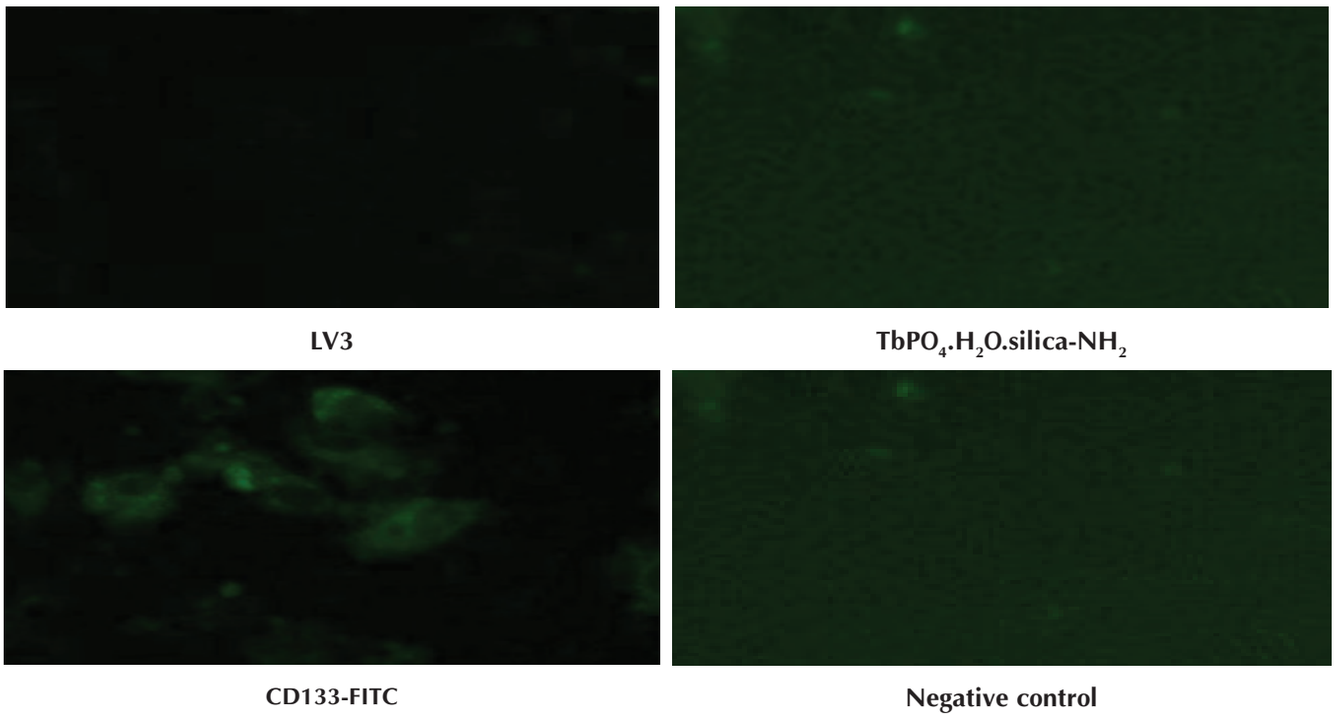

Fig. 2. CCD-18Co cells was probed after 1 h of incubation either with LV3, $TbPO_4.H_2O$.silica-NH_2, CD133-FITC, or without LV3 (negative control) by fluorescence microscopy on an Olympus Scan^R.

Table 1. Labelling performance of cancer stem cells and healthy cells.

Samples	The number of fluorescent detected cells (%)	
	Cancer stem cells (NTERA-2)	*Healthy cells (CCD-18Co)*
LV3	99.68±3.85	1.44±0.11
$TbPO_4.H_2O$.silica-NH_2	0.57±0.07	0.31±0.02
CD133-FITC	95.83±7.31	1.17±0.06
Negative control	0.10±0.02	0.20±0.04

Table 2. Total intensity of samples in examined cell lines.

Samples	Total intensity	
	NTERA-2	*CCD-18Co*
LV3	6011±62.62**	0
CD133-FITC	5497±42.87	0
Negative control	19.00±3.07	0

Negative control sample; LV3 - Experimental sample. Data is expressed as mean ± SE (n=3) combined from three repeated experiments. *Significant differences (t-test, p≤0.05) and **p≤0.01.

The fluorescent intensity was analysed in the LV3-treated NTERA-2 cell line by fluorescence microscope as shown in Table 2. By fluorescence spectroscopy, NTERA-2 emits fluorescence intensity at 6011±62.62 FU, which is statistically significant compared to the negative control. Meanwhile, fluorescence intensity in healthy cells were not measurable. This result is consistent with the study of L.N. Minh, et al. (2019) [9] and is demonstrated in Fig. 1.

3.2. LV3 fluorescent labelling performance by flowcytometry evaluation

We used flow-cytometry to evaluate the labelling specificity of LV3. Detailed results are shown in Table 1 and Fig. 3.

The results showed that the LV3 probed 99.68% of NTERA-2 cells, which was higher than the respective number (0.10%) of the negative control. As a result, it is seen that LV3 labelled NTERA-2 cells more efficiently than the RT labelling of the colorectal cancer cell [9]. Further research is required to elucidate how LV3 could label a cancer stem cell better than in other cancer cell lines.

Besides, LV3 could not label and distinguish CCD-18Co. Thus, LV3 is an effective material for labelling CSCs. These preliminary results demand more studies *in vivo* and clinical testing.

Recent clinical studies have shown that high expression of CD133 in tumours plays an important role as a prognostic marker of disease progression. As such, a spectrum of immunotherapeutic strategies has been developed to target these CD133 positive cells with the goal of translation into the clinic. In one report, the researcher Mi Y used salinomycin-loaded poly (lactic-co-glycolic acid) - poly (ethylene glycol) nanoparticles conjugated with CD133 antibodies (CD133-SAL-NP) to eliminate $CD133^+$ ovarian CSCs. The CD133-SAL-NPs efficiently bound to the $CD133^+$ ovarian cancer cells resulting in an increased

cytotoxic effect toward $CD133^+$ ovarian cancer cells when compared with the untargeted SAL-NPs and salinomycin. The CD133-SAL-NPs reduced the percentage of $CD133^+$ ovarian CSCs in ovarian cells more effectively than treatment with salinomycin or SAL-NPs, suggesting that CD133-SAL-NP targeted $CD133^+$ ovarian CSCs [11].

Herein, rare-earth nano-ion Tb^{3+} conjugated with anti-CD133 mAb to formulate LV3 presents promising CSC labelling and specific targeting capacities. This might also be the first developing stage of rare-earth-based nanomaterials for valuable applications in cancer diagnostics and treatment.

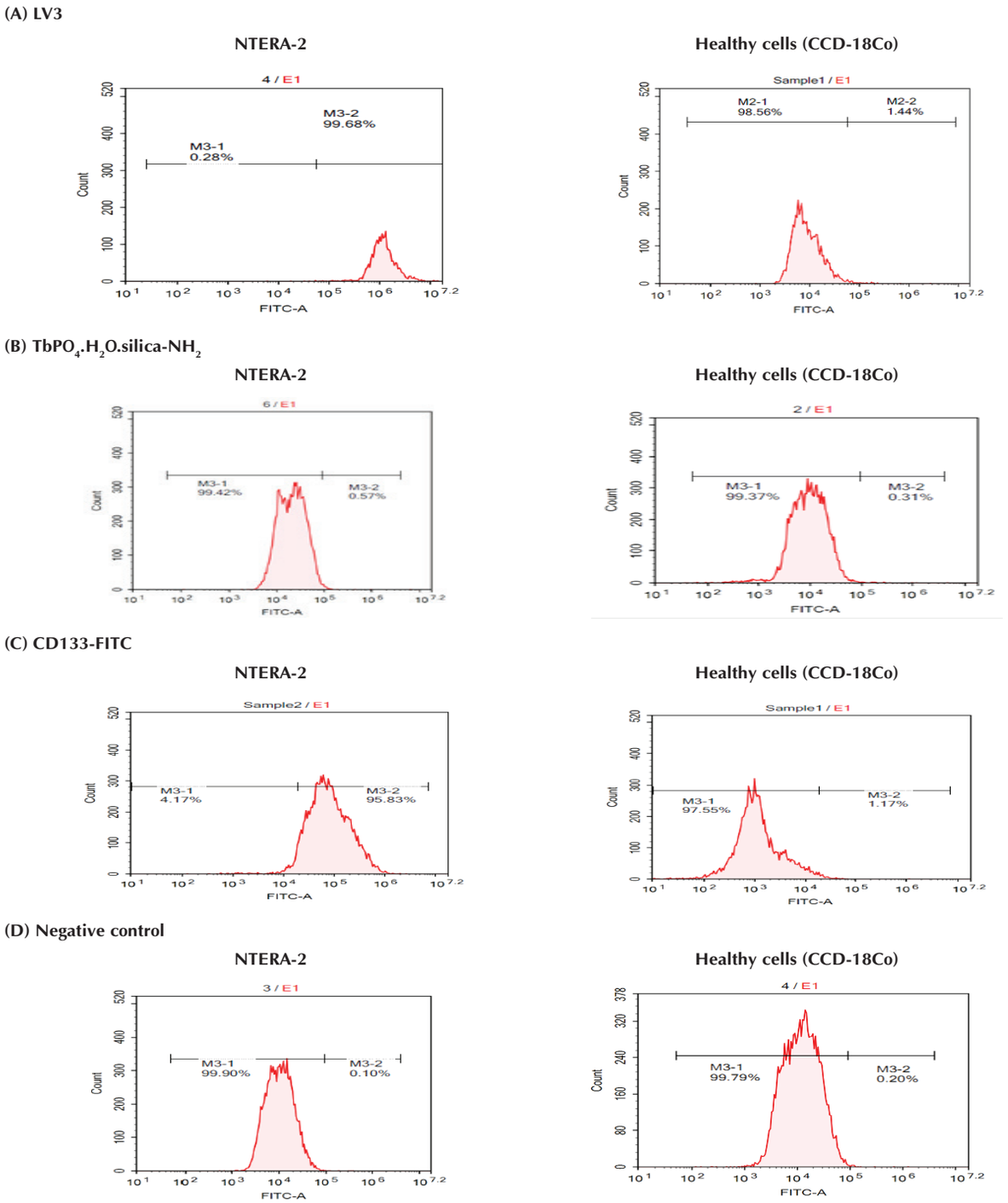

Fig. 3. Flow-cytometry analysis to determine the number of fluorescent labelled cells with various materials: (A) LV3, (B) $TbPO_4.H_2O$.silica-NH_2, (C) CD133-FITC, and (D) negative control.

3.3. Effect of LV3 on the proliferation of NTERA-2

The proliferation of LV3-treated NTERA-2 cell was assessed by using MTT assays. LV3 showed the ability to inhibit the growth of NTERA-2 cells up to 11.14% at a concentration of 10 µg/ml (Table 3). The anti-proliferation of LV3 on NTERA-2 cells was slightly higher than that on CCD-18Co cells.

Table 3. The proliferation of complex on NTERA-2 cells and CCD-18Co cells.

Samples	% proliferation	
	NTERA-2	*CCD-18Co*
LV3	88.86±2.13	95.05±0.68
Negative control	100	100

3.4. Effect of LV3 on NTERA-2 spheroids co-culture with macrophages

Although several CSCs markers have been reported, one of the most promising and possibly least ubiquitous is CD133, a frequently expressed surface marker on CSCs. Some evidence has indicated that directly targeting CD133 with biological drugs might eliminate CSCs effectively [12].

Table 4. 3D tumour spheroids inhibited under the treatment of LV3.

Samples	3D tumour spheroids (%)	Standard deviation
LV3	69.50*	0.81
Negative control	100.00	0.09

Negative control sample; LV3 - Experimental sample. Data is expressed as mean ± SE (n=3) combined from three repeated experiments. * Significant differences (t test, p≤0.05).

In this study, the activity of LV3 inhibited 3D-tumor growth *in vitro* formed by co-culturing 3D NTERA-2 spheroids with macrophages (Table 4; Fig. 4). As a result, the diameters of 3D spheroids dropped to 69.50% in comparison with that of the untreated negative control after a 3-d treatment. Herein, although LV3 slightly inhibited the growth of NTERA-2 cells (11.14%) *in vitro*, this nanocomplex strongly inhibited the growth of these 3D NTERA-2 spheroids (30.5%) when co-cultured with macrophages.

Among the reported markers of the cancer stem cells, CD133 is the most well-known marker for isolating and studying CSCs in different types of cancer. The CD133 high population of cancer cells are not only capable of self-renewal and proliferation but are also highly metastatic and resistant to therapy. Despite limited information on the physiological functions of CD133, many ongoing studies aim to reveal the mechanisms that CD133 utilizes to modulate cancer dissemination and drug resistance [13]. Thus, the role of anti-CD133 antibodies in the LV3 may reduce the function of CD133 and result in the inhibition of CSCs.

According to another report that investigates the cytotoxic, radiation dose-enhancing, and radio-sensitizing ability of five rare-earth oxide nanoparticles on the two immortalized mammalian cell lines U-87 MG and Mo59K, a significant cytotoxicity of Nd_2O_3 and La_2O_3 was observed in U-87 MG cells. As aforementioned, the component of LV3 is terbium (Tb^{3+}), which is a typical lanthanide with green fluorescence that has the potential for biomedical labelling and imaging. Seemingly, terbium in LV3 is likely to have an inhibitory effect on CSCs. In this study, LV3 was

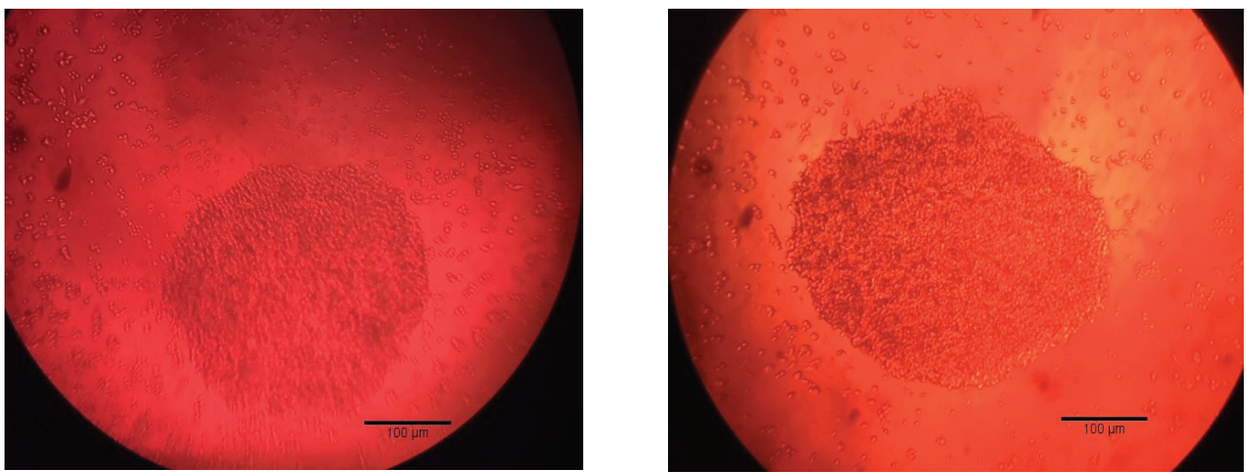

3D tumour treated with LV3 — 3D tumour – negative control

Fig 4. The 3D tumourspheres at the day 3 under the treatment of LV3 and negative control under the fluorescence microscope system Olympus Scan^R 100X.

demonstrated to be a promising target for drug delivery to CSCs and may be useful as an agent to inhibit the growth of cancer by targeting CSCs. LV3 may, therefore, represent a promising approach for the treatment of cancer.

4. Conclusions

LV3, which was a combination between the rare-earth-based Tb^{3+} nanorod and CD133 monoclonal antibody, was assessed for its fluorescent properties and tumoursphere inhibition using cancer stem cells (NTERA-2) and healthy human colon cells (CCD-18Co). The LV3-probed NTERA-2 cells exhibited strong emission under fluorescent microscopic observation. The NTERA-2 labelling efficiency of the LV3 was 99.68% from flow cytometric analysis whereas healthy cells (CCD-18Co) were weakly probed (1.44%). Also, LV3 was shown to be a promising anti-CSC factor in which 11.14% survived inhibition *in vitro* and 30.50% tumourspheroid inhibition of NTERA-2 cells. In conclusion, LV3 has presented as highly effective in targeting cancer stem cells *in vitro*.

CRediT author statements

Le Nhat Minh, Vo Trong Nhan, Thi Thao Do, Tran Thu Huong: Conceptualization, Methodology, Data curation, Formal analysis, Writing - Review & Editing; Le Tri Vien, Phung Thi Kim Hue: Conceptualization, Methodology, Writing original draft preparation, Writing - Review & Editing.

ACKNOWLEDGEMENTS

This research was conducted at Institute of Materials Science and Institute of Biotechnology, Vietnam Academy of Science and Technology, Hanoi, Vietnam. This research was supported and funded by the Institute of Health Research and Educational Development in Central Highlands.

COMPETING INTERESTS

The authors declare that there is no conflict of interest regarding the publication of this article.

REFERENCES

[1] P.M. Glumac, A.M. LeBeau (2018), "The role of CD133 in cancer: A concise review", *Clinical and Translational Medicine*, **7(1)**, DOI: 10.1186/s40169-018-0198-1.

[2] J. Gil, A. Stembalska, K.A. Pesz, et al. (2008), "Cancer stem cells: The theory and perspectives in cancer therapy", *Journal of Applied Genetics*, **49(2)**, pp.193-199, DOI: 10.1007/BF03195612.

[3] T.T. Huong, T.K. Anh, H.T. Khuyen, et al. (2014), "Study on optical properties of nanorods containing rare earth ion Tb^{3+} and Eu^{3+} for biomedical labelling applications of fluorescence", *Vietnam Journal of Science and Technology*, **50(1A)**, pp.126-132.

[4] S. Vinogradov, X. Wei (2012), "Cancer stem cells and drug resistance: The potential of nanomedicine", *Nanomedicine*, **7(4)**, pp.597-615, DOI: 10.2217/nnm.12.22.

[5] W. Arap, R. Pasqualini, M. Montalti, et al. (2015), "Luminescent silica nanoparticles for cancer diagnosis", *Current Medicinal Chemistry*, **20(17)**, pp.2195-2211, DOI: 10.2174/0929867311320170005.

[6] S. Asha, A.N. Ananth, G.V. Kumari, et al. (2017), "Biocompatible fluorescent nano-apatite with ionic silver - its antibacterial activity and cytotoxicity towards cancer cells", *Materials Today: Proceedings*, **4(2)**, pp.4309-4318, DOI: 10.1016/j.matpr.2017.04.001.

[7] D.T. Thao, N.T. Nga, T.T. Huong, et al. (2019), "Evaluate the ability of detecting colorectal cancer cells (HT-29) of nanomaterials from Tb^{3+} rare earth", *Vietnam Journal of Biotechnology*, **3(1A)**, pp.27-32.

[8] L.N. Minh, V.T. Nhan, D.T. Thao, et al. (2020), "Evaluation of potential targeting *in vitro* to colorectal cancer cell from nano Tb^{3+} - monoclonal antibody (RT) transport system", *Journal of Science and Technology*, **56(1)**, pp.95-99.

[9] L.N. Minh, V.T. Nhan, N.T. Nga, et al. (2019), "Labelling efficiency of Tb^{3+} conjugated CD133 monoclonal antibody nanocomplex targeting *in vitro* metastatic cancer cells", *Vietnam Journal of Biotechnology*, **17(3)**, DOI: 10.15625/1811-4989/17/3/14775.

[10] T. Mosmann (1983), "Rapid colorimetric assay for cellular growth and survival: application to proliferation and cytotoxicity assays", *Journal of Immunological Methods*, **65(1-2)**, pp.55-63, DOI: 10.1016/0022-1759(83)90303-4.

[11] Y. Mi, Y. Huang, J. Deng (2018), "The enhanced delivery of salinomycin to CD133+ ovarian cancer stem cells through CD133 antibody conjugation with poly(lactic-co-glycolic acid)-poly(ethylene glycol) nanoparticles", *Oncology Letters*, **15(5)**, pp.6611-6621, DOI: 10.3892/ol.2018.8140.

[12] J.U. Schmohl, D.A. Vallera (2016), "CD133, selectively targeting the root of cancer", *Toxins*, **8(6)**, DOI: 10.3390/toxins8060165.

[13] G.Y. Liou (2019), "CD133 as a regulator of cancer metastasis through the cancer stem cells", *The International Journal of Biochemistry & Cell Biology*, **106**, pp.1-7, DOI: 10.1016/j.biocel.2018.10.013.

DOI: 10.31276/VJSTE.63(1).54-58

Meningococcal disease in one soldier patient: Case report from Vietnam

Nguyen Thanh Viet[1], Nguyen Minh Nam[2], Nguyen Vu Trung[2], Do Tuan Anh[2*], Hoang Van Tong[1, 3*]

[1]Institute of Biomedicine and Pharmacy, Vietnam Military Medical University, 160 Phung Hung Street, Phuc La Ward, Ha Dong District, Hanoi, Vietnam
[2]103 Military Hospital, Vietnam Military Medical University, 261 Phung Hung Street, Phuc La Ward, Ha Dong District, Hanoi, Vietnam
[3]Departments of Pathophysiology, Vietnam Military Medical University, 160 Phung Hung Street, Phuc La Ward, Ha Dong District, Hanoi, Vietnam

Received 1 October 2020; revised 11 December 2020; accepted 23 December 2020

Abstract:

Meningococcal disease is caused by an infection with *Neisseria meningitidis* bacteria, which is responsible for two major forms of the disease including meningitis and/or septicaemia. Humans are the only natural host of *N. meningitidis* and approximately 10% of adults and 24% of adolescence are infected. *N. meningitidis* infection is responsible for two major forms of disease including meningitis and septicaemia globally. *N. meningitidis* remains a significant cause of an endemic and leads to significant morbidity and mortality. Diagnosis of meningococcal disease may be challenging due to clinical signs that vary widely and are often similar to those of other illnesses. Meningococcal disease persists in Vietnamese military populations despite the availability of antibiotics and vaccines. The rate of meningococcal disease in Vietnam is low and no meningococcal sepsis case has yet been reported from Vietnam. Herein, we describe the first meningococcal sepsis case in a Vietnamese military unit and emphasize the beneficial application of a molecular method in the diagnosis of *N. meningitidis* and the successful use of antibiotic treatment.

Keywords: **meningitis, meningococcal disease, *Neisseria meningitidis*, sepsis.**

Classification number: **3.2**

1. Background

Neisseria meningitidis is a Gram-negative diplococcus and aerobic or facultative anaerobic bacterium [1]. Humans are the only natural host of *N. meningitidis* and approximately 10% of adults and 24% of adolescence are infected [2, 3]. *N. meningitidis* infection is responsible for two major forms of disease including meningitis and septicaemia globally [4]. This disease mainly affects infants, preschoolers, and young people [5]. Humans can carry *N. meningitidis* in their nose and throat without any clinical symptoms [1, 3] and thus they are the main source of *N. meningitidis* spread. *N. meningitidis* is transmitted through close contacts such as among family members and military populations [6]. *N. meningitidis* can cause sporadic cases, infect small groups, or cause large epidemics over the world with seasonal variations and the prevalence of asymptomatic carriers varies among countries [7].

Rapid recognition and treatment of meningococcal infection are very important in reducing morbidity and mortality [8]. Therefore, understanding the signs of infection is particularly crucial in Vietnam where the prevalence of disease is low and doctors are likely to ignore [9]. Also, meningococcal disease is an uncommon infection in Vietnam, especially in military units. Sporadic cases of meningococcal disease in soldiers have been reported globally [10-12] but no meningococcal disease case in soldiers has been reported from Vietnam so far. In this report, we provide an attention to this disease in Vietnam and to discuss the clinical aspects such as diagnosis and treatment related to this meningococcal case.

*Corresponding author: Email: hoangvantong@vmmu.edu.vn, drtuananh103@gmail.com

2. Case presentation

2.1. Medical history

A 23-year-old male soldier residing in an army unit located in Phu Man village, Quoc Oai district, Hanoi metropolis, Vietnam was admitted to the the 103 Military Hospital of the Vietnam Military Medical University (VMMU). In the last few years, this military unit had several soldiers infected with *N. meningitidis*. He did not have a history of any infection or travelled to other areas with reported epidemics or exposure to individuals with meningitis.

2.2. Clinical features

On May 1st, 2020, the patient presented with a sore throat, a sudden high fever, chills, impaired consciousness, and haemorrhagic rash on the body. He was taken to a local hospital where he was treated with antipyretics and antibiotic injection (cefotaxime 2 g powder for solution). Once stabilized, he was immediately referred to the 103 Military Hospital of the VMMU and was admitted to the Department of Infectious Disease in critical condition on May 2nd, 2020. On admission, the patient was found with a stiff neck, high fever, confusion, headaches, hypotension (80/50 mmHg), nasal bleeding, oral bleeding, oliguria, and haemorrhagic rash on the body but no photophobia, no nausea, and no vomiting (Fig. 1). Heart rate was increased with a regular rhythm and no rubs, murmurs, or gallops were heard. The lungs were clear to auscultation, the abdomen was tender to palpation, and bowel sounds were positive but no significant distention.

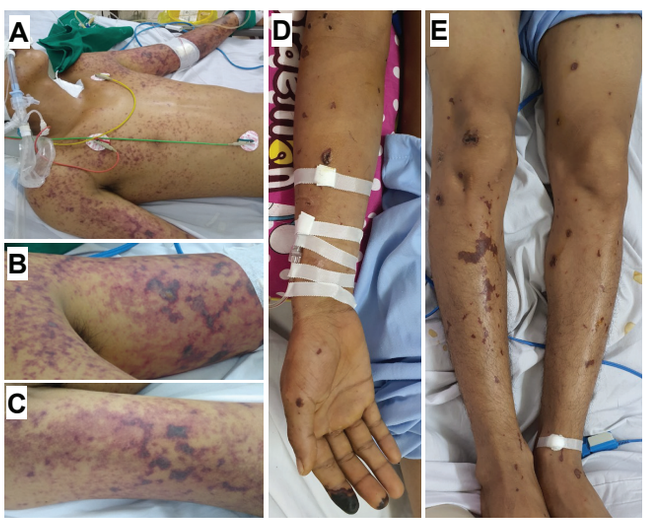

Fig. 1. Widespread purpuric and ecchymotic rash (on day 2). (**A**) Upper body; (**B**) Upper left limb; (**C**) Right limb; (**D**) Right arm; (**E**) Lower limbs.

2.3. Identification of meningitis

Bacterial culture, Gram staining and real-time PCR were immediately performed with the peripheral blood, spinal fluid, and nasopharyngeal specimens. The collection and transport of these specimens and the culture method were followed according to WHO guidelines [13]. The results of the bacterial culture and Gram staining showed that the tested samples were negative for *N. meningitidis*. The real-time PCR results showed positive for *N. meningitidis* in peripheral blood sample only. For the real-time PCR, DNA extraction was performed using the automatic nucleic acid extraction system SaMag-12 (Sacace, Italia) according to the manufacturer's instructions. The real-time PCR assay was performed using the Meningitidis real-time PCR kit for *in vitro* diagnostics (IVD) on the SaCycler-96 real-time PCR system (Sacace, Italia) according to manufacturer instructions.

2.4. Laboratory tests

The results from the laboratory blood tests during hospitalization are shown in Table 1. On admission (day 2 or D2), the laboratory tests showed anaemia, low haemoglobin level, leukopenia, lymphocytopenia, neutrophilia, thrombocytopenia, coagulopathy, decreased fibrinogen and prothrombin levels, and increased international normalized ratio (INR) and activated partial thromboplastin time (APTT) levels. Increased lactate levels revealed tissue hypoperfusion and the increased creatinine and urea nitrogen levels revealed an acute renal failure. The aspartate aminotransferase (AST) and alanine aminotransferase (ALT) levels were in the normal range, which revealed normal liver function. There were significantly increased inflammatory markers such as C-reactive protein and procalcitonin. Arterial blood gas showed acidosis with pH of 7.29 (reference range: 7.35-7.45), bicarbonate of 17.7 mEq/l (reference range: 22-26 mEq/l), and base excess of -9.1 mEq/l (reference range: -2 to +2 mEq/l). Normal values for $PaCO_2$ (36.3 mm of Hg) and PaO_2 (85.7 mm of Hg) were observed. Laboratory parameters also showed leukocytosis on day 3 (D3), day 4 (D4), and extreme leukocytosis on day 6 (D6) and day 8 (D8) as well as impaired myocardial function (significant increase of total Creatine Kinase (CK) and CK subunits M and B (CKMB) on D4). Real-time PCR was negative for *N. meningitidis* on day 15 (D15). Other parameters appeared within the normal range except for liver function and anaemia on D18 (Table 1).

Table 1. Laboratory data of biochemical and clinical tests.

Laboratory data	Reference range	D2	D3	D4	D5	D6	D7	D8	D11	D14	D15	D18
Red blood cells (t/l)	4.2-6.0	4.1	4.3	3.9	-	3.9	-	3.76	3.62	-	-	3.58
Hemoglobin (g/l)	130-170	122	128	113	-	116	-	110	105	-	-	104
White blood cells (g/l)	4.0-10.0	3.8	23.6	16.5	-	30.6	-	30.2	14.7	-	-	8.2
Neutrophil (%)	43-76	89.7	91.6	89.3	-	87.1	-	80.9	79.3	-	-	66.2
Lymphocytes (%)	19-48	8.8	5	6.5	-	4.6	-	10.6	11.3	-	-	22.06
Platelet count (g/l)	150-350	51	12	25	-	73	-	129	257	-	-	494
Fibrinogen (g/l)	2-4	1.68	3.2	6	-	6.9	-	-	-	-	-	-
Prothrombin (%)	70-140	40	42	55	-	89	-	79	89	-	-	-
INR	0.8-1.2	1.9	1.86	1.5	-	1.08	-	1.16	1.08	-	-	-
APTT (sec)	30-40	55	104	37	-	29	-	-	-	-	-	-
Urea (mmol/l)	2.5-7.5	9.2	9	8.9	-	9.7	-	-	-	-	-	-
Creatinine (mmol/l)	62-120	206	159	141	-	102	-	93	70	-	-	56
Glucose (mmol/l)	3.9-6.4	5.1	5.6	5.6	-	6.6	-	8.8	6.6	-	-	4.4
Total bilirubin (mol/l)	3.4-17.1	15.7	17	16	-	-	-	18.8		-	-	-
Bilirubin direct (µmol/l)	0-7	4	3	4	-	-	-	-	-	-	-	-
Total protein (g/l)	60-80	51.4	-	-	-	-	-	-	-	-	-	-
Albumin (g/l)	38-54	28.3	32	32	-	-	-	36	30.6	-	-	-
AST (U/l)	10-40	42	49	179	-	260	-	-	-	-	-	49
ALT (U/l)	10-40	38	37	53	-	96	-	158	178	-	-	77
Total CK (U/l)	38-174	-	-	6395	-	5274	-	-	-	-	-	-
CKMB (U/l)	1-25	-	-	82	-		-	-	-	-	-	-
Procalcitonin (ng/ml)	<0.05	>100	>100	>100	64.6	-	11.6	-	-	0.44	-	-
CRP (mg/l)	0.5-10	56	-	-	-	-		107	-	-	-	11.2
pH	7.35-7.45	7.29	7.31	7.48	-	-	7.56	-	-	-	-	-
HCO_3 (mEq/l)	22-26	17.7	18.4	28	-	-	34.1	-	-	-	-	-
Base excess (mEq/l)	-2- +2	-9.1	-7.9	4.3	-	-	11.8	-	-	-	-	-
Lactat (mmol/l)	<2.1	7.3	4	2.7	-	-	1.6	-	-	-	-	-
Gram stain*	Negative	Negative	-	-	-	-	-	-	-	-	-	-
Realtime PCR*	Negative	Positive**	-	-	-	-	-	-	-	-	Negative	-

*: gram stain and real-time PCR to detect *N. meningitidis* in spinal fluid, blood, and throat specimens; **: positive with peripheral blood sample; (-): not available; CRP: C-Reactive Protein.

2.5. Treatment and intervention

Because of sepsis shock, the patient had to undergo a gastrostomy and tracheotomy. To avoid delay, antimicrobial therapy was initiated as quickly as possible after the performance of the lumbar puncture and collection of peripheral blood. The patient was initially treated with IV meronem 2 g/24 h and IV ciprobay 800 mg/24 h. Once *N. meningitidis* had been definitively identified, ciprobay was stopped and meronem was continued. The patient became hemodynamically unstable with a blood pressure of 80/50 mmHg, therefore noradrenalin and dobutamin were administered. In addition, other supportive therapies were used including saline infusions, electrolytes, antipyretics, and oxygen therapy. He also had begun to receive one unit of platelet transfusions on day 2 (D2). Consequently, the patient showed clinical improvement and was discharged after 20 days. He underwent another blood test after 20 days, which showed normal ranges, and had good mental status and was without the presence of haemorrhagic rash.

3. Discussion

In this case, the patient only presented nonspecific prodrome of fever, sore throat, and a nonspecific rash. Therefore, it was difficult to distinguish meningococcal disease from other common bacterial and viral febrile illnesses.

Early signs of sepsis are hypotension and tachycardia and the distinguishing feature such as rash, which may initially appear as small lesions that may appear urticarial, macular, or papular. The rash can develop into petechiae, purpura, or ecchymosis. These may be early signs of thrombocytopenia and purpura fulminant. The sensitivity of Kernig's and Brudzinski's signs was only 55.5 and 53.3%, respectively, which makes them unreliable in excluding meningitis [14]. The nonspecific features progress to sepsis with signs of circulatory insufficiency, shock, and the pathognomonic purpuric rash in about 40-70% of patients with meningococcal diseases [15]. In this study, the patient presented hypotension, shock, tachycardia and purpura, he also had stiff neck and thrombocytopenia. The presence of a non-blanching haemorrhagic rash is pathognomonic of meningococcal disease and reflects coagulopathy with the decreased fibrinogen, prothrombin, and increased INR and aPTT. In this case, the haemorrhagic rash has developed into ecchymosis on day 2. The stiff neck presented in this patient is consistent with Magazzini's report that elderly patients are less likely to present with neck stiffness and are more likely to present with altered consciousness compared to those aged <30 years [16]. Shock due to meningococcal septicaemia is a consequence of several pathophysiologic processes including myocardial dysfunction and impaired cellular metabolism [17]. Septic shock can lead to the consequence of impaired myocardial function and metabolic derangements, which were also found in this case.

N. meningitidis can be identified by microbiological culture, real-time PCR, or Gram staining from a purpuric skin lesion, blood, or cerebrospinal fluid. Microbiological culture is considered the standard method for *N. meningitidis* detection, but the sensitivity is limited particularly when antibiotics were previously administered. Microbiological culture is time-consuming and is frequently compromised by previous antibiotic treatment. Although this method has been used for decades to detect *N. meningitidis*, testing of respiratory specimens to detect *N. meningitidis* using microbiological culture is often discouraged [18]. Gram staining was negative for *N. meningitidis* in blood likely due to the previous use of cefotaxime. Cefotaxime interferes the final transpeptidation step during the biosynthesis of bacterial cell walls, thus reduces their stability and causes bacterial lysis [19]. Real-time PCR is not affected by antibiotics used previously [20] and thus the use of real-time PCR has quickly identified *N. meningitidis* and improved the detection rate [21]. In this case, the positive result for *N. meningitidis* in the blood sample by real-time PCR significantly helped physicians provide appropriate antibiotic treatment for the patient.

Approximately 10% of the general population carry *N. meningitidis* without any signs of disease [3] but this rate is drastically higher in certain living environments such as college dormitories or military units [22, 23]. Meningococcal disease is relatively frequent in military units in Vietnam. The drug of choice for treatment of meningococcal disease used to be penicillin and chloramphenicol [24]. However, due to resistance to these and some other antibiotics, third-generation cephalosporins are currently the most common choice of treatment. These drugs, however, are not readily available in many medical units in Vietnam. Cefotaxime, ceftriaxone, and penicillin are preferred as initial therapy in patients clinically diagnosed with invasive meningococcal disease [25], thus cefotaxime was already used in this case. However, according to WHO, 88-97% of drug stores dispense antibiotics without a prescription despite prohibition of this in Vietnam. One-third of inpatients used an inappropriate antibiotic during their admission. Antibiotics account for more than 50% of drugs used and are the most commonly sold drugs in Vietnam [26]. According to the Vietnam Ministry of Health, penicillin resistance is common in Vietnam [27]. Empiric treatment with a third-generation cephalosporin is recommended in developed countries. Chloramphenicol and meropenem can be used in cases of penicillin allergy [25]. Ciprofloxacin antibiotic is the antibiotic of choice, and ceftriaxone is an alternative [5]. In this case, we used IV meronem in treatment as recommended by most national and international guidelines [28, 29] and the patient recovered after 20 days of treatment.

4. Conclusions

Meningococcal meningitis may persist in Vietnam military populations, particularly during periods of military recruits. This is the first meningococcal sepsis case among soldier patients in a Vietnamese military unit. The clinical presentations of *N. meningitidis* vary widely making it difficult to diagnose, especially in Vietnam military units. The source of *N. meningitidis* should be investigated to propose suitable deterrence methods for *N. meningitidis* infection.

Consent for publication

Written informed consent from the patient was obtained for publication of the case report, including any accompanying images.

CRediT author statements

Nguyen Thanh Viet, Nguyen Minh Nam, Nguyen Vu Trung: Conceptualization, Methodology, Data curation, Formal analysis, Writing - Review & Editing; Do Tuan Anh, Hoang Van Tong: Conceptualization, Methodology, Writing original draft preparation, Writing - Review & Editing.

ACKNOWLEDGEMENTS

The authors wish to thank the collaborative staffs at the Department of Infectious Diseases of 103 Military Hospital for their assistance in the care of this patient and the Department of Medical Microbiology of the 103 Military Hospital for their information of real-time PCR method.

COMPETING INTERESTS

The authors declare that there is no conflict of interest regarding the publication of this article.

REFERENCES

[1] S. Takada, S. Fujiwara, T. Inoue, et al. (2016), "Meningococcemia in adults: A review of the literature", *Intern. Med.*, **55(6)**, pp.567-572, DOI: 10.2169/internalmedicine.55.3272.

[2] H. Christensen, M. May, L. Bowen, et al. (2010), "Meningococcal carriage by age: A systematic review and meta-analysis", *Lancet Infect. Dis.*, **10(12)**, pp.853-861, DOI: 10.1016/S1473-3099(10)70251-6.

[3] D.A. Caugant, E.A. Hoiby, P. Magnus, et al. (1994), "Asymptomatic carriage of Neisseria meningitidis in a randomly sampled population", *J. Clin. Microbiol.*, **32(2)**, pp.323-330, DOI: 10.1128/jcm.32.2.323-330.1994.

[4] C.L. Trotter, M.E. Ramsay (2007), "Vaccination against meningococcal disease in Europe: review and recommendations for the use of conjugate vaccines", *FEMS Microbiol. Rev.*, **31(1)**, pp.101-107, DOI: 10.1111/j.1574-6976.2006.00053.x.

[5] World Health Organization (2018), *Meningococcal Meningitis*, https://www.who.int/teams/health-product-policy-and-standards/standards-and-specifications/vaccine-standardization/meningococcal-meningitis, accessed 14 May 2020.

[6] S. Bosis, A. Mayer, S. Esposito (2015), "Meningococcal disease in childhood: Epidemiology, clinical features and prevention", *J. Prev. Med. Hyg.*, **56**, pp.e121-e124.

[7] L.C. Garfunkel, J.M. Kaczorowski, C. Christy (2007), *Pediatric Clinical Advisor (Second Edition)*, Philadelphia, pp.364-366.

[8] World Health Organization (2015), *Meningococcal Meningitis Fact Sheet*, accessed 14 May 2020.

[9] W.R. Taylor, K. Nguyen, D. Nguyen, et al. (2012), "The spectrum of central nervous system infections in an adult referral hospital in Hanoi, Vietnam", *PLOS ONE*, **7(8)**, DOI: 10.1371/journal.pone.0042099.

[10] A.S. Kushwaha, S.K. Aggarwal, M.M. Arora (2010), "Outbreak of meningococcal infection amongst soldiers deployed in operations", *Med. J. Armed Forces India*, **66(1)**, pp.4-8, DOI: 10.1016/S0377-1237(10)80082-6.

[11] J.F. Brundage, M.A. Ryan, B.H. Feighner, et al. (2002), "Meningococcal disease among United States military service members in relation to routine uses of vaccines with different serogroup-specific components, 1964-1998", *Clin. Infect. Dis.*, **35(11)**, pp.1376-1381, DOI: 10.1086/344273.

[12] S.O. Lee, S. Ryu, S. Park, et al. (2003), "Meningococcal disease in the Republic of Korea army: Incidence and serogroups determined by PCR", *Journal of Korean Medical Science*, **18(2)**, pp.163-166, DOI: 10.3346/jkms.2003.18.2.163.

[13] World Health Organization (2020), *Laboratory Methods for The Diagnosis of Meningitis Caused by Neisseria meningitidis*, *Streptococcus pneumoniae*, *and Haemophilus influenzae*, https://www.who.int/docs/default-source/documents/publications/laboratory-methods-for-diagnosis-of-meningitis.pdf, accessed 14 May 2020.

[14] A. Ala, F. Rahmani, S. Abdollahi, et al. (2018), "Accuracy of neck stiffness, Kernig, Brudzinski, and Jolt Accentuation of headache signs in early detection of meningitis", *Emerg. (Tehran)*, **6(1)**, https://www.ncbi.nlm.nih.gov/pmc/articles/PMC5827054/pdf/emerg-6-e8.pdf, accessed 14 May 2020.

[15] M.J. Thompson, N. Ninis, R. Perera, et al. (2006), "Clinical recognition of meningococcal disease in children and adolescents", *Lancet*, **367(9508)**, pp.397-403, DOI: 10.1016/S0140-6736(06)67932-4.

[16] S. Magazzini, P. Nazerian, S. Vanni, et al. (2012), "Clinical picture of meningitis in the adult patient and its relationship with age", *Intern. Emerg. Med.*, **7(4)**, pp.359-364, DOI: 10.1007/s11739-012-0765-1.

[17] R. Sinha, S. Nadel (2013), "Understanding shock", *Paediatrics and Child Health*, **23(5)**, pp.187-193, DOI: 10.1016/j.paed.2012.11.002.

[18] K.A. Cartwright, J.M. Stuart, D.M. Jones, et al. (1987), "The Stonehouse survey: nasopharyngeal carriage of meningococci and *Neisseria lactamica*", *Epidemiol. Infect*, **99**, pp.591-601, DOI: 10.1017/s0950268800066449.

[19] S. Mitsuhashi, M. Inoue, S. Masuyoshi (1980), "Antibacterial activity of cefotaxime", *J. Antimicrob. Chemother.*, **6**, Suppl. A, pp.37-46.

[20] H.M. Wu, S.M. Cordeiro, B.H. Harcourt, et al. (2013), "Accuracy of real-time PCR, Gram stain and culture for *Streptococcus pneumoniae*, *Neisseria meningitidis* and *Haemophilus influenzae* meningitis diagnosis", *BMC Infect. Dis.*, **13**, DOI: 10.1186/1471-2334-13-26.

[21] X. Wang, M.J. Theodore, R. Mair, et al. (2012), "Clinical validation of multiplex real-time PCR assays for detection of bacterial meningitis pathogens", *J. Clin. Microbiol.*, **50(3)**, pp.702-708, DOI: 10.1128/JCM.06087-11.

[22] K. Tryfinopoulou, K. Kesanopoulos, A. Xirogianni, et al. (2016), "Meningococcal carriage in military recruits and university students during the Pre MenB vaccination Era in Greece (2014-2015)", *PLOS ONE*, **11(12)**, DOI: 10.1371/journal.pone.0167404.

[23] T.X. Tran, T.T. Le, L.P. Trieu, et al. (2019), "Whole-genome sequencing and characterization of an antibiotic resistant *Neisseria meningitidis* B isolate from a military unit in Vietnam", *Ann. Clin. Microbiol. Antimicrob.*, **18**, DOI: 10.1186/s12941-019-0315-z.

[24] S. Nadel (2016), "Treatment of meningococcal disease", *J. Adolesc. Health*, **59(2)**, pp.S21-S28, DOI: 10.1016/j.jadohealth.2016.04.013.

[25] L.K. Pickering (2003), *Meningococcal Infections*, American Academy of Pediatrics, 11pp.

[26] World Health Organization (2020), *Antimicrobial Resistance in Vietnam*, https://www.who.int/vietnam/health-topics/antimicrobial-resistance, accessed 14 May 2020.

[27] Ministry of Health (2013), *National Action Plan on Combatting Drug Resistance in The Period from 2013-2020*, Decision No 2174/QD-BYT dated 21st June 2013 (in Vietnamese).

[28] A. Rhodes, L.E. Evans, W. Alhazzani, et al. (2016), "Surviving sepsis campaign: international guidelines for management of sepsis and septic shock", *Intensive Care Med.*, **43**, pp.304-377, DOI: 10.1007/s00134-017-4683-6.

[29] E. Garaci, P. Sinibaldi, G. Rasi (1996), "A new tumour associated antigen of non-small cell lung cancer: tumour liberated proteins (TLP) - A possible new tumor marker", *Anticancer Res.*, **16(4B)**, pp.2253-2255.

DOI: 10.31276/VJSTE.63(1).59-63

Effect of *Centella asiatica* on cognitive deficits caused in trimethyltin-induced neurotoxicity model mice

Hang Thi Nguyet Pham[1*], Hong Nguyen Tran[1], Xoan Thi Le[1], Khoi Minh Nguyen[1], Hiep Tuan Nguyen[1], Lap Thi Nguyen[2], Folk R. William[3]

[1]National Institute of Medicinal Materials, 3 Quang Trung Street, Trang Tien Ward, Hoan Kiem District, Hanoi, Vietnam
[2]Hanoi Pharmacy University, 15 Le Thanh Tong, Phan Chu Trinh Ward, Hoan Kiem District, Hanoi, Vietnam
[3]University of Missouri, Columbia City, Missouri State, USA

Received 2 October 2020; revised 15 December 2020; accepted 30 December 2020

Abstract:

***Centella asiatica* (L.) Urb. is a nootropic that has been widly used medicinally around the world for centuries. In this study, the authors investigates the anti-dementia effect of an n-butanol extract of *Centella asiatica* in a mouse model of neurodegeneration caused by trimethyltin (TMT). Mice were administered *Centella asiatica* extract (150 and 540 mg/kg) or a reference drug, tacrine (2.1 mg/kg), daily for one week before the TMT injection and during tests to analyse the spatial short-term and the spatial working memory. The treatment of mice with TMT caused deficits in short-term spatial working memory and decreased the number of pyramidal cells in the hippocampal CA1 and CA3 regions elucidated by Nissl staining at 28 d of the post-TMT treatment. The administration of *Centella asiatica* extract or tacrine significantly attenuated the behavioural and histochemical changes caused by the TMT. As a result, the author suggest that *Centella asiatica* extract improved memory deficits partly by protecting hippocampal neurons from TMT-induced damage.**

Keywords: ***Centella asiatica*, dementia, hippocampus, neuroprotection, trimethyltin.**

Classification number: **3.3**

1. Introduction

Alzheimer's chronic neurodegenerative disease (AD) causes memory loss and cognitive deficits, which develop slowly for 20-30 years until symptoms become apparent in patients at 65 years of age and over. AD is the most common dementia with the number of AD patients reaching more than 40 million worldwide [1, 2].

For AD patients with a severely damaged brain, health care costs are estimated to be hundreds of billions of dollars each year. Currently, no cure for AD is available, but medicines such as acetylcholinesterase inhibitors are employed to temporarily reduce the symptoms of AD patients although they have significant side effects. Development of effective treatments/drugs with fewer undesirable effects is critically important.

Centella asiatica (L.) Urb. is used in Ayurvedic medicine [3] to treat depression, anxiety, convulsion, and cognitive deficits [4, 5]. However, studies on the potential benefits of this plant for memory loss associated with AD are limited. Therefore, this study aims to evaluate the effects of *Centella asiatica* collected in Vietnam on memory deficits caused in an animal model of trimethyltin-induced neurodegeneration to explore possible mechanisms underlying the effects.

2. Materials and methods

2.1. Preparation of Centella asiatica extract

Centella asiatica (L.) Urban was collected in the Thanh Hoa province in August 2019 and identified by the staff (Department of Resource Medicinal Materials) of the National Institute of Medicinal Materials, Hanoi, Vietnam (NIMM). *Centella asiatica* extract was prepared by cutting aerial parts into small pieces and drying at 55°C. Plant material (650 g) was extracted with 80% alcohol (1:7 w/v) at room temperature for 24 h, filtered, and dried in vacuo at 50°C. The residue was suspended in H_2O and then partitioned three times with n-butanol, successively. The

*Corresponding author: Email: nguyethangpt@nimm.org.vn

combined n-butanol extracts were concentrated *in vacuo* at 60°C and yielded 40 g dried extract.

Centella asiatica extract was analysed for candidate secondary metabolites by UPLC (with diode detection) - TOF-MS plus MS/MS (with lockspray ionization operated in the ESI negative mode). Tentative identification of the peaks was performed by comparing data with published values.

2.2. Chemicals and reference drug

Reference drug: Tacrine (Sigma-Aldrich, USA) was dissolved in a phosphate-buffered saline (PBS) for peritoneal injection (i.p.) in mice at a dose of 2.1 mg/kg body weight.

2.3. Animal and drugs treatment

Male *Swiss albino* mice 6-7 weeks old were obtained from the National Institute of Hygiene and Epidemiology, Hanoi, Vietnam. Food and water were provided *ad libitum*. The animals were habituated for at least one week in quarters that were thermostatically maintained at 22±1°C with constant humidity (65%) and a 12-h light-dark cycle (lights on: 07:00-19:00). The behavioural experiments were performed during the light phase from 9:00 to 18:00 according to experimental schedules shown in Fig. 1.

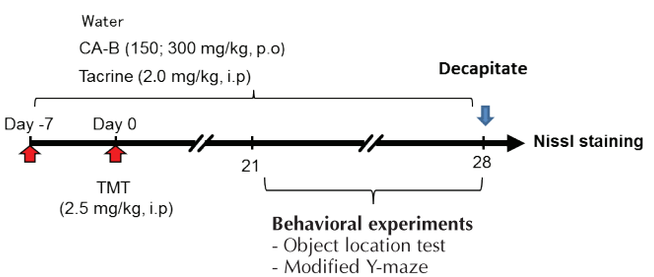

Fig. 1. Experimental schedule.

2.4. Behavioural study

The TMT-induced memory deficits were induced as previously described [6]. Briefly, mice were randomly divided into 5 groups (9-12 animals/group), namely, Groups 1 through 5. As shown in Fig. 1, Groups 2-5 received TMT injection on day 0.

Group 1 (naïve group) and Group 2 (TMT-group) were administered distilled water (p.o.) daily during the experimental period.

Groups 3-4 (TMT+*Centella asiatica* extract) and Group 5 (TMT+Tacrine) were administered *Centella asiatica* extract (150 and 300 mg/kg, p.o.) and tacrine (2.1 mg/kg, i.p.), respectively, at a volume of 0.1 ml/10 g body weight from day 7 to day 28.

After completion of the behavioural assays, the animals were decapitated under anaesthesia (pentobarbital, 50 mg/kg, i.p.) on day 28 to isolate brains for Nissl staining.

Object location test (OLT): The object location test was performed from 09:00 to 17:00 at 4-5 lux, without noise from day 21 to day 23, as previously described [6, 7]. Briefly, after acclimatization to an observation box (35×35×50 cm) for 10 min, a sample phase trial was conducted. Each mouse was placed in the observation box for 5 min and exposed to two identical objects. The total time spent to explore each object was measured and the mouse was then returned to the home cage. The test phase trial was conducted 30 min after the sample phase trial. In the test trial, objects were replaced by identical copies. One was placed in the same position and the other was placed diagonally on opposite corners. The animals were exposed to the objects for 5 min and the total time spent exploring each object was measured using Any Maze system® (Stoelting Co., IL, U.S.A.).

Modified Y-maze: The modified Y-maze test was performed from 9:00 to 17:00, at 8-9 lux, without noise on days 27 and 28, as previously described [8, 9]. This test consisted of a sample trial and a test trial, which were separated by an interval. In the sample trial, each mouse was placed in the maze with one arm closed. The animal was allowed to explore the other two arms freely for 5 min. In the test trial conducted 30 min after the sample trial, the animal was placed in the maze with 3 arms open and allowed to explore the arms freely. The previously closed arm was defined as the novel arm, and the time the animals spent in the new arm was measured using an Any Maze system® (Stoelting Co., IL, U.S.A.).

2.5. Nissl staining

The Nissl staining was conducted according to H.T.N. Pham, et al. (2019) [6] and A. Kádár, et al. (2009) [10]. After completing behavioural tests, mice were anesthetized with a peritoneal injection of pentobarbital (50 mg/kg; i.p) and then perfused intracardially with heparinized saline followed by 10% formalin saline. The brains were excised and post-fixed in 10% formalin saline for 3 h. The brains were soaked in a graded strength of sucrose solutions (12, 15, and 30%) for 48 h and then stored at -80°C until histological analysis. Coronal sections (slice thickness 20 µm) were taken at an appropriate position (Bregma -1.96 to -2.30 mm) using a freezing microtome (Leica CM 1950, Japan) and stained with 0.5% cresyl violet. Three sagittal brain sections prepared from each mouse were used for Nissl staining. The images of CA1 and CA3 regions were captured using a microscope (Olympus PROVIS®, Olympus Corporation, Tokyo, Japan) and the average intensity was analysed by Image-J software (ver. 1.41, NIH; Bethesda, MD, U.S.A.).

2.6. Statistical analysis

Data were expressed as the mean±standard error of the mean (S.E.M.). All the data obtained in the present study, except those from the OLT, were analysed by a one-way ANOVA followed with a post hoc comparison test (Student-Newman-Keuls/Dunnett). OLT data were analysed using a paired Student's t-test. Differences of $p<0.05$ were considered significant.

3. Results and discussion

3.1. Centella asiatica extract treatment improved memory deficits in TMT mice using object location test and modified Y-maze

The spatial short-term memory of the mice was evaluated on day 21 using the object location test. In the sample phase trials, no significant differences were observed in time spent exploring each identical object between the animal groups. In the test phase trial, the naïve group spent a significantly longer time exploring the object placed in the new location than the object placed in the familiar location ($p<0.05$). *Centella asiatica* extract (300 mg/kg) and tacrine-treated TMT mice were able to recognize a difference between objects placed in novel and familiar locations ($p<0.05$) (Fig. 2).

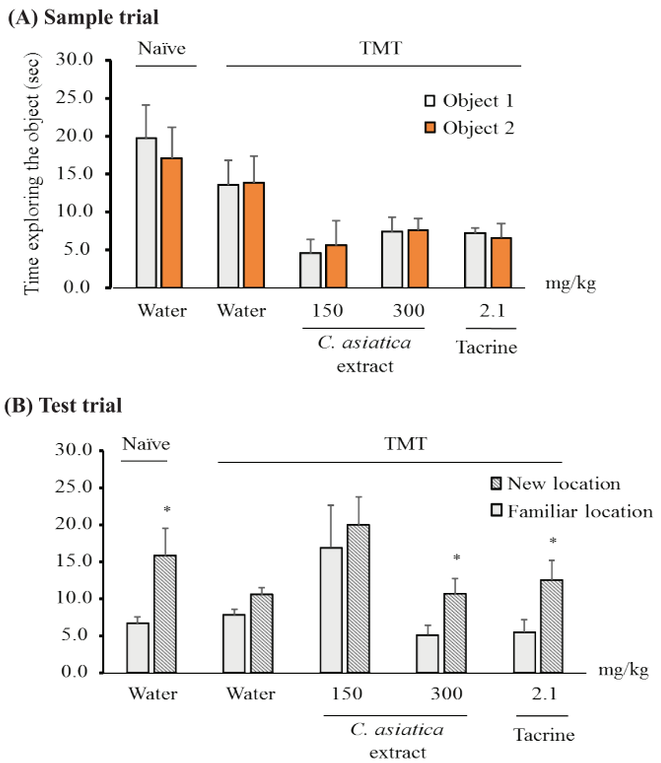

Fig. 2. Effect of *Centella asiatica* extract (150 and 300 mg/kg) on spatial short-term memory deficits in TMT-treated mice. (**A**) Time exploring the object in the sample trial; (**B**) Time exploring the object in the test trial; n=9-12 animals/group; *p<0.05 vs. the time spent exploring the non-displaced object.

To further study the effects of *Centella asiatica* extract on spatial working memory deficits in TMT mice, we conducted the modified Y-maze test on days 27-28 using the same animals.

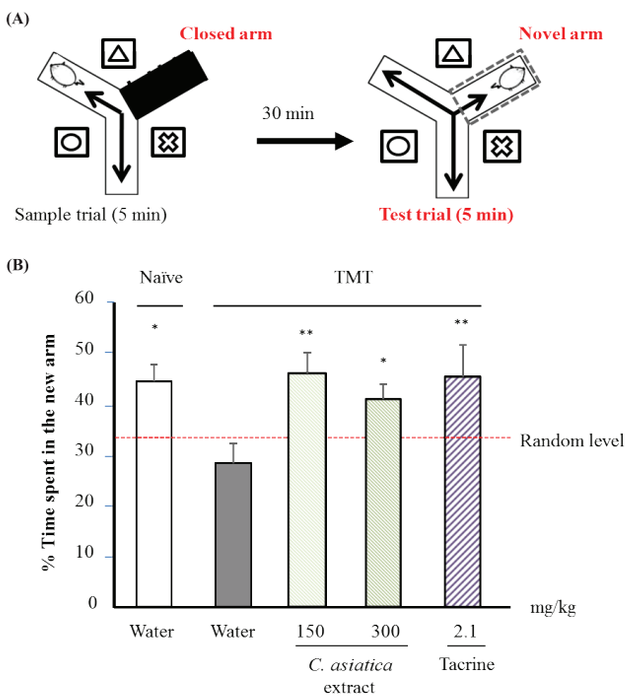

Fig. 3. Effect of *Centella asiatica* extract (150 and 300 mg/kg) on spatial working memory deficits in TMT-treated mice. (**A**) Experiment protocol of the modified Y-maze test; (**B**) Results are expressed as % time animals spent exploring the novel arm in the test trial; n=9-12 animals/group; *p<0.05; **p<0.01 vs. the water-treated TMT group.

As shown in Fig. 3, naïve mice preferred to visit the new arm compared to two familiar arms (higher than the chance level of 33.3%). Water-treated TMT mice significantly spent a shorter time in the new arm than untreated mice ($p<0.05$), indicating TMT-induced spatial working memory deficits. TMT mice treated with *Centella asiatica* extract (150 and 300 mg/kg) or tacrine (2.1 mg/kg) significantly spent a long time exploring the new arm compared to water-treated TMT mice (P values as shown in Fig. 3).

3.2. Centella asiatica extract exerts neuroprotective effects on TMT-induced hippocampal cell damage in vivo

Next, we evaluated the effect of *Centella asiatica* extract on the protection of hippocampal neurons in TMT mice. The hippocampal tissues were stained with crystal violet and then morphological changes were observed. The density of cresyl violet-stained cells in CA1 and CA3 regions were analysed by Image-J software. The results in Fig. 4 showed that mice exposed to TMT had a severe loss of pyramidal neurons in the hippocampal CA1 and CA3 regions and that

the administration of *Centella asiatica* extract (150 and 300 mg/kg) prevented the TMT-induced damage in the CA1 and CA3 regions.

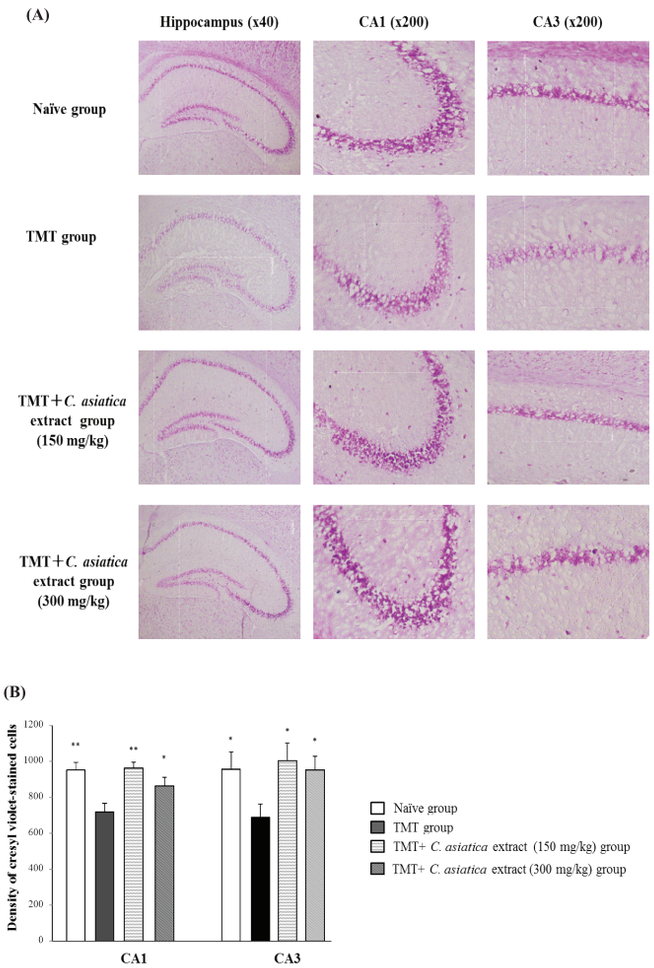

Fig. 4. Effects of Centella asiatica extract (150 and 300 mg/kg) on TMT-induced neuronal cell damage in the CA1 and CA3 of the hippocampus. (**A**) The upper, middle, and bottom panels are representative photos obtained from the naïve group, water-treated TMT group, and Centella asiatica extract-treated TMT groups (150 and 300 mg/kg), respectively; (**B**) The relative percentage values of the cell density in the CA1 and CA3 regions of each animal group. Each data column represents the mean±S.E.M. calculated from 8-10 animals in each group; *p<0.05; **p<0.01 vs. the water-treated TMT group at the same area of the mice hippocampus.

Centella asiatica is consumed in daily meals and used as a nootropic for emotional disorders such as depression, sedation, anxiety, mental weakness, and memory deficits [5, 11] via its neuroprotective, neurogenesis, and antioxidant properties [12]. Clinical studies have shown that *Centella asiatica* attenuates age-related decline in cognitive function and mood disorders in the elderly [13, 14]. Bioactive compounds of *Centella asiatica* include triterpenoids glycosides (asiaticoside and madecassoside) and aglycons (asiatic acid and madecassic acid) [15, 16]. In this study, by analyses with UPLC-TOF-MS plus MS/MS, we determined the constituents of the *Centella asiatica* extract used in these experiments to include madecassoside and asiaticosid (Fig. 5).

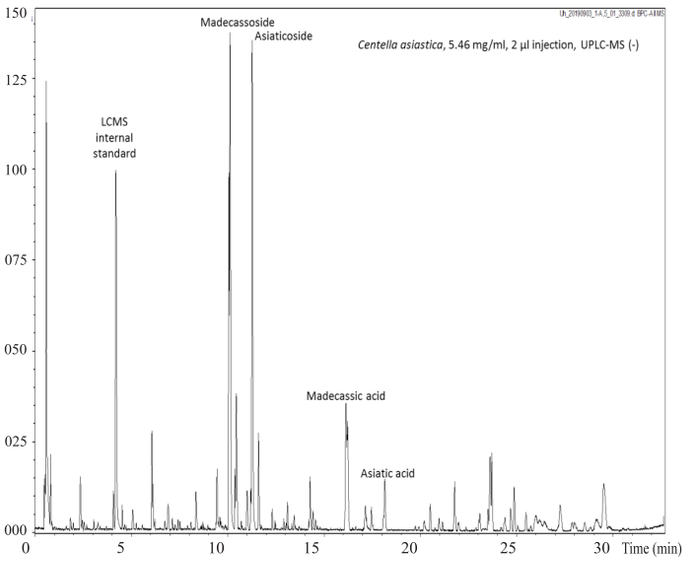

Fig. 5. UPLC-TOF-MS plus MS/MS chromatogram of *Centella asiatica* extract.

The hippocampus is a part of the limbic system and plays important roles in the consolidation process of information from short-term memory to long-term memory and spatial memory that enables navigation. The hippocampus proper consists of Cornu ammonis and dentate gyrus, and Cornu ammonis is divided into CA1, CA2, CA3, and CA4 regions. In dementia patients, the hippocampus is first affected, which induces initial symptoms of short-term memory impairment and disorientation [17]. TMT is a neurotoxicant that damages the hippocampal CA1 and CA3 regions. Thus, TMT-induced neuronal and cognitive impairments have been proposed as an experimental animal model for neurodegeneration in the hippocampus [18, 19]. The present study showed that TMT causes neuronal damage in the hippocampal CA1 and CA3 regions and spatial memory impairment in mice. An important finding in the present study is that *Centella asiatica* extract treatment attenuates memory impairments and prevents neuronal damage in CA1 and CA3 regions in TMT mice. A previous study reported by M.R.K. Gadahad, et al. (2008) [20] demonstrated that the administration of *Centella asiatica* juice stimulated the proliferation and morphological changes of neuronal cells in CA1 and CA3 regions in adult rats. Moreover, A. Sirichoat, et al. (2015) [21] reported that asiatic acid isolated from *Centella asiatica* improved hippocampus-

dependent memory deficits via a mechanism involved in neuronal proliferation. Taken together, it is likely that *Centella asiatica* extract ameliorates cognitive deficits in TMT-treated mice via preventing neuronal cell damages or stimulating neuronal cell proliferation, or both in the hippocampus.

4. Conclusions

The present study indicated that *Centella asiatica* extract has a protective effect against TMT-induced neuronal and cognitive impairments in mice suggesting that *Centella asiatica* extract treatment may be beneficial for the prevention/therapy of dementia.

CRediT author statements

Hang Thi Nguyet Pham, Hong Nguyen Tran, Xoan Thi Le: Conceptualization, Methodology, Data curation, Formal analysis, Writing - Review & Editing; Khoi Minh Nguyen, Hiep Tuan Nguyen, Lap Thi Nguyen, Folk R. William: Conceptualization, Methodology, Writing original draft preparation, Writing - Review & Editing.

ACKNOWLEDGEMENTS

This research was funded by National Institute of Medicinal Materials, Hanoi, Vietnam. We thank Dr. Zhentian Lei and University of Missouri Metabolomics Center for conducting the HPLC-MS analyses.

COMPETING INTERESTS

The authors declare that there is no conflict of interest regarding the publication of this article.

REFERENCES

[1] D.J. Selkoe (1991), "The molecular pathology of Alzheimer's disease", *Neuron*, **6(4)**, pp.487-498, DOI: 10.1016/0896-6273(91)90052-2.

[2] H.W. Querfurth, F.M. LaFerla (2010), "Alzheimer's disease", *New England Journal of Medicine*, **362(4)**, pp.329-344, DOI: 10.1056/NEJMra0909142.

[3] K.J. Gohil, J.A. Patel, A.K. Gajjar (2010), "Pharmacological review on *Centella asiatica*: A potential herbal cure-all", *Indian Journal of Pharmaceutical Sciences*, **72(5)**, pp.546-556, DOI: 10.4103/0250-474X.78519.

[4] P. Chanana, A. Kumar (2016), "Possible involvement of nitric oxide modulatory mechanisms in the neuroprotective effect of *Centella asiatica* against sleep deprivation induced anxiety like behaviour, oxidative damage and neuroinflammation", *Phytotherapy Research*, **30(4)**, pp.671-680, DOI: 10.1002/ptr.5582.

[5] N.E. Gray, A.A. Magana, P. Lak, et al. (2018), "*Centella asiatica* - phytochemistry and mechanisms of neuroprotection and cognitive enhancement", *Phytochemistry Reviews*, **17(1)**, pp.161-194, DOI: 10.1007/s11101-017-9528-y.

[6] H.T.N. Pham, S.V. Phan, H.N. Tran, et al. (2019), "*Bacopa monnieri* (L.) ameliorates cognitive deficits caused in a trimethyltin-induced neurotoxicity model mice", *Biological and Pharmaceutical Bulletin*, **42(8)**, pp.1384-1393, DOI: 10.1248/bpb.b19-00288.

[7] Q. Zhao, Y. Murakami, M. Tohda, et al. (2007), "Chotosan, a kampo formula, ameliorates chronic cerebral hypoperfusion-induced deficits in object recognition behaviors and central cholinergic systems in mice", *Journal of Pharmacological Sciences*, **103(4)**, pp.360-373, DOI: 10.1254/jphs.fp0061457.

[8] M. Yamada, M. Hayashida, Q. Zhao, et al. (2011), "Ameliorative effects of yokukansan on learning and memory deficits in olfactory bulbectomized mice", *Journal of Ethnopharmacology*, **135(3)**, pp.737-746, DOI: 10.1016/j.jep.2011.04.010.

[9] X.T. Le, H.T.N. Pham, P.T. Do, et al. (2013), "Bacopa monnieri ameliorates memory deficits in olfactory bulbectomized mice: Possible involvement of glutamatergic and cholinergic systems", *Neurochemical Research*, **38(10)**, pp.2201-2215, DOI: 10.1007/s11064-013-1129-6.

[10] A. Kádár, G. Wittmann, Z. Liposits, et al. (2009), "Improved method for combination of immunocytochemistry and Nissl staining", *Journal of Neuroscience Methods*, **184(1)**, pp.115-118, DOI: 10.1016/j.jneumeth.2009.07.010.

[11] D. Roy, S. Barman, M.M. Shaik (2013), "Current updates on *Centella asiatica:* phytochemistry, pharmacology and traditional uses", *Med. Plant Res.*, **3**, pp.20-36.

[12]G. Sbrini, P. Brivio, M. Fumagalli, et al. (2020), "*Centella asiatica* L. phytosome improves cognitive performance by promoting bdnf expression in ratprefrontal cortex", *Nutrients*, **12(2)**, DOI: 10.3390/nu12020355.

[13] J. Wattanathorn, L. Mator, S. Muchimapura, et al. (2008), "Positive modulation of cognition and mood in the healthy elderly volunteer following the administration of *Centella asiatica*", *Journal of Ethnopharmacology*, **116(2)**, pp.325-332.

[14] R. Dev, S. Mohamed, Z. Hambali, et al. (2009), "Comparison on cognitive effects of *Centella asiatica* in healthy middle age female and male volunteers", *European Journal of Scientific Research*, **31(4)**, pp.553-565.

[15] K. Ghosh, D. Indra (2014), "Phytochemistry, *in vitro* free radical scavenging, chelating and toxicity of *Centella asiatica* L. (apiaceae) ethanolic leaf extract", *International Journal of Pharmaceutical Sciences Review and Research*, **29(1)**, pp.328-334.

[16] Z.Z. Hafiz, M.A.M. Amin, R.M.J. James, et al. (2020), "Inhibitory effects of raw-extract *Centella asiatica* (reca) on acetylcholinesterase, inflammations, and oxidative stress activities via *in vitro* and *in vivo*", *Molecules (Basel, Switzerland)*, **25(4)**, DOI: 10.3390/molecules25040892.

[17]P. Andersen, R. Morris, D. Amaral, et al. (2006), *The Hippocampus Book*, Oxford University Press, DOI: 10.1093/acprof:oso/9780195100273.001.0001.

[18] A. Fiedorowicz, I. Figiel, B. Kamińska, M. Zaremba, et al. (2001), "Dentate granule neuron apoptosis and glia activation in murine hippocampus induced by trimethyltin exposure", *Brain Research*, **912(2)**, pp.116-127, DOI: 10.1016/s0006-8993(01)02675-0.

[19] K. Ogita, Y. Nitta, M. Watanabe, et al. (2004), "*In vivo* activation of c-Jun N-terminal kinase signaling cascade prior to granule cell death induced by trimethyltin in the dentate gyrus of mice", *Neuropharmacology*, **47(4)**, pp.619-630, DOI: 10.1016/j.neuropharm.2004.06.012.

[20] M.R.K. Gadahad, M. Rao, G. Rao (2008), "Enhancement of hippocampal CA3 neuronal dendritic arborization by *Centella asiatica* (Linn) fresh leaf extract treatment in adult rats", *Journal of the Chinese Medical Association*, **71(1)**, pp.6-13, DOI: 10.1016/s1726-4901(08)70066-2.

[21] A. Sirichoat, W. Chaijaroonkhanarak, P. Prachaney, et al. (2015), "Effects of asiatic acid on spatial working memory and cell proliferation in the adult rat hippocampus", *Nutrients*, **7(10)**, pp.8413-8423, DOI: 10.3390/nu7105401.

DOI: 10.31276/VJSTE.63(1).64-70

Development of inducer-free expression plasmids using IPTG-inducible P*spac* promoter for *Bacillus subtilis*

Phuong Thi Bich Chu[1, 2, 3, 4], Hanh Thi Thu Phan[1, 2], Hoang Duc Nguyen[1, 2, 4*], Trang Thi Phuong Phan[1, 2, 5*]

[1]*Center for Bioscience and Biotechnology, University of Science, Vietnam National University - Ho Chi Minh City, 227 Nguyen Van Cu Street, Ward 4, District 5, Ho Chi Minh City, Vietnam*

[2]*Vietnam National University - Ho Chi Minh City, Linh Trung Ward, Thu Duc City, Ho Chi Minh City, Vietnam*

[3]*Faculty of Pharmacy, Ho Chi Minh city University of Technology (HUTECH), 475A Dien Bien Phu Street, Ward 25, Binh Thanh District, Ho Chi Minh City, Vietnam*

[4]*Department of Microbiology, University of Science, Vietnam National University - Ho Chi Minh City, 227 Nguyen Van Cu Street, Ward 4, District 5, Ho Chi Minh City, Vietnam*

[5]*Laboratory of Molecular Biotechnology, University of Science, Vietnam National University - Ho Chi Minh City, 227 Nguyen Van Cu Street, Ward 4, District 5, Ho Chi Minh City, Vietnam*

Received 1 December 2019; revised 14 February 2020; accepted 3 March 2020

Abstract:

An inducer-free expression vector for the low expression levels in *Bacillus subtilis (B. subtilis)* is necessary for fundamental research. In this study, we constructed inducer-free expression plasmids carrying P*spac*, a well-known IPTG-inducible promoter, by removing a part of the *lacI* gene. After that, we analysed the expression of the target genes *bgaB* and *gfp*$^+$ in *B. subtilis.* Western blot experiments demonstrated that the reporters from the inducer-free plasmids with P*spac* could be produced at low levels in *B. subtilis* strains and were equivalent to their corresponding inducible constructs with 1 mM IPTG. The reporter activities showed that inducer-free expression from the P*spac* promoter was dramatically less than that of the inducer-free plasmids with the strong promoters P*grac*01 and P*grac*100 reported previously, about 16.2 to 20.3 times for BgaB and 24.7 to 34.3 times for GFP$^+$, respectively. To summary the idea, the inducer-free expression vectors carrying P*spac* promoters allow the constitutive expression of heterologous recombinant proteins at low levels in *B. subtilis*.

Keywords: ***Bacillus subtilis*, inducer-free, pHT vector, P*spac*, weak promoter.**

Classification number: **3.5**

1. Introduction

B. subtilis is an important host for the production of heterologous proteins because of its advantages such as easy handling, safe, non-pathogenic, endotoxin-free, effective protein secretion mechanisms, and industrial fermentation. Besides, *B. subtilis* is a model organism for studying Gram-positive bacteria and the biological systems of cellular differentiation, stress responses, and multicellular organization [1, 2]. Thus, scientists have paid more attention to its expression systems for industrial applications and basic research [3].

Fundamental research has shown it is essential to have a weak promoter that can be controlled to express low levels of recombinant proteins within the cells. IPTG-inducible P*spac*, a well-characterized hybrid promoter, is composed of the *B. subtilis* phage SPO-1 promoter and the *E. coli lac* operator, which leads to transcription activation for low levels of gene expression. The P*spac* promoter allows low-expression levels of reporter expression [4, 5], which is approximately 50 times weaker than the P*grac* promoter. Many plasmids containing the IPTG-inducible P*spac* promoter, such as pHCMC05, pAL01, and the improved plasmid pHT2002 [6], are suitable to express a modest amount of the heterologous protein in the induction of IPTG in *B. subtilis*. One example of requiring low protein expression level is sortase, which is a membrane-associated protein needed for anchoring recombinant proteins to the cell wall. Low levels of sortase are necessary to avoid membrane clogging [7]. The weak promoter P*spac* is also an appropriate choice when the recombinant protein, or a protein of interest in any pathway, is harmless to the host cells after overproduction.

Induction of protein expression is stimulated by the addition of the inducer IPTG, a non-metabolizable analogue

*Corresponding authors: Email: ptptrang@hcmus.edu.vn; ndhoang@hcmus.edu.vn

of allolactose. After induction, the RNA polymerase enzyme specially transcribes the coding sequence of the protein of interest present in the expression plasmid under the control of the promoter. IPTG is very useful to control gene expression in many microorganisms. However, IPTG has several limitations: (i) it requires cell culture monitoring to ensure that IPTG is added at the appropriate time. Because the induction point varies significantly from one recombinant protein to another, the process becomes challenging to manipulate, particularly when several proteins are expressed in parallel (e.g., for a screening study) and (ii) it presents toxicity limitations that affect cell viability [8]. Therefore, inducers are sometimes not necessary for low and continuous protein expression in the cell.

Some auto-inducible and constitutive expression vectors were constructed such that heterologous proteins can be expressed in *B. subtilis* during continuous culture without adding the inducer. In the last few years, inducer-free expression systems were developed by deleting a part of or the entire *lacI* gene in the vector carrying the IPTG-inducible promoters, P*grac*01, P*grac*57, and P*grac*100 [9, 10]. These strong inducer-free expression vectors have shown a prospective yield of recombinant proteins for industrial and medical applications. However, an inducer-free expression vector system based on a weak promoter controlling the expression of heterologous proteins at low levels has not yet been studied. In this work, inducer-free expression plasmids were developed by deleting the *lacI* gene on plasmids carrying the P*spac* promoter, which allows the system to express proteins of interest without using any inducers. Two widespread reporter genes, *bgaB* and *gfp*$^+$, were used to investigate the expression levels of these vectors.

2. Materials and methods

2.1. Strains, plasmids and growth conditions

Escherichia coli OmniMAX™ was used as the host for gene cloning and *B. subtilis* 1012 was used for gene expression and integration. The final concentrations of antibiotics were as follows, in mg/l: ampicillin (Amp), 100 for *E. coli*; and chloramphenicol (Cm), 10 for *B. subtilis*. The strains were cultivated in Luria-Bertani (LB) medium consisting of 1% tryptone, 0.5% yeast extract, and 0.5% NaCl. Strains were cultivated at 37°C in shaking flasks at 200 rpm. The cell density was determined by measuring the OD_{600} with an S-20 spectrophotometer (Boeco, Germany). Table 1 shows a list of the plasmids and oligonucleotides used in this study.

Table 1. Bacterial strains, plasmids and oligonucleotides used in this study.

Bacterial strains	**Genotype**	**Source/references**
E. coli OmniMAX	F′ {*pro*AB *lacI*^{q} *lacZ*ΔM15 *Tn*10(Tet^R) Δ(*ccdA*B)} *mcr*A Δ(*mrr hsd*RMS-*mcr*BC) Φ 80(*lacZ*)ΔM15 Δ(*lac*ZYA-*arg*F)U16 9 *end*A1 *rec*A1 *sup*E44 *thi*-1 *gyr*A96 *rel*A1 *ton*A *pan*D; used for cloning	Invitrogen
B. subtilis 1012	*leuA8 metB5 trpC2 hsrM1*	Mobitec
Plasmids	**Description**	**Source/references**
pHCMC05	P*spac* promoter, no reporter gene, negative control	[4]
pHCMC05-bgaB	P*spac-bgaB*, inducible, used to construct pHT1672	[4]
pHT1675	P*grac*100-*gfp,* Δ*lacI, lacO1-lacO3* 406 bp; used to construct pHT1692	This study
pHT2002	P*spac-bgaB*, inducible	[6]
pHT1535	P*spac-gfp*$^+$, inducible plasmid	This study
pHT1692	P*spac-gfp*$^+$, Δ*lacI* 406 bp	This study
pHT1672	P*spac-bgaB*, Δ*lacI* 787 bp	This study
Oligonucleotide	**Sequence 5' → 3'**	**Used for**
ON1896	CGGTTCGATCTTGCTCCAACTG	pHT 1672, plasmid sequencing
ON925	GAATTAGCTTGGTACCAAAGGAGGTAAGGATCACTAG	pHT1672, screening *E. coli* colonies
ON1278	GGCCATGACGTCTTTGTAAAGCTCATCCATGCCATGTGT	
ON780	CCCGCGGTCAGCTAGCCTAAACCTTCCCGGCTTCATCATGCTC	pHT1672, screening *B. subtilis* colonies
ON779	AAAGGAGGAAAGATCTATGAATGTGTTATCCTCAATTTGTTAC	
ON1512	ATCTCCATGGACGCGTGACG	pHCMC05, receiving P*spac* promoter
ON1249	CGTTTCCACCGGAATTAGCTTG	
ON926B ON1273	GACGTCGACTCTAGACATGGATCCTTCCTCCTTTATATGG CCCGGTACCCACTTCCTAGAATATATATTATGTAAACAAAGGAGGTA AGGATCACTAG	pHT1692, screening *E. coli* colonies
ON1280	GGCCATGACGTCTTATTTGTAAAGCTCATCCATGCCATGTGT	pHT1692, screening *B. subtilis* colonies
ON867B	GTGAAGGTGATGCTACAAACGGAAAGCTTACCCTTAAA	

2.2. Materials

Taq DNA polymerase and enzymes, including *Sna*BI, *Apa*I, T4 DNA ligase, *Kpn*I, *Bam*HI, Alkaline phosphatase, and Klenow, were supplied by Thermo Scientific. PCR kit, cloning kit, and basic materials for molecular biology were supplied by Qiagen, Thermo Scientific, Sigma-Aldrich, Merck-Millipore, and BioBasic. The plasmid pHCMC05-*bgaB*, and the plasmid pHT1675 were used as the origin plasmids to create the inducer-free plasmids. The plasmid pHCMC05 without the *bgaB* or *gfp*$^+$ gene was used as a negative control. All primers for PCR were described in Table 1.

2.3. Construction of the inducer-free expression plasmid based on the Pspac promoter

The plasmid pHCMC05-*bgaB* [4], a popular IPTG-inducible plasmid based on the P*spac* promoter, was engineered by removing 787 bp from the *lacI* gene to generate the auto-inducible plasmid pHT1672 (Fig. 1A). First, the plasmid pHCMC05-*bgaB* was treated by the restriction enzymes *Sna*BI and *Apa*I, in which *Apa*I created sticky end products while *Sna*BI created blunt end products. Second, the sticky ends were deleted by the Klenow Fragment to optimize the ligation reaction. Then, the ligation reaction of these products was carried out by T4 ligase and subsequently transformed into *E. coli*. The transformants were analysed by colony PCR using restriction analysis. Finally, the gene sequence of pHT1672 was confirmed by an improved Sanger method using an ON1896 primer on a Big Dye™ terminator (Macrogen - Korea). The structure of the pHT1672 plasmid is shown in Fig. 1B.

2.4. Transformation of recombinant plasmids into B. subtilis 1012 competent cells

The procedure for the transformation of recombinant plasmids into *B. subtilis* 1012 competent cells was carried out as described elsewhere [11]. First, the *B. subtilis* 1012 competent cells were shaken in 50-ml flasks containing 10 ml of LS medium at 50 rpm in a 30°C-shaking incubator for 2 h. Then, 100 µl of 0.1 M ethylene glycol tetraacetic acid (EGTA) was added into the prepared 50-ml flask with *B. subtilis* competent cells and this flask was kept at room temperature (25°C) for 10 min. After that, 1 ml of *B. subtilis* competent cells was removed and transferred into a 1.5-ml tube containing the recombinant plasmid. Next, this tube was shaken at 200 rpm in 37°C for 2 h before being centrifuged at 7000 rpm for 5 min to receive the recombinant cells. The cells were resuspended in the left supernatant and spread on LB agar plates containing 10 µg/ml Cm and 40 µg/ml 5-Bromo-4-chloro-3-indolyl-β-D-galactopyranoside (X-gal). The plates were incubated at 37°C overnight. Then, *B. subtilis* colonies were screened using ON780/ON779 primers by colony PCR. Finally, the LB liquid media was used for breeding *B. subtilis* cells from selected colonies.

2.5. Evaluation of expression of the reporter protein

The evaluation protocol of BgaB expression has been described in previous articles [6, 9, 12]. First, three single colonies of each recombinant *B. subtilis* 1012 strain were cultured in LB liquid medium. The shaking culture flask of each clone was incubated at 37°C at 200 rpm to the mid-log phase when the OD_{600} of the culture reached 0.8-1. Then, IPTG was added at 0 (control), 0.1, and 1.0 mM to each culture. The cells were collected at 0 h (before induction), 2 h, and 4 h after induction for measurement of the BgaB activity and Western Blot analysis. In terms of this purpose, the volume of cell suspension was received at OD of 1.2 and 2.4, respectively.

For the investigation of BgaB activity, *B. subtilis* cells were lysed in 500 µl of a LacZ buffer containing 200 µg/ml of lysozyme and incubated at 37°C for 2 h. All samples were centrifuged at 10000 rpm for 5 min before the determination of the activities. The BgaB activity was represented by MUG units, which were calculated by measuring the fluorescence intensity at E_x/E_m=360/460 nm. We used 4-methylumbelliferyl-β-D-Galactopyranoside (MUG) as a substrate to realize the presence of the target protein β-galactosidase through the fluorescence. A microplate fluorometer (Clariostar, BMG Labtech) was used to measure the amount of fluorescence created by β-gal-dependent MUG hydrolysis, in which a culture medium sample without cell was used as a blank reference. The β-galactosidase activity (MUG units) were calculated by the following equation: $(V_l/V_s)\times F_{360/460}/(t\times OD_{600})$; where V_l is the volume of cell lysate; V_s is the sample volume used for the assay; $F_{360/460}$ is the fluorescence signals measured with the excitation - emission wavelengths of 360±8 nm and 460±8 nm, respectively; t is the reaction time (30 min); and OD_{600} is the OD of the cell samples at 600 nm (OD_{600}=1.2) [9, 12].

In Western Blot analyses, separation of the cell's proteins was conducted by SDS-PAGE and the transferation of these proteins to the nitrocellulose membrane was performed using

a transfer apparatus (Bio-Rad). Western Blot was carried out with primary antibodies that were complementary to the BgaB that were created in the mice in our lab, while the secondary antibody Anti-Mouse IgG - Peroxidase antibody was supplied by Sigma. Five-percent skimmed milk was used for blocking and antibody incubation, in which the concentration of primary antibodies was 1:20000 while the concentration of secondary antibodies was 1:10000. The proteins were stained by using a Pierce™ ECL Western Blotting Substrate (Thermo Scientific) and the chemiluminescent signal was detected by the iBright™ CL1500 Imaging System (Invitrogen).

2.6. Inducer-free expression of GFP at a low level in B. subtilis

In this procedure, the plasmid pHT1675, an inducer-free plasmid based on the P*grac*100 promoter, was engineered to form pHT1692. Firstly, the P*spac* gene was received from the basic plasmid pHCMC05 by using PCR with the primer pair ON1512/ON1249. Next, the PCR products were treated by *Kpn*I/*Bam*HI enzymes while the origin plasmid pHT1675 was treated with *Kpn*I/*Bam*HI and alkaline phosphatase to remove the P*grac*100 gene. Then, the enzymatic products were ligated by T4 DNA ligase, resulting in the pHT1692 vector containing the P*spac* promoter. Finally, we checked the GFP expression levels of this self-inducible *B. subtilis* expression system to demonstrate its potential application in basic research.

For the investigation of GFP activity, *B. subtilis* cells were lysed in a 500 µl PBS buffer that contained 137 mM NaCl, 2.7 mM KCl, 8 mM Na_2HPO_4, 2 mM KH_2PO_4, and 400 µg/ml lysozyme. Then, these mixtures were incubated at 37°C for 2 h. Immediately after centrifugation at 10000 rpm for 5 min, all samples were used for determination of the activities. GFP fluorescence was measured by using a microplate fluorometer (Clariostar, BMG LabTech) and a 384-well plate (Black) with an excitation wavelength of 470±8 nm and an emission wavelength of 515±8 nm. The determination of the GFP expression was calculated as the relative fluorescence unit (RFU) divided by the OD_{600}. All data were averaged from three independent samples of each time point [9]. The Western Blot was conducted with the primary antibodies against the GFP created in the mice in our lab and the secondary antibody Anti-Mouse IgG (whole molecule)-Peroxidase antibody was supplied by Sigma. The Western Blot procedure used is described above.

3. Results and discussion

3.1. Construction of the inducer-free expression plasmid pHT1672 based on Pspac promoter

The inducer-free plasmid pHT1672 was constructed successfully by deleting 787 bp between *Apa*I and *Sna*BI from the *lacI* gene of the plasmid pHCMC05-*bgaB* (Fig. 1). The results of DNA sequencing analysed by the Clone Manager showed 100% sequence homology between the analysed and designed DNA sequences of pHT1672. Because the plasmid lacks the regulatory gene, it will express the target protein in *B. subtilis* cells at the maximum level of the promoter without an inducer.

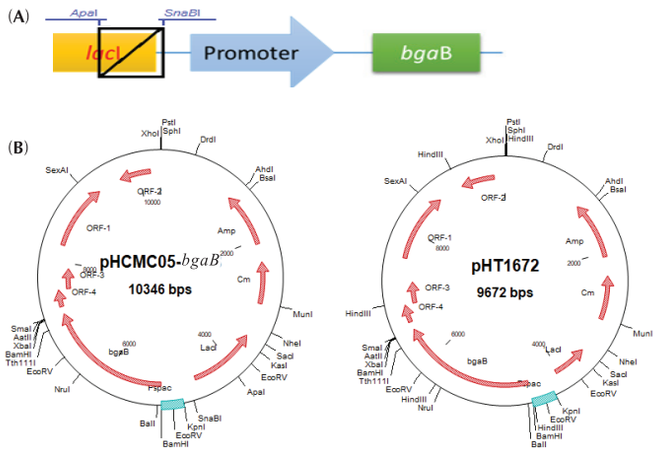

Fig. 1. The development of an inducer-free expression vector from an IPTG-inducible expression vector for *B. subtilis*. (**A**) A schematic depicting the deletion of a part of the *lacI* gene from the IPTG-inducible vector resulting in an inducer-free expression vector (**B**) a map of the pHCMC05-*bgaB* (inducible vector) and pHT1672 (inducer-free vector).

3.2. Non-inducible expression of BgaB from plasmid pHT1672 with the Pspac promoter in B. subtilis

In this experiment, we investigated the expression levels of the target protein in *B. subtilis,* which contains pHT1672 under the control of the P*spac* promoter by using the inducer IPTG. *B. subtilis* strains containing the origin plasmid pHCMC05-*bgaB* and the inducible expression plasmid based on the P*spac* promoter pHT2002 [9] were also tested for comparison. *B. subtilis* with pHCMC05, a similar expression system without the *bgaB* gene, was used as a negative control. The *BgaB* expression of these four *B. subtilis* strains are shown in Fig. 2.

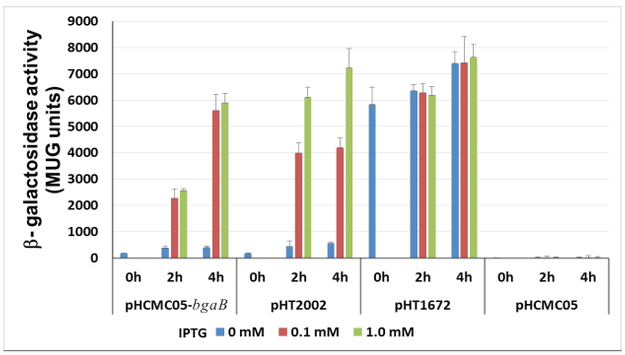

Fig. 2. The *BgaB* expression of the inducible and inducer-free plasmids in *B. subtilis* 1012. The production of the reporter protein *BgaB* over the four different *B. subtilis* strains haboring surveyed vectors pHCMC05-*bgaB* (origin plasmid, P*spac*, inducible), pHT2002 (P*spac*, inducible), pHT1672 (P*spac*, inducible-free), and pHCMC05 (P*spac*, negative control without *bgaB* gene), were evaluated in the presence of different IPTG concentrations (0, 0.1, 1.0 mM IPTG). The activities of β-galactosidase (MUG units) was measured in all samples. All cultures were grown three times and each experiment was repeated at least twice under similar conditions. Error bars denote standard deviations.

At the same time we collected the aliquots, the MUG units of the *B. subtilis* strain containing the inducer-free plasmid pHT1672 were equivalent in spite of different IPTG concentrations. After 2 and 4 h, the expression level of *BgaB* from the inducer-free plasmid pHT1672 in the absence of IPTG were compared to those of the origin inducible plasmids, pHCMC05-*bgaB* and pHT2002, with 1 mM IPTG. As shown in Fig. 2, the MUG units of pHT1672 after 2 h without induction were about 16.5 times higher than those of pHCMC05-*bgaB*. These ratios reached about 18.6 for samples received after 4 h of culture. In addition, the expression levels of *B. subtilis* containing the inducible-free construct pHT1672 were at least 13.2 times higher than that of pHT2002 without induction after 2 and 4 h. After 4 h induction with 1.0 mM IPTG, the value of β-galactosidase activity was equivalent when the comparison of different strains pHT1672 and 2002 was performed. It could be deduced that the deletion of the *lacI* gene has no effect on the strength of the P*spac* promoter and the conversion from inducible to inducer-free plasmids in *B. subtilis*.

The *BgaB* expression levels of the inducer-free plasmid based on the P*spac* promoter pHT1672 were about 16.2 to 20.3 times lower than that of the inducer-free plasmids based on the P*grac*01 and P*grac*100 promoter [9]. A previous study [6] showed that the heterologous *bgaB* could be induced for the expression at modest amounts in the *B. subtilis* containing pHT2002 by using IPTG as inducer. As a result of this study, we concluded that the inducible-free plasmid pHT1672 could express the recombinant protein *BgaB* at a low level without the addition of IPTG. This auto-inducible system can control the expression of target proteins continuously in the *B. subtilis* host strain without an inducer.

The expression of heterologous proteins controlled by the P*spac* promoter in *B. subtilis* was so low that they could not be detected by SDS-PAGE (Fig. 3A). This result was comparable with a previous study [6]. To confirm whether or not *BgaB* was expressed from these four *B. subtilis* strains, the Western Blot was conducted with the aliquots of these cells and the volume of the cell suspension was received at an OD of 2.4 after 4 h of induction. The presence of *BgaB* is shown in Fig. 3.

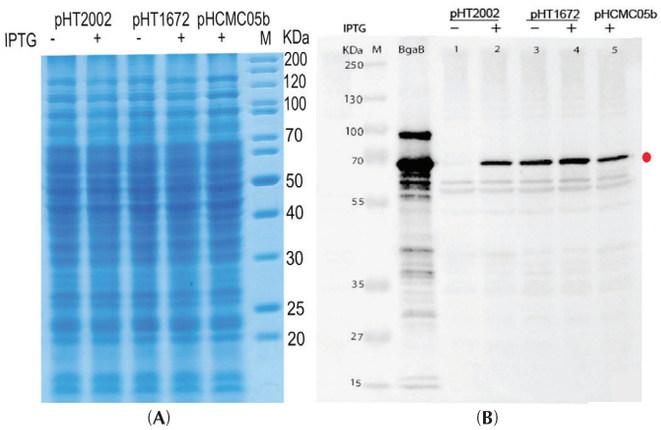

Fig. 3. The Western Blot results showing the *BgaB* expression of inducer-free plasmids based on the P*spac* promoter in *B. subtilis* 1012. The aliquots of surveyed *B. subtilis* strains (pHT1672, pHT2002) in the induced conditions (+, 1 mM IPTG) and the non-induced conditions (-, 0 mM IPTG). The origin plasmid pHCMC05- *bgaB* (pHCMC05b) was used as a positive control. The three different bacterial strains containing the surveyed vectors were cultured in an LB liquid medium at 37°C to the mid-logarithmic growth phase. Then, each culture was divided into two subcultures, where one was continuously incubated without an IPTG induce (0 mM) and the other was in inducible conditions with 1 mM IPTG (the positive controls were induced at 1 mM IPTG). The samples were collected 4 h after induction. The size of the *BgaB* lane was about 78 kDa. (**A**) The SDS-PAGE result shows fuzzy *BgaB* lines that are difficult to identify and (**B**) The Western Blot result clearly reflects the expression of *BgaB* in the *B. subtilis* strains.

As shown in Fig. 3, we confirmed that using polyclonal antibodies developed in our laboratory could detect a 78 kDa protein corresponding to the molecular size of *BgaB*. The thickest band of each line was *BgaB*, while the other fuzzy bands were non-specific binding proteins of the cells. The *BgaB* expression levels of the two surveyed *B. subtilis* strains that contained the inducer-free plasmids (pHT1672, pHT2002) were similar. Besides, there was no significant difference between the *BgaB* bands of these strains in the presence or absence of the inducer IPTG. The expression level of heterologous protein *BgaB* in the *B. subtilis* strain pHT1672 was equivalent to the level of that in the *B. subtilis* strain pHT2002, which is an inducer-free plasmid based on P*spac* promoter recently published in Ref. [6]. These levels were higher than that of the positive control pHCMC05-*bgaB*. Thus, we conclude that the inducer-free vectors based on the P*spac* promoter could express modest amounts of the heterologous protein. Therefore, these vectors are suitable for basic research to express proteins for metabolic engineering or membrane proteins.

3.3. Inducer-free production of GFP from plasmid pHT1692 with the Pspac promoter in B. subtilis

The target protein using an inducer-free expression system is continuously expressed in the *B. subtilis* host strain without inducer. Therefore, protein overexpression under strong promoter systems might cause a change of the protein's structure, resulting in inactivation of the protein's function [12]. Basic research has shown that it is important to use an inducer-free vector to allow the target heterologous protein to be produced continuously at low levels. To reconfirm the potential application of inducer-free plasmids based on the P*spac* promoter, the expression of another target protein was also investigated. For this study, the auto-inducible plasmid pHT1692 was created by engineering the origin of the inducer-free plasmid pHT1675 (P*grac*100-*gfp, ΔlacI, lacO1-lacO3* 406 bp) [9]. First, the P*spac* gene was received from the basic plasmid pHCMC05 by using PCR with the primer pair ON1512/ON1249. Next, the PCR products were treated with *Kpn*I/*Bam*HI enzymes while the origin plasmid pHT1675 was treated with *Kpn*I/*Bam*HI and alkaline phosphatase to remove the P*grac*100 promoter. Then, the enzymatic products were ligated by T4 DNA ligase, resulting in the pHT1692 vector consisting of a P*spac* promoter. The activity of GFP produced by the *B. subtilis* strain with an inducer-free vector based on P*spac* promoter pHT1692 was evaluated by fluorescent spectrometry (plate reader). *B. subtilis* with pHCMC05, a similar expression system without *gfp*$^+$ gene, was used as a negative control. The *B. subtilis* strain containing the inducible expression plasmid based on the P*spac* promoter pHT1535 was also tested for comparison. The GFP expression of these *B. subtilis* strains is shown in Fig. 4.

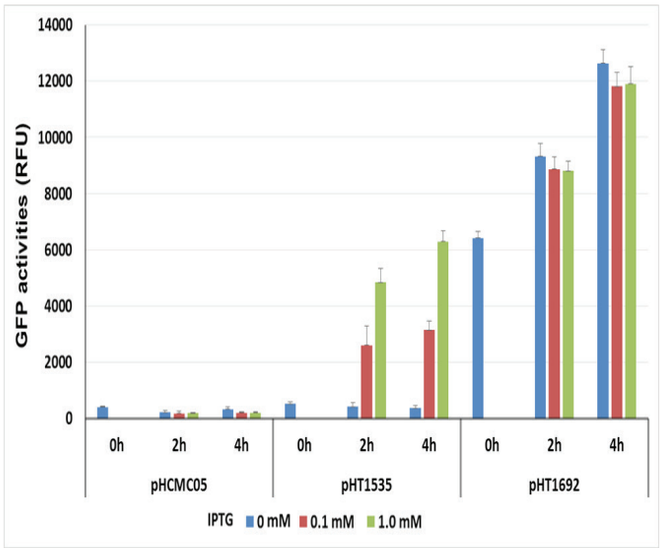

Fig. 4. The GFP expression of the inducible and inducer-free plasmids in *B. subtilis* 1012. The production of the reporter protein GFP in the different *B. subtilis* strains contained surveyed vectors pHT1535 (P*spac,* inducible), pHT1692 (P*spac,* inducible-free), and pHCMC05 (P*spac,* negative control without *gfp+* gene) was evaluated in the presence of different IPTG concentrations (0, 0.1, 1.0 mM IPTG). The activities of GFP (RFU units) was measured in all samples. All cultures were grown three times and each experiment was repeated at least twice with similar conditions. Error bars denote standard deviations.

GFP activities of the *B. subtilis* strain pHT1692 changed from 6416 to 12640 RFU and were significantly different between the surveyed samples in non-induced conditions by time. The activity of GFP measured from the strain pHT1692 achieved the highest activity of 12640 RFU, which was 2-fold higher than that of the inducible plasmid pHT1535. The expression levels of the strain pHT1692 were about 24.7 to 34.3 less than that of some inducer-free plasmids based on *Pgrac*01 and *Pgrac*100 previously reported in Ref. [9].

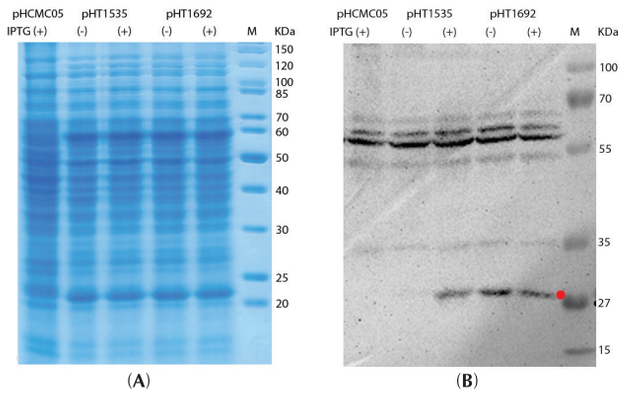

Fig. 5. The Western Blot results showing the GFP expression of inducer-free plasmids based on the P*spac* promoter in *B. subtilis* 1012. The suspension of the surveyed *B. subtilis* strains (pHT1692, pHT1535) under induced conditions (+, 1 mM IPTG) and non-induced conditions (-, 0 mM IPTG). The plasmid pHCMC05 without the *gfp*$^+$ gene was used as a negative control. The three different bacterial strains containing the surveyed vectors were cultured in an LB liquid medium at 37°C to the mid-logarithmic growth phase. Then, each culture was divided into two subcultures where one was continuously incubated without IPTG inducer (0 mM) and the other was under inducible conditions with 1 mM IPTG (the positive controls were induced at 1 mM IPTG). The samples were collected 4 h after induction. The size of the GFP lane was about 27 kDa. (**A**) The SDS-PAGE result shows fuzzy GFP lines that are difficult to identify and (**B**) The Western Blot result clearly reflects the expression of GFP in the *B. subtilis* strains.

The Western Blot results (Fig. 5B) also corresponded with previous publications and the sample of surveyed strains (pHT1672, pHT1535) indicated that the GFP protein was present in small quantities. These results certainly demonstrate that the newly constructed inducer-free expression plasmid based on the P*spac* promoter could allow low-level GFP expression without controlling.

4. Conclusions

P*spac*, a well-known IPTG-inducible promoter for *B. subtilis*, is suitable for studying the role of proteins that are produced at modest concentrations in the cell. We successfully engineered a P*spac* cassette by deleting a part of the *lacI* gene to create the inducer-free expression plasmids, pHT1692 and pHT1672, that express recombinant reporter proteins at low levels in *B. subtilis* without the addition of IPTG. The inducer-free expression plasmids for low protein expression in *B. subtilis* could be useful for investigating heterologous proteins at low levels.

CRediT author statements

Phuong Thi Bich Chu, Hanh Thi Thu Phan: Conceptualization, Methodology, Data curation, Formal analysis, Writing - Review & Editing; Hoang Duc Nguyen, Trang Thi Phuong Phan: Conceptualization, Methodology, Writing original draft preparation, Writing - Review & Editing.

ACKNOWLEDGEMENTS

This research is funded by Vietnam National Foundation for Science and Technology Development (NAFOSTED) under Grant Number 106-NN.02-2015.24.

COMPETING INTERESTS

The authors declare that there is no conflict of interest regarding the publication of this article.

REFERENCES

[1] L. Westers, H. Westers, W.J. Quax (2004), "*Bacillus subtilis* as cell factory for pharmaceutical proteins: A biotechnological approach to optimize the host organism", *Biochim. Biophys. Acta.*, **1694(1-3)**, pp.299-310, DOI: 10.1016/j.bbamcr.2004.02.011.

[2] J.M. Dijl, M. Hecker (2013), "*Bacillus subtilis:* From soil bacterium to super-secreting cell factory", *Microb. Cell Factories*, **12(3)**, DOI: 10.1186/1475-2859-12-3.

[3] C. Zhou, B. Ye, S. Cheng, et al. (2019), "Promoter engineering enables overproduction of foreign proteins from a single copy expression cassette in *Bacillus subtilis*", *Microb. Cell Factories*, **18(1)**, DOI: 10.1186/s12934-019-1159-0.

[4] H.D. Nguyen, Q.A. Nguyen, R.C. Ferreira, et al. (2005), "Construction of plasmid-based expression vectors for *Bacillus subtilis* exhibiting full structural stability", *Plasmid*, **54(3)**, pp.241- 248, DOI: 10.1016/j.plasmid.2005.05.001.

[5] D.G. Yansura, D.J. Henner (1984), "Use of the *Escherichia coli* lac repressor and operator to control gene expression in *Bacillus subtilis*", *Proc. Natl. Acad. Sci. USA*, **81(2)**, pp.439-443, DOI: 10.1073/pnas.81.2.439.

[6] H.T.T. Phan, N.N.Y. Nhi, L.T. Tien, et al. (2019), "Construction of expression plasmid for *Bacillus subtilis* using P*spac* promoter and *BgaB* as a reporter", *Sci. Technol. Dev. J.*, **22(2)**, pp.239-246, DOI: 10.32508/stdj.v22i2.1284.

[7] H.D. Nguyen, W. Schumann (2006), "Establishment of an experimental system allowing immobilization of proteins on the surface of *Bacillus subtilis* cells", *J. Biotechnol.*, **122(4)**, pp.473-482, DOI: 10.1016/j.jbiotec.2005.09.012.

[8] L. Briand, G. Marcion, A. Kriznik, et al. (2016), "A self-inducible heterologous protein expression system in *Escherichia coli*", *Sci. Rep.*, **6**, pp.33-37, DOI: 10.1038/srep33037.

[9] D.T.M. Tran, T.T.P. Phan, T.K. Huynh, et al. (2017), "Development of inducer-free expression plasmids based on IPTG-inducible promoters for *Bacillus subtilis*", *Microb. Cell. Factories.*, **16(1)**, DOI: 10.1186/s12934-017-0747-0.

[10] P.T.P. Trang, T.T.A. Dao, T.T. Lan, et al. (2018), "Developing auto-inducible P*grac*57 promoter in *Bacillus subtilis*", *Natural Sciences and Technology*, **15(3)**, pp.100-108.

[11] T. Phan, P. Huynh, T. Truong, et al. (2017), "A generic protocol for intracellular expression of recombinant proteins in *Bacillus subtilis*", *Methods Mol. Biol.*, **1586**, pp.325-334, DOI: 10.1007/978-1-4939-6887- 9_21.

[12] F.V. Aroca, M. Giannattasio, E. Brunelli, et al. (2006), "One-step high-throughput assay for quantitative detection of beta-galactosidase activity in intact gram-negative bacteria, yeast, and mammalian cells", *BioTechniques*, **40(4)**, pp.433-434, DOI: 10.2144/000112145.

DOI: 10.31276/VJSTE.63(1).71-76

Co-digestion of domestic wastewater and organic fraction of food waste using anaerobic membrane bioreactor: A pilot scale study

Hong Ha Bui[1], Lan Huong Nguyen[2*], Thanh Tri Nguyen[1], Phuoc Dan Nguyen[3]

[1]Institute for Tropicalization and Environment (ITE), 57A Truong Quoc Dung Street, Ward 10, Phu Nhuan District, Ho Chi Minh City, Vietnam
[2]Ho Chi Minh City University of Food Industry (HUFI), 140 Le Trong Tan Street, Tay Thanh Ward, Tan Phu District, Ho Chi Minh City, Vietnam
[3]Ho Chi Minh City University of Technology, 268 Ly Thuong Kiet Street, Ward 14, District 10, Ho Chi Minh City, Vietnam

Received 24 February 2020; revised 8 July 2020; accepted 20 July 2020

Abstract:

In this study, a co-digestion pilot scale study of a mixture of domestic wastewater and the organic fraction of food waste using an anaerobic membrane bioreactor was developed. As a result, it show that the removal efficiencies of the chemical oxygen demand (COD) and total suspended solids (TSS) were high and reached more than 90%. However, the removal of nitrogen and phosphate was not remarkable. The daily biogas yield reached 2.12 m^3/d. The obtained biogas per COD removed was 0.22 m^3/kgCOD. The average generated methane yield was 1.33 m^3/d,which is equivalent to 0.14 m^3/kgCOD. A high efficiency of organic compound removal combined witha large amount of retained nutrients and high biogas yield suggests the results of this pilot scale study can be practically applied to the recovery of nutrients for agricultural use along with biogas for cooking. These benefits remarkably reduce environmental pollution, especially for decentralized residential areas and independent-stationed military units located far from concentrated wastewater treatment plants.

Keywords: **anaerobic, AnMBR, biogas yield, co-digestion, domestic wastewater, food waste, pilot scale.**

Classification number: **3.5**

1. Introduction

Municipal wastewater and solid waste from decentralized residential areas and independent-stationed military units are rapidly increasing because of remarkable population growth. Almost all of this wastewater has not yet been treated to meet to allowable standards due to its distance away from wastewater treatment plants. Besides, municipal solid waste is also difficult to treat because of high cost and the generation of secondary pollution from landfills. Generally, these wastes are usually collected and treated separately by aerobic biological technologies, which leads to high cost, high energy consumption, and is ineffective for decentralized discharge sources. Meanwhile, anaerobic biological degradation is a technology that poses many advantages, such as low waste sludge and low energy consumption, while offering superb energy recovery potential from biogas, which reduces greenhouse gas emission and increases the energy recovery from waste treatment effluent [1, 2] However, the application of anaerobic technology has been limited by its long biomass retention time and poor biomass settling, leading to washout of biomass from the effluent [1, 3]. In order to overcome these disadvantages, recent research has developed membrane technologies; specifically, a submerged membrane technology that permits retaining complete microbial biomass in the reactor while also maintaining low reactor volume [4]. With regard to the recovery of biogas, a fraction of organic food waste can increase the biogas yield thanks to the growth of influent organic loading. Theoretically, the obtained CH_4 yield from anaerobic digestion is about 0.35 $m^3/kgCOD_{removed}$. Research results achieved by some scholars have shown a similar or lesser CH_4 yield when conducting experiments with a mixture of wastewater and the organic fraction of solid waste in anaerobic digestion. For instance, in Gouveia's research that uses a

*Corresponding author: Email: lanhuongba@gmail.com

pilot scale anaerobic membrane bioreactor (AnMBR) for the treatment of municipal wastewater, the methane yield achieved 0.18-0.23 Nm^3 CH_4/kg $COD_{removed}$ [5]. An AnMBR combined with activated carbon (GAC) was studied by D.W. Gao, et al. (2014) [6] to treat urban wastewater and obtained a methane yield of 140, 180, and 190 l CH_4/$kgCOD_{removed}$ corresponding to a hydraulic retention time (HRT) of 8, 6, and 4 h, respectively. M. Galib, et al. (2016) [7] studied the treatment of food wastewater by anaerobic membrane (AnMBR) with a retention time of 5 d, 2 d, and 1 d and the biogas production generated ranged from 0.13 to 0.18 l CH_4/$gCOD_{removed}$.

Anaerobic membrane technology has been widely applied to the treatment of various biodegradable wastewater on both the lab and pilot scale, such as a pilot AnMBR for the treatment of urban wastewater [8] and the decolonization of dye wastewater [9]. Anaerobic co-digestion of wastewater and solid waste have also been investigated by scholars over recent decades, for example, J.W. Lim (2011) [10] conducted a study on the co-digestion of a mixture of brown wastewater and food waste and the co-digestion of food waste and domestic wastewater by an upflow anaerobic sludge blanket (UASB) [11]. The mechanism of anaerobic digestion is the conversion of organic matter into valuable biogas without energy consumption. However, rarely has a study of the co-digestion of a mixture of wastewater and food waste submerged in an anaerobic membrane bioreactor (AnMBR) been conducted, especially a pilot scale study.

Therefore, in this work, a pilot scale study using the anaerobic co-digestion of a mixture of wastewater and organic fraction of food waste in a constantly-stirred, submerged anaerobic membrane bioreactor set up at an independent-stationed military unit far from residential areas. Based on the practical data collected of the discharge amount of domestic wastewater and organic fraction of food waste at various independent-stationed military units, together with inherited lab scale study results, the study found a suitable mixture ratio between these wastes to conduct the pilot scale study. Hence, the aim of this study is to evaluate the removal efficiency of organic compounds (COD), nutrients (N, P), total suspended solid, and pathogens and to estimate the biogas yield produced from the pilot scale co-digestion process.

2. Materials and methods

2.1. Domestic wastewater (DWW) and organic fraction of food waste (OFFW)

Domestic wastewater was directly taken from the septic tank at Radar Station 33 of the independent-stationed military unit in Ba Ria-Vung Tau province, Vietnam. The characteristics of this wastewater are presented in Table 1.

Table 1. Properties of domestic wastewater.

No.	Parameter	Unit	Value (n=10)
1	pH	-	7.1±0.5
2	COD	mg/l	152.0±51.0
3	TN	mg/l	113.05±18.5
4	$N\text{-}NH_4^+$	mg/l	103.08±11.8
5	TP	mg/l	8.95±1.25
6	TSS	mg/l	82.0±23.0

Food solid waste was collected from the residue of the kitchen at Radar Station 33, which included rice, fruit, and vegetable remains as well as meat and fish residues. The collected solid waste was then removed of its inorganic components (i.e. grit and plastic). In the next step, the residues were cut into small pieces and blended by blender to a size less than 0.5 mm. Finally, blended OFFW (BOFFW) samples were stored in plastic containers and kept in the refrigerator at 4°C. The characteristics of blended organic fraction of food waste are shown in table 2.

Table 2. Characteristics of blended organic fraction of food waste (BOFFW).

No.	Parameter	Unit	Value (n=3)
1	pH	-	6.8±0.5
2	Moisture	%	86.0±2.0
3	C/N	-	32.0±1.03
4	TS	g/kg wet	235.0±13.0
5	VS	g/kg wet	213.0±12.0

Based on the data collected of the discharge of domestic wastewater and solid waste at ten independent-stationed military units and some decentralized residential areas (data not shown), the ratio of BOFFW to DWW was at 5:1 (5 kg of BOFFW:1 m^3 of DWW). After mixing, the characteristics of the influent of the AnMBR-CSTR system are presented in table 3.

Table 3. Characteristic of influent wastewater after a mixture.

No.	Parameter	Unit	Value (n=3)
1	pH	-	7.3±0.3
2	COD	mg/l	2093.0±126.0
3	TN	mg/l	188.4±17.3
4	$N\text{-}NH_4^+$	mg/l	130.2±7.9
5	$P\text{-}PO_4^{3-}$	mg/l	6.0±0.3
6	TSS	mg/l	844.0±52.0

2.2. Set up treatment model

Because anaerobic sludge was not available, the sludge for this model was cultivated from probiotics, cow dung, and mud (500 l). The microbial culture process was carried out over 35 d. Firstly, the cow dung was finely ground then mixed with probiotic and molasses according to the ratio presented in Table 4. The mixture was then pumped into anaerobic tanks that contained the available wastewater. In the following step, the wastewater was stirred completely such that microorganisms make thorough contact with the cow dung, molasses, and sewage contained in the wastewater. The supplemented substrates were calculated as follows.

Table 4. The supplemented substrates used to cultivate microbials in the setup stage of the model.

Stage	Time (d)	Supplemented substrates					
		Wastewater (m^3)	*Fresh water (m^3)*	*Organic fraction of food waste (kg)*	*Probiotic (g)*	*Cow dung (kg)*	*Molasses (g)*
1	1-5	1	3	5	100	5	200
2	6-13	2	3	10	200	10	400
3	14-20	3.5	1.5	17.5	200	10	300
4	21-35	5	0	25	100	0	200

The initial culture sludge volume required to add into the tank:

$V_s = (V \times C)/MLSS = (5000 \times 6000)/11200 \approx 2678.6$ (l) (choose 2.7 m^3)

where V_s is the volume (l) of sludge to be added to the tank, V is the volume (l) of the mixing anaerobic tank, C is the optimal anaerobic sludge concentration in the mixing tank with a range of $4000 \leq C \leq 6000$ mg/l and C=6000 mg/l was chosen for this study, and MLSS is the concentration of anaerobic sludge added to the original tank, where MLSS=11200 mg/l.

The amount of probiotics, molasses, cow dung, clean water, and sewage added is presented in Table 4.

During the sludge culture process, the sludge volume must be checked and compared with the volume of sludge needed for the treatment process by turning off the agitator, letting the sludge settle for 30 min, and then measuring the volume of sludge. If the amount of obtained sludge was less than that of above-calculated sludge amount, the cultivating process needs to continue. If the amount of obtained sludge was enough or more than 10% in comparison with the calculated amount, the cultivating process was stopped.

2.3. The pilot model description

The pilot AnMBR-CSTR model is shown in Fig. 1. The model consists of an anaerobic continuous stirred reactor (AnCSTR) of 5 m^3 total volume with a diameter of 1.42 m, a height of 3.44 m, and a membrane tank that has the same total volume as the AnCSTR. One ultrafiltration membrane module (0.05 µm pore size) with a total membrane surface area of 10 m^2 was placed in this membrane tank. The model was operated with a flux of 10-50 l/m^2h.

Fig. 1. The pilot scale AnMBR-CSTR model.

2.4. Operation of the model

Figure 2 shows the flow diagram of the pilot model. The system's treatment medium flowrate was 210 l/h. The pilot system consisted of one continuous-stirred anaerobic tank with a volume of 10 m^3 and one submerged membrane tank with the same volume. Both tanks were connected each other to ensure that the sludge concentration in the two modules were the same and a circulating pump was continuously operated to circulate sludge from the membrane tank into the anaerobic continuously-stirred tank. The pilot model was fed with wastewater pre-treated as above description. The wastewater was first pumped into the anaerobic continuously-stirred tank. The AnCSTR was completely mixed using a paddle to increase the contact between the anaerobic sludge and the wastewater. After a certain retention time period, the wastewater was continuously pumped into the membrane tank. Both modules were equipped with biogas, temperature, and pressure meters. In order to control membrane fouling and maintain of the trans-membrane pressure (TMP), the membrane was cleaned with an operating cycle of 3 min of backwash, 5 sec of relaxation time, and 10 min filtration followed by 5 sec of relaxation time.

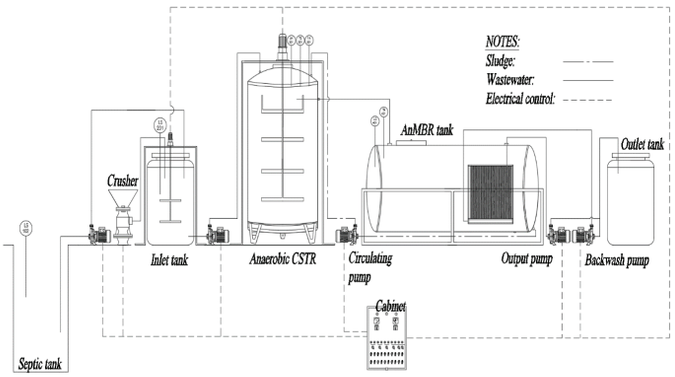

Fig. 2. Process flow diagram of the pilot scale AnMBR.

The operation conditions of AnMBR-CSTR were summarized in Table 5.

Table 5. AnMBR system operation parameters.

Parameter	Symbol	Unit	Value
pH	pH	-	7-8
Temperature	-	^oC	32.4-34.7
Hydraulic retention time	HRT	d	2
Sludge retention time	SRT	d	60
Organic load	OLR	kg COD/m^3.d	<1.3
Effective volume of the system	V	m^3	10
Flow input	Q	m^3/d	5

2.5. Analysis

The pH, COD of the influent, effluent, and membrane tank, and biogas yield in the effluent were analysed on a daily basis. TSS, N-NH_4^+, and P-PO_4^{3-} were measured at every other day. The operation time (total time of model) was 60 d.

The pH was measured by an online pH meter system that was directly installed into the treatment system. The COD, TSS, N-NH_4^+, and P-PO_4^{3-} were determined according to the standard methods for the examination of water and wastewater (APHA, 2012). The biogas yield was regularly monitored by an airflow measurement system and the obtained data were analysed using computer software.

3. Results and discussion

During 60 operation days, the pH of the influent and effluent of the AnMBR-CSTR at a SRT of 48 h ranged between 6.8-7.9±0.3 and 6.7-7.8±0.3, respectively. The pH was quite stable during the anaerobic degradation process of the mixture of BOFFW and DWW and suitable for the growth of anaerobic microorganisms. The pH of the effluent was slightly higher than that of the influent due to the accumulation of volatile fatty acids (VFAs) during acidification stage. However, the fluctuation of the pH was not significant, which showed there was a good balance between the metabolism of acidification and methane groups.

3.1. Total suspended solids (TSS) removal

The data in Fig. 3 shows the TSS of the influent and effluent and TSS removal efficiency of the pilot scale AnMBR-CSTR over a 60-d period of operation. It can be seen from Fig. 3 that despite the very high TSS in the influent, the effluent's TSS was low. The highest TSS removal efficiency reached greater than 95%.

The average TSS concentration in the influent was 844 mg/l and the TSS in the effluent was 52 mg/l. This result can be explained due to the presence of the ultrafiltration module in the AnMBR-CSTR system. The results were similar to the results obtained by a lab scale co-digestion model [12] and other studies [4, 5, 8, 9].

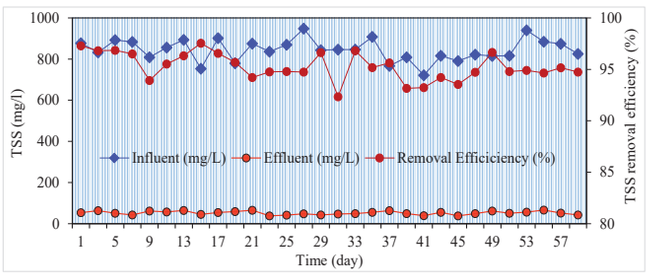

Fig. 3. The TSS removal efficiency.

3.2. The removal efficiency of COD

The influent and effluent COD and COD removal efficiency are presented in Fig. 4. A total removal efficiency higher than 90% was achieved with total COD values in the effluent ranging from 103 to 182 mg/l during the 60-d operation period despite an excellent COD in the influent (1807-2300 mg/l). The COD in the effluent was fairly stable during the treatment process. With the same HRT of 48 h, the pilot scale AnMBR-CSTR gave a similar removal efficiency of COD to the lab scale AnMBR-CSTR [12].

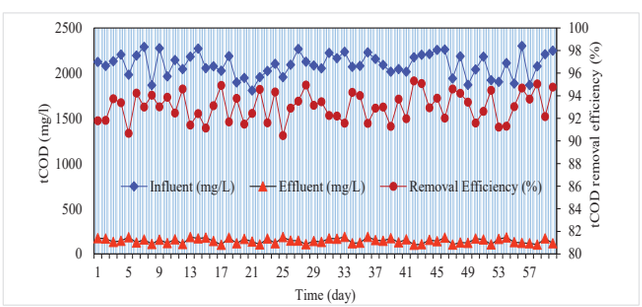

Fig. 4. The COD removal efficiency.

3.3. Nitrogen and phosphorus removal

The data in Figs. 5A and 5B show the concentrations of N-NH_4^+ and TKN, respectively, in the influent and effluent of the pilot scale AnMBR-CSTR. As can be seen from Fig. 5A, the N-NH_4^+ in the influent and effluent of was high and reached 112-149 and 139-198 mg/l, respectively. There was an increase in N-NH_4^+ in the effluent, which can be explained by the anaerobic degradation process where organic nitrogen derived from urine and some food wastes were converted into ammonium nitrogen by anaerobic microbial. Additionally, a part of N-NH_4^+ is used for cell synthesis of microorganisms. The results in Fig. 5B indicate that the TKN in the influent and effluent was significantly changed. From Fig. 5A and 5B, it can be seen that most of the N-TKN in the wastewater existed in the form of N-NH_4^+. These results agree with the work of J. Gouveia, et al. (2015) [5].

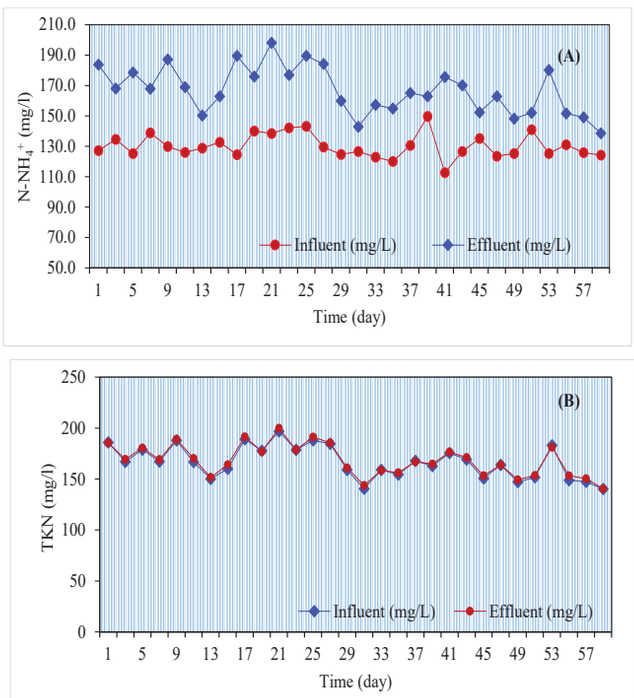

Fig. 5. Nitrogen removal (A) N-NH_4^+, (B) TKN.

The P-PO_4^{3-} concentration also significantly changed. The results in Fig. 6 indicate that there was a slight decline in P-PO_4^{3-} in the effluent, ranging from 6.0 mg/l to 3.9 mg/l. This decline in phosphorus is due to its use for the synthesis of microorganism cells.

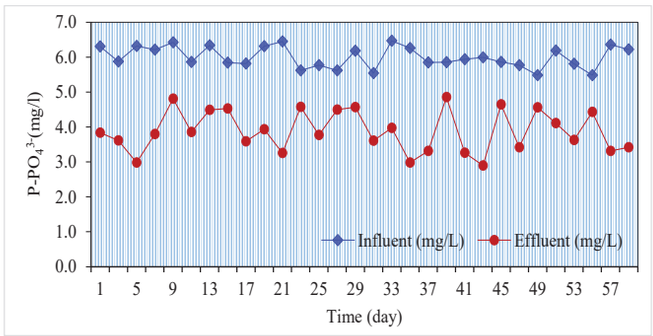

Fig. 6. Phosphate removal.

3.4. Biogas yield

The measured daily biogas yield had an average value of 2.12 m^3/d (the highest was 2.56 m^3/d and the lowest was 1.76 m^3/d). The amount of obtained biogas per removed COD was 0.22 $m^3/kgCOD_{removed}$ (the highest was 0.24 $m^3/kgCOD_{removed}$ and the lowest was 0.19 $m^3/kgCOD_{removed}$). The biogas yield data is presented in Fig. 7.

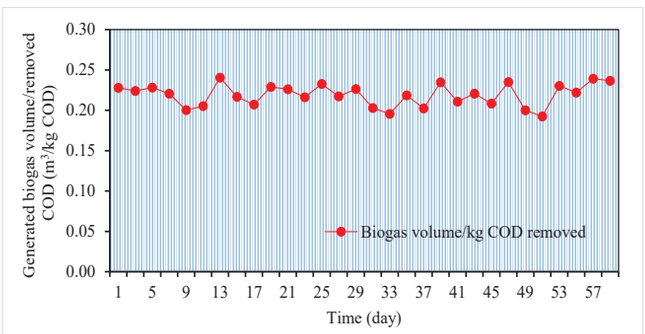

Fig. 7. The biogas yield generated per COD removed.

4. Conclusions

The co-digestion of domestic wastewater and food waste by a pilot scale anaerobic membrane bioreactor can solve both issues of wastewater treatment and food waste management for decentralized residential areas and independent-stationed military units. The removal efficiency of COD and TSS was quite high, especially with the presence of the membrane, from which TSS was completely removed. Moreover, supplementing with the organic fraction of food waste improved biogas generation. In summary, the pilot scale co-digestion technology performed in this study can be applied to a wider scale to resolve both wastewater and solid waste for decentralized areas that are far from concentrated treatment plants.

CRediT author statements

Hong Ha Bui, Lan Huong Nguyen: Conceptualization, Methodology, Data curation, Formal analysis, Writing - Review & Editing; Thanh Tri Nguyen, Phuoc Dan Nguyen: Conceptualization, Methodology, Writing original draft preparation, Writing - Review & Editing.

COMPETING INTERESTS

The authors declare that there is no conflict of interest regarding the publication of this article.

REFERENCES

[1] H. Kjerstadius, S. Haghighatafshar, Å. Davidsson (2015), "Potential for nutrient recovery and biogas production from blackwater, food waste and greywater in urban source control systems", *Environ. Technol.*, **36**, pp.1707-1720, DOI: 10.1080/09593330.2015.1007089.

[2] D. Goulding, N. Power (2013), "Which is the preferablebiogas utilisation technology for anaerobic digestion of agricultural crops in Ireland: Biogas to CHP or biomethane as a transport fuel?", *Renew. Energy*, **53**, pp.121-131, DOI: 10.1016/j.renene.2012.11.001.

[3] H. Lin, W. Peng, M. Zhang, et al. (2013), "A review on anaerobic membrane bioreactors: Applications,membrane fouling and future perspectives", *Desalination*, **314**, pp.169-188, DOI: 10.1016/j.desal.2013.01.019.

[4] Z. Huang, S.L. Ong, H.Y. Ng (2011), "Submerged anaerobic membrane bioreactor for low-strength wastewater treatment: effect of HRT and SRT on treatment performance and membrane fouling", *Water Res.*, **45**, pp.705-713, DOI: 10.1016/j.watres.2010.08.035.

[5] J. Gouveia, F. Plaza, G. Garralon, et al. (2015), "Long-term operation of a pilot scale anaerobic membrane bioreactor (AnMBR) for the treatment of municipal wastewater under psychrophilic conditions", *Bioresource Technology*, **185**, pp.225-233, DOI: 10.1016/j.biortech.2015.03.002.

[6] D.W. Gao, Q. Hu, C. Yao, et al. (2014), "Integrated anaerobic fluidized-bed membrane bioreactor for domestic wastewater treatment", *Chem. Eng. J.*, **240**, pp.362-368, DOI: 10.1016/j.cej.2013.12.012.

[7] M. Galib, E. Elbeshbishy, R. Reid, et al. (2016), "Energy-positive food wastewater treatment using an anaerobic membrane bioreactor (AnMBR)", *J. Environ. Manage.*, **182**, pp.477-485, DOI: 10.1016/j.jenvman.2016.07.098.

[8] A.S.J.B. Giménez, A. Robles, L. Carretero, et al. (2011), "Experimental study of the anaerobic urban wastewater treatment in a submerged hollow- fibre membrane bioreactor at pilot scale", *Bioresour. Technol.*, **102**, pp.8799-8806, DOI: 10.1016/j.biortech.2011.07.014.

[9] A. Spagni, S. Casu, S. Grilli (2012), "Decolourisation of textile wastewater in a submerged anaerobic membrane bioreactor", *Bioresour. Technol.*, **117**, pp.180-185, DOI: 10.1016/j.biortech.2012.04.074.

[10] J.W. Lim (2011), *Anaerobic Co-digestion of Brown Water and Food Waste for Energy Recovery*, 11th Ed. World Wide Work. Young Environ. Sci. (WWW-YES-2011)-Urban waters: resource or risks, pp.6-10.

[11] P.C. Chan, R.A. Toledo, H.I. Iu, et al. (2018), "Co-digestion of food waste and domestic wastewater - effect of copper supplementation on biogas production copper supplementation on biogas production", *Energy Procedia*, **153**, pp.237-241, DOI: 10.1016/j.egypro.2018.10.008.

[12] B.H. Ha (2018), "Co-digestion of food waste and domestic wastewater by using upflow anaerobic sludge blanket (Uasb) couped with a microfiltration membrane (Mf)", *Vietnam J. Sci. Technol.*, **56**, pp.118-125, DOI: 10.15625/2525-2518/56/2c/13038.

DOI: 10.31276/VJSTE.63(1).77-82

Fluctuations in agriculture and sediment in the Mekong delta of Vietnam due to increased upstream water use

Viet Hung Bui[1*], Ngoc Diep Nguyen[2]

[1]Faculty of Environment, University of Science, Vietnam National University - Ho Chi Minh City, 227 Nguyen Van Cu Street, Ward 4, District 5, Ho Chi Minh City, Vietnam
[2]Faculty of Economic Institution, University of Labor and Social Affairs, Ho Chi Minh City, 1018 To Ky Street, Tan Chanh Hiep Ward, District 12, Ho Chi Minh City, Vietnam

Received 12 August 2020; revised 15 November 2020; accepted 3 December 2020

Abstract:

The Mekong delta (MD) of Vietnam rests at the end of the lower Mekong basin (LMB) where it is met with serious adverse effects from all upstream activities with severe consequences like landslides and complicated subsidence phenomena. Because the Vietnamese MD is a wetland, it carries many advantages such as an abundant water resource in both quality and quantity, large soil resource area, diversity in bioecology, and harmonious climate (large rainfall, warm), all of which expand the production, ecology, and environmental sectors. Researchers agree that the main reason for these consequences are the lack of sediment deposited in MD due to the absence of floods and upstream hydropower development. To better understand the causes of the above phenomena, research on the transboundary impact between Vietnam and Cambodia in the MD was carried out [1]**. This article develops more reliable scientific evidence of the impacts of upstream water use on the economic, social, and environmental factors of its four national members. It also scientifically demonstrates the transboundary impacts of upstream hydropower and irrigation developments in LMB such as the decline of sediment and the extreme decline of the quantity/yield from natural fisheries under all development scenarios.**

Keywords: **hydropower plant, irrigation, lower Mekong basin, transboundary impacts, water resource, water use.**

Classification number: **5.1**

1. Introduction

Because the Vietnamese MD is a wetland, it carries many advantages such as an abundant water resource in both quality and quantity, large soil resource area, diversity in bioecology, and harmonious climate (large rainfall, warm), all of which expand the production, ecology, and environmental sectors. Now, these advantages coincide with many adverse impacts from upstream the Mekong river basin. With this comes many opinions from inside and outside stakeholders, researchers, and experts presented with this situation in the MD.

The external causes of impacts on the MD are the hydropower projects, irrigation systems, and industrial zones along upstream countries that make hydrological flow and drought more serious during the dry season [1]. The internal causes of impacts on the MD is the quality of surface water that is too polluted, which leads to the critical problem of water security [2]. With the current economic development of both upstream and downstream countries, especially those in energy development, the adverse effects are focused on mainstream hydropower plants and irrigation in the Mekong river basin [3].

To provide foundational scientific knowledge to this discussion, in 2011, the Mekong River Commission (MRC) implemented a Council Study Program (CSP), namely "Study on the sustainable management and development of the Mekong river, including impacts of mainstream hydropower projects", which was completed in 2018. The main objective of the CSP is to enhance the scientific knowledge of the potential impacts of economic development on the water, people, as well as the natural environment of the Mekong river basin [4]. Transboundary impacts have been an issue of interest to Vietnam because the MD in Vietnam is the most vulnerable region in the whole basin [3]. The results of the consultant group's assessment of

*Corresponding author: Email: bvhung@hcmus.edu.vn

Vietnam, which contributed to the CSP's results, presented the transboundary impacts between Vietnam (downstream) and the upstream region on agriculture production and sediment condition.

While the transboundary impacts studied in the CSP included agriculture, aquaculture, water quality, and labour, in this research the sections are the environmental (water quality, sediments), economic (production rice fluctuations), and social sectors (labour force).

2. Materials and methods

The CSP is a complicated body of research with many kinds of data and information with different steps, activities, and subjects in its process. The general approach of the research is summarised by the following steps:

The CSP is implemented via 2 pathways. These pathways are (1) impacts of water resource development via both positive and negative changes to the hydrological regime (i.e., hydropower or irrigation projects changing timing, quantity, quality, etc.) and (2) positive and negative impacts not transmitted via the hydrological regime. The CSP's assessment approach is illustrated in Fig. 1.

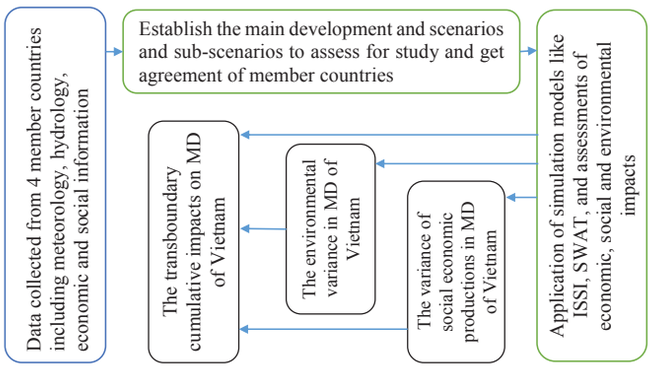

Fig. 1. CSP's integrated assessment approach [4].

The CSP divided the region of interest in the LMB into 6 subzones. Zone 6, including zone 6A - freshwater MD of Vietnam and zone 6B - saline MD of Vietnam, is the study region in Vietnam (Fig. 2). So, the area researched in zone 6 is the whole region of the MD in Vietnam. The transboundary cumulative impact assessment caused by the identified upstream development activities for zone 6 is the most comprehensive compared with those of the upper zones in the LMB [4].

With the above assessment and geographical scopes, the CSP created some scenarios to specifically research and assess as well as to form the scientific basis for the analysis of causal impacts. There are 3 kinds of development scenarios including the M1 scenario, which represents the baseline condition of research and the referential conditions for comparisons with others. The development scenarios are (i) the early development scenario (M2); (ii) the definite future scenario (M3) and with climate change (M3CC); and (iii) planned development scenarios with 12 sub-scenarios, namely, C2, C3, A1, A2, F1, F2, F3, H1a, H1b, H3, I1, and I2 with focus on irrigation, hydropower, and flood conditions (Table 1).

Table 1. Composite indicators for use in the transboundary Cumulative Impact Assessment (CIA).

Approach	Dimensions	Indicators for transboundary CIA
Qualitative and Quantitative synthesis	Social - Economic	Income (fish and rice surplus) (USD) Production (fish and rice values) (USD)
	Environmental	Water quality and sediment conditions in mainstream of Mekong river
	Integrated	Resilience, vulnerability

The transboundary impact assessment is a part of the Integrated Multi-Sector Cumulative Impact Assessment. The transboundary impact assessment between Vietnam and Cambodia is one part of this sector.

The assessment of the transboundary impacts on the MD of Vietnam caused by the construction of hydropower plants and extended irrigation areas included the upstream countries of China, Laos, Thailand, and Cambodia along with their cumulative characteristics of potential impacts [3, 4].

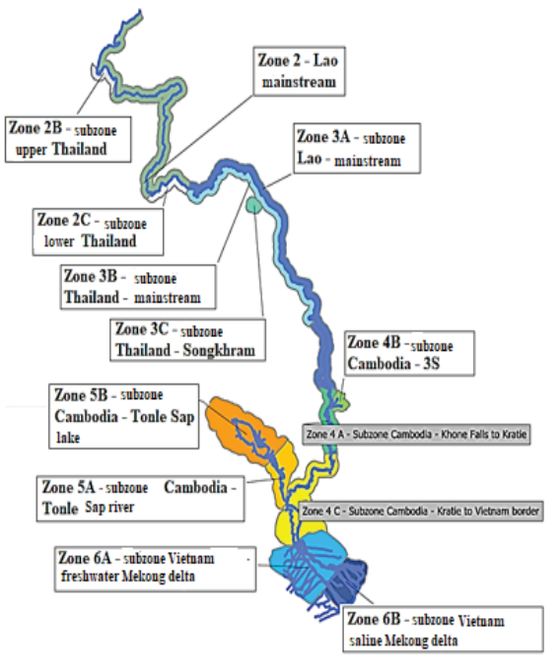

Fig. 2. Map sub-zones used for the assessment of impacts in Council Study [4].

For more detail of the transboundary impacts as well as their effectiveness, the approach from transboundary impact assessment was used, which is implemented using the following indicators as seen in Table 1. The 6 sub-scenarios in Table 2 (F2, F3, I1, A1, A2, and A3) were used to estimate the consequences of transboundary socio-economic assessment. The matrix of scenario comparisons for the transboundary socio-economic assessment is considered in Table 3.

Table 2. Main development scenarios.

Sc.	Describes	Sc.	Describes
M1	Early development scenario 2007	C2	Planned development 2040+wetter CC
M2	Definite future scenario 2020	C3	Planned development 2040+drier CC
M3	Planned development scenario 2040	F1	Planned development 2040 without FPF
M3CC	Planned development scenario 2040 with CC	F2	Planned development 2040 with FPF2
A1	Planned development 2040 without ALU	F3	Planned development 2040 with FPF3
A2	High level ALU implementation	H1a	Planned development 2040 without HPP
I1	Planned development 2040 without IRR	H1b	Planned development 2040 (Chinese, tributary and mainstream dam)
I2	Planned development 2040 with IRR HIGH	H3	Planned development 2040 with HPS3

Table 3. Scenario and sub-scenario comparisons for the socio-economic assessment.

Effects tested	Scenario comparisons	Socio-economic
Surplus of fish and rice production	(All)	X
Climate change	M3CC vs C2, C3	X
Irrigation development	M3CC vs I1, I2	X
Hydropower development	M3CC vs H1a, H1b, H3	X
Agriculture and land-use development	M3CC vs A1, A2	X
Flood protection infra-structure development	M3CC vs F1, F2, F3	X

A: agriculture; C: climate change; I: irrigation development; H: hydropower; F: flood protection.

3. Results and discussion

Based on the results of all the scenarios (i.e., main and sub-development scenarios), the changes in social, economic, and environmental dimensions in zone 6 (MD of Vietnam) due to the transboundary impacts caused by upstream development activities along upstream countries are identified and summarised below.

3.1. The variance of social economic productions in MD of Vietnam

The transboundary social economic assessment was implemented by identifying food security from surplus of fish and rice production. In fact, there are many other factors related to the food security, but, at this time, they are out of the scope of this research. The surpluses of rice and fish production in the sub-scenarios are presented with the variances of transboundary impacts caused by the upstream development activities on MD of Vietnam in Figs. 3, 4.

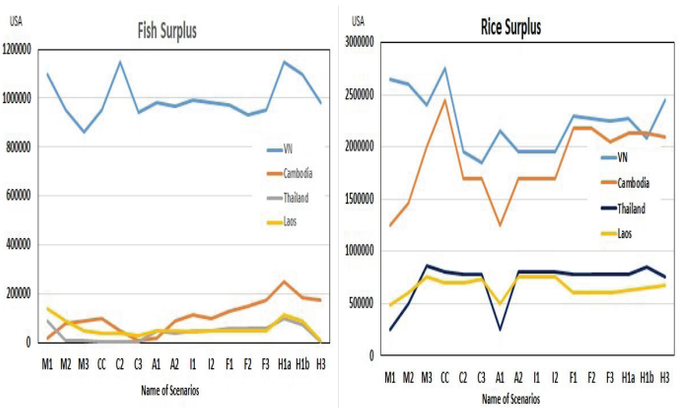

Fig. 3. National fish and rice surplus for all scenarios [4].

Figure 3 indicates that Vietnam's fish and rice production are influenced by all of the upstream water development activities described in the sub-scenarios. However, the variance of fish and rice surplus is not large and could be explained by the dependence of fish and rice surplus on the export market.

With changes in rice and fish production, poor households become more vulnerable in sub-scenarios C3 and F2, which cause major dips in fish surplus, as well as C2, C3, A1, A2, IRR2, IRR3, and H1b, which all reduce rice surplus. When considering climate change conditions, Vietnam could help the conditions of increasingly poor households and would likely to see a substantial reduction in vulnerability if less dams or no dams were built (H1a or H1b) (Fig. 4).

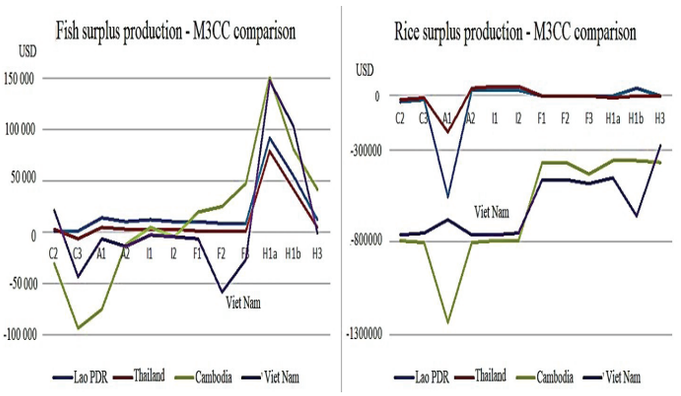

Fig. 4. Fish and rice surplus for sub-scenarios if compared with M3CC [4].

The rice production in zone 6 (MD of Vietnam) estimated over a 24-year period under the main development scenarios is illustrated in Fig. 5. The rice production's variance over the 24-year development scenario is not much because the local water infrastructure has been nearly completely constructed, which protects the rice land and local residences.

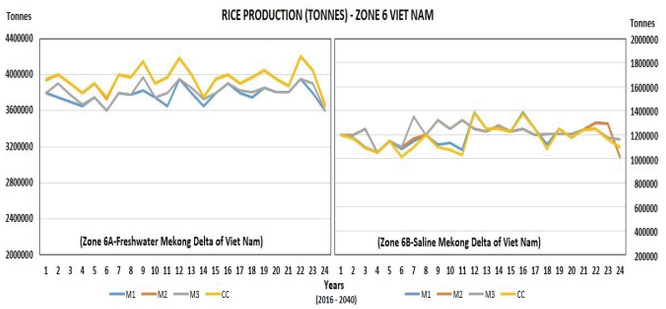

Fig. 5. Rice production (tons) over the 24 year by main development scenarios [4].

The variance in fish production in zone 6 over the 24-year development scenarios are shown in Fig. 6. The fish sector (including the native fish catch and aquaculture) changed because it depends on a lot on the flow of both quality and quantity, which is significantly impacted by the development activities of upstream countries.

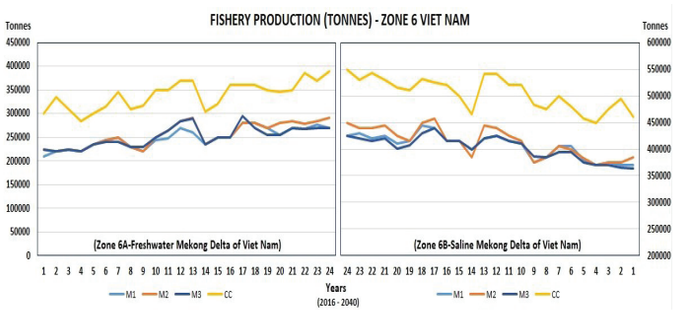

Fig. 6. The native fish catch and aquaculture production estimated in zone 6 (6A, 6B) [4].

The CSP's sector approach has shown that even until 2040, significant impacts from climate change are likely and could be caused by transboundary impacts of water resource development coupled with the changing climate. When considering climate change, one striking finding is the significant reduction of future GDP for all climate scenarios. The change of GDP in zone 6 is listed in Table 4. The reducing rates in the climate change scenarios clearly showed that climate change will directly affect the LMB including zone 6 - MD of Vietnam.

Besides the transboundary impacts of Cambodia caused by its economic decline of rice and fish production, MD of Vietnam has to face the adverse variance of water resource due to the rise in sea level, which makes salinity intrusion penetrate deeply into the area.

Table 4. The GDP projection (average) and its (%) reduction for 2040 due to climate change [4].

Scenarios	GDP (billion USD)	Rate (%)
M1 trend	82.3	
M2	82.7	-0.6%
M3 (No CC)	82.5	-0.2%
M3CC	81.3	1%
C2 (Wet)	78.9	4%
C3 (Dry)	78.7	5%

3.2. The environmental variance in MD of Vietnam

The modelling study of CSP considered the effects from different scenarios on a variance/change of issues such as flow, sediment, and nutrient regimes due to the cumulative effects of upstream development activities including climate change. The natural phenomena regime is changed significantly due to the impacts of upstream reservoirs and dams. The variance of flow regime is different between the time scenarios, which means the seasonal or annual average or tidal flows.

Seasonal flow changes: With the development of hydropower projects in the basin, there is a change in flow regime between the wet season with lower flows and the dry season with increased flows in MD. A potential benefit may appear when the dry seasonal flow increases, and oppositely, when flood areas and the reversal of the Tonle Sap lake to the MD are reduced, which impacts flood pulse-dependent ecosystems. The reversal in flow will be 8% lower for (M2), 5% (M3), and 9% (M3CC). In a different way, a dry year would have a reversal of 58% (M2), 60% (M3), or 55% (M3CC) of the baseline average.

Annual average flow change: The change in annual average mainstream flow did not increase or reduce by much. The variance was between -3.4 and 2.4% when the authors compared the main development scenarios to the baseline scenario M1 (Fig. 7).

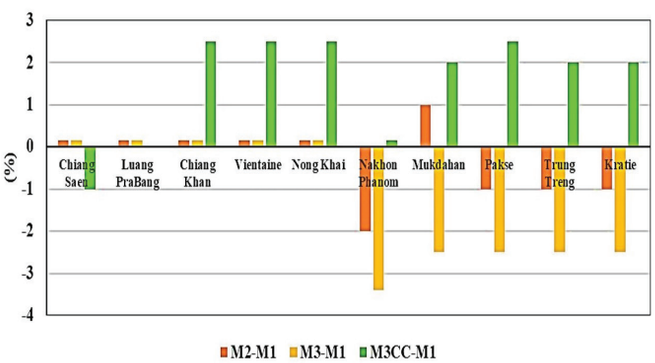

Fig. 7. The percent different annual average flow at key stations along river [4].

Sediment flux: The change in volume of sediment flux is the most striking finding from the modelling so far. The retaining of sediment passage by the cumulative effect of reservoirs in the upstream river basin's region, in tributaries, and as proposed in the mainstream all but take out the sediment from the river when it reaches to downstream region. At Kratie, there was only 3% sediment flux continuing to the delta as highlighted in red in Fig. 8. The figure also shows the adverse effect of trapped sediment on hydropower reservoirs along the mainstream is significant. For example, the volume of sediment from MRB through Kratie toward the delta was simulated to be about 143 Mt/y (M1). It was reduced in 2020 (M2) to only 47.4% of the natural value and for M3 and M3CC to less than 4% for the 2040 scenarios that have full hydropower development.

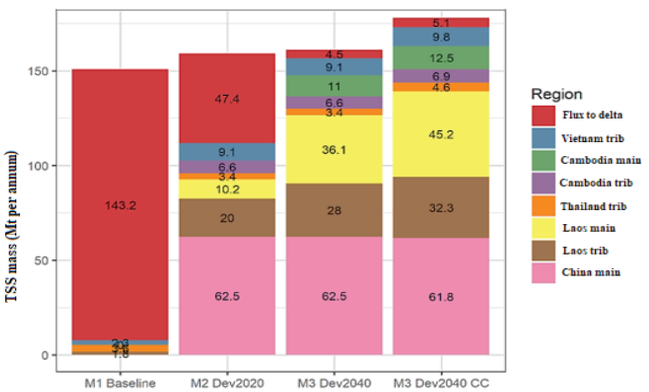

Fig. 8. Reservoir sediment trapping by region main scenarios [4].

3.3. The transboundary cumulative impacts on MD of Vietnam

The authors integrated all figures of the positive and negative impacts of all upstream development activities in upstream countries through the main and sub-development scenarios. The assessment of the transboundary effects/ adverse impacts on the MD of Vietnam can be considered as connections between benefit and cost-sharing mechanisms, which require the consideration of very complex socio-economic interactions. This assessment focused on the most critical trade-off between hydropower and fisheries. The integration echoed many of the themes raised by other assessments. The transboundary assessment impacts are only focused on a few themes like:

- The emerging trade-offs between hydropower and fisheries are substantial and suggest a project-by-project assessment to identify the most harmful and the most efficient investment projects.

- Transboundary effects were significant and include positive effects for Thailand and Vietnam as a consequence of their investments in hydropower. While Cambodia had negative effects due to losses in fisheries and sediment.

The approach for addressing benefit sharing is to compare sector impacts (hydropower and fisheries) in key sub-scenarios. Sub-scenario H1a quantifies the negative external impacts the combined bundle of hydropower project is likely to have on fisheries. Sub-scenario H1b limits the effects on mainstream hydropower.

Table 5. Comparison of hydropower benefits and fisheries cost for H1a and H1b [4].

Scenario	Country	Hydropower benefits ($)	Fisheries costs ($)	National cost-benefit ratio	Possible benefit transfer levy
H1a	Cambodia	11.1	6.5	58%	Mainstream HPP: 18.9%
	Lao PDR	36.3	4.0	11%	
	Thailand	82.9	6.5	8%	
	Vietnam	26.7	2.5	9%	
H1b	Cambodia	3.7	2.3	61%	On tributary HPP: 8.6%
	Lao PDR	17.3	2.1	12%	
	Thailand	63.7	3.1	5%	
	Vietnam	15.2	1.2	8%	

Table 5 compares country-specific hydropower benefits with the costs of fisheries, which results in a side-effect of hydropower investments. Critical to this comparison is that hydropower benefits do not remain in the countries where dams are or would be located. However, it should be noted that the fisheries sectors are likely to experience substantial losses when there is increasing investment on hydropower development. The economic losses of the fisheries sector are not only about the price and fishing catch, but also the reduction of both nutrient, sediment, and the variance of flow due to the impacts of upstream hydropower development. So, Table 5 is a clear demonstration of a synthesis of the combined impacts of upstream development activities on the MD of Vietnam.

4. Conclusions

The transboundary cumulative impact assessment helps us understand the relationships between upstream water development activities and the adverse variations occurring in the MD. Additionally, we found significant cause for all impact factors. The significant trade-off in hydropower development in the lower basin may cause damage to the MD of Vietnam specifically to the fisheries sector and by significantly reducing the sediments deposited in reservoirs (by about 4%) and decreasing the amount of sediment and nutrients moving downstream compared to 2007. Besides, the results of this research also showed the inter-dependence of LMB countries in the economic-social development of each country.

Although the scope of our study is focused on the transboundary cumulative impacts of upstream water development activities, especially upstream hydropower development impacts on the mainstream, the research results are still logically useful scientific bases and a methodical investment compared with many related studies in the Mekong region so far.

CRediT author statements

Viet Hung Bui, Ngoc Diep Nguyen: Conceptualization, Methodology, Data curation, Formal analysis, Writing - Review & Editing.

ACKNOWLEDGEMENTS

This research is small component of whole results of the Council Study of MRC, which made more clearly the transboundary impacts to MD of Vietnam. The research is supported by the Vietnam National Mekong Committee. The authors would like to express the gratitude to the Southern Institute of Water Resource Research (SIWRR) for supporting data for this research.

COMPETING INTERESTS

The authors declare that there is no conflict of interest regarding the publication of this article.

REFERENCES

[1] T. Trinh (2018), "Mekong delta faced on warning 'be submersible'", *Tuoi Tre Online*, https://tuoitre.vn/dbscl-truoc-canh-bao-bi-nhan-chim-20180404160602866.htm, accessed 5 April 2020 (in Vietnamese).

[2] L. Quynh (2017), *Mekong Delta: A Lot Water but Still Lack of Available Water*, Center for International Studies, University of Social Sciences and Humanities, Ho Chi Minh city, http://scis.hcmussh.edu.vn/?ArticleId=291ed61c-6aac-4335-bc20-cdf6f3e5d50e, accessed 5 April 2020 (in Vietnamese).

[3] Ministry of Agriculture and Rural Development (2019), *Research on Solutions and Technologies to Prevent River Erosion in Bac Lieu and Ca Mau Provinces*, Ministry - level Science and Technology Research, http://www.siwrr.org.vn/?mod=list&id=84&cid=712&page=&lang, accessed 5 April 2020 (in Vietnamese).

[4] Mekong River Commission (2020), http://www.mrcmekong.org/highlights/the-council-study-reports/, accessed 5 April 2020.

DOI: 10.31276/VJSTE.63(1).83-89

Removal of greenhouse gas in biofilter using organic and inorganic media

Nguyen Thanh Tung[1], Wilai Chiemchaisri[1], Chart Chiemchaisri[1*], Samunya Sanguanpak[2]

[1]Department of Environmental Engineering, Faculty of Engineering, Kasetsart University, 50 Ngamwongwan Road, Lat Yao District, Chatuchak District, Bangkok, Thailand
[2]National Metal and Materials Technology Center, National Science and Technology Development Agency, 11 Thailand Science Park (TSP), Phahonyothin Road, Khlong Nueng, Khlong Luang District, Pathum Thani Province, Thailand

Received 27 April 2020; revised 14 June 2020; accepted 26 June 2020

Abstract:

A biofilter using organic (compost) and inorganic (pumice, porous silica pellet or poremat) media was applied to the removal of methane (CH_4) and nitrous oxide (N_2O) to minimize the impact of off-gasses from municipal solid waste disposal global. The objective was to determine the appropriate biofilter media for CH_4 oxidation and N_2O conversion. The off gas (59.6% CH_4, 1.0% N_2O) was fed simultaneously with air (1:3 ratio) into the biofilter. CH_4 oxidation and N_2O conversion rates were observed over a 101-day period through the analysis of gas concentration along the biofilter's depth using gas chromatography. Higher CH_4 oxidation in the biofilters containing organic and inorganic media was achieved, especially for the compost-poremat biofilter with 70.1 g $CH_4/m^3/d$ realised. The most active methane oxidation zone was found near the gas inlet at the bottom of the biofilter. The presence of inorganic material helped promote aerobic conditions for CH_4 oxidation, especially during the initial period. N_2O was also more completely removed with the biofilter containing inorganic media. Higher methanotrophic activities in matured biofilter media and the presence of methanotrophs type I, which prefer oxygen-rich conditions, were confirmed.

Keywords: **biofilter, compost, greenhouse gas, inorganic media, methane oxidation.**

Classification number: **5.1**

1. Introduction

Municipal solid waste (MSW) disposal on land either by sanitary landfilling or open dumping are the most common methods used in Asian countries [1]. Their major environmental impacts include pollution from leachates and greenhouse gas emissions. Highly potent greenhouse gases, including methane (CH_4) and nitrous oxide (N_2O), could be produced during solid waste decomposition in waste landfills as well as leachate treatments [2-5]. Therefore, the mitigation of CH_4 and N_2O emissions from emitted gas is required to minimize the overall environmental impact from MSW management.

Biofiltration is considered to be a cost-effective and efficient means to mitigate diffuse CH_4 emissions [6]. In a biofilter, CH_4 is oxidized to CO_2 by methanotrophic bacteria under the presence of oxygen [7]. Previous studies have reported the application of biofilters to alleviate CH_4 in off-gases from landfills [8] and wastewaters [9, 10]. Different organic materials have been applied successfully as biofilter media including compost [11] and stabilized wastes [12]. It was reported that the loose texture of the organic media provided sufficient oxygen while supplementing nutrients for methanotrophic activities [11]. Nevertheless, high CH_4 oxidation could not be sustained over long-term operation due to the shortage of oxygen supply from media clogging as a result of excessive extracellular polysaccharide (EPS) production from methanotrophic activities [13]. On the other hand, inorganic media such as gravels and porous clay particles have been used as biofilter media [14], but the optimum nutrient solution needs to be continuously supplemented to maintain its methanotrophic activities [15]. To deal with these difficulties, a combination of organic and inorganic packing materials for CH_4 biofiltration systems were studied in this research. In our hypothesis, the organic materials played a role in supplying nutrients for methanotrophs while the clogging problems of filter media were alleviated by the presence of granular inorganic materials that preserve the stability of the filter media structure and allow uniform gas distribution. Moreover, we also investigated N_2O conversion, which occurred simultaneously with CH_4 oxidation, during gas treatment in the biofilter.

**Corresponding author: Email: fengccc@ku.ac.th*

2. Materials and methods

In this study, three different materials, including one organic material (compost) and two inorganic materials (pumice, porous silica pellet), were used to investigate their methane removal capacities. Specifically, the organic material was commercial grade leaf compost for garden applications and the inorganic materials were pumice of 3-5 mm diameter (commonly used as filter material in fishponds or aquariums and for garnishing soil for flowering and ornamental plants) and porous silica pellets called "poremat", which is commonly used as media in biological water treatment and controlled planting systems.

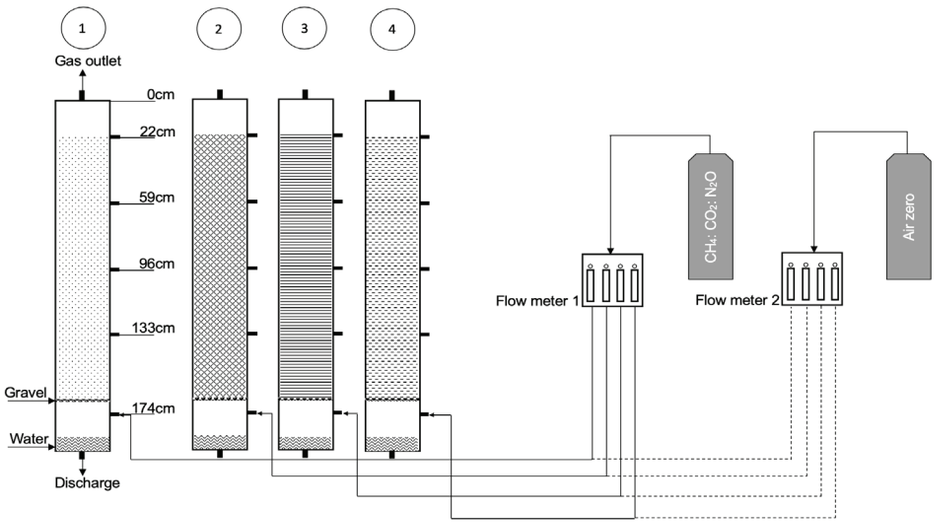

Fig. 1. Schematic of experimental column with different media: (1) compost, (2) compost-pumice, (3) compost-poremat, and (4) compost-pumice-poremat.

Four acrylic closed-top columns of 5 cm diameter and 180 cm length (Fig. 1) were used. The columns were equipped with gas sampling ports sealed with butyl rubber stoppers. Each column contained 3 l of filter material placed over 2 cm of gravel and a perforated plate located 15 cm from the bottom of the column. The 1st column was filled with 100% compost whereas the 2nd, 3rd, and 4th columns were filled with a mixture of compost and pumice at 70:30% (w/w), a mixture of compost and poremat at 70:30% (w/w), and a mixture of compost, pumice, and poremat at 70:15:15% (w/w), respectively. The placement of the biofilter material was performed by homogeneously mixing the indicated material proportions and placing it into the biofilter as a 10 cm layer until the total media depth (150 cm) was reached. The amount of media placed into each biofilter was as follows: column 1 had 1,708 g of compost; column 2 had 1,340 g of compost and 574 g of pumice, column 3 had 1,381 g of compost and 592 g of poremat, and column 4 had 1,361 g of compost, 292 g of pumice, and 292 g of poremat. The mixed media samples were also kept for characterization. The physicochemical characteristics of the biofilter materials in each column were analysed following standard methods [16] and the results are shown in Table 1. Artificial gas (CH_4:CO_2:N_2O=59.94:39.96:0.10%) and laboratory grade purified air (or air zero) were continuously fed to the bottom of the columns at 0.5 and 1.5 ml/min flow rates. These gas concentrations were set to simulate the emission of CH_4 (20-60%) and N_2O concentrations (up to 300 ppm) from open dumpsites and aerated closed landfill sites reported in previous studies [17, 18]. The experiment was conducted at room temperature (28-30°C) and the moisture content of each media were adjusted from their initial values of 10-15% (Table 1) to 25% after being placed in the biofilter to optimize methanotrophic activities [19]. At the end of the column experiment, the biofilter materials in the columns were sampled and analysed for methanotrophic activity and responsible microorganisms.

Table 1. Characteristics of biofilter media.

Parameters (unit)	Column No.			
	1	*2*	*3*	*4*
pH	7.5	7.5	7.7	7.6
Moisture content (%)	15.2	10.4	10.6	10.5
Porosity (%)	39.7	61.5	54.6	58.3
Bulk density (g/cm^3)	0.58	0.65	0.67	0.66
Total Nitrogen (µg/g)	10,008	7,718	7,823	5,465
NH_4^+ (µg/g)	69.9	39.7	19.3	27.0
NO_3^- (µg/g)	1,059	942	833	726
PO_4^{3-} (µg/g)	5,268	4,010	3,941	3,803

The column experiment was initialized one month prior to the methane oxidation rate (MOR) measurements. There was no initial inoculation of methanotrophs in the biofilter media, thus an initial start-up operation was required to allow indigenous methanotrophic bacteria to develop naturally in the biofilters. During the experiment, gas samples were collected from the sampling ports and analysed for their composition (CH_4, CO_2, O_2 and N_2O) using gas chromatography (GC). For CH_4, CO_2, and O_2 gas analysis, an Agilent GC6890 equipped with a CTR I (Alltech®) column and thermal conductivity detector (TCD) was used. The operating conditions were an inlet temperature of 105°C, column temperature of 35°C, and a detector temperature of 150°C with helium (He) carrier gas

flow rate of 65 ml/min. Meanwhile, a Perkin Elmer Clarus 580 GC equipped with a Heyesep D column and electron capture detector (ECD) was used for N_2O analysis. The operating temperatures of the injector, column, and detector temperatures of 400, 60, and 300°C, respectively, with a He carrier gas flow rate of 20 ml/min.

For CH_4 and N_2O, the MOR and nitrous oxide conversion rate (NCR) were calculated from the inflow and outflow gas concentrations from each section of the biofilter media depth as shown in the following equation:

$$R\ or\ NCR = \frac{Q[(C)_{in}-(C)_{out}]}{V_{media}} \quad (1)$$

where MOR = methane oxidation rate (g $CH_4/m^3/d$); NCR = nitrous oxide conversion rate (g $N_2O/m^3/d$); Q = gas flow rate (m^3/d); $(C)_{in}$ = inflow CH_4 or N_2O gas concentration (g/m^3); $(C)_{out}$ = outflow CH_4 or N_2O gas concentration (g/m^3); V_{media} = volume of filter media at corresponding depth (m^3). The t-test analysis was used to verify any significant difference between the experimental columns at 95% confidence interval ($p<0.05$). Microsoft Excel version 2019 was used to perform the statistical analysis.

Batch experiments were conducted to evaluate the methanotrophic activities and carbon dioxide production rates of biofilter media. Ten grams of media were taken from the columns at the end of experiment (day 101) and transferred into 108-ml serum bottles capped with rubber septa and aluminium rings. Each experiment was conducted in duplicate. Subsequently, 10 ml of artificial gas (CH_4:CO_2:N_2O) was added to the serum bottle and incubated at room temperature (28-30°C), then the gas composition in the headspace was analysed by GC daily over a 3-day period. During the batch experiments, the methanotrophic activity (MOA) and carbon dioxide production rate (CPR) of the biofilter media and methane or carbon dioxide concentration gradients were determined and input into the following equation:

$$MOA\ or\ CPR = \frac{pV_{gas}}{M}\frac{dC}{dt} \quad (2)$$

where MOA = Methanotrophic activities (mg CH_4/g media/h); CPR = Carbon dioxide production rates (mg CO_2/g media/h); ρ = CH_4 or CO_2 gas density at room temperature (mg/cm^3); V_{gas} = head space gas volume (cm^3); M = dried mass of media (g); dC/dt = CH_4 or CO_2 concentration gradient (vol. fraction/h).

The microbial population attached on the organic (compost) and inorganic (poremat) media were analysed by next generation sequencing. The isolation of the microbial genomic DNA from the test materials were performed by the DNeasy PowerSoil Pro Kit. The 16S rRNA gene was amplified using 341F and 805R primers (Quanta bio, USA). Cluster generation and 250-bp paired-end read sequencing were performed on an Illumina MiSeq and examined using FASTQC software. The methanotrophic, nitrifying, and denitrifying microorganisms responsible for CH_4 oxidation and N_2O production were targeted in this study.

Results and discussion

Methane oxidation rate (MOR) in biofilter

Figure 2 shows the MOR observed among the different biofilters after the start-up period. During the initial period (day 39-60), the biofilters containing organic and inorganic media provided a higher MOR compared to the compost material. Among them, the highest average MOR of 79.7 g $CH_4/m^3/d$ was observed in the compost-poremat media. Afterwards, the MOR of the compost media gradually increased from 61.1 g $CH_4/m^3/d$ during day 64-88 to 70.6 g $CH_4/m^3/d$ during day 91-101. During the biofiltration progression, the MOR in the biofilters with compost-pumice, compost-poremat biofilter, and compost-pumice-poremat biofilter were found to be slightly reduced over time. Nevertheless, the average MOR over the entire operation period of 101 days was found to be higher in the biofilters containing both organic and inorganic media. Among them, the highest MOR was achieved in compost-poremat biofilter at 70.1 g $CH_4/m^3/d$ (Table 2). Compared to other low CH_4 loading biofilters operated under passive gas flow conditions, the MOR achieved in the biofilter containing both organic and inorganic materials in this study was found in between those of sandy loam (96-176 g $CH_4/m^3/d$) [11], compost (176-224 g $CH_4/m^3/d$) [11], and stabilized wastes (7.6-34 g $CH_4/m^3/d$) [12]. Nevertheless, a higher MOR was also reported in a biofilter containing a compost and pumice mixture than that of compost media alone, even when the biofilter was operated under active gas flow conditions [20].

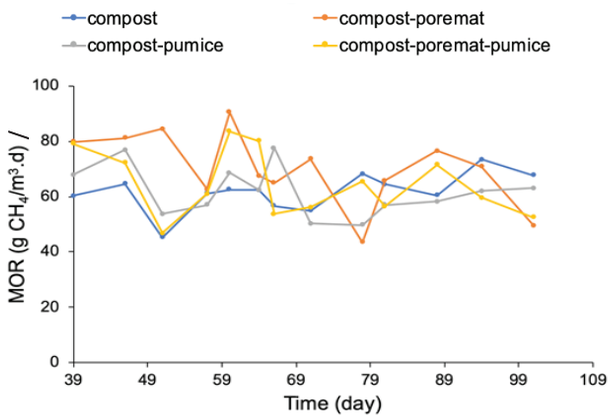

Fig. 2. Methane oxidation rate observed in biofilters containing different media.

Table 2. MOR (g CH_4/m^3/d) in biofilters at different operation period.

Biofilter media	day 39-60	day 64-88	day 94-101	overall
Compost	58.7 (7.7)[a]	61.1(4.9)	70.6 (4.0)	61.7 (6.9)[a]
Compost-poremat	79.7 (10.4)[a,b]	65.3(11.6)	60.2 (14.9)	70.1(13.3)[a,b]
Compost-pumice	64.8 (9.4)[b]	59.1(10.2)	62.5 (0.8)	61.8 (9.0)[b]
Compost-pumice-poremat	68.5 (14.9)	63.9 (10.5)	56.0 (5.1)	64.4 (11.9)

The numbers show average (SD) values; a and b show significant difference ($p<0.05$) between the biofilters, i.e. compost and compost-poremat biofilter, compost-poremat and compost-pumice, respectively.

The results suggest that the incorporation of inorganic media helped to achieve higher CH_4 oxidation rates in the biofilter, especially during the initial period. The CH_4 oxidation reaction produces water vapor as a product, so the increase and condensation of water within the biofilter media could reduce the mass transfer of CH_4 into the biofilm by blocking gas diffusion into available material pore space [21], thus decreasing CH_4 oxidation. Owing to the high porosity characteristics of inorganic materials, the mixture of inorganic materials and compost helped to increase the porosity of the biofilter media from 39.7 to 61.5, 54.6, and 58.3% in the biofilters with compost-pumice, compost-poremat, and compost-poremat-pumice media, respectively (Table 1). Under high porosity conditions, an enlarged pore space within the biofilter media could facilitate the diffusion of CH_4 and O_2 into methanotrophic biofilm CH_4 oxidation. This could explain the reason for achieving higher CH_4 oxidation in the biofilters containing both organic and inorganic media. In previous studies, it was also reported that the high porosity of biofilter media was favourable for CH_4 oxidation [8, 22]. Oppositely, a higher porosity media in compost-pumice biofilter and compost-pumice-poremat biofilter yielded a lower MOR as compared to the compost-poremat biofilter. This might be due to their shorter CH_4 retention times in the filter media. With the low solubility of CH_4 in the biofilm layer and the fact that only dissolved CH_4 can be consumed by methanotrophs, the retention time should be sufficient to ensure that CH_4 is converted to a form in which it becomes available to methanotrophic bacteria [18]. Therefore, these results reveal that the porosity of the biofilter media should be properly designed to achieve high CH_4 removal in the biofilter.

Figure 3 presents the gas concentration profiles within the biofilter, which confirmed the presence of CH_4 oxidation. An increase in CO_2 concentration and a decrease of CH_4 and O_2 clearly demonstrate ongoing biological methane oxidation. The most active zone of methane oxidation in all four biofilters was observed at the layer of 1.33-1.74 m depth from the top of biofilter. Meanwhile, there were smaller changes to the CH_4, CO_2, and O_2 concentrations in the upper part of the biofilter. Fig. 3A demonstrates that the CH_4 concentration in the biofilter with organic-inorganic media decreased to a larger extent than that within the compost biofilter in the active zone. Among the tested biofilters, the compost-poremat biofilter had the largest decrease in CH_4 concentration from 17% at the inlet to 6.2% at 1.33 m depth and the CH_4 concentration was mostly unchanged at the top of biofilter. Meanwhile, the CH_4 concentration in the compost biofilter was reduced to 8% at 1.33 m depth and slightly decreased to 7% at the top of the biofilter. The decrease in O_2 concentration corresponded to CH_4 oxidation by methanotrophs. However, it was noticed

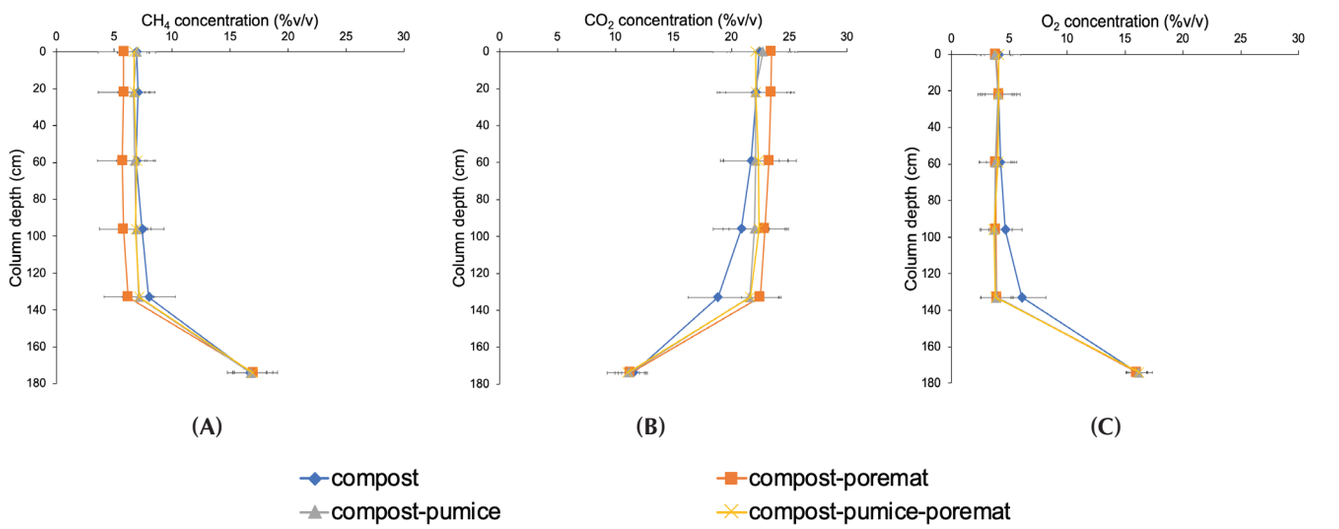

Fig. 3. Profiles of (A) CH_4, (B) CO_2 and (C) O_2 concentrations along the biofilter depths. The error bar indicates standard deviation of gas concentrations.

that O_2 concentrations became limited (<5%) in the biofilter above 1.33 m depth and this might indicate that microbial CH_4 oxidation might be inhibited by the shortage of O_2 above this height. Therefore, a limited CH_4 oxidation was observed in the biofilter above 1.33 m depth.

Methanotrophic activities in biofilter media

At the end of the experiment, 10 g of filter media from the most active CH_4 oxidation zone (1.33-1.74 m depth) in each biofilter was collected to investigate the methanotrophic activities via batch experiments. As shown in Table 3, the filter media with different physiochemical properties exhibited different methanotrophic activities. The highest methanotrophic activities were observed for compost-poremat media at 35.4 µg CH_4/g dried wt/h. Meanwhile, the lowest methanotrophic activities were observed in compost at 22.3 µg CH_4/g dried wt/h. These results imply that the presence of the inorganic biofilter (with high porosity) helped facilitate oxygen transfer into the media while the compost material supplied nutrients for methanotrophic activities. Therefore, the co-existence of organic and inorganic media could benefit CH_4 oxidation. The results obtained from the batch experiment were in agreement with those observed during column operation. During the batch experiments, the CPR trends followed that of the MOR. The CH_4:CO_2 mol ratio observed during batch experiments was found to be 1:1.25-1.43, which suggests that the presence of organic oxidation comes from other organic carbon contained within the biofilter media.

Table 3. Methanotrophic activities of different biofilter materials.

Biofilter media	MOA ($x10^{-3}$ mg/g media/h)	CPR ($x10^{-3}$ mg/g media/h)	CH_4:CO_2 (mol:mol)
Compost	22.3	81.63	1:1.33
Compost-poremat	35.4	121.9	1:1.25
Compost-pumice	25.1	99.1	1:1.43
Compost-pumice-poremat	30.9	109.4	1:1.28

MOR: methane oxidation rate; CPR: carbon dioxide production rate.

3.3. Methanotrophic bacterial population

The methanotrophic bacteria population in compost-poremat media, which exhibited the highest MOR in the column experiment and largest methanotroph activities, was investigated. The sequencing of the 16S rRNA genes amplified from the active bacterial communities of the compost-poremat biofilter revealed the presence of microorganisms classified in 21 phyla, 47 classes, 114 orders, 188 families, and 332 genera in total. Among them, they predominantly belonged to Actinobacteria (46.6±1.9%) followed by Proteobacteria (20.5±1.7%) and Firmicutes (18.0±2.3%). The presence of methanotrophs (Fig. 4) included *Methylobacter* and *Methylocaldum*, both classified as Methanotroph type I. Previous research has reported that a high oxygen environment favours the growth for methanotroph type I whereas type II was found to favour methane-rich conditions [19]. There was a similar microbial profile detected in organic and inorganic media. In the compost, *Methylobacter* and *Methylocaldum* accounted for 9.2 and 2.1% of the total bacteria, respectively, and were found to be 8.5 and 2.6% in the poremat media, respectively. These results suggest that the biofilter media provided favourable conditions for Methanotroph type I growth in both organic and inorganic media. The predominance of similar microbial species was also reported in biofilters using a mixture of compost and lava rock and compost and a wood-based biochar mixture [22].

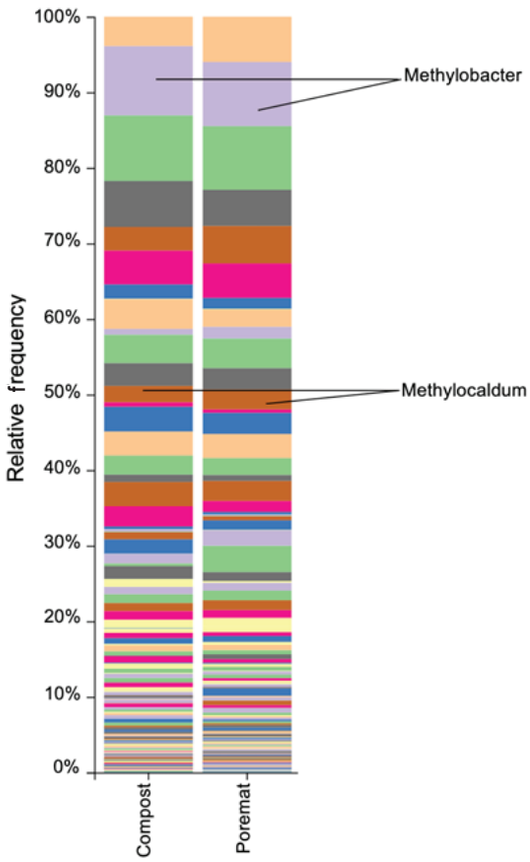

Fig. 4. Bacterial population in compost-poremat media at 1.50 m depth.

3.4. N_2O removals in the biofilter

Figure 5 shows the NCR in the biofilters with different media. In the compost biofilter, negative conversion rates were determined that indicated N_2O production during day

39 to day 81, but they became positive or were removed afterwards until the end of experiment. The production of N_2O in the compost biofilter could possibly be provided from a high nitrogen content maintained in the compost biofilter together with the formation of preferential air flow and stagnant zones. These conditions can create zones with low oxygen penetration leading to the development of potentially anoxic/anaerobic microbial metabolic conditions that yield incomplete nitrification. Diffusion limitations in thick biofilms could also create the formation of oxygen-depleted anoxic zones. When nitrification proceeds under oxygen-limiting conditions, ammonia-oxidizing bacteria use NO_2^- as the terminal electron acceptor instead of O_2, which leads to higher N_2O production as a by-product during incomplete nitrification [23]. Similar observations of N_2O production in organic material-based biofilters were also reported [24].

A shift from N_2O production to removal in the compost biofilter occurred simultaneously with an increase in CH_4 oxidation in the same biofilter (Fig. 2). This observation revealed the improvement of aerobic conditions in the compost biofilter over time. Meanwhile, the compost-pumice, compost-poremat, and compost-pumice-poremat biofilters yielded N_2O removal during the entire experimental period (Table 4). The removal of N_2O concentrations in these biofilters suggest that the use of organic and inorganic materials could promote oxygen availability to achieve complete nitrification in the biofilter media. In previous research, it was reported that N_2O emissions from biofilters containing inorganic (pumice) media was negligible due to a much lower microbial N content in compost compared to that in compost-based biofilters [20].

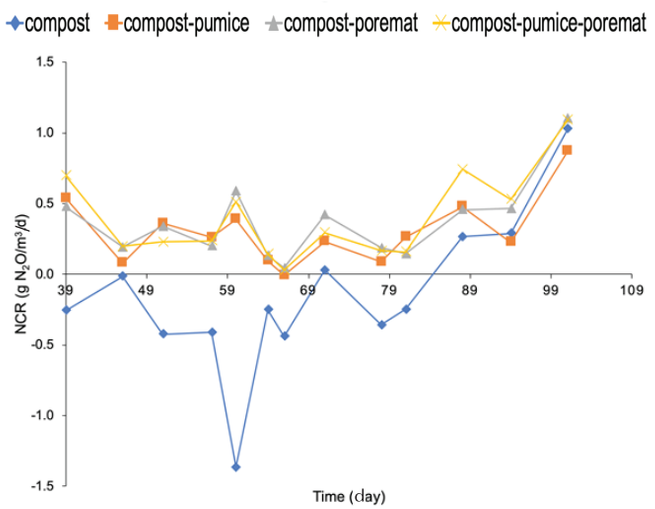

Fig. 5. N_2O emission rates in different filter materials.

Table 4. NCR (g $N_2O/m^3/d$) in biofilters at different operation period.

Biofilter media	day 39-60	day 64-88	day 94-101	overall
Compost	-0.5 (0.5)^{a,b,c}	-0.2 (0.3)	0.7 (0.5)	-0.2 (0.5)^{a,b,c}
Compost-poremat	0.4 (0.2)^{a}	0.2 (0.2)	0.8 (0.5)	0.4 (0.3)^{a}
Compost-pumice	0.3 (0.2)^{b}	0.2 (0.2)	0.5 (0.5)	0.3 (0.2)^{b}
Compost-pumice-poremat	0.4 (0.2)^{c}	0.3 (0.3)	0.8 (0.4)	0.4 (0.3)^{c}

The numbers show average (SD) values; a, b, and c significant difference ($p<0.05$) between the compost biofilter and other biofilters respectively.

4. Conclusions

The compost-poremat biofilter was found to be the most effective filter material providing an average methane oxidation rate of 70.1 g $CH_4/m^3/d$ over a 101-day period. The high porosity of the biofilter media containing a mixture of organic and inorganic media allowed sufficient oxygen transfer for methane oxidation, even at the bottom of biofilter media bed of 1.5 m depth. High methanotrophic activities and the presence of type I methanotrophs confirmed active methane oxidation under oxygen-rich conditions in the biofilter media. N_2O was also found to be removed from the biofilter containing inorganic media, while it was mainly produced in the compost biofilter.

CRediT author statements

Nguyen Thanh Tung, Wilai Chiemchaisri: Conceptualization, Methodology, Data curation, Formal analysis, Writing - Review & Editing; Chart Chiemchaisri, Samunya Sanguanpak: Conceptualization, Methodology, Data curation, Formal analysis, Writing - Review & Editing.

ACKNOWLEDGEMENTS

The authors are grateful to financial support from AUN/SEED-Net Collaborative Research (CR) Grant provided by Japan International Cooperation Agency (JICA).

COMPETING INTERESTS

The authors declare that there is no conflict of interest regarding the publication of this article.

REFERENCES

[1] A. Idris, B. Inanc, M.N. Hassan (2004), "Overview of waste disposal and landfills/dumps in Asian countries", *J. Mater. Cycles Waste Manag.*, **6**, pp.104-110, DOI: 10.1007/s10163-004-0117-y.

[2] H.G. Bingemer, P.J. Crutzen (1987), "The production of methane from solid wastes", *J. Geophys. Res.*, **92**, pp.2181-2187, DOI: 10.1029/JD092iD02p02181.

[3] T. Ishigaki, M. Nakagawa, M. Nagamori, et al. (2016), "Anaerobic generation and emission of nitrous oxide in waste landfills", *Environ. Earth Sci.*, **75**, pp.751-756, DOI: 10.1007/s12665-016-5543-3.

[4] X. Wang, M. Jia, X. Chen, et al. (2014), "Greenhouse gas emissions from landfill leachate treatment plants: a comparison of young and aged landfill", *Waste Manag.*, **34**, pp.1156-1164, DOI: 10.1016/j.wasman.2014.02.004.

[5] L. Lin, C. Lan, L. Huang, et al. (2008), "Anthropogenic N_2O production from landfill leachate treatment", *J. Environ. Manage.*, **87(3)**, pp.341-349, DOI: 10.1016/j.jenvman.2007.01.014.

[6] H. La, J.P.A. Hettiaratchi, G. Achari, et al. (2018), "Biofiltration of methane", *Bioresour. Technol.*, **268**, pp.759-772, DOI: 10.1016/j.biortech.2018.07.043.

[7] P. Boeckx, O.V. Cleemput, I. Villaralvo (1996), "Methane emission from a landfill and the methane oxidising capacity of its covering soil", *Soil Biol. Biochem.*, **28(10-11)**, pp.1397-1405, DOI: 10.1016/S0038-0717(96)00147-2.

[8] J. Streese, R. Stegmann (2003), "Microbial oxidation of methane from old landfills in biofilters", *Waste Manag.*, **23(7)**, pp.573-580, DOI: 10.1016/S0956-053X(03)00097-7.

[9] Y. Zhao, F. Shao (2004), "Use of an aged-refuse biofilter for the treatment of feedlot wastewaters", *Environ. Eng. Sci.*, **21(3)**, pp.349-360, DOI: 10.1089/109287504323066996.

[10] T.L. Gómez-Borraz, A. González-Sánchez, W. Bonilla-Blancas, et al. (2017), "Characterization of the biofiltration of methane emissions from municipal anaerobic effluents", *Process Biochem.*, **63**, pp.204-213, DOI: 10.1016/j.procbio.2017.08.011.

[11] N. Tanthachoon, C. Chiemchaisri, W. Chiemchaisri (2007), "Utilisation of municipal solid waste compost as landfill cover soil for reducing greenhouse gas emission", *Int. J. Environ. Technol. Manag.*, **7(3/4)**, pp.286-297, DOI: 10.1504/IJETM.2007.015146.

[12] W. Chiemchaisri, C. Chiemchaisri, J. Boonchaiyuttasak (2013), "Utilization of stabilized wastes for reducing methane emission from municipal solid waste disposal", *Bioresour. Technol.*, **141**, pp.199-204.

[13] W. Chiemchaisri, J.S. Wu, C. Visvanathan (2001), "Methanotrophic production of extracellular polysaccharide in landfill cover soils", *Water Sci. Technol.*, **43(6)**, pp.151-158.

[14] J. Nikiema, M. Heitz (2010), "The use of inorganic packing materials during methane biofiltration", *Int. J. Chem. Eng.*, pp.1-8, DOI: 10.1155/2010/573149.

[15] J. Nikiema, M. Girard, R. Brzezinski, M. Heitz (2014), "Biofiltration of methane using an inorganic filter bed: influence of inlet load and nitrogen concentration", *J. Environ. Eng. Sci.*, **9(1)**, pp.38-45.

[16] J.M. Anderson, J.S.I. Ingram (1993), *Tropical Soil Biology and Fertility: A Handbook of Methods*, 2nd Edn., Oxford University Press, ISBN 9780851988214.

[17] M. Nagamori, M.I.M. Mowjood, Y. Watanabe, Y. Isobe,

T. Ishigaki, K. Kawamoto (2016), "Characterization of temporal variations in landfill gas components inside as open solid waste dumpsite in Sri Lanka", *J. Air Waste Manag. Assoc.*, **66(12)**, pp.1257-1267.

[18] M. Nag, T. Shimaoka, H. Nakayama, T. Komiya, C. Xiaoli (2016), "Field study of nitrous oxide production with in situ aeration in a closed landfill site", *J. Air Waste Manag. Assoc.*, **66(3)**, pp.280-287.

[19] C. Scheutz, P. Kjeldsen (2004), "Environmental factors influencing attenuation of methane and hydrochlorofluorocarbons in landfill cover soils", *J. Environ. Qual.*, **33(1)**, pp.72-79.

[20] C. Pratt, J. Deslippe, K.R. Tate (2013), "Testing a biofilter cover design to mitigate dairy effluent pond methane emissions", *Environ. Sci. Technol.*, **47(1)**, pp.526-532.

[21] H. Wang, J. Einola, M. Heinonen, M. Kulomaa, J. Rintala (2008), "Group-specific quantification of methanotrophs in landfill gas-purged laboratory biofilters by tyramide signal amplification-fluorescence in-situ hybridization", *Bioresour. Technol.*, **99**, pp.6426-6433.

[22] H. La, J.P.A. Hettiaratchi, G. Achari, T.J. Verbeke, P.F. Dunfield (2018), "Biofiltration of methane using hybrid mixtures of biochar, lava rock and compost", *Environ. Pollut.*, **241**, pp.45-54, DOI: 10.1016/j.envpol.2018.05.039.

[23] T.P. Nguyen, J. Clemens, C. Cuhls (2014), "The effects of biofilter on the removal of greenhouse gases at anaerobic digestion plants". *J. Viet. Environ.*, **6(1)**, pp.65-68.

[24] R. Melse, J. Hol (2014), "Biofiltration of exhaust air from animal houses: removal efficiencies and practical experiences", *Biosyst. Eng.*, **159**, pp.56-69, DOI: 10.1016/j.biosystemseng.2017.04.007.

DOI: 10.31276/VJSTE.63(1).90-96

Sustainability assessment of community-based water resource management of irrigation systems for agriculture

Huynh Thi Lan Huong[1*], Pham Ngoc Anh[2]

[1]Vietnam Institute of Meteorology, Hydrology and Climate change, 23, Lane 62, Nguyen Chi Thanh Street, Lang Thuong Ward, Dong Da District, Hanoi, Vietnam
[2]Ministry of Natural Resources and Environment, 10 Ton That Thuyet Street, My Dinh Ward, Nam Tu Liem District, Hanoi, Vietnam

Received 20 August 2020; revised 25 October 2020; accepted 5 November 2020

Abstract:

To study community-based water resource management (CbWRM) of irrigation for agriculture, the participation of the community in the management of the irrigation system must be considered. CbWRM is the cooperation between a farming organization (the water-using cooperative group) and state-related organizations (such as the Department of Water Resources Management and commune-level authorities) in the process of the operation and management of water. In the CbWRM model, the community participates in the selection and election of the management board, meetings to collect ideas to build a CbWRM model, and financial contributions to water use fees. The community also participates in the annual operational planning of water use. Therefore, this study aimed to develop indicators to assess the sustainability of the CbWRM model of irrigation for agriculture in the Hau Giang province, Vietnam. With an assessment result of 0.54 (relatively sustainable), this study shows a picture of water resource management in general and community participation in particular. These research results can help managers and policymakers promote community participation to achieve high-efficiency water resource management in the agriculture of the Hau Giang province.

Keywords: **agriculture, community-based, irrigation system, water resource management.**

Classification number: **5.2**

1. Introduction

The ever increasing water demand of communities has caused serious problems in water resource management. Because there are many methods of water resource management, assessments of the sustainability of a particular scheme of water resource management are of great importance. A meaningful assessment can help a policymaker select the most suitable method to apply to water resource management.

A large number of rural areas around the world, mainly in developing countries, have applied various models of CbWM. Nevertheless, retaining CbWM sustainability has faced difficulties due to lack of the continuous provision of the necessary technical, financial, and social resources from the responsible stakeholders. In several circumstances, the development of a number of community organizations has contributed to CbWM sustainability, which is the key role of community in the process of policy-making [1].

Community participation in the process of water resource management is considered as an inevitable rule. According to F. Molle (2005) [2], CbWRM is a participatory process in which the community is the centre of an effective water management system. From planning to operating to maintaining the water supply system, the community is responsible for the resource from which they benefit. This engagement can be both considered as a tool for better management or as a process for community empowerment as it can be established under a consumer association, by community action groups in urban areas, or by water-user groups and irrigation cooperatives in rural areas [3]. The capacity of the community in CbWRM is strongly emphasized in W.S. Madeleen (1998) [4]. This study addressed the potential for technical, labour, and financial contributions, as well as community support in the planning process, implementation, and sustainable maintenance of a water supply system. The work also demonstrated that the

*Corresponding author: Email: huynhlanhuong@gmail.com.

community has a decisive role in resolving contradiction and conflicts in the use, exploitation, and sustainability of water resource management [4].

In Vietnam, according to N.V. Dung, et al. (2006) [5], community participation in water resource management has a long history, especially around the northern and southern deltas. There are two basic approaches of water resource management. The first considers water as a common property. This approach is common in the upland and mountainous areas and in some lowlands of Vietnam. The second approach considers water as a commodity. Such an approach pays attention to the multiple purposes of water such as for agriculture, domestic use, aquaculture, industry, and services. This approach was taken by the Participatory Irrigation Management (PIM), which was applied in Vietnam in the early 1990s after the government officially decided to transfer agricultural land use rights to households. This is seen as an effective method for CbWRM because the communities are involved as water users, managers, and protectors of water resources, especially for small-scale irrigation systems. The PIM has been experimentally applied in many provinces such as Tuyen Quang, Bac Kan, Thanh Hoa, Nghe An, Quang Tri, Quang Ngai, Binh Dinh, and Hau Giang.

According to I. Juwana, et al. (2010) [6], a great number of indicators of water resource sustainability have been deployed in numerous countries such as the Canadian Water Sustainability Index (CWSI), Water Poverty Index, Watershed Sustainability Index (WSI), and West Java Water Sustainability Index (WJWSI). All of these indicators aim to provide the current condition of a water resource and generate inputs for policymakers to prioritize water issues.

I. Juwana, et al. (2012) [7] has proposed a list of six sub-component indicators for accessing water resource sustainability. Based on the literature review of indicator-based water sustainability in this study, water stakeholders can apply and customize existing indicators and/or develop new indicators. From these indicators, the community can learn about their current water resource situation and which element can improve its condition. In addition, the water sustainability indicators can support policymakers during the process of prioritization of problems, challenges, and water resource programs.

In a study by P. Kamalesh, et al. [8], a framework based on technical, environmental, financial and institutional criteria was developed. Similar to the above study [7], Tier I indicators were described through several component indicators. The author also provides weights for each Tier I indicator and the lower tier indicators, which make the water sustainability assessment process more accurate and reasonable. The weights were determined based on interviews and consultations with experts in sustainable water resource development. The information obtained was integrated into the scoring system to help evaluate whether the project under consideration was sustainable. The score was divided into 3 types: sustainable, partly sustainable, and unsustainable.

B.D. Richter, et al. (2018) [9] developed a set of indicators for assessing the sustainability of urban water supply systems including: (1) governance of water resource and its role; (2) preparedness for droughts and other capabilities for emergency response; (3) monitoring of water resources; (4) capacity to pay for water resources and social justice; (5) efficiency and conservation in water usage and water quality; and (6) protection of the watershed. The indicators presented in this work supports cities with improving the sustainability of their water supply systems. While it is straightforward to quantify and evaluate the subcomponents of these indicators, in some cases subjective judgement and ultimate weighting are needed. In order to enhance the service reliability, financial viability, customer satisfaction, and environmental health, these indicators can be evaluated and tracked by utilities over time.

R. Popawala, et al. (2011) [10] provided a set of indicators to evaluate the sustainability of an urban water management system, including primary, secondary, and first-level indicators that encompass social, economic, environmental, and technical aspects. The second-level indicators include, for example, population with access to water supply, sewage, rainwater, investment capital, maintenance costs and repair, daily water supply per person, per capita water production waste per day, covered pipe area, and energy consumption. In addition, the authors also weighted the indicators for levels 1 and 2 based on expert opinions combined with findings from field surveys.

In Vietnam, a variety sustainable assessment methods have been proposed and applied. In the study of [11], the authors analysed the social elements of model management in terms of community participation. The authors used six key indicators: (1) water sustainability; (2) sustainability of the project; (3) community participation; (4) technology sustainability; (5) sustainable financial economy; and (6) organizational sustainability.

T.L.H. Nguyen (2010) [12] defined seven requirements for assessing the sustainability and effectiveness of a water supply system as follows: (1) adequate water supply for at least 70% of the households in the community; (2) the quality of water supply services meets the needs of the community; (3) technical problems are promptly solved and water supply interruptions should not exceed 1 day per year and the leakage rate is below 20%; (4) transparency in finance; (5) no negative social impacts on the community; (6) having technical support and access to financial resources for maintenance and repairs; and (7) the functional lifetime of the system is not less than 30 years.

N.V. Dung, et al. (2006) [5] explained the concept of a sustainable water resource management model. It has been said that community participation is very diverse both in form and level, so it is difficult to say which model is the best overall because each one corresponds to a community with specific populational, geographical, institutional, and cultural characteristics. Therefore, in order to consider the success of a sustainable CbWRM model, specific criteria and indicators are needed.

Within the framework of this study, the authors aim to develop a set of indicators to evaluate the sustainability of CbWRM models at the local level. The results of the evaluation will help managers identify priority issues and devise strategies, plans, and action programs to balance factors in the process of developing a specific model of CbWRM.

The Hau Giang province was selected for study. A survey of irrigation in Hau Giang showed that there is a community-based model in their agriculture known as "water use cooperatives", which is a form of PIM. This approach to CbWRM of irrigation for agriculture in Hau Giang can be described as follows:

First, the Government invests in an electric pumping station. Through the Provincial Department of Irrigation and the commune authorities, the government assigns a water cooperative group (WCG) to manage and operate the system. The WCG develops the plans to pump water and collect fees from the households. All villagers participated in the selection of a management board and meetings to collect ideas to develop the system. The villagers also paid water use fees and participated in the meetings for annual operational planning.

According to the survey, the model in place at Hau Giang has significant economic benefits such as reduced investment costs, increased productivity, and profits. The second-most significant benefit is social benefits such as to stabilize people's lives and increase their connectivity in the community. However, most of models only work for a short time (2 years), so it will take time for people to get used to using and managing the system. The model is based on an existing irrigation infrastructure that did not involve the community from the beginning and thus they did not participate in the planning, designing, and construction stages. The community was only involved in the management.

2. Methodology and data

2.1. Methodology

To assess the sustainability of CbWRM of irrigation for agriculture in Hau Giang, the research team used several methods: (1) data collection and social surveys; (2) expert consultation; and (3) a set of indicators to evaluate the sustainability.

2.2. Data collection, social surveys

The data included information related to community participation in irrigation works; ability and willingness to pay for irrigation services of community; information related to economic, technical, and environmental factors, and benefits of water supply services. A questionnaire was used and applied to the communities (people living in the area) and managers. The details of the application of this method are described below.

2.2.1. Expert consultation

Experts were consulted to determine the weights of the Tier I and Tier II indicators to serve the assessment of the sustainability CbWRM in the study area.

2.2.2. Development of the set of indicators

A set of indicators was developed based on the following criteria:

- Comprehensive: The indicators should provide an overview and capture the multidimensional nature of sustainable state management community models. Sustainability aspects need to be assessed for each type of model.

- Simplicity: The indicators must be simple enough to facilitate data collection, analysis, and evaluation.

- Clarity: The indicators must be clearly defined and given specific calculation instructions.

- Availability: The given indicators should be consistent with the data available to collect and assess. This will contribute to time and cost saving during the evaluation. However, it should be noted that when data collection and evaluation are not available, it is necessary to ensure reasonable data collection time and cost.

- Relevance: The indicators will be compatible with the objectives of the national and local strategies and master plans.

To develop the set of indicators, five steps were followed:

Step 1: Develop the frame of indicators

The objective of this step is to clearly identify the area being assessed and the scope of the evaluation indicators including Tier I and Tier II indicators. To develop the frame of indicators, this study was based on an evaluation of indicators developed by previous research including the study by I. Juwana, et al. (2012) [7]; P. Kamalesh, et al. (2008) [8]; R. Popawala, et al. (2011) [10]; H.T. Dai, et al. (2007) [11], and T.L.H. Nguyen (2010) [12]. Then, the results from these evaluations will be combined with the local survey to develop a set of indicators.

Step 2: Selection of Tier I and Tier II indicators

The selection of Tier I and II indicators needs to follow certain criteria: (1) feasibility of the data; (2) simplicity of data; and (3) validity of the data. From the frame of indicators developed in Step 1, the research team set up a common set of indicators (level 1) for irrigation water supply in agriculture (Table 1).

Table 1. Set of indicators to assess the sustainability of CbWRM.

Tier I indicators	Tier II indicators	Sources of data
Social indicator	Conflict possibility in using water resources	From survey data
	The level of community participation in developing model	From survey data
	The level of community involvement in operating the model	From survey data
	The level of community participation in maintenance / repairing model	From survey data
	The level of community participation compared to the model design	From survey data
	The level of community participation in the financial decisions of the model	From survey data
	Service complaints regarding the model	From survey data
	Qualifications of managers and operators of model	From survey data
	Percentage of model managers and operators who participate in technical training and operational management	From survey data
	The percentage of people participating in technical training on how to operate and use the model	From survey data
	Executive board of the model	From survey data
Technical indicator	Degree of meeting the demand of using water in agricultural production	From survey data
	Access ability to water resources	From hydro-meteorological data
	Water quality	From environmental data
	Frequency of malfunctioning of models	Survey data from the irrigation company
	The frequency of periodic maintenance of the model	Survey data from the irrigation company
	The rate of water loss	Survey data from the irrigation company
Environmental indicator	Possibility of the influence of the natural environment on the model	From environmental data
	Risk of natural environmental pollution from the model	From environmental data
Economic indicator	Capital for developing models	Survey data from the irrigation company
	Capital for operating the model	Survey data from the irrigation company
	Capital for model maintenance/repair.	Survey data from the irrigation company

Step 3: Collecting data

After setting up the indicators, the data is collected. This data is very important and helpful for the calculation.

Step 4: Calculating the sustainable index

The sustainability index (SI) of the CbWRM is calculated directly through the values of the four Tier I indicators: economic, social, environmental, and technical by Eq. (1):

$$\text{Sustainable Index (S.I)} = \sum_{i=1}^{m} \text{Mi}*\text{Wi} \quad (1)$$

where Mi is the normalized value of a Tier I indicator number *i*; W_i is the weight of Tier I indicator number *i*; and m is number of Tier I indicators.

The value Mi of a Tier I indicator number *i* is calculated based on the Tier II indicators by Eq. (2):

$$\text{Mi} = \sum_{j=1}^{n} \frac{Xij}{n} \quad (2)$$

where X_{ij} is the normalized value of a Tier II indicator number *j* and N is the number of the Tier II indicator *i* that belongs to the Tier I indicator.

As each Tier II indicator is calculated in different units, it is necessary to calibrate each of these indicators to the same standard system [13].

(+) If the value of a Tier II indicator is proportional to vulnerability, then Eq. (3) will be applied to normalize its value:

$$\text{Xij} = \frac{\text{S}-\text{S}_{\min}}{\text{S}_{\max}-\text{S}_{\min}} \quad (3)$$

where *s* is a Tier II indicator; s_{min} is the minimum value of a Tier II indicator, and s_{max} is the maximum value of a Tier II indicator.

(+) On the other hand, if the value of a Tier II indicator is inversely proportional to vulnerability, then the value will be normalized by Eq. (4):

$$\text{Xij} = \frac{\text{Smax}-\text{S}}{\text{Smax}-\text{Smin}} \quad (4)$$

where *s* is a Tier II indicator; s_{min} is the minimum value of a Tier II indicator; and s_{max} is the maximum value of a Tier II indicator.

- Step 5: Sustainability assessment

After calculating the sustainability index, it is necessary to determine the level corresponding to the values. By referring to previous studies, combined with expert advice of the actual situation, the authors divided the value in intervals to represent the levels of sustainability for the CbWRM model as follows:

SI: ≥0.7-1 : sustainable

SI: ≥0.5-0.7 : relatively sustainable

SI: <0.5 : not sustainable

2.2.3. Delphi method

The Delphi method was conducted in the study to select indicators and the weights of the indicators. In the practical application of the Delphi method, the authors followed the following steps:

1. Define the purpose of selecting indicators and evaluating weights of indicators to assess the sustainability of the CbWRM in Hau Giang.

2. Select a team of 10 experts with solid knowledge and interest in the field of water resources in particular and natural resources and environment in genera.

3. Establish level I and level II indicators, assign initial values of weights to level I indicators and send to each member of the expert group.

4. The feedback results from each expert are collected, tabulated, and summarized.

5. Summary of the results sent back to experts for comments to emphasize opposing, extreme, or special opinions different from the majority.

6. Experts have the option to revise their previous estimates after reviewing information received from other (unnamed) members.

7. Repeat steps 3 through 5 until there are no longer any significant changes (i.e. the experts reach an agreement).

The results of the Tier I indicator weights identified based on the Delphi method are summarized in Table 2.

Table 2. Tier I indicator weights.

No	**Weight before Delphi**		**Weight after Delphi**	
	Tier I indicators	***Weight***	***Tier I indicators***	***Weight***
1	Social	0.25	Social	0.28
2	Economic	0.25	Economic	0.24
3	Environmental	0.25	Environmental	0.24
4	Technical	0.25	Technical	0.24

2.3. Data

To collect the data, the authors conducted a survey in the study area and had meetings with representatives from the Department of Agriculture and Rural Development as well as the Department of Natural Resources and Environment, Centre for Rural Water Supply and Sanitation in Hau Giang and interviewed people from the Hoa Luu commune, Vi Thanh city, Hau Giang province.

Information collected during the survey in Hau Giang to serve for the development and calculation of indicators includes:

- The model of CbWRM in Hau Giang in the field of irrigation in agriculture.

- Local policies and mechanisms related to the model of CbWRM in Hau Giang in the field of irrigation in agriculture.

- The technical parameters of the model of CbWRM in Hau Giang in the field of irrigation in agriculture.

- Construction investment capital and recurring expenses for the model of CbWRM in Hau Giang in the field of irrigation in agriculture.

- People's participation in the operation of the model of CbWRM in Hau Giang in the field of irrigation in agriculture.

- The operation of the model of CbWRM in the field of irrigation in Hau Giang agriculture.

- The limitations of the model of CbWRM in the field of irrigation in Hau Giang agriculture.

- Benefits that the model of CbWRM in the field of irrigation in Hau Giang agriculture.

- Assessing the effectiveness of each model of CbWRM of irrigation in Hau Giang agriculture.

- Proposing how to sustainably develop the model of CbWRM of irrigation in agriculture in Hau Giang.

The required data are described in the questionnaire of both levels (managers and communities). These data include: the specifications of the model; information related to investment capital and periodic model costs; how the model works; people's participation in the operation of the model; benefits and limitations that the model brings along with its socio-economic-environmental impacts; and the effectiveness of each model and information on the proposal to replicate an effective model. Data on policy mechanisms are directly consulted with local leaders. The survey sites were carefully considered by the method of overview and direct consultation with local leaders, from which the locations for each agriculture field in Hau Giang province was identified.

The survey took place in Hau Giang from March 3, 2017 to March 7, 2017. The authors interviewed a few organizations under DARD and DONRE in Hau Giang such as the Department of Water Resources, under Department of Natural Resources and Environment of Hau Giang province; the Department of Irrigation, under the Department of

Agriculture and Rural Development of Hau Giang province; the Center for Rural Water Supply and Sanitation in Hau Giang province; and interviewed people from the Hoa Luu commune, Vi Thanh city, Hau Giang province.

The total number of questionnaires was 200, of which 100 were for managers and 100 were for people in Hau Giang. The questionnaire was built based on the purpose of the survey, the subject matter investigated, and the scope of the survey. The questionnaire forms for managers and communities are shown in Annex 1 and Annex 2. Data collected during the survey was analysed and synthesized by simple statistical methods (e.g. aggregating data, averaging, etc.).

3. Results and discussion

This study developed 4 Tier I indicators (social, economic, environmental, and technical) and 22 Tier II indicators. They were applied to assess the sustainability of CbWRM for agriculture in Hau Giang. The results are summarized in Table 3.

Table 3. The value of Tier II indicators.

Tier I indicators	Tier II indicators	Value
Social indicator	Conflict possibility in using water resources	0.33
	The level of community participation in developing model	0.00
	The level of community involvement in operating the model	0.50
	The level of community participation in maintenance / repairing model	0.89
	The level of community participation compared to the model design	1.00
	The level of community participation in the financial decisions of the model	0.50
	Service complaints regarding the model	0.50
	Qualifications of managers and operators of model	1.00
	Percentage of model managers and operators who participate in technical training and operational management	1.00
	The percentage of people participating in technical training on how to operate and use the model	1.00
	Executive board of the model	0.10
Technical indicator	Degree of meeting the demand of using water in agricultural production	1.00
	Access ability to water resources	1.00
	Water quality	0.00
	Frequency of malfunctioning of models	1.00
	The level of periodic maintenance of the model	0.50
	The rate of water loss	0.10
Environment indicator	Possibility of the influence of the natural environment on the model	0.50
	Risk of natural environmental pollution from the model	0.50
Economic indicator	Capital for developing models	0.00
	Capital for operating the model	1.00
	Capital for model maintenance/repair	1.00

The final result of sustainability assessment for CbWRM model of irrigation for agriculture in Hau Giang province are shown in Table 4.

Table 4. The results of sustainability assessment.

Tier I indicators	Value of Tier I indicators	Weight of Tier I indicators	Final value	Sustainable Index
Social (A)	0.58	0.28	0.16	0.54
Technical (B)	0.75	0.24	0.18	
Environment (C)	0.50	0.24	0.12	
Economy (D)	0.33	0.24	0.08	

This result shows the superiority of the closed model design, which has been implemented in many provinces and cities nationwide. The design and financial participation in the construction investment, as well as major repairs of the irrigation system, were carried out by state agencies without the participation of the community.

The overall sustainability assessment result of 0.54 is considered "relatively sustainable". This shows that the model is in the early stages of formation and many factors, especially issues related to community, need to be improved (Fig. 1).

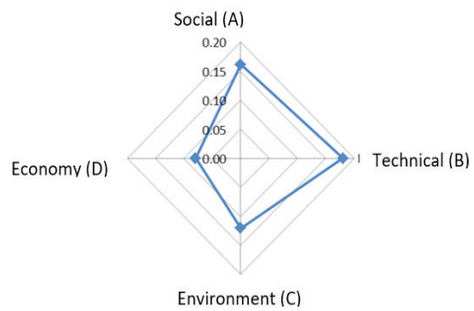

Fig. 1. Sustainability assessment.

The CbWRM model in the agricultural sector is assessed to be relatively sustainable due to the low values of the calculated indicators. These indicators relate to the disputed abilities of water use and the level of community participation in model development and management. The indicators related to the modelled capital sources with focus on the capital source of the state, private investors, and people are still limited. Therefore, for the next period, the model needs more investment from community capital for operation and maintenance. However, the cooperation model of the investment management and exploitation of irrigation works in Hau Giang and other provinces in the Mekong delta is on the right track and consistent with the policy of the Ministry of Agricultural and Rural Development. This model works by reducing the investment of the state budget, enhancing the role of the people and the private sector, improving the

efficiency of the irrigation system, and increased agricultural output. Such a model should be comprehensively studied in order to apply to the entire Mekong delta and other regions across the country. However, it is necessary to solve the shortcomings arising from what is currently happening in Hau Giang. The problems identified in the sustainability assessment need to be addressed before replicating the model. There is a particular need for a gradual enhancement of community participation, not only in management, but also in investment and system design. One of the factors essential to the development and replication of the model is the issue of capital investment in infrastructure and policy institutions.

4. Conclusions

CbWRM of irrigation for agriculture is a typical system found in Vietnam. While it is a relatively new type of system, CbWRM has shown its role to the local community. The entire community should engage in the system by participating in the following activities: selection of management boards, community meetings to collect ideas for developing the system, paying water use fees, and participating in relevant meetings for developing an annual operation plan.

This study introduced a set of indicators to evaluate the sustainability of the CbWRM. The set of indicator includes four Tier I indicators: social, technical, environment, and economy. Each indicator had Tier II indicators to assess the sustainability of CbWRM for agriculture practice.

On the basis of the evaluation results, it was possible to identify factors affecting the sustainability of the model to support managers in making appropriate adjustments. The results of this study can be extended to other regions in the Mekong delta, and the whole country, to evaluate existing models and propose appropriate adjustments.

CRediT author statements

Huynh Thi Lan Huong, Pham Ngoc Anh: Conceptualization, Methodology, Data curation, Formal analysis, Writing - Review & Editing.

COMPETING INTERESTS

The authors declare that there is no conflict of interest regarding the publication of this article.

REFERENCES

[1] A.V.M. Machado, J.A.N. dos Santos, L.M.C. Alves, et al. (2019), "Contributions of organizational levels in community management models of water supply in rural communities: Cases from Brazil and Ecuador", *Water*, **11(3)**, DOI: 10.3390/w11030537.

[2] F. Molle (2005), "Irrigation and water policies in the Mekong region: Current discourses and practices Colombo, Sri Lanka", *IWMI* (Research report 95), 43pp.

[3] Cap-Net (2014), *IWRM as A Tool for Adaptation to Climate Change*, Training Manual and Facilitator's Guide, 195pp.

[4] W.S. Madeleen (1998), *Community Management Models for Small Scale Water Supply Systems*, IRC International Water and Sanitation Center, A Preliminary Review.

[5] N.V. Dung, N.D. Tinh (2006), *Community-based Water Resources Management in Vietnam - A Literature Review of Experiences and Best Practices*, 35pp.

[6] I. Juwana, B. Perera, N. Muttil (2010), "A water sustainability index for West Java. Part 1: Developing the conceptual framework", *Water Sci. Technol.*, **62(7)**, pp.1629-1640, DOI: 10.2166/wst.2010.452.

[7] I. Juwana, N. Muttil, B.J.C. Perera (2012), "Indicator-based water sustainability assessment - A review", *Science of The Total Environment*, **438**, DOI: 10.1016/j.scitotenv.2012.08.093.

[8] P. Kamalesh, B. Shashi (2008), "A framework to assess sustainability of community-based water projects using multi-criteria analysis", *First International Conference on Construction In Developing Countries (ICCIDC-I)*, pp.464-472.

[9] B.D. Richter, M.E. Blount, C. Bottorff, et al. (2018), "Assessing the sustainability of urban water supply systems", *Journal - American Water Works Association*, **110(2)**, pp.40-47.

[10] R. Popawala, N.C. Shah (2011), "Evaluation of Sustainability index for Urban Water Management System", *P. Int. Conf. Environ. Sci. & Dev. (ICESD 2011)*, **4**.

[11] H.T. Dai, M.Q. Phuc (2007), "Assessing the sustainability of clean water supply systems in Bac Giang province", *Technical Journal of Irrigation and Environment*, 9pp.

[12] T.L.H. Nguyen (2010), *Doctoral Dissertation Study on Community-based Management Forms of Centralized Water Supply Works in Rural Vietnam*, Code No: 62.31.10.01, National Economics University, Hanoi.

[13] T.L.H. Huynh, A.T. Do, T.M. Dao (2020), "Climate change vulnerability assessment for Can Tho city by a set of indicators", *International Journal of Climate Change Strategies and Management*, **12(1)**, pp.147-158, DOI: 10.1108/ IJCCSM-01-2018-0003.

Vietnam Journal of Science, Technology and Engineering (VJSTE): Manuscript Template

General Instructions on using this template and submitting a manuscript to VJSTE: Thank you for preparing a manuscript for submission to VJSTE. Using this template, or following the guidelines below, will help us in processing your article.

The structure of different types of articles may vary according to the type of study, and the content of the article.

The following are the detailed main components of the original research and review articles submitted to the journal.

Original research

The original research should have three following parts:

Preliminary section: It includes title, list of all contributing authors with their institutional affiliation, and abstract (160-250 words) with at least 3 keywords.

Title: How to format a science article (replace with your real title)

Author(s): List the author name(s) separated by commas. Use superscript numbers to link affiliations, and symbols *†‡ for author notes. For example, Y. Obsie[1*], S.A. Adem[1, 2]

**Corresponding author(s):* Include the email addresses or telephone numbers of the corresponding author(s). Please use the asterisk (*) symbol for the corresponding author information. This information is at the bottom of the manuscript's first page.

Author's affiliation addresses:

[1]Affiliations should be preceded by superscript numbers corresponding to the author list

[2]For any institutions, please provide the institution name, street, district, city, country

Received ; revised ; accepted

Abstract:
Start your abstract here…
Keywords: **keyword 1, keyword 2, keyword 3…**
Classification number(s): **1.1, 3.4, 5.3, etc.**

Abstract: The abstract should range between 160 and 250 words and be structured in a single paragraph following keywords in a separate line. The abstract should represent the main part of the research manuscript. It should reflect a brief and comprehensive background following the aim of the study (main questions to be addressed), methods used for investigating the problem, a summary of significant findings, main conclusions, and implications of the results.

Keywords: They should come immediately after the abstract and contain 3-7 specific and relevant keywords. They should reflect the research study and the relevant field of research.

Classification numbers: Depend on the Journal's Classification Scheme.

Author(s) are encouraged to write a "Highlights" that summarises the most exciting, interesting points from your manuscript.

Manuscript section: It is the main body of the scientific manuscript including: 1) Introduction; 2) Material(s) and method(s); 3) Results and discussion (separation of these two sections is acceptable); 4) Conclusions; 5) Recommendations/Suggestions/ Implications/Study limitations...(if any). These sections may slightly vary depending on the type of research approach and design used in the research. Each section should be numbered.

All of the Figures, Tables, and Equations should be cited in numerical order.

Figures

Fig. #: (Begin each figure caption with a label, "**Fig. 1.**" for example, as a new paragraph).

Fig. 1. The figure caption should begin with an overall descriptive statement of the figure followed by additional text. They should be immediately after each figure. Figure parts are indicated with capital letters **(A)**. If you prefer, you can place both the actual figures and captions logically through the text near where they are cited rather than at the end of the file (but not both). If a paragraph in the main text begins with the name of a figure, write out "Figure" in full (e.g., <para> "Figure 1 shows...").

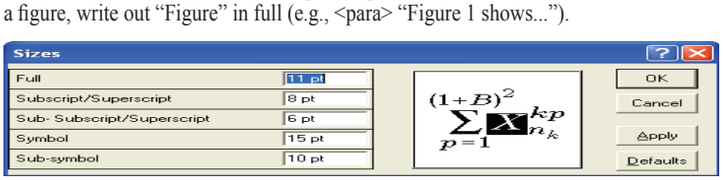

Fig. 1. The figure caption.

Tables

Table #: (Begin each table caption with a label "**Table 1.**", etc. as a new paragraph).

Table 1. Start this caption with a short description of your table. Format tables using the Word Table commands and structures. Do not create tables using spaces or tabs characters.

Table 1. Caption.

a	b	c	d	e
f				
g				
h				

Equations

$$\int_a^b x dx \tag{1}$$

Equations can be included. We do not recommend using the native Word 2007, 2008, 2010 or 2011 equation editor. This can in some cases produce less reliable MathML, the online markup language we use, which may result in display errors. Instead, use the legacy equation editor in Word (Insert menu; select insert object; select word equation) or use MathType (recommended). If you enter equations in simple LaTeX, check that they will convert accurately (Word 2007 and higher can convert simple LaTeX equations).

Closing section: It includes appendices/supplementary materials/data availability statement (if applicable), CRediT author statement (for multiple authors), acknowledgements (if applicable), competing interests, ethics (if any) and a complete list of references corresponding to all the citations given in the text of the manuscript. The appendices/supplementary materials may include data files and other material relevant to the research that should be submitted in separate files if required.

APPENDICES (if any)

The appendices should ideally be under 1000 words (approximately 2 A4 pages) for printing version. With longer appendices, they are only accepted for online publication.

CRediT author statement (for multiple authors)

CRediT offers authors the opportunity to share an accurate and detailed description of their diverse contributions to the published work.

ACKNOWLEDGEMENTS (if applicable)

This section is for the researchers who were funded for the research projects, and it should enclose all sources of financial support.

COMPETING INTERESTS

The author(s) declare(s) that there is no conflict of interest regarding the publication of this article.

REFERENCES

For in-text citation: References should be cited in the bracket with a number [1]. Multiple reference citations are separated by commas [2, 3] or if a series, dashes [4-6]. When citing sources with the author(s) and the year, they should be shortened to the first author's name, followed by et al. (with more than one author) and the year.

For reference list: With less than or equal to three authors, list all the author(s). With more than three authors, the first three should be listed and followed by et al.

References are listed in numerical order, and in the same order in which they are cited in text. The reference list should include all and only those references you have cited in the text. The reference list appears at the end of the article.

The reference consists of: Initial(s) and first/last name of the author(s), author' names separated by commas (Year of publication), "Titles of journal articles or chapter of book", *Title of Journal, Book or Other Publication*, **Volume(Number)** (if any), page numbers (if any), DOI (if any), URL and accessed date (if any) (in its original language if not English).

To cite a website and online/electronic resources, please include the accessed date (day month year).

Example of a reference list:

[1] T. Binzoni, T.S. Leung, D. Boggett, et al. (2003), "Non-invasive laser Doppler perfusion measurements of large tissue volumes and human skeletal muscle blood RMS velocity", *Phys. Med. Biol.*, **48(1)**, pp.2527-2549, DOI: 10.1088/0031-9155-48-15-318.

[2] H.W. Bischoff, H.C. Bold (1963), *Some Soil Algae from Enchanted Rock and Related Algal Species*, University of Texas Publications, 95pp.

[3] R. Busi (2016), "Weedy rice in the Philippines and Vietnam", https://www.aciar.gov.au/publication/technical-publications/weedy-rice-philippines-and-vietnam-final-report, accessed 15 July 2018.

Review articles

They should be different from the original research as they would contain different sections on the literature review. Authors may structure this part as per nature, background, and available literature on the issue argued in the manuscript.

For more detailed instructions, please visit our website: vietnamscience.vn or vietnamscience.vjst.vn

This manuscript template has been used from 2021 onwards.

P-ISSN 2525-2461 • E-ISSN 2615-9937

Vietnam Journal of Science, Technology and Engineering

MARCH 2021 • VOLUME 63 NUMBER 1

EDITORIAL OFFICE

113 Tran Duy Hung Str., Cau Giay Dist., Hanoi, Vietnam

Tel: (84.24) 39436793; Fax: (84.24) 39436794

Email: vjste@most.gov.vn

Website: vietnamscience.vn or vietnamscience.vjst.vn

PUBLICATION LICENCE

No.1153/GP-BTTTT 26th July 2011

No.2528/GP-BTTTT 26th December 2012

No.592/GP-BTTTT 28th December 2016